Universidade de São Paulo
Faculdade de Medicina de Ribeirão Preto
Departamento de Genética

Juliana Yumi Sakita

Mastócitos e câncer colorretal: uma complexa interação com potencial terapêutico

Ribeirão Preto – SP
2022

Juliana Yumi Sakita

Mastócitos e câncer colorretal: uma complexa interação com potencial terapêutico

Tese apresentada à Faculdade de Medicina de Ribeirão Preto da Universidade de São Paulo, como requisito para obtenção do título de Doutora em Ciências, área de concentração: Genética

Orientador: Dr. Vinicius Kannen Cardoso

Ribeirão Preto - SP

2022

FICHA CATALOGRÁFICA

Sakita, Juliana Yumi

Mastócitos e câncer colorretal: uma complexa interação com potencial terapêutico

316p. : il.; 30cm
Tese apresentada ao Programa de Pós-graduação em Genética da Faculdade de Medicina de Ribeirão Preto da Universidade de São Paulo para obtenção do título de Doutora em Ciências Médicas.
Área de concentração: Genética.

FOLHA DE APROVAÇÃO

Janus

Universidade de São Paulo

ATA DE DEFESA

Aluno: 17135 - 10132285 - 2 / Página 1 de 1

Ata de defesa de Tese do(a) Senhor(a) Juliana Yumi Sakita no Programa: Ciências Biológicas (Genética), do(a) Faculdade de Medicina de Ribeirão Preto da Universidade de São Paulo.

Aos 15 dias do mês de novembro de 2022, no(a) FMRP-USP realizou-se a Defesa da Tese do(a) Senhor(a) Juliana Yumi Sakita, apresentada para a obtenção do título de Doutora intitulada:

"Mastócitos e câncer colorretal: uma complexa interação com potencial terapêutico"

Após declarada aberta a sessão, o(a) Sr(a) Presidente passa a palavra ao candidato para exposição e a seguir aos examinadores para as devidas arguições que se desenvolvem nos termos regimentais. Em seguida, a Comissão Julgadora proclama o resultado:

Nome dos Participantes da Banca	Função	Sigla da CPG	Resultado
Vinicius Kannen Cardoso	Presidente	FMRP(FMRP)	Não Votante
Wilson Araújo da Silva Junior	Titular	FMRP - USP	APROVADA
Jaqueline Carvalho de Oliveira	Titular	UNIFAL - Externo	APROVADO
Fernando Chahud	Suplente	FMRP - USP	APROVADA

Resultado Final: Aprovada

Parecer da Comissão Julgadora *

Eu, Ísis Sawasaki Silveira Leme _____, lavrei a presente ata, que assino juntamente com os(as) Senhores(as). Ribeirão Preto, aos 15 dias do mês de novembro de 2022.

Wilson Araújo da Silva Junior

p/ Jaqueline Carvalho de Oliveira

Fernando Chahud

Vinicius Kannen Cardoso
Presidente da Comissão Julgadora

* Obs: Se o candidato for reprovado por algum dos membros, o parecer circunstanciado é obrigatório.

A defesa foi homologada pela Comissão de Pós-Graduação em _____ e, portanto, o(a) aluno(a) _____ jus ao título de Doutora em Ciências obtido no Programa Ciências Biológicas (Genética) - Área de concentração: Genética.

_____
Presidente da Comissão de Pós-Graduação

Conforme a Resolução nº 7493/2018, artigo 91, § 2º, a CCP autorizou que esta defesa fosse realizada de **modo híbrido**, com a participação de um ou mais examinadores por meio de videoconferência ou outro suporte eletrônico à distância equivalente.
Portanto, declaro que os membros **Profa. Dra. Jaqueline Carvalho de Oliveira** e **Prof. Dr. Wilson Araújo da Silva Junior** participaram remotamente e consideraram a aluna aprovada.

Ribeirão Preto, 15 de novembro de 2022.

Prof. Dr. Vinicius Kannen Cardoso
Presidente da Banca

APOIO E SUPORTE FINANCEIRO

O presente trabalho foi realizado com apoio da Coordenação de Aperfeiçoamento de Pessoal de Nível Superior – Brasil (CAPES) – Código de Financiamento 001.

O presente trabalho foi realizado com apoio do **CNPq**, Conselho Nacional de Desenvolvimento Científico e Tecnológico – Brasil.

DEDICATÓRIA

Este trabalho é dedicado em memória da minha mãe, **Edna Sakita**. Que você continue olhando e zelando por mim como sempre o fez. Que meu trabalho possa ajudar as pessoas, assim como os princípios que a senhora me deu. Meu amor e gratidão por você serão eternos.

AGRADECIMENTOS

Eu gostaria de agradecer meu orientador **Dr. Vinicius Kannen**, por todos os ensinamentos durante todos esses anos, tanto no âmbito profissional, quanto no pessoal. Mesmo me orientando à distância, esteve disponível para tirar dúvidas, conversar sobre as minhas dificuldades e me dar todo o apoio necessário.

Gostaria de agradecer também o **Prof. Dr. Sérgio Akira Uyemura**, por permitir que eu desenvolvesse minha pesquisa em seu laboratório e por todo apoio durante meu mestrado e doutorado. Obrigada por todas as discussões pertinentes, por dar o suporte científico e por deixar as portas abertas para conversarmos sobre prospecções futuras.

Ao **Prof. Dr. Jeremy Squire**, meu co-orientador, por aceitar esse papel durante meu doutorado. Obrigada por todo suporte e discussões pertinentes.

Meus sinceros agradecimentos à minha família: ao meu pai, **Edgar Sakita**, por acreditar no meu potencial, por ser meu apoio e abrigo. **Karim Sakita**, minha tia e madrinha, que tem o dom de ser ouvinte e conselheira; obrigada por todo apoio durante todos esses anos. **Henrique** e **Isabela**, agradeço por todo o carinho e por terem me dado o privilégio de ser tia da **Maria Flor**, que é a criança mais amável desse mundo. À minha segunda família, **Alice**, **Cesário** e **Simone Ozawa**, por me acolherem tão bem na família de vocês, por todo carinho e por compartilharem essa longa jornada ao meu lado.

Aos meus amigos, **Ualter Cipriano**, **Aline Viana Bernardi**, **Stefania Minto**, **Suziene Cardoso**, **Maycon Marção**, **Renan Simões**, **Lorenna Evelyn**, por todos os momentos compartilhados e ensinamentos. Obrigada por sempre me incentivarem, me escutarem e até discutirem os experimentos comigo.

Agradeço aos técnicos do nosso laboratório: **Emerson Santos**, **Lucas Souza**, **João Franco**; obrigada por todas as discussões pertinentes e por tornarem o nosso ambiente de trabalho muito mais leve e prazeroso.

À **Drª Tathiane Malta**, obrigada pelos ensinamentos de bioinformática, pela paciência e disposição em me ensinar e por todas as análises que

acrescentaram e enriqueceram muito meu trabalho. Aprendi muito a nível científico e pessoal.

Também agradeço aos professores colaboradores: **Profª Dra Daniela Carlos** e **Prof. Dr. Fernando Cunha**, por todo apoio científico e por deixarem as portas do seu laboratório abertas para parcerias e colaborações. Agradecimento em especial ao doutorando **Jefferson Elias**, aluno da Profª Daniela, pela ajuda nos experimentos finais do meu artigo e pela disponibilidade de chegar as 4h da manhã e ficar até o final do experimento.

Aos técnicos responsáveis pelo biotério da Faculdade de Ciências Farmacêuticas: **Reinaldo**, **Fábio** e **Ronaldo**; agradeço por toda ajuda nas trocas e limpeza das caixas de animais, por prepararem os materiais necessários e discussões pertinentes.

Obrigada aos funcionários e ao **Departamento de Genética** da Faculdade de Medicina de Ribeirão Preto, por todo suporte durante o desenvolvimento da minha pesquisa.

Agradecimento ao meu filho de quatro patas, **Hashi**, por me dar tanto amor, por me alegrar nos momentos difíceis e sempre estar ao meu lado.

Por fim, gostaria de agradecer ao meu esposo, **André Ozawa**, por compartilhar e acreditar nos meus sonhos, por toda a compreensão e fazer com que minha jornada científica e pessoal seja tão mais leve e proveitosa.

Sem vocês, nada disso seria possível! Espero um dia, poder retribuir tudo o que fizeram e fazem por mim.

Seja humilde se queres obter sabedoria. Porém, seja ainda mais humilde quando a tiver adquirido.

Helena Blavatsky

RESUMO

SAKITA, J.Y. “**Mastócitos e câncer colorretal: uma complexa interação com potencial terapêutico**”. 2022, 316 p. Tese de Doutorado – Faculdade de Medicina de Ribeirão Preto, SP, Brasil, 2022.

Introdução: O câncer colorretal (CCR) tem uma alta taxa de mortalidade e pode se desenvolver de forma associada à colite ou de forma esporádica. Existem debates significativos se mastócitos (MCs) podem promover ou inibir o desenvolvimento do CCR. Neste trabalho, a atividade dos MCs durante os diferentes estágios do CCR foi investigada.

Métodos: Foram analizadas amostras pareadas de pacientes (tecido saudável *versus* CCR), bem como uma meta-análise imunogenômica baseada nas amostras de CCR do *The Cancer Genome Atlas* (TCGA). Também foram realizados ensaios *in vitro* e múltiplos experimentos com modelos de camundongos geneticamente modificados (GEM).

Resultados: A análise das amostras de CCR de pacientes revelou que MCs podem estar ativados ou não em tumores. Além disso, a análise dos dados presents no TCGA revelou que um aumento na população de MCs ativada ocorre concomitantemente com uma redução na população de células T CD8 tumorais. Em camundongos, o cultivo de MCs previamente expostos a células CCR juntamente com células tumorais revelou que elas podem induzir as células malignas à apoptose. Em modelos GEM, a deficiência de MCs reduziu o desenvolvimento de tumores associados à colite apesar de promover um maior infiltrado de linfócitos T CD8 nestas lesões. Do contrário, esta deficiência de MCs promoveu a multiplicidade de tumores colorretais esporádicos. O uso de outros modelos GEM demonstrou que diferentes respostas imunes alteram e são alteradas pela atividade dos MC, influenciando diretamente a tumorigênese do cólon. Através do resgate da atividade de MCs via transplante de medula óssea em camundongos deficientes em MC foi possível demonstrar mecanisticamente que estas células definem o desenvolvimento tumoral desde as etapas tumorigênicas iniciais. Descobertas similares foram observadas através da inibição farmacológica dos MCs em momento anterior or posterior da indução das lesões tumorigênicas iniciais. Com base nisso, buscou-se explorar o

potencial terapêutico de MCs contra o CRC. A atividade de MCs promoveu o desenvolvimento de tumores alográficos e inibiu a infiltração de células $CD8^+$ nestas lesões. Do contrário, a inibição farmacológica da atividade de MCs reduziu o desenvolvimento de tais tumores e aumentou a população de células CD8 tumorais. Nenhum resultado positivo desta terapia se observou em animais imunossuprimidos. Finalmente, esta estratégia terapêutica potencializou a atividade citotóxica do quimioterápico fluorouracil.

Conclusão: Os MCs possuem um duplo papel no desenvolvimento do CCR e são potenciais alvos terapêuticos contra essa doença.

Palavras chaves: Colite; tumor; Sistema imune; eixo mastócito-linfócito; azoximetano.

ABSTRACT

SAKITA, J.Y. "**Mast cells and colorectal cancer: a complex interaction with therapeutic potential**". 2022, 316 p. Ph.D. Thesis – Medicine School of Ribeirão Preto, University of São Paulo, SP, Brazil, 2022.

Background Colorectal cancer (CRC) has a high mortality rate. It can develop in either colitis-dependent (CA-CRC) or -independent (sCRC) manner. There has been a significant debate about whether mast cells (MCs) promote or inhibit the development of CRC. Herein we investigated MC activity throughout the multi-stepped development of CRC.

Methods: Patient-matched samples (healthy colon *versus* CRC tissue) were histopathologically analyzed. A cohort of The Cancer Genome Atlas (TCGA) CRC samples underwent an immunogenomic meta-analysis. We also performed in vitro assays and multiple experiments with genetically engineered mouse (GEM) models.

Results: Analysing human CRC samples revealed that MCs could be active or inactive in this disease. Furthermore, an increase in the activated MC population occurs concomitantly with a reduction in the tumour-residing CD8 T cells. In mice, MC deficiency decreased the development of CA-CRC lesionswhile it increased the density of tumour-based CD8 infiltration. Moreover, co-culture experiments revealed that tumour-primed MCs promote apoptosis in CRC cells. In GEM models, MC deficiency reduced the development of colitis-associated tumours despite promoting a higher infiltrate of CD8 T lymphocytes in these lesions. Conversely, this condition increased the number of tumours induced by the sCRC protocol. The use of other GEM models demonstrated that different immune responses alter and can be altered by MC activity, directly influencing colon tumorigenesis. Through the rescue of MC activity via bone marrow transplantation in MC-deficient mice, it was possible mechanistically demonstrate that these cells define tumour development from the initial tumorigenic steps onwards. We observed similar findings through the pharmacological inhibition of MCs before or after the induction of initial tumorigenic lesions. These findings led us to explore the therapeutic potential of MCs against CRC. The activity of MCs promoted the development of allograft tumors and inhibited the infiltration of

CD8+ cells in these lesions. However, pharmacologically inhibiting MCs activity blocked the growth of such tumours and increased the CD8 T cell tumour population. This therapy did not impact tumour growth in immunosuppressed animals. Nevertheless, this therapeutic strategy potentiated the cytotoxic activity of fluorouracil chemotherapy.

Conclusion: MCs have a dual role throughout CRC development and are potential druggable targets against this disease.

Keywords: Colitis; tumours; immune system; mast cell-lymphocyte axis; azoxymethane.

LISTA DE FIGURAS

*p=0,04). **B**: Crescimento relativo entre os tumores com células de melanoma (B16F10) tratados com cromoglicato dissódico (CA; vermelho) e não tratados (CT; preto) por 15 dias (n = 11). **C**: Gráficos representativos das gates utilizadas na análise da citometria de fluxo para MCs ($CD45^+$ $CD117^+FcεRI^+$) e linfócitos T CD8 ($CD45^+$ $CD3^+CD8^+$) de células isoladas dos tumores B16F10. **D-E**: Gráficos demonstrando a porcentagem e MCs ($CD45^+CD117^+FcεRI^+$) e linfócitos T CD8 ($CD45^+CD8^+CD3^+$) isolados das amostras de tumor (n = 8; *p=0,002). Os dados estão mostrados como mediana, com os valores mais altos e mais baixos. Os valores de p foram calculados usando o teste t two-tailed Mann-Whitney. 151

Figura 27: A atividade dos mastócitos pode ser usada como alvo da terapia contra os tumores colorretais em camundongos. **A**: Razão do volume tumoral relativo de tumores colorretais pelo peso corpóreo do animal tratado com CA ou não após 26 dias do início do experimento (n = 17; ****p<0,0001). **B**: Crescimento relativo dos tumores colorretais avançados em camundongos. O grupo tratado com cromoglicato dissódico (CA; 25mg/kg/dia; verde) apresentou menor crescimento quando comparado com o grupo não tratado (CT; preto) (n = 17; 26 dias de experimento). **C**: Gráfico demonstrando o acompanhamento do peso corporal dos animais durante os tratamentos. Os dados estão representados como média ± desvio padrão. **D**: Gráficos demonstrando a estratégia de gates para a avaliação do número de células $CD45^+$ $CD3^+CD8^+$ e $CD45^+FcεRI^+CD117^+$ isoladas de amostras de tumores colorretais avançados. **E**: Gráficos demonstrando a porcentagem de células $CD45^+$ $CD3^+CD8^+$ isoladas de amostras de tumores colorretais avançados (n = 8; *p=0,02). **F**: Gráfico demonstrando a porcentagem de MCs ($CD45^+CD117^+FcεRI^+$) isolada das amostras de tumor (n = 17). Os dados estão representados como mediana, com

LISTA DE TABELAS

LISTA DE ABREVIATURAS E SIGLAS

Abreviatura	Significado	Abreviatura	Significado
AB/AM	Antibiótico e Antimicótico	MAT	Microambiente tumoral
AC	Cripta aberrante	MCs	Mastócitos
AOM	Azoximetano	Mcpt	Metaloproteinase
APC	Polipose adenomatosa coli	MEC	Matrix extracelular
CA	Cromoglicato dissódico	MGMT	O^6-metil-transferase
CAB	Cripta aberrante	MHC-I	Complexo principal de histocompatibilidade classe 1
CCR	Câncer colorretal	MHC-II	Complexo principal de histocompatibilidade classe 2
CDNA	DNA complementar	mm^2	Milímetros quadrados
Cpa3	Carboxipeptidase A3	mm^3	Milímetros cúbicos
Cm	Centímetro	PAF	Polipose adenomatosa familiar
DMEM	*Dulbeccos* modificado	PARP2	Poli [ADP ribose] polimerase 2
FCA	Foco de cripta aberrante	PL	Lesão preneoplásica
FCFRP	Faculdade de Ciências Farmacêuticas de Ribeirão Preto	qRT-PCR	PCR quantitativa em tempo real
FMRP	Faculdade de Medicina de Ribeirão Preto	RNAseq	Sequenciamento de RNA
GAPDH	Gliceraldeído 3-fosfato dehidrogenase	RPMI	*Roswell Park Memorial Institute*
GFP	Proteína verde fluorescente	SFB	Soro fetal bovino
HE	Hematoxilina e Eosina	SNE	Sistema nervoso entérico
H1R	Receptor de histamina tipo 1	SNG	Sequenciamento de nova geração
H4R	Receptor de histamina tipo 4	TBE	Tribromoetanol
IHC	Imunohistoquímica	TCGA	The Cancer Genome Atlas
IL	Inteleucina	TGI	Trato gastrointestinal
Il33r	Receptor da Interleucina 33	TLR	Receptor Toll like
Ip	Intraperitoneal	TMA	Tissue microarray
IR	Radiação ionizante	Treg	Linfócitos T regulatórios
Lgr5	Repetições ricas em leucinas contendo receptor acoplado à proteína G	TRPV1	Receptor vanilóide de potencial transitório tipo 1
LTC	Linfócito T citotóxico	VT	Volume tumoral
KO	*Knockout*	WB	Western blotting

SUMÁRIO

1. Introdução

1.1 Cólon: anatomia comparativa (Humanos *vs* camundongos)

O intestino grosso é formado pelo céco, apêndice vermiforme (presente somente nos humanos), cólon, reto e ânus. Em ambas as espécies, a função primária do intestino grosso é reabsorver água e estocar o conteúdo fecal (TREUTING, ARENDS, DINTZIS, 2018). Macroscopicamente, o cólon humano pode ser diferenciado do intestino delgado pela presença das bandas musculares longitudinais externas, ou *taenia coli* (ELLIS, MAHADEVAN; 2014). Já em roedores, o cólon apresenta a camada serosa lisa (MARTINEZ *et al*., 2016).

O cólon pode ser dividido em quatro regiões de acordo com a sua posição anatômica: cólon ascendente, transverso, descendente e sigmoide (TREUTING, ARENDS, DINTZIS, 2018). Em adultos, mede cerca de 1,5 metros, tendo início na região terminal do íleo e término no reto (MARTINEZ *et al*., 2016). Em roedores, o cólon mede cerca de 18 centímetros (cm) (HUGENHOLTZ, de VOZ, 2018).

Em camundongos o cólon ascendente é caracterizado pela presença de dobramentos transversos na camada serosa. O cólon ascendente continua em direção à região pilórica do estômago, onde passa a se chamar cólon transverso. O cólon distal, ou cólon descendente é a região de ligação do cólon transverso e o reto (KARARLI, 1995).

Em humanos, o cólon ascendente tem cerca de 15 a 20cm de comprimento, e se situa próximo ao lóbulo direito do fígado (MARTINEZ *et al*., 2016). O cólon transverso possui 40 a 45cm de comprimento e se localiza na porção superior do abdômen, posteriormente ao estômago, se estendendo até o hipocôndrio

esquerdo, abaixo da borda inferior do baço (ELLIS, MAHADEVAN; 2014; MARTINEZ *et al*.; 2016). O cólon transverso está conectado à margem inferior do pâncreas e ao omento maior por meio do mesocólon transverso, uma lâmina dupla de peritônio (LIU, CRAWFORD, 2005).

O cólon descendente mede aproximadamente 25cm e é a porção mais estreita do cólon humano (TREUTING, ARENDS, DINTZIS, 2018). O cólon sigmóide, tem aproximadamente 25cm e se inicia na abertura pélvica. Este, se insere anteriormente ao sacro, com leve desvio a direita no assoalho pélvico. Ao nível da terceira linha da fusão sacral, há uma leve curvatura a esquerda do cólon sigmóide antes deste descender rumo ao reto (MARTINEZ *et al*., 2016).

1.2 Características histológicas do colón

As diferenças entre o epitélio do intestino delgado e o cólon estão diretamente relacionadas com as funções fisiológicas de cada órgão. Ambos os epitélios são formados por uma única camada de células epiteliais colunares (ELLIS, MAHADEVAN; 2014). Entretanto, o intestino delgado tem um importante papel na absorção de nutrientes, enquanto o epitélio do cólon tem a função de absorção de água e eletrólitos (BOWCULTT *et al.,* 2014). Assim, a principal diferença microscópica entre os intestinos é a presença de vilosidades (projeções do epitélio intestinal) no intestino delgado, maximizando a superfície de absorção (BOOTH, POTTEN, 2000).

O tecido colônico, é composto por quatro camadas denominadas mucosa, submucosa, muscular própria e a camada serosa (BOOTH, POTTEN, 2000). A camada mucosa é composta por uma única camada de células epiteliais

colunares que formam protusões luminais, constituindo as criptas de Lieberkühn (HUMPHRIES, WRIGHT, 2008). A lâmina própria compõe o estroma da mucosa colônica, e contém vasos sanguíneos, linfáticos, e células do sistema imune. Dentre essas células, estão presentes os eosinófilos, macrófagos, linfócitos e os mastócitos (MCs) (JASSO *et al*.; 2022). A camada submucosa é composta por uma abundante quantidade de tecido adiposo (presente somente nos humanos). A camada muscular é composta de uma camada circular interna e uma camada longitudinal externa (HUGENHOLTZ, de VOZ, 2018).

Por estar em constante atrito com o bolo fecal, a mucosa intestinal precisa resistir às forças mecânicas que podem comprometer a integridade epitelial (GEHART, CLEVERS, 2019). Esse processo só é possível devido a presença de um nicho de células tronco teciduais intestinais (CTCi). O gene codificante de Lgr5 é um dos marcadores mais populares para as CTCi, garantindo assim a constante renovação tecidual necessária (HAGEMAN *et al*., 2020). A natureza proliferativa de células $Lgr5^{+}$ se deve a atividade molecular da via de sinalização Wnt (Wingless e Int-1) e Notch, bem como a estimulação de EGF (fator de crescimento epidermal) (GEHART, CLEVERS, 2019). Essas células possuem a capacidade de se diferenciar terminalmente em quatro linhagens celulares: colonócitos (células absortivas no cólon) ou enterócitos (células absortivas no intestino delgado), células globulares (CG) secretoras de muco, células neuroendócrinas, e células Paneth (CHENG, LEBLOND, 1974).

1.3 Mastócitos

Os MCs são células pertencentes a resposta imune inata, e foram descobertas por Friedrich Daniel von Recklinghausen em 1863 (RECKLINGHAUSEN, EITER, 1863). Posteriormente, em 1877, essas células foram minuciosamente descritas por Paul Ehrlich (EHRLICH, 1877). De início, os MCs receberam o nome de *Mastzellen* devido à sua estrutura rica em grânulos, e se sugeriu que estes grânulos fossem reservatórios intracelulares (RECKLINGHAUSEN, EITER, 1863; EHRLICH, 1877). Agora, sabe-se que estes grânulos são ricos em mediadores imunes, histamina, triptase e quimase. Além disso, os MCs são agora reconhecidos como células efetoras e reguladoras tanto da imunidade inata, quanto da resposta adaptativa intestinal (BULFONE-PAUS, BAHRI, 2015).

Os MCs são células imunes derivadas de células tronco hematopoiéticas $CD34^{+}$, e são liberadas pela medula óssea para a circulação sanguínea em sua forma imatura. Determina-se como MCs maduros aqueles que são residentes nos tecidos alvos (WEST, BULFONE-PAUS, 2022). Os MCs também estão presentes em diferentes órgãos e entre as áreas epitileiais e estromais (DWYER, BARRETT, AUSTEN, 2016). Além disso, os MCs modulam tanto a resposta imunidade inata quanto a adaptativa devido a sua capacidade de reconhecer e responder a alterações endógenas e exógenas, além de recrutar outras células imunes para o local de dano (ALBERT-BAYO *et al*., 2019).

A ativação dos MCs pode ser desencadeada através de vários receptores de reconhecimento de padrão. Especificamente, os receptores Fc expressos por MC ou receptores acoplados à proteína G rastreiam e reconhecem um grande

número de produtos associados a patógenos, produtos inflamatórios do hospedeiro e complexos imunes (ABRAHAM, ST JOHN, 2010; WEST, BULFONE-PAUS, 2022). Dentre esses receptores, pode-se citar os FcεRI para os anticorpos IgE, FcγR para os anticorpos IgG, receptores Toll-like (TLRs 1-7-9) e os receptores de reconhecimento padrão, c-Kit, CD117 e CD48 (KAMBAYASHI, KORETZKY, 2007; SANDIG, BULFONE-PAUS, 2012; KANAGARATHAM *et al*., 2020).

Um MC devidamente ativado sofre degranulação, o que significa que os compostos armazenados em suas vesículas intracelulares são imediatamente liberados ao seu redor, ou ocorre a síntese *de novo* (TRAINA, 2021). O processo de degranulação pode ocorrer por dois mecanismos: degranulação fragmentada ou anafilática (DVORAK *et al.*, 1992; ALBERT-BAYO *et al*., 2019). A degranulação fragmentada leva ao esvaziamento parcial ou total dos grânulos, causando uma liberação seletiva sem as fusões inter-grânulos ou grânulos-membrana plasmática. Esse tipo de degranulação é promovido por neuropeptídios, citocinas e produtos microbianos que interagem com os MCs, comum em doenças como a síndrome inflamatória intestinal (DVORAK *et al.*, 1992). Já na degranulação anafilática, o conteúdo mastocitário é liberado de forma explosiva através das fusões dos grânulos ou grânulos-membrana plasmática, e estão associados às reações de hipersensibilidade (DVORAK *et al*., 1991).

O tipo de estímulo patogênico, o paradeiro da ameaça e os níveis de ativação dos MCs, determinarão o tempo, o caráter da resposta e as mudanças no meio inflamatório (ABRAHAM, ST JOHN, 2010). Os MCs podem promover uma

resposta imune negativa ou positiva pela qual o problema imunológico pode ser resolvido ou agravado (WERNERSSON, PEJLER, 2014).

Por serem as maiores células produtoras de histamina, os MCs estão envolvidos principalmente em processos alérgicos (THANGAM, *et al.,* 2018). Durante as reações alérgicas, a histamina regula o balanço entre as células Th1 (interferon-γ [IFN- γ], interleucina [IL] -12, e IL-2) e Th2 (IL-5, IL-4, IL-10 e IL-13) (JUTEL, 2007). Além disso, a histamina regula processos fisiológicos como a secreção de ácido gástrico, inflamação, além de atuarem como neurotransmissor e na regulação da vasodilatação e broncoconstrição (BARNES, 1991; HILL, 1992).

1.4 Ação dos MCs no cólon

A barreira intestinal separa os ambientes interno e externo e é essencial para a homeostase intestinal. Dentre as suas principais funções, a barreira garante o controle da permeabilidade intestinal e proteção contra as substâncias tóxicas ou bactérias (ALBERT-BAYO *et al*., 2019). Devido à sua alta variedade de receptores, os MCs são capazes de responder a diversos tipos de estímulos, incluindo os neurais, microbianos, hormonais, metabólicos e químicos (TRAINA, 2021). Essa característica faz com que essas células tenham um papel central na homeostase da barreira intestinal (OVERMAN, RIVIER, MOESER; 2012; VANUYTSEL *et al*., 2014). Do ponto de vista fisiológico, os MCs induzem um aumento no fluxo sanguíneo e aumentam a motilidade intestinal. Essas ações constituem uma estratégia de defesa cujo objetivo é a lavagem e eliminação de antígenos ou substâncias tóxicas no lúmen intestinal (WOOD; 2007).

A primeira resposta dos MCs em meio aos estímulos, é a liberação dos mediadores presentes em seus grânulos e corpos lipídicos (WERNERSSON, PEJLER, 2014). Na mucosa intestinal, a sua ativação afeta a integridade e viabilidade epitelial, promove a secreção de íons e água, estimula a resposta imune inata e adaptativa, fluxo sanguíneo, coagulação e permeabilidade intestinal, fibrose, facilitam as interações neuro-imunes, promovem o peristaltismo e a percepção da dor (BISCHOFF, 2007).

O recrutamento dos MCs intestinais depende da ligação da α4β7 integrina com os receptores do tipo-2 das quimiocinas CXC, ou com as moléculas de adesão expressas nos MCs (ABONIA *et al*.; 2005). Dependendo da sua localização, essas células podem ser categorizadas como MCs de tecido conectivo ou MCs mucosais (XING *et al*., 2011).

O grau e o tipo de ativação dos mastócitos (fragmentada ou anafilática), em resposta as interações do microambiente, determinam a manutenção da homeostase e a manutenção das funções de defesa na mucosa intestinal (ALBERT-BAYO *et al*., 2019).

1.4.1 Mastócitos atuam como reguladores neuro-imunes no cólon

O trato gastrointestinal (TGI) sofre regulação e controle do sistema nervoso entérico (SNE), composto por diferentes tipos de neurônios como as células gliais e os neurônios entéricos, presentes na camada muscular e na lâmina própria (GUPTA K, HARVIMA, 2018; MITTAL *et al.*; 2019) Embora o TGI se comunique com o sistema nervoso central (SNC) através do sistema nervoso

simpático e parassimpático, o SNE é capaz de controlar a maioria das funções fisiológicas, tais como a motilidade, secreção e função imune de maneira independente (TRAINA, 2021).

A comunicação entre o SNC e o SNE, permite a regulação da barreira intestinal pelo monitoramento da secreção de íons, espessura epitelial, função imune e peristaltismo (ALBERT-BAYO *et al*., 2019; FORSYTHE, 2019). Os MCs são componentes fundamentais nessas interações via sinalização parácrina (mais comum), transgranulação (fragmentos dos grânulos ou dos mediadores são distribuídos diretamente ao corpo neuronal) ou através das integrinas (sinapses físicas) (FORSYTHE, 2019).

A proximidade dos MCs com os nervos entéricos aferentes cria uma comunicação bidirecional entre o SNC e o SNE (TRAINA, 2021). Os neurônios entéricos, vagais e os aferentes, expressam receptores para as moléculas liberadas pelos MCs (principalmente proteases, neuropeptídios, hormônios e fatores de crescimento), no qual estimulam os nervos terminais e determinam o limiar de disparo. Similarmente, os neuropeptídios e neurotransmissores liberados pelos neurônios estimulam a secreção dos mediadores mastocitários, que posteriormente ativam os receptores neuronais (FORSYTHE, 2019).

A relação entre os MCs e o SNE está relacionada com a transmissão de sinais de dor (FORSYTHE, 2019). A triptase liberada pelos MCs ativa PARP2 (poli [ADP ribose] polimerase 2) nas terminações nervosas periféricas. Essa ativação por sua vez, sensibiliza os receptores TRPV1 (receptor vanilóide de potencial transitório I), que quando combinados com a ativação dos MCs fazem a transmissão de sinais viscerais de dor em resposta à estímulos infecciosos ou condições de estresse (VAN DIEST *et al*., 2012). Por sua vez, o SNE estimula a

liberação de mediadores vasoativos, inflamatórios e algogênicos (CORRIGAN, 2016).

Além disso, o SNC influencia no processo de degranulação dos MCs intestinais através do nervo vago (TRAINA, 2021). A liberação de histamina e quimase modulam a permeabilidade da barreira intestinal e a secreção de água. Essas alterações estão correlacionadas com um aumento da infiltração de MCs, criando um loop positivo (DONG *et al*., 2017).

1.4.2 Mastócitos e a imunidade inata no epitélio colônico

Os MCs possuem um papel protetor contra as infecções virais e bacterianas através do recrutamento de neutrófilos, eosinófilos e macrófagos para mucosa intestinal e da ativação de respostas defensivas (ALBERT-BAYO *et al*., 2019). Quando ativados, os MCs liberam fosfolipase A2 e enzimas extracelulares com propriedades pró-inflamatórias e antibactericidas, capazes de eliminar os pátogenos (TRIGGIANI M, *et al*.; 2009). Os MCs formam extensões extracelulares compostas de DNA, histonas, proteases, tripase e peptídeos anti-microbianos, que funcionam como armadilhas quando não são capazes de exercer uma fagocitose eficiente. A formação dessas armadilhas é induzida pela condição de hipóxia e depende da produção de espécies reativas de oxigênio e culminam na morte dos MCs (MÖLLERHERM, von KÖCKRITZ-BLICKWEDE, BRANITZKI-HEINEMANN, 2016).

A triptase é um componente essencial no combate da infecção bacteriana através do recrutamento dos neutrófilos (SHIN *et al*.; 2008). A quimase contribui

inibindo a ligação do *Streptococcus* à matrix extracelular via degradação proteolítica da fibronectina (GENDRIN *et al.*, 2018). A carboxipeptidase A favorece a limpeza endógena e exógena das toxinas (SCHNEIDER *et al*.; 2007), enquanto a histamina liberada pelos MCs inicia o processo de infiltração neutrofílica na mucosa colônica via H4R (receptor de histamina tipo 4) (WECHSLER *et al*., 2018).

1.4.3 MCs e a resposta imune adaptativa no cólon

Os MCs tem sido demonstrado como células capazes de ativar e serem ativados pelos linfócitos T (ALBERT-BAYO *et al*., 2019). Sua ativação via células T ocorre através da liberação de citocinas pró-inflamatórias específicas, ou em menor porcentagem, a partir de microvesículas derivadas dos linfócitos (SHEFLER I, *et al*., 2010). Por sua vez, os MCs promovem a ativação, recrutamento, proliferação e secreção de citocinas em múltiplos tipos de linfócitos T. Além disso, os MCs promovem a polarização da resposta Th através da liberação de mediadores especifícos como IL-12 e IFN-γ para resposta Th1; IL-4 para resposta Th2; IL-6 e TGF-β para reposta Th17; e IL-6 e TNF-α para Th22 (SHEFLER I, *et al*., 2014).

Além disso, os MCs também estão envolvidos na apresentação de antígenos às células T. Graças aos seus receptores de reconhecimento de patógenos, os MCs internalizam e processam os antígenos que são apresentados para os linfócitos T via sistema MHCII (complexo principal de histocompatibilidade classe II) (VALITUTTI, ESPINOSA; 2010). A secreção de IL-6 e histamina pelos MCs

tem sido relatada como um regulador negativo e supressor da função das células T regulatórias (Treg) (MEKORI *et al*., 2016).

Já na resposta imune humoral, os MCs estão envolvidos na proliferação e diferenciação das células B em células plasmáticas secretoras de IgA (ALBERT-BAYO *et al*., 2019). Os MCs também dão suporte para a produção de IgE através da secreção de IL-4 e IL-13 e por meio da interação entre CD40L e CD40 expresso nos MCs e nas células B respectivamente (PAWANKAR *et al*.; 1997). Outras citocinas liberadas pelos MCs, IL-5 e IL-22, estão envolvidas na produção de IgM e desenvolvem um papel crucial na homeostase e defesa contra os patógenos da mucosa intestinal (BAUMGARTH, 2011). Além disso, a sobrevivência e proliferação dos linfócitos B são influenciadas pela secreção de citocinas e quimiocinas dos MCs, até mesmo em locais distantes através da liberação de exossomos que contém proteínas, RNA, mediadores solúveis, receptores FCεRI, proteínas MHC II e moléculas co-estimulatórias (CAMUSSI, 2010).

1.5 Ação dos MCs no desenvolvimento dos tumores

Os MCs localizam-se nas margens dos tumores e no microambiente tumoral (MAT), comumente ao redor dos vasos sanguíneos (TAMMA *et al.*, 2017). Os MCs são recrutados com a ajuda de quimioatraentes liberados por células tumorais, como o fator de células tronco (SCF) ou Ccl15 (YU, 2018). Após sua ativação, tornam-se altamente pró-inflamatórias e recrutam ativamente células do sistema imune inato, principalmente neutrófilos, macrófagos e eosinófilos e células do sistema imune adquirido (células B e T) para orquestrar respostas

imunes antitumorais (KOMI, REDEGELD, 2020). Uma variedade de citocinas liberadas por MCs, incluindo IL-1, IL-4, IL-8, IL-6, MCPT-3, MCPT-4, TNF-α, IFN-γ, LTB4, TGF-β e quimase contribuem para o desenvolvimento da inflamação, inibindo o crescimento de células tumorais e induzindo-as à apoptose (RIBATTI, CRIVELLATO, 2012).

Por outro lado, os mediadores liberados pelos MCs, tais como FGF-2, NGF, PDGF, VEGF, IL-8 e IL-10 promovem a expansão das células tumorais (RIBATTI, 2015). A histamina também é capaz de induzir a proliferação das células tumorais agindo nos receptores H1 expressos na superfície do tumor (H1R) (RIBATTI, 2015).

Além disso, os MCs são capazes de facilitar a vascularização tumoral e seu potencial maligno de invasão (RIBATTI, CRIVELLATO, 2012; KOMI, REDEGELD, 2020). Os MCs liberam uma série de mediadores angiogênicos no MAT, incluindo IL-8, TNF-α, TGF-β e ativador de plasminogênio tipo uroquinase (DE PALMA, BIZIATO, PETROVA, 2017). A triptase liberada por MCs também promove a proliferação de células endoteliais, induzindo a formação de novos vasos e fornecendo novas fontes de oxigênio e trocas gasosas (GUO *et al.,* 2016). Além disso, a histamina age sobre os receptores H1R e H2R, estimulando a formação de novos vasos (DE PALMA, BIZIATO, PETROVA, 2017). Além de desempenhar um papel na angiogênese via VEGF-A e VEGF-B, os MCs também estão envolvidos na linfangiogênese pela liberação de VEGF-C e VEGF-D (DETORAKI *et al*., 2009).

As metaloproteinases (Mcpts) são capazes de degradar e remodelar a matrix extracelular (MEC) levando a uma alteração do microambiente celular, sendo a MCPT-9 a principal delas (KNIGHT *et al*., 2007). Sob a influência da quimase

liberada pelos MCs, as moléculas de E-caderina que conectam as células epiteliais nas junções aderentes são clivadas e sua expressão é diminuída (VISCIANO *et al.*, 2015). Portanto, a quimase pode promover a separação, proliferação e realocação de aglomerados de células, agindo direta e indiretamente na MEC para apoiar a metástase (GORZALCZANY, *et al*., 2017).

Os MCs que expressam *Mcpt4* estão presentes principalmente no estroma tecidual (XING *et al*., 2011) e são um dos responsáveis pela manutenção da homeostase da barreira intestinal (GROSCHWITZ *et al*., 2009). Durante o desenvolvimento dos tumores em animais $Apc^{Min/+}$, a expressão de *Mcpt4* e *Cma* (quimase) foi encontrada aumentada (MAYWALD *et al*., 2015). Já o aumento da expressão de *Mcpt1* (expresso pelos MCs localizados na mucosa tecidual; XING *et al*., 2011) associado com a deleção do receptor de quimiocinas (*Ackr2*) em animais $Apc^{Min/+}$, demonstraram proteger o epitélio contra a formação dos pólipos intestinais (BODDULURI *et al*., 2018).

Por outro lado, outros trabalhos têm evidenciado que a expressão de *Mcpt6* possui um papel protetor no desenvolvimento dos tumores alográficos de melanoma (GRUJIC *et al*., 2020). Utilizando um modelo triplo *knockout* (KO) para *Mcpt6*, *Mcpt4* e carboxipeptidase A3 (*Cpa3*), eles também demonstraram que essas Mcpts protegem os animais contra o desenvolvimento de metástases pulmonares em casos de melanoma (GRUJIC *et al*., 2017).

1.6 Câncer colorretal: epidemiologia

O câncer colorretal (CCR) é o terceiro câncer maligno mais comum na população mundial e o segundo câncer que mais letal (SONG, 2022; SUNG *et al*.; 2021). Em 2020, o CCR correspondia a cerca de 10% da incidência global, e a 9,4% das causas de morte relacionadas ao câncer (GLOBOCAN, 2020). O número global de novos casos está predito em 3,2 milhões em 2040. Esse número foi baseado nos dados de envelhecimento, crescimento populacional e desenvolvimento humano (SUNG *et al*.; 2021)

No Brasil, estima-se que o triênio de 2020 a 2022, a incidência dos casos de CCR seja de cerca de 20.540 em homens e 20.470 em mulheres (INCA; 2022). A análise da incidência de acordo com as regiões do Brasil revelou que a maior parte dos casos ocorre nas regiões Sudeste, Centro-Oeste e Sul (MARTIN et al., 2021; INCA; 2022).

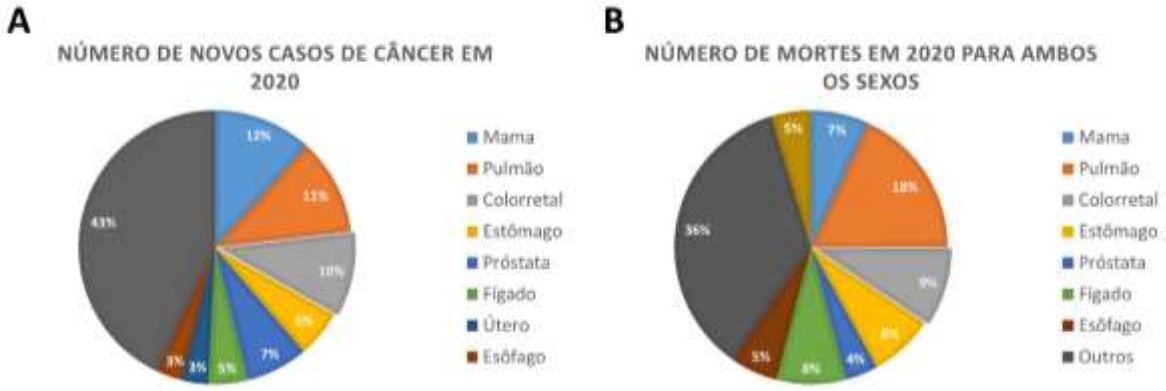

Figura 1: Incidência e mortalidade do câncer colorretal (CCR) na população mundial. **A**: Gráfico demonstrando a incidência de novos casos no ano de 2020 de acordo com a Organização mundial da saúde. O CCR corresponde a 10% de todos os casos (cinza claro, em destaque). **B**: Gráfico em porcentagem demonstrando a letalidade de cada tipo de câncer. O CCR é a segunda neoplasia com maior letalidade. Os gráficos foram adaptados do GLOBOCAN (2020).

1.7 Etiologia e fatores de risco associados

O CCR pode ser subdividido em diferentes tipos de acordo com a sua etiologia: CCR esporádico, associado à colite e os casos hereditários.

O tipo hereditário corresponde a cerca de 5% de todos os casos de CCR e são comumente associados à polipose adenomatosa familiar (PAF) (HEINIMANN, DARMKREBS, 2020). Nestes casos, múltiplos adenomas colônicos surgem precocemente e se proliferam ao longo do cólon de pacientes. A formação dos pólipos está relacionada com mutações em *APC* (polipose adenomatosa coli), e a descoberta do CCR normalmente ocorre em pacientes adultos jovens (35-45 anos) (DINARVAND *et al*., 2019; LYNCH, CHAPELLE, 2003).

O CCR associado à colite se desenvolve em pacientes que possuem uma doença inflamatória crônica, tais como a Síndrome do Intestino Irritado e a doença de Crohn (SHAH, ITZKOWITZ, 2021). A inflamação crônica gera um dano de DNA induzido por estresse oxidativo, levando a uma instabilidade genômica e aumentando a susceptibilidade de mutações em oncogenes ou genes supressores tumorais (ITZKOWITZ, 2004). As mutações que ocorrem no processo carcinogênico associado à colite são muito similares aos casos esporádicos: *APC*, *KRAS*, *P53*, *PIK3CA*, *SMAD4*, *ARID1A* e *MYC* (RAJAMÄKI *et al*., 2021; ROBLES *et al*., 2016; YAEGER *et al*. 2016). Porém, a frequência e o tempo em que ocorrem essas alterações genéticas diferem em ambos os processos. A mutação no gene *APC* ocorre tardiamente, durante a transição para o adenocarinoma. Já a mutação em *P53*, ocorre nas primeiras etapas da

carcinogenese associada à colite, antes mesmo da displasia (SHAH, ITZKOWITZ, 2021).

A maior incidência do CCR é de casos esporádicos, correspondendo a 70-75% de todos os casos (KEUM, GIOVANNUCCI, 2019). O desenvolvimento do CCR esporádico está associado ao acúmulo de mutações somáticas e/ou alterações epigenéticas induzidos pelo estilo de vida ocidental e hábitos não saudáveis (SAKITA *et al*. 2016; KEUM, GIOVANNUCCI, 2019, ARAI *et al.*, 2021). Esses hábitos estão relacionados principalmente à alimentação, uma vez que o epitélio colônico fica exposto à diversos tipos de compostos carcinogênicos que provocam dano ao DNA (SAKITA *et al*. 2016).

A integridade genômica nas células epiteliais e principalmente nas CTCis, dependente do sistema de reparo ao dano de DNA (GRONKE *et al*., 2019; SAKITA et al., 2019). Esse sistema, garante uma pausa transitória no ciclo celular para que o DNA seja reparado, ou caso o dano seja muito extenso, a indução da célula à apoptose (ARAI *et al.*, 2021). As alterações no sistema de reparo, favorecem o desenvolvimento da instabilidade genômica, que permite que as CTCis acumulem novas mutações e prossigam para a transformação maligna (BLOKZIJL *et al*., 2016).

1.8 Estágios de desenvolvimento do CCR

O processo tumorigênico se desenvolve através de três amplas fases: iniciação, promoção e progressão (BIRD, 1995; VOLGELSTEIN, 1996). Uma possível hipótese para o entendimento da tumorigênese intestinal, incluindo

malignidades do intestino delgado e cólon, sugere que somente as CTCi possuem longevidade suficiente para acumular mutações (BARKER *et al*, 2009).

A iniciação é o processo no qual as células normais adquirem a primeira mutação em genes *driver* que fornecem vantagens de crescimento e sobrevivência (oncogenes) sobre as células vizinhas (BERENBLUN; SHUBIK, 1948; VOGELSTEIN, KINZLER, 2015). A mutação em *APC*, gene driver do CCR foi relatado na maioria dos casos esporádicos (POWELL *et al.*, 1992). A perda do complexo de destruição formado por APC induz a altos níveis de β-catenina, que atua como um importante co-ativador transcricional (FODDE 2002).

A promoção tumoral, ou fase de expansão, corresponde a fase de crescimento do tumor de uma única célula iniciada em um tumor primário completamente desenvolvido. Geralmente está associada a alterações morfológicas e/ou fenotípicas (BIRD, 1995). Nesta fase, as células iniciadas adquirem uma segunda mutação em gene driver, garantindo o descontrole da proliferação celular e a desordenada arquitetura tecidual (BIRD, 1995; KANNEN *et al*., 2012; KANNEN *et al*., 2013; VOGELSTEIN, KINZLER, 2015).

As PL do cólon foram inicialmente observadas em 1987 no cólon de camundongos expostos à carcinógenos. Essas lesões foram identificadas como criptas aberrantes (CAB) ou focos de criptas aberrantes (FCA) quando havia a ocorrência de um agrupamento de criptas displásicas (BIRD, 1987). Posteriormente, essas lesões foram observadas em pacientes diagnosticados com câncer de cólon (PRETLOW, TP. *et al.*; 1991; RONCUCCI, 1992). A análise molecular dos FCA de pacientes revelou a presença de mutações em *KRAS* e *APC* (JEN *et al*.; 1994). Essas pesquisas precursoras revelaram que o tamanho

e número de FCAs variam conforme o risco para o desenvolvimento do carcinoma colorretal (BIRD, 1995; RONCUCCI L. *et al*.; 2000).

Durante o processo tumorigênico, o nicho de células $Lgr5^{+}$ iniciadas tumoralmente apresentam um aumento na divisão através do mecanismo de fissão criptal, bifurcação na base da cripta, empurrando as células para cima e para fora para dar origem a novas criptas colônicas (FUJIMITSU Y. *et al*.; 1996). Este evento tem sido sugerido participar da expansão das PL colônicas (MCLELLAN *et al*.; 1991). Existem debates se a progressão das criptas displásicas ocorre somente através da conversão clonal das células tronco mutadas via fissão criptal (HUMPHRIES, WRIGHT, 2008), ou se elas invadem as criptas adjacentes em um processo top-down (SHIH, WANG, 2001).

A progressão tumoral se refere ao estágio mais avançado da tumorigênese: a metástase. Nessa fase, as células tumorais adquirem uma ou mais mutações em genes driver, como em *TP53*, *SMAD4*, *PIK3CA*, que fazem com que essas células consigam invadir o tecido adjacente (FODDE 2002; VOGELSTEIN, KINZLER, 2015).

1.9 Mastócitos e CCR

No CCR em humanos, uma redução da população de MCs tem sido associada a um bom prognóstico, enquanto números elevados parecem estar associados a piora da doença e menores taxas de sobrevivência do paciente (NIELSEN *et al*., 1999; MEHDAWI *et al.*, 2016). Recentes pesquisas também

demonstraram que os mastócitos ativados estavam positivamente correlacionados com os tumors colorretais metastáticos (FLORES *et al.*, 2020).

A avaliação dos precursores dos MCs em amostras de sangue periférico de pacientes com CCR revelou que tais células não estavam associadas à progressão dos tumores (ZHAO *et al.*, 2022). No modelo animal exposto a carcinógenos, a deficiência de MC reduziu a carga tumoral (WEDEMEYER, GALLI, 2005). A inibição farmacológica da atividade de MCs também diminuiu o risco de CCR (MOTAWI *et al.*, 2017).

Outros grupos de pesquisa sugeriram que os MCs promovem o desenvolvimento de CCR associado à colite em camundongos (RIGONI *et al*., 2015; TANAKA, ISHIKAWA, 2013). Em contrapartida, outros trabalhos demonstraram a ação protetora contra o desenvolvimento de tumores no cólon de camundongos portadores da mutação heterozigótica em *Apc* (*Apc*$^{Min/+}$) (BODDULURI *et al*., 2018; e SINNAMON *et al.*, 2008).

Esses trabalhos demonstram que ainda não está claro qual é a ação dos MCs ao longo do desenvolvimento do CCR. Além disso, os MCs são células com ação complexas, e o entendimento da sua ação nas diferentes etapas revelará se a sua atividade pode ser explorada terapeuticamente.

1.10 Modelo experimental

1.10.1 Carcinógeno azoximetano (AOM)

A exposição ao carcinógeno AOM é o modelo experimental que melhor mimetiza em camundongos o processo carcinogênico que ocorre no cólon de humanos. O AOM é um carcinógeno indireto, ou seja, requer ativação metabólica para formar produtos reativos que reagem com DNA. O seu metabólito ativo é o metilazoximetanol (MAM), que possui a capacidade de alquilar macromoléculas no cólon e no fígado por meio da adição de grupamentos metil na posição O^6 ou N^7 da guanina (ROSENBERG, GIARDINA, TANAKA, 2009). Essas adições de grupamentos metil foram os adutos de DNA, que caso não sejam removidos por meio da via das metiltransferases (MGMT), farão com que ocorra um despareamento de bases nitrogenadas por erros no processo de reparo a oxidação do DNA. Tais eventos promovem altas taxas de morte celular, e induzem a iniciação carcinogênica de colonócitos (KONDO *et al*., 2010).

1.10.2 Dextran sulfato de sódio (DSS)

Para estudar o modelo do CCR associado à colite, Neufert e colaboradores padronizaram o uso do AOM juntamente com dextran sulfato de sódio (DSS) (NEUFERT, BECKER, NEURATH, 2007). O DSS é um importante indutor de colite por meio de dano ao epitélio colônico, mimetizando as condições da colite ulcerativa e da Doença de Crohn (OKAYASU *et al*., 1990). Esse modelo tem como característica a formação de tumores localizados na porção distal do cólon

(De ROBERTIS *et al*. 2011), além de ser essencial para o estudo das vias de sinalização do receptor Toll-like (FUKATA *et al.*, 2007).

1.10.3 Animais *knockout* para mastócitos

Existem modelos de animais KO para MCs para se explorar a atividade dos MCs *in vivo*. Os camundongos $Kit^{W/wv}$ e $Kit^{W/sh}$ carreiam uma mutação no locus W (c-kit) e exibem uma redução da sinalização de c-kit tirosina quinase, resultando na deficiência dos MCs (LYON, GLENISTER, 1982).

Os animais $Kit^{W/wv}$ possuem uma deficiência profunda de MCs, e exibem menos de 1% dos MCs na pele em comparação com os animais *wild type* (WT) (KITAMURA, GO, HATANAKA; 1978). Porém, a deficiência de c-kit nesses animais também provoca outras alterações fenotípicas, como anemina macrocítica, esterilidade, melanogênese prejudicada, deficiência nas células intersticiais de Cajal e redução dos linfócitos intraepiteliais intestinais (NAKANO *et al*., 1989; TSAI *et al*.; 2002).

Os animais $Kit^{W/sh}$ são resultado de uma mutação espontânea entre duas linhas puras (C3H/HeJ x 101/H) (LYON, GLENISTER, 1982). W-sash (Wsh) é uma mutação por inversão nos elementos regulatórios da transcrição de c-kit, presente no cromossomo 5 (NAGLE et al., 1995). Como resultado, os animais apresentam deficiência para os MCs em múltiplos sítios anatômicos, e prejuízo na pigmentação da pele (GRIMBALDESTON *et al*., 2005). Por não apresentar as inúmeras alterações fenotípicas dos animais $Kit^{W/Wv}$, esse modelo foi o escolhido para o desenvolvimento do trabalho.

2. Hipótese

Este projeto baseia-se na hipótese de que os MCs são células imunes com uma complexa ação modulatória, podendo orquestrar uma ampla gama de reações imunológicas em resposta ao desenvolvimento do CCR. É de especial importância o entendimento da interação entre MCs e LTCs como um eixo de interação celular determinante para expansão ou inibição do desenvolvimento do CCR. O entendimento mecanístico destas interações é essencial para que os MCs sejam terapeuticamente explorados contra o CCR (**Figura 2**).

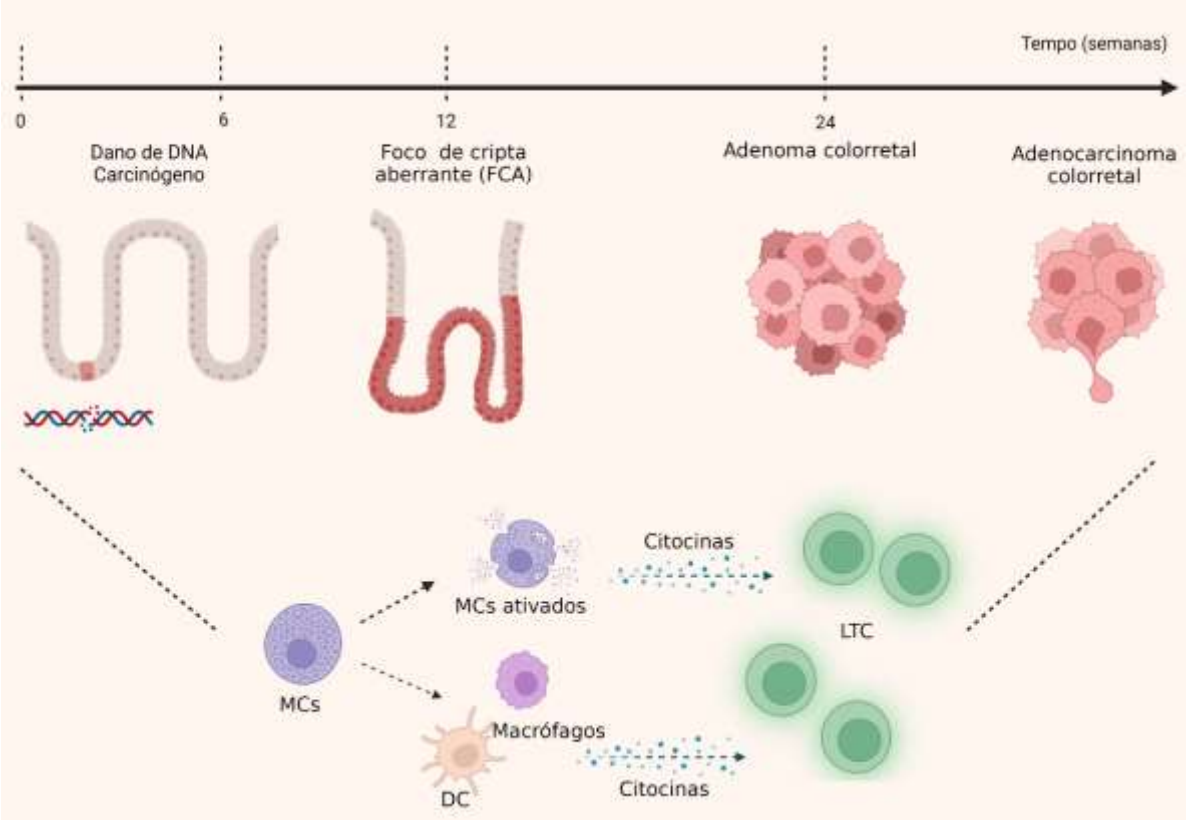

Figura 2: Esquema ilustrativo demonstrando a hipótese do trabalho. A interação entre mastócitos (MCs) e linfócitos T (LTCs) é demonstrada como um eixo de interação celular determinante para expansão ou inibição do desenvolvimento do CCR. Fonte: Do autor. Criado no Biorender.com.

3. Objetivo

3.1 Objetivo geral

Este estudo investigou se o entendimento do eixo MC-linfocitos T citotóxico (LTC) sobre as diferentes fases da tumorigenese colorectal poderia desvendar possíveis alternativas terapêuticas para o tratamento do CCR.

3.2 Objetivo específico

A hipótese e o objetivo geral foram explorados através dos seguintes objetivos específicos (**Figura 3**):

1- Investigar a existência de um possível eixo MC-LTC em pacientes humanos diagnosticas com CRC;
2- Investigar se um possível eixo MC-LTC reage diferencialmente à indução da tumorigenese colorretal esporádica ou daquela associada à colite;
3- Investigar se diferentes fatores imunológicos podem alterar o eixo MC-LTC durante o desenvolvimento das lesões tumorigenicas colônicas iniciais;
4- Investigar o efeito do eixo MC-LTC durante as fases iniciais da tumorigenese colorretal esporádica;
5- Investigar se o eixo MC-LTC pode ser explorado como alvo terapêutico contra o CCR.

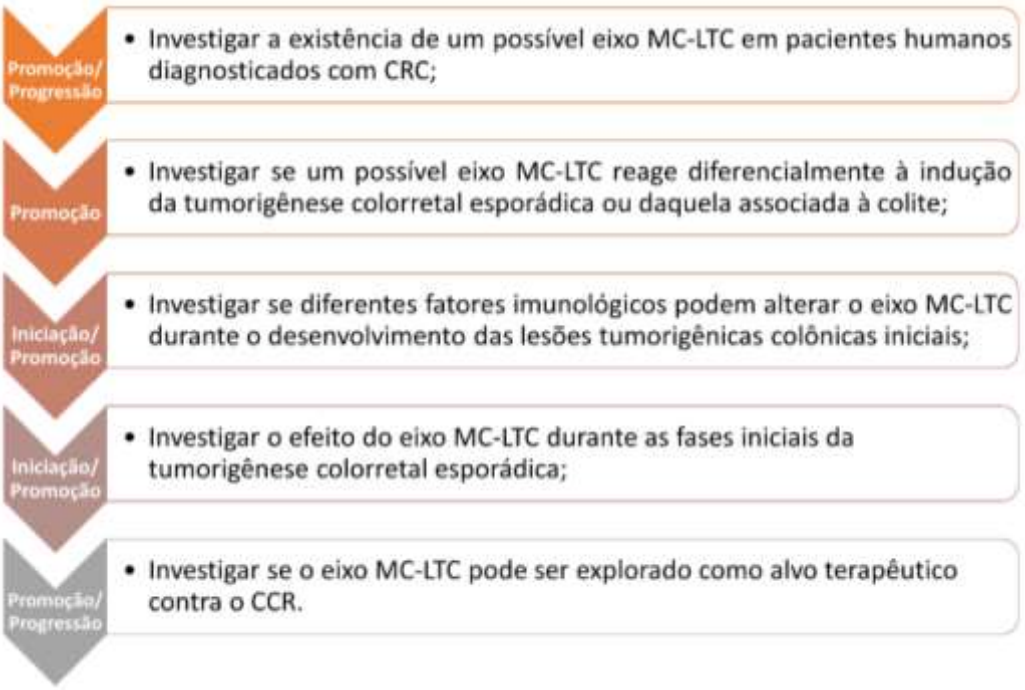

Figura 3: Fluxograma demonstrando uma visão geral dos objetivos específicos do presente trabalho.

4. Materiais e métodos

4.1 Estudo em humanos

O Comitê de Ética e Pesquisa da Faculdade de Medicina da USP de Ribeirão Preto (FMRP) aprovou o uso de 38 amostras pareadas de 19 pacientes do Hospital das Clínicas de Ribeirão Preto (12873/2014). Os pacientes não haviam sido submetidos à tratamentos quimioterápicos e radioterápicos anteriores às coletas cirúrgicas. Para cada paciente, foram coletadas uma amostra de tecido saudável e uma amostra de tecido tumoral. As amostras estavam estocadas no banco cirúrgico da Faculdade de Medicina de Ribeirão Preto (FMRP).

4.1.1 Experimento I: Comparação dos MCs no cenário do CCR e margem de segurança cirúrgica

Para entender se o número de MCs estava alterado no CCR, foram comparadas amostras pareadas de pacientes em material parafinado. Amostras combinadas (tecido saudável e tumoral) de 13 pacientes foram analisadas por reações de imunohistoquímica (IHC) para o anticorpo anti-triptase (Tópico 4.10). Outras 6 amostras combinadas foram adicionadas ao *cohort* para validação do número de MCs através da coloração de azul de toluidina. A população de MCs foi determinada pelo número de células positivas por amostra em objetiva de 40x, e a contagem normalizada pela área tecidual.

4.1.2 Experimento II: Análise *in silico* para avaliação do número de MCs no CCR

Para explorar o efeito da atividade dos MCs em casos de CCR, foram realizadas uma compreensiva revisão sistemática nos casos de CCR (n = 604) do *The Cancer Genome Atlas* (TCGA). Uma aprovação do comitê de ética não se aplica a este tipo de análise. As populações de células imunes foram estimadas por CIBERSORT (NEWMAN AM *et al*.; 2015). Foram selecionadas apenas as amostras de CCR classificadas como tendo genoma estável. Esses dados foram utilizados para realizar correlação de Pearson entre os fatores (1) infiltração linfocitária e (2) frações relativas de MCs (MCs totais, MCs ativados e MCs inativos). As amostras ainda foram subdivididas em dois grupos com base na frequência de MC ativado, estabelecendo uma dicotomia comparando o quarto superior (alta frequência de MCs ativados, HMCA) com o quarto inferior (baixa frequência de MCs ativados, LMCA). As amostras com frequência intermediária foram excluídas da análise.

4.2 Estudo com modelos experimentais: *Mus musculus*

Todos os experimentos foram aprovados pela Comissão de Ética no Uso de Animais do Campus de Ribeirão Preto da Universidade de São Paulo (15.1.229.60.8 e 22.1233.60.2). Colônias foram estabelecidas no Biotério da Faculdade de Ciências Farmacêuticas de Ribeirão Preto (FCFRP). As salas de experimentação foram mantidas com temperatura ambiente constante e ciclo

noite-dia 12/12h. Os animais seguiram um regime *ad libitum* que é baseado no livre acesso ao alimento e água 24 horas por dia, com consumo médio de 5g de ração e 6ml de água por animal adulto.

Para o desenvolvimento do estudo, camundongos geneticamente modificados foram adquiridos do biotério central ou do biotério de animais especiais da FMRP-USP (**Tabela 1**).

Tabela 1: Descrição das cepas de animais utilizadas no desenvolvimento do estudo.

Sigla	Descrição	Código
$Kit^{W/sh}$	Animal KO para mastócitos	12861
B2m KO	Animal KO para o complexo de histocompatibilidade I (MHCI)	002087
Ciita KO	Animal KO para o complexo de histocompatibilidade II (MHCII)	003239
Il-6 KO	Animal KO para a interleucina 6	002650
NOD	Animal diabético não obeso	001976
NOD *scid γ*	Animal imunodeficiente	005557
St2 KO	Animal KO para o receptor de Il33	Cepa doada e desenvolvida pelo Dr. Andrew McKenzie.
BALB/cJ	Animal utilizado como grupo controle da cepa *St2*	000651
C57BL/6- Tg (CAG-EGFP)131Osb/LevSopJ	Animal que expressa a proteína EGFP utilizado como doador de medula óssea	006567
C57/BL6J	Animal utilizado como grupo controle do $Kit^{W/sh}$, B2m e Ciita	000664

4.3 Cultura de células tumorais

Células murinas de carcinoma colorretal (MC38) foram cultivadas em meio *Dulbeccos* modificado (DMEM; Merck D6429, Alemanha) suplementado com soro fetal bovino 10% (SFB; Cód 12103C, Merck, Alemanha) e solução de antibiótico e antimicótico (AB/AM; Cód A5955, Merck, Alemanha). As células foram cultivadas em estufa incubadora à 37°C e 5% de CO_2.

A linhagem celular B16F10 (melanoma murino) foi doada pelo Professor Fernando Cunha (FMRP/SP). As células foram cultivadas em meio Roswell Park Memorial Institute (RPMI), suplementado com SFB 10% e solução de AB/AM, e mantidas em estufa incubadora à 37°C e 5% de CO_2.

4.3.1 Experimento III: Análise da ação dos MCs *in vitro*

Para observar os efeitos dos MCs observados nas análises histológicas e *in silico*, nós buscamos realizar uma co-cultura da linhagem MC38 com MCs isolados do peritônio de animais. Para isso, os camundongos receberam 10^6 células/ml via i.p. para indução da ascite; e após uma semana os MCs foram isolados da cavidade peritoneal por lavagem (procedimento detalhado no tópico 4.3.1.1). No dia anterior ao experimento, foram plaqueadas 10^5 células MC38 em placas de 12 poços para a adesão das mesmas. A proporção de células imunes utilizada foi de 10% de mastócitos para a quantidade de células tumorais plaqueadas. Essa proporção foi baseada nas contagens histológicas com o objetivo de mimetizar o processo que acontece *in vivo*. As células foram co-

cultivadas por 48 horas e coletadas para análise de apoptose/necrose (Tópico 4.11), proliferação celular (IHC para Mki67) e estudo clonogênico.

4.3.1.1 Isolamento de MCs

O isolamento de MCs do peritônio de camundongos foi realizado para os experimentos de co-cultura com as células MC38. Brevemente, os animais foram eutanasiados e a área abdominal higienizada com álcool 70%. Uma incisão foi realizada na pele de forma cautelosa para manter a integridade da cavidade peritoneal. Injetar 10ml de solução Hank's Balanced Salt Solution (HBSS; Cód 140600040; Thermofisher scientifics; EUA) livre de Ca^{2+} e $Mg^{2+,}$ de forma que não atinja nenhum órgão interno. O peritônio do animal foi homogeneizado com o intuito de coletar o máximo de células imunes. Recoletar o meio HBSS com o conteúdo celular. O líquido deve sair com coloração amarela, indicando a acidez da cavidade, e turvo, indicando a presença de células. O procedimento foi realizado 2 vezes; e a suspensão de células centrifugada por 5 minutos a 400g. O sobrenadante foi retirado e o *pellet* foi ressuspendido com uma solução para lise de hemácias (0,8% NH_4Cl; Cód A9434; Merck; Alemanha) por 5 minutos. A reação foi interrompida com a adição de 15 ml de HBSS. Esta etapa foi realizada até que o *pellet* não apresentasse mais a presença de hemácias (coloração vermelha). Uma solução de Percoll 70% (Cód P1644; Merck; Alemanha) foi adicionada para a seleção dos mastócitos, que após a centrifugação (15 minutos a 580g) permanecerá no fundo do tubo.

Após o isolamento do lavado peritoneal, os MCs foram corados com uma solução de azul de tripan (0,4%; Cód 72571; Merck; Alemanha) para análise da

viabilidade celular; e outra alíquota foi corada com azul de toluidina, para confirmação do tipo celular isolado.

4.3.1.2 Análise clonogênica

Uma vez que nós determinamos a ação dos MCs sobre as células de adenocarcinoma colorretal, nós exploramos esses resultados de forma a avaliar a interferência dos MCs na formação de colônias tumorais. Assim, foram plaqueadas 300 células MC38 em uma placa de 12 poços. A proporção de 10% de MCs foi mantida e as células foram co-cultivadas por cinco dias à 37°C e 5% CO_2. Posteriormente, o sobrenadante foi retirado e as colônias coradas com uma solução de cristal violeta 0,2% (SAMOSZUK, TAN, CHORN, 2005). As colônias foram contadas e normalizadas pela área da placa (mm^2).

4.4 Preparo e aplicação do carcinógeno

O preparo do carcinógeno AOM (Cód A5486; Sigma-Aldrich, EUA) foi realizado em capela com sistema de exaustão e sua diluição feita com soro fisiológico, sendo que alíquotas (100mg/ml) foram conservadas à -20ºC. A solução de aplicação no camundongo foi preparada imediatamente antes do uso na dose de 10mg/kg (NEUFERT *et al*. 2007). Este carcinógeno foi aplicado através de uma injeção intraperitoneal (i.p.) no quadrante abdominal inferior direito.

4.5 Eutanásia dos animais

O anestésico utilizado para a eutanásia foi o tribromoetanol (TBE). Para o preparo do anestésico, 5mL de álcool amino terciário (Cód 240486; Sigma-Aldrich, EUA) foi aquecido à 50ºC para a dissolução do TBE (2,5g; Cód T48402; Sigma-Aldrich, EUA). Em um Becker contendo 200mL de água milliQ sob agitação (vórtex), a solução de TBE foi gotejada para total dissolução. O pH foi ajustado para 7,0 e a solução filtrada com o auxílio de um microfiltro de 0,22 µm. As alíquotas foram conservadas à -20ºC.

Para a realização da eutanásia, os animais foram pesados individualmente para que a dose de TBE (250 mg/kg) fosse calculada e aplicada (i.p.). A responsividade do animal foi testada através da pressão digital na base da cauda e face plantar das patas traseiras. Quando não apresentava mais reação de dor ou fuga, o animal foi fixado à plataforma de eutanásia. Uma incisão foi realizada na porção abdominal para a exposição do diafragma. Este foi então rompido, induzindo o colabamento pulmonar, e uma média de 800 ± 200uL de sangue foi retirado do ventrículo esquerdo com uma seringa heparinizada. A cavidade abdominal foi completamente aberta e o cólon dissecado do intestino delgado e mesentério. Após a retirada do cólon, o mesmo foi aberto longitudinalmente e lavado com solução salina para a retirada do conteúdo luminal. O cólon foi seccionado em amostras de 1cm cada. As duas primeiras amostras distais foram fixadas em formol 10% (270ml de formaldeído 37 % (Cód F8775, Merck, Alemanha) + 4g de fosfato monobásico de sódio (Cód S0751, Merck, Alemanha) + 6,5g de fosfato dibásico de sódio (Cód S3264, Merck, Alemanha) para 1 litro água destilada) durante 24 horas para análises

histopatológicas. As outras amostras foram armazenadas em criotubos devidamente identificados e armazenados em freezer -80ºC para análises de biologia molecular.

4.6 Experimentos utilizando diferentes modelos de camundongos geneticamente modificados

4.6.1 Experimento IV: Ação dos MCs no desenvolvimento dos tumores colorretais associados à colite

Para verificar a ação dos mastócitos sobre a formação dos tumores colorretais *in vivo* foram utilizados camundongos KO para MCs ($Kit^{W/sh}$).

Buscando investigar o papel dos mastócitos durante a formação dos tumores colorretais associados à colite, camundongos $Kit^{W/sh}$ (n = 8) e Kit^{B6} (n = 8) receberam uma dose de AOM (10mg/kg) e 3 ciclos de dextran sulfato de sódio 2% (DSS, Merck 42867, Alemanha) (NEUFERT, BECKER, NEURATH, 2007). O DSS foi pesado e dissolvido em água de beber autoclavada. Os animais foram acompanhados quanto à perda de peso e qualquer sinal de sofrimento. A eutanásia foi realizada na 10ª semana após a exposição ao carcinógeno e o cólon coletado e avaliado quanto ao número e tamanho dos tumores.

Os tumores foram divididos em duas porções: histologia (fixadas em formol 10% tamponado) e coletadas em solução RNAlater (Cód: R0901; Merck, Alemanha; solução inativadora de RNases) e armazenadas à -80º-C até o momento da análise.

4.6.2 Experimento V: Ação dos MCs no desenvolvimento dos tumores colorretais esporádicos

Para verificar se a ação dos mastócitos difere no desenvolvimento de tumores colorretais esporádico, camundongos $Kit^{W/sh}$ (n = 8) e C57BL/6 (n = 8) receberam 6 doses de AOM (10mg/kg/semana) e foram eutanasiados após 18 semanas da última exposição ao carcinógeno. Os tumores foram macroscopicamente avaliados, pesados e divididos para análises genéticas e histológicas.

4.6.3 Experimento VI: Avaliação nas alterações imunes causadas pelo carcinógeno

Com o intuito de investigar as alterações imunes que o AOM provoca no microambiente colônico, camundongos C57BL/6 (n = 6/grupo) receberam 6 doses de AOM (10mg/kg/semana) ou salina, para avaliação do recrutamento de linfócitos. O cólon dos animais foi coletado e digerido para análise de linfócitos T CD4 e CD8 por citometria de fluxo (protocolo descrito no Tópico 4.12). Esse experimento foi usado como um guia para as principais alterações imunes e possíveis vias a serem exploradas juntamente com os MCs.

4.6.4 Experimento VII: Determinar a ação dos MCs e a interação com o microambiente colônico: sistema MHC

Buscando avaliar a influência do sistema MHCI e MHCII na ação e número de MCs, foram utilizados camundongos *B2m* (MHCI KO, n = 6) e *Ciita* (MHCII KO; n = 6) com seus respectivos grupos controle (C57BL/6, n = 6 cada). Foi administrado a todos os grupos 6 doses do carcinógeno AOM (10mg/kg/semana) e a eutanásia realizada após uma semana da última exposição.

O cólon foi coletado para análises histológicas e moleculares. O número de MCs foi avaliado através da expressão gênica dos marcadores *Mctp1* e *Mctp4* (XING *et al*.; 2011).

4.6.5 Experimento VIII: Determinar a ação dos MCs e a interação com o microambiente colônico: imunossupressão

Ainda explorando a relação dos MCs com o microambiente tumoral, buscou-se investigar a ação de tais células em camundongos imunossuprimidos. Para isso, camundongos NOD (n = 6) e camundongos NOD *scidγ* (n = 6) receberam 3 doses de AOM (10mg/kg/semana) e foram eutanasiados após 3 semana da última exposição ao carcinógeno. O cólon foi coletado para análises histológicas e moleculares. O número de criptas aberrantes foi avaliado através da coloração de Hematoxilina e Eosina e normalizado pela área tecidual (mm^2).

4.6.6 Experimento IX: Determinar a ação dos MCs e a interação com o microambiente colônico: Il6

Para investigar a relação dos MCs em um ambiente sem a ação das interleucinas pró-inflamatórias, camundongos Il6 KO (n = 6) e seu grupo controle (C57BL/6, n = 6 cada), foram expostos a 3 doses de AOM (10mg/kg/semana) e eutanasiados após 3 semanas da última exposição ao carcinógeno. O cólon foi coletado para análises histológicas e moleculares. O número de criptas aberrantes foi avaliado através da coloração de Hematoxilina e Eosina (Tópico 4.8) e normalizado pela área tecidual (mm^2).

4.6.7 Experimento X: Determinar a ação dos MCs e a interação com o microambiente colônico: Il33

Já foi demonstrado que as interleucinas 33 (Il33) atuam como uma alarmina de dano de DNA. Com base nisso, e na sua interação já descrita com os MCs (EISSMANN *et al*. 2020), buscou-se avaliar essa relação no processo da tumorigenese colorretal esporádica. Assim, camundongos *St2* KO (Il33r KO, n = 6) e camundongos BALB/cJ (n = 6) receberam 6 doses de AOM (10mg/kg/semana) e foram eutanasiados após uma semana da última exposição.

4.6.8 Experimento XI: Determinar a ação dos Ação dos MCs no desenvolvimento das lesões preneoplásicas

Após avaliar a função dos MCs durante a formação dos tumores esporádicos e associados à colite, e a sua relação com as alterações imunes no microambiente tumoral, foi investigada a ação de tais células imunes na formação das lesões preneoplásicas. Para isso, camundongos $Kit^{W/sh}$ (n = 6) e C57BL/6 (n = 6) receberam 6 doses de AOM (10mg/kg/semana) e foram eutanasiados após 6 semanas da última exposição ao carcinógeno. O tecido foi corado e as lesões preneoplásicas avaliadas por microscopia (coloração HE), e parte do cólon foi armazenado para análise da expressão gênica.

4.6.9 Experimento XII: Ação dos MCs no dano de DNA precursor da tumorigenese colorretal

Considerando que os MCs são células pertencentes à resposta imune inata, foi avaliada a ação de tais células em resposta ao dano de DNA precursor das lesões preneoplásicas. Então, camundongos $Kit^{W/sh}$ (n = 6) e C57BL/6 (n = 6) receberam 6 doses de AOM (10mg/kg/semana) e foram eutanasiados após uma semana da última exposição ao carcinógeno.

4.6.10 Experimento XIII: Ação dos MCs no dano de DNA inicial

Voltando algumas etapas da carcinogênese colorretal, foi investigada a ação dos MCs durante o desenvolvimento das criptas aberrantes, e a sua resposta ao dano de DNA inicial. Para isso, camundongos $Kit^{W/sh}$ (n = 6) e C57BL/6 (n = 6) receberam 3 doses de AOM (10mg/kg/semana) e foram eutanasiados após 3 semanas ou 72 horas da última exposição ao carcinógeno. As criptas aberrantes foram contadas por microscopia e as alterações genéticas avaliadas por técnicas de biologia molecular.

4.6.11 Experimento XIV: Avaliação do resgate da atividade dos MCs em animais $Kit^{W/sh}$

Para a validação dos resultados, camundongos $Kit^{W/sh}$ (n = 6) e C57BL/6 (n = 6) receberam um transplante de medula óssea de um animal que expressava a proteína EGFP. Após a confirmação da enxertia dos camundongos, os animais receberam 3 doses de AOM (10mg/kg/semana) e foram eutanasiados após 3 semanas da última exposição ao carcinógeno.

4.6.11.1 Transplante de medula óssea (TMO)

Os animais foram irradiados no Centro de Medicina Nuclear do Instituto de Radiologia do HCFMUSP. A grade de proteção contendo água e ração foi retirada da caixa dos camundongos antes da exposição à irradiação ionizante

(IR) no irradiador RS 2000 (Biological System-Rad Source, EUA). A dosagem à qual os animais foram expostos foi de 900cGy, sendo duas doses de 450cGy com intervalo de 4 horas. Após 24 horas da IR, foi realizada a enxertia dos animais.

Os animais positivos para a proteína verde fluorescente (GFP) foram sacrificados para a obtenção da medula óssea (camundongos doadores). Para isso, uma dose letal de TBE foi administrada (ip) e os reflexos vitais testados. Para a obtenção da óssea, os músculos foram dissecados e os ossos dos membros superiores medula e inferiores foram macerados com uma solução de PSB + soro fetal bovino (10%). Centrifugar a solução contendo as células da medula óssea por 5 minutos a 1200 rpm. O sobrenadante foi retirado e as células incubadas com uma solução de hemólise (Tris-HCl 10mM; MgCl 5mM; NaCl 10mM) por 5 minutos. As células foram lavadas com PBS e contadas em câmara de Neubauer. Cerca de $12x10^6$ células foram transplantadas via endovenosa nos animais irradiados.

A confirmação da enxertia foi realizada após 7 semanas do TMO a partir da coleta de sangue endovenoso. As células foram avaliadas quanto a expressão de GFP em citometria de fluxo (Guava easyCyte BHT; Millipore).

4.6.12 Experimento XV: Avaliar a resposta dos MCs em diferentes momentos do desenvolvimento das lesões preneoplásicas

Para investigar a ação dos MCs em diferentes momentos do processo de carcinogênese, foi utilizado o cromoglicato de sódio (CA – 25 mg/kg/dia). Esse

fármaco, bloqueia os canais de cálcio dos MCs, impedindo a liberação conteúdo celular e consequentemente, bloqueando a sua ação (WARGOVICH *et al*., 1996).

Camundongos C57BL/6 foram divididos em três grupos (n = 6) de forma randomizada. Os grupos foram classificados como: (1) grupo controle (3 doses de AOM + 3 semanas de salina); (2) CA administrado em conjunto com o AOM (3 doses de AOM e CA diariamente durante 3 semanas + 3 semanas de salina) e (3) CA administrado após a exposição ao carcinógeno (3 doses de AOM + 3 semanas de CA) (**Figura 4**). O cólon dos animais foi coletado para análises histológicas (número de criptas aberrantes) e análise da expressão gênica.

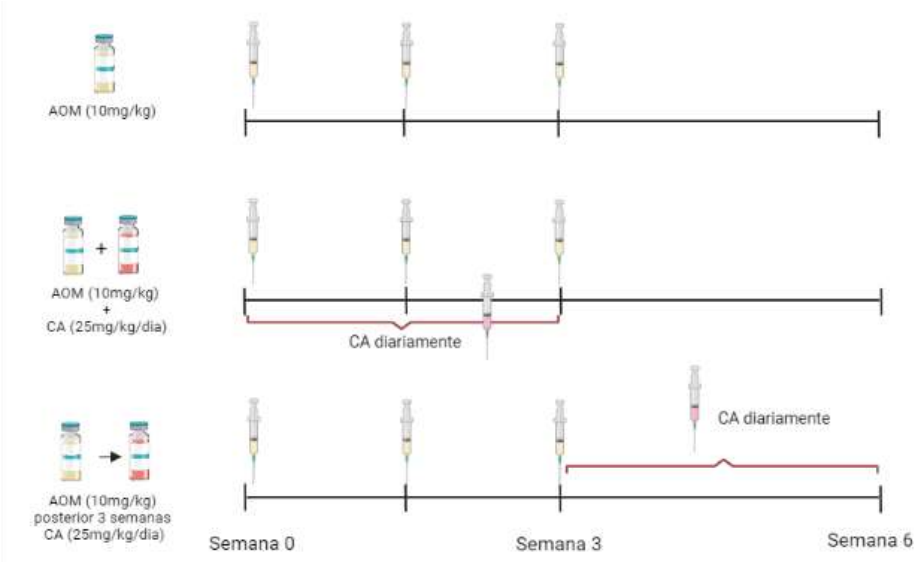

Figura 4: Desenho experimental XVI. Camundongos C57BL/6 receberam intervenções farmacológicas com cromoglicato de sódio (CA – 25mg/kg/dia) em diferentes condições experimentais. As setas vermelhas indicam aplicações do carcinógeno azoximetano (AOM – 10mg/kg/semana) e as setas verdes, indicam o tratamento com CA. A linha tracejada indica que os animais receberam somente salina durante o período indicado.

4.6.13 Experimento XVI: Avaliar a ação dos MCs durante a formação dos tumores alográficos

Os experimentos anteriores buscaram avaliar a ação dos MCs nas diferentes fases da CCR esporádica. Para investigar a ação dos MCs fora do microambiente colônico e a sua influência direta sobre o adenocarcinoma colorretal, camundongos C57BL6 (Kit^{B6} n = 6) e $Kit^{W/sh}$ (n = 6) receberam um implante alográfico. O desenvolvimento do tumor foi acompanhado durante todo o experimento através das aferições com o paquímetro. Os tumores foram coletados no 17º dia após o implante para análise molecular e histológica.

4.6.13.1 Implante alográfico

Para a realização do implante alográfico, as células MC38 foram previamente cultivadas (Item 4.3) e $2x10^6$ células foram implantadas em cada animal. As células foram contadas em câmara de Neubauer e separadas em tubos individuais. Cada tubo foi centrifugado e o pellet de células ressuspendido em 100µl de PBS 1x estéril. As células foram mantidas no gelo até o momento do implante.

Brevemente, os animais foram anestesiados com TBE (cerca de 300µl) e os pêlos do dorso foram tricotomizados com o auxílio de uma máquina. A injeção das células foi realizada no flanco direito dos animais, de forma subcutânea com o auxílio de seringa acoplada de uma agulha de calibre 22G. No 7º dia após o

implante, os tumores foram medidos com o auxílio de um paquímetro para então, os animais receberem os seus respectivos tratamentos.

O volume tumoral (VT) foi calculado de acordo com as medidas realizadas com o paquímetro. Os tumores foram medidos a cada 3 dias e os animais acompanhados quanto a perda de peso e outros efeitos adversos.

Os tumores foram medidos quanto a largura e o comprimento. O volume tumoral é o resultado da fórmula:

VT = (4/3*(3,14159)*(comprimento/2)*(largura/2)^2)

A taxa de crescimento foi calculada pela diferença do volume final pelo inicial dividido pela quantidade de dias de experimento:

Taxa de crescimento = (volume final – volume inicial)/17

4.6.14 Experimento XVI: Explorar a atividade dos MCs terapeucaticamente

Almejando explorar os resultados obtidos e aplica-los futuramente na terapia convencional contra o CCR, o MCs foram utilizados como alvo terapêutico. Para isso, camundongos C57BL/6 receberam o implante das células de adenocarcinoma colorretal (MC38) e foram divididos em quatro grupos (n = 6 cada) de acordo com a tabela 2. O CA foi utilizado para inibir a ação dos MCs (25mg/kg/dia). A variação de tempo para o início dos tratamentos teve como objetivo investigar se o CA possuía ação sobre um adenocarcinoma mais avançado. Os animais foram acompanhados durante todo o experimento para avaliação do crescimento tumoral, bem como possíveis efeitos colaterais

(diarreia ou perda de peso excessiva). Os tumores foram coletados e avaliados quanto ao tamanho e células imunes.

Tabela 2: Descrição dos grupos experimentais de acordo do experimento XVIII.

Grupo	Início do tratamento
Controle salina	7 dias após o implante
Cromoglicato dissódico (CA)	7 dias após o implante
Controle salina	14 dias após o implante
Cromoglicato dissódico (CA)	14 dias após o implante

4.6.15 Experimento XVII: Determinar se a atividade dos MCs pode ser alvo terapêutico do melanoma

Com o objetivo de testar se a inibição da ação dos MCs também possuía ação sobre outros tipos de células tumorais, o CA foi testado em células de melanoma (B16F10).

Camundongos C57BL/6 receberam um implante alográfico das células Bl16 previamente cultivadas. Após 7 dias do implante, os animais foram divididos em dois grupos: controle (tratado com salina) ou tratado com CA (25mg/kg/dia). O tratamento teve duração de 10 dias (eutanásia realizada no 17º dia após o implante). Os tumores foram medidos e pesados e divididos para análises histológicas, imunes (citometria de fluxo) e moleculares.

4.6.16 Experimento XIX: Avaliar se a ação do CA está atrelada aos linfócitos

Para verificar se os efeitos observados pelo CA estavam associados com a ativação dos linfócitos T, foram utilizados camundongos RAG-1, que não possuíam linfócitos T e B maduros. Os animais RAG-1 tiveram início ao tratamento com o CA (25mg/kg/dia), ou salina, 3 dias antes do implante alográfico com as células MC38. O tratamento se estendeu durante todo o experimento, que teve ao todo, 14 dias.

O tamanho dos tumores foi aferido com o paquímetro a cada 3 dias e os animais pesados para acompanhamento.

4.6.17 Experimento XVIII: Avaliar se a inibição da atividade dos MCs tem efeito no CCR avançado

Por fim, com o objetivo de adicionar o CA aos tratamentos já utilizados contra o CCR, foram testados a combinação do CA com anticorpo anti-Pd1 (Cód RMP1-14; Invivogen; EUA). Camundongos C57BL/6 receberam o implante alográfico das células MC38 e após 7 dias, foram divididos em grupos de forma randomizada para o início do tratamento. Os grupos foram: controle de salina; CA (25mg/kg/dia); anti-Pd1 (10µg/camundongo/a cada 3 dias) e CA+anti-Pd1. O crescimento dos tumores e o peso dos animais foram acompanhado a cada 3 dias. No 17º dia após o implante, os animais foram eutanasiados e os tumores coletados para análises histológicas.

4.7 Coloração de hematoxilina e eosina (HE)

A coloração de hematoxilina e eosina (HE) foi utilizada para avaliar a formação de criptas aberrantes, lesões preneoplásicas avanças e para a categorização dos tumores.

Brevemente, as lâminas foram seccionadas a 4µm (RM2125 RTS; Leica, DE) e devidamente identificadas. Para a coloração, os cortes foram desparafinizados em estufa a 60°C e passaram por uma bateria de xilol e álcoois (100%- 100% - 95%- 70%) até a completa hidratação do tecido. O processo de coloração das lâminas então prosseguiu com uma incubação de um minuto e meio na Hematoxilina de Harris (Cód.H3136 – Merck, Alemanha). As lâminas foram lavadas e permeabilizadas em álcool 70% para posterior coloração com eosina (30 segundos; Cód.102439 – Merck, Alemanha). Após esta etapa, as lâminas foram desidratadas por uma bateria crescente de álcoois (70%- 95%- 100%- 100%- xilol) e montadas com entellan e lamínula.

4.8 Análises histopatológicas

A análise do risco para o desenvolvimento do CCR foi realizada através da contagem do número de CAB e FCA no epitélio colônico dos animais expostos ao AOM.

As CAB foram observadas nos experimentos no qual os animais foram expostos à 3 doses de AOM e eutanasiados após 3 semanas da última

exposição. Já os FCA foram observados em animais expostos à 6 doses de AOM e avaliados na 12ª semana de experimento (**Figura 5**).

A identificação das CAB e dos FCA foi realizada de acordo com a descrição de Bird em 1988 (MCLELLAN, BIRD, 1988). As CAB apresentam como características: tamanho aumentado e contorno distorcido com relação às criptas normais, maior espaço pericriptal, núcleo hipercromático, perda da polaridade celular, e geralmente possuem aberturas ovais em vez de circulares (MCLELLAN, BIRD, 1988). Além disso, também é possível observar a presença de outras alterações nucleares, como micronúcleo, corpos apoptóticos e cariorrexis (GOLDBERG, BLAKEY, BRUC, 1983).

Os FCA foram identificados como um agrupamento de CAB, que dependendo do estágio, podem não apresentar a separação entre as criptas displásicas (BIRD, 1987).

As CAB e FCA foram contadas na objetiva de 40x, e normalizadas pela área em cm^2 de tecido.

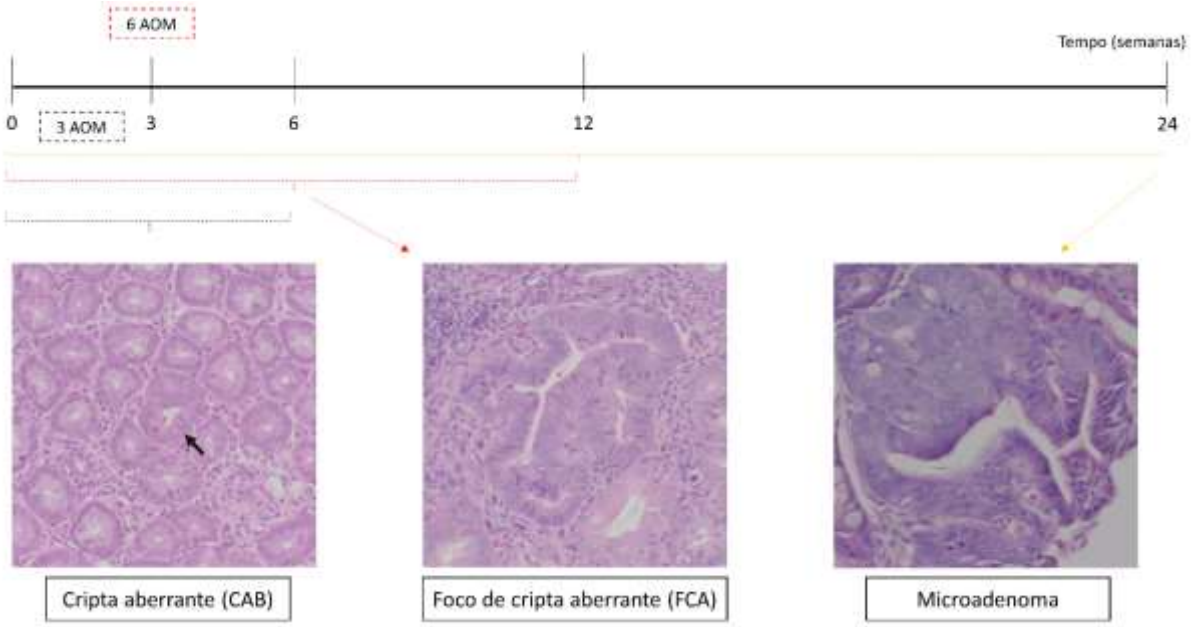

Figura 5: Modelo de tumorigênese colorretal esporádica. As criptas aberrantes (CAB, seta preta) foram induzidas no epitélio colônico dos camundongos através da administração de 3 doses de azoximetano (AOM; 10mg/kg/semana) e eutanásia após outras 3 semanas. Já os focos de CAB (FCA), foram desenvolvidas após 6 AOM e os animais eutanasiados após 6 semanas da última exposição. Os tumores esporádicos foram desenvolvidos após 18 semanas da última exposição ao AOM (6AOM + 18 semanas).

4.9 Coloração Azul de toluidina

As amostras foram seccionadas a 4 µm (RM2125 RTS; Leica, DE) e fixadas em uma lâmina histológica. As lâminas foram desparafinizadas em estufa a 60°C e reidratadas através de uma bateria decrescente de álcoois. As amostras foram coradas com uma solução de azul de toluidina 0,5% (Cód 198161; Merck; Alemanha) por 2 minutos. Posteriormente, as lâminas foram lavadas com água destilada para retirada do excesso de corante; e desidratadas através de uma bateria crescente de álcoois. As lâminas foram montadas com entellan (Cód 107960; Merck; Alemanha) e lamínula, e o número de MCs contados em uma

objetiva de 40x. Os MCs apresentam uma coloração azul mais intensa por conta dos seus grânulos de heparina e histamina, sendo possível diferenciar dos outros tipos celulares. O número de MCs contados foi normalizado com a área tecidual (mm^2).

4.10 Imunohistoquímica (IHC) e IHC multiplex

Lâminas de microscopia com amostras seccionadas a 4µm (RM2125 RTS; Leica, Alemanha) foram marcadas com o Ac primário (**Tabela 3**) de acordo com as instruções do fabricante. Brevemente, as amostras foram desparafinizadas *overnight* em uma estufa (60ºC). Posteriormente, as lâminas passaram por duas incubações com xilol para retirar a parafina residual e por uma bateria decrescente de álcoois (100%- 100%- 95% - 70%) para hidratarem. Amostras foram submetidas à recuperação antigênica em tampão citrato (2,101g de Ácido cítrico [C7129; Merck; Alemanha]/ litro pH=6,0) durante 30 minutos em panela de pressão elétrica. Em seguida, as amostras foram incubadas por 15 minutos com uma solução de H_2O_2 3% (Merck, Alemanha) para o bloqueio da peroxidase endógena. Outro bloqueio com 3% de albumina de soro bovino (BSA – Sigma, EUA) foi realizado durante 30 minutos com o intuito de reduzir as ligações inespecíficas. As amostras foram então incubadas com o Ac primário durante 16 horas a 4ºC. A reação foi revelada pelo Picture^{TM}–MAX Polymer Detection Kit (Thermo Fisher; EUA), conforme indicado nas instruções do fabricante. Finalmente, as lâminas foram contracoradas com hematoxilina de Harris (Merck; Alemanha), desidratadas em bateria crescente de álcoois e xilol.

As células positivas apresentaram coloração marrom devido à precipitação do DAB e foram contadas e normalizadas pela área tecidual ou pelo número de criptas por amostras.

Foram realizados controles positivos e negativos para cada reação. Como controle da reação, foram feitas lâminas utilizando somente o Ac secundário com o DAB. Dessa forma, foi possível verificar se as células positivas não eram marcações inespecíficas entre ambos os reagentes. Além disso, também foram utilizadas amostras controles, ou seja, uma amostra em que não deveria haver marcação (cérebro) e uma amostra positiva para marcação do Ac (baço) (**Figura suplementar 1**).

Para a IHC multiplex, foi utilizado o kit Vector AEC (Cód SK-4200; Vector Laboratories, EUA) como substrato cromógeno ao invés do DAB. As lâminas foram contracoradas com a solução de hematoxilina, montadas com uma solução de glicerol 70% (Cód G5516; Merck; Alemanha) e fotografadas em um microscópio óptico capaz de escanear a lâmina inteira (Aperio ImageScope AR system; Leica Biosystem; Alemanha). Essa técnica permite que a marcação com o AEC seja subtraída do corte tecidual e que sejam realizadas outras marcações. Para isso, as lâminas foram mergulhas em água destilada para o descolamento da lamínula. Posteriormente, elas foram incubadas em álcool 95% até que o corte tecidual ficasse translucido. Por fim, uma solução de 0,15 mM de $KMnO_4$/0.01 M H_2SO_4 foi adicionada aos cortes por 2 minutos em temperatura ambiente. As lâminas foram lavadas e o processo da IHC prosseguido a partir da etapa de bloqueio de sítios inespecíficos com BSA. Uma vez que todas as marcações foram realizadas e escaneadas, foi feito a pseudo-coloração e

sobreposição das imagens. O núcleo foi pseudo-colorido em azul, e cada Ac foi corado em cores que pudessem ser sobrepostas (**Figura suplementar 2**).

Tabela 3: Anticorpos utilizados para reações de imunohistoquímica (IHC) e IHC multiplex.

Anticorpo	Código de referência	Concentração
Triptase	Ab2378	1:150
CD4	Ab183685	1:750
CD8	Ab203035	1:150
CD68	Ab955	1:400
CD3	Ab5690	1:500
Ki67	Ab16667	1:150

4.11 Western blotting (WB)

A extração de proteínas foi realizada com 30mg de amostra congelada em tampão de lise RIPA (Sigma R0278), 60µL de inibidor de fosfatase (Cód. P0044; Merck; Alemanha) e 15µL de inibidor de protease (Cód. P2714; Merck; Alemanha). A lise das amostras foi realizada com o auxílio de um Tissue lyser (Dremel; México) e de um sonicador ultrassônico (Merck; Alemanha). A quantificação das proteínas extraídas foi realizada com kit Pierce BCA (Cód. 23225; Thermofisher; EUA) e comparadas com uma curva padrão de BSA.

Para a eletroforese, foram utilizados géis de poliacrilamida 10%. Uma solução de Laemmli + 2-βmercaptoetanol (10µL) foi adicionada à 30µg de proteínas e desnaturadas durante 5 minutos à 98ºC. Após a eletroforese, as proteínas foram transferidas do gel de poliacrilamida para uma membrana de PVDF por meio do sistema sanduíche com tampão bicarbonato (0,84g de Bicarbonato de sódio (S6014, Merck, Alemanha) e 0,318g de carbonato de sódio

(07047, Grupo Química, Brasil). Uma etapa de bloqueio foi realizada com uma solução de BSA (Cód. A7906, Merck, Alemanha) 5% para evitar que ligações proteicas inespecíficas ocorressem. Os anticorpos primários utilizados foram γH2AX (ab81299; 1:5000) e GAPDH (ab181602; 1:10000). Todos os anticorpos primários foram ligados com seus respectivos secundários (anticorpo IgG de cabra anti IgG de coelho; ab6717; 1:10000), para posterior revelação com ECL (enzima-substrato; Luminol Cód. A4685; ácido p-cumárico Cód. C9008; Tris-glicina Cód. T6066; Merck, Alemanha). As membranas foram reveladas em um fotodocumentador Chemidoc (Bio-rad; EUA).

4.12 Citometria de fluxo

A análise de viabilidade do ensaio de co-cultura (Tópico 4.3.1) foi realizada utilizando Anexina V e 7-AAD (Cód. 88-8006-74; Thermofisher scientifcs; EUA) para análise de viabilidade celular. As placas de cultivo foram centrifugadas para que os MCs e as células que entraram em apoptose não fossem descartadas juntamente com o meio de cultura. Posterior à etapa de tripsinização, as células foram incubadas com o kit de viabilidade celular e o anticorpo para $CD45^{+}$ para confirmação da presença de MCs. As células em apoptose foram caracterizadas como positivas para Anexina V, uma vez que esse reagente tem afinidade com a fosfotidilserina, presente no folheto interno da bicamada lipídica. Já as células em estágio de apoptose tardia ou necrose, foram caracterizadas como positivas para 7-AAD, que tem alta afinidade às moléculas de DNA.

Para o experimento de transplante de medula óssea, uma amostra de sangue da veia caudal foi coletada e as células brancas extraídas. A confirmação da enxertia foi realizada através da detecção das células positivas para EGFP no equipamento Guava easyCyte BHT (Merck Millipore, Alemanha) (Tópico 4.6.11).

Para análise das células imunes presentes no cólon ou nos tumores alográficos, as amostras foram digeridas utilizando uma solução contendo 0,125 mg/mL de colagenase tipo 2 (Cód. C6885 Merck; Alemanha) e 0,2 mg/mL de DNase tipo 1 (Cód. 10104159001; Merck; Alemanha). As amostras foram cortadas em pequenas partes para auxiliar no processo de digestão tecidual e incubadas à 37ºC por 45 minutos. Posteriormente, as células foram passadas em um filtro de 100µm duas vezes para completa dissolução dos grumos celulares (RAVINDRAN *et al*., 2018). As células foram então incubadas com os anticorpos (**Tabela 4**) e as amostras analisadas no equipamento Facs Canto II (BD Biosciences, EUA).

A estratégia de *gating* aplicada (**Figura 6**) levou em consideração somente as células *singlets*, ou seja, as células únicas que passaram no capilar de forma isolada. Na avaliação dos linfócitos T $CD8^+$, foi feito uma pre-seleção após análise dos singlets de acordo com o tamanho (FSC) e complexidade dessas células (SSC). Posteriormente, em ambas as amostras (MCs e Linfócitos T $CD8^+$) foram selecionadas somente as células vivas (FVS negativas). A próxima *gate* aplicada foi para a seleção das células $CD45^+$, excluindo as células não leucocitárias. Dentro dessa população (células únicas, vivas, $CD45^+$), os MCs e os linfócitos foram avaliados de acordo com os seus respectivos marcadores. Os linfócitos T CD8 foram caracterizados como células $CD45^+CD8a^+CD3^+$ e os MCs determinados como $CD45^+Fc\varepsilon RI^+CD117^+$.

Na normalização dos dados, foi levado em consideração o número absoluto de células por tubo que foram avaliadas na citometria. Posteriormente, foram calculadas as porcentagens de MCs e $CD8^+$ dentro da população leucocitária. As células positivas foram normalizadas pelo número de células $CD45^-$ para a checagem do número de células imunes recrutadas para a população de células tumorais.

As combinações de anticorpos e corantes (FITC, APC, APC Cy-7, BV421, PE-Cy7, PE) foram realizadas de forma que não houvesse a sobreposição das cores e que cada anticorpo fosse reconhecido por um filtro do equipamento Facs Canto II (BD Biosciences, EUA).

Tabela 4: Lista de anticorpos utilizados para análise por citometria de fluxo.

Anticorpo	Número de catálogo	Concentração
CD45-FITC	11-0451-82	1:250
CD45-APC	561873	1:250
CD45-BV421	103133	1:300
CD117-PE-Cy7	55863	1:250
FcεRI-PE	134307	1:250
CD8a-PE	553032	1:300
CD3-FITC	557354	1:250
CD4-FITC	100405	1:300
Foxp3-APC	77-5775-40	1:300
FVS-APC Cy-7	565388	1:250

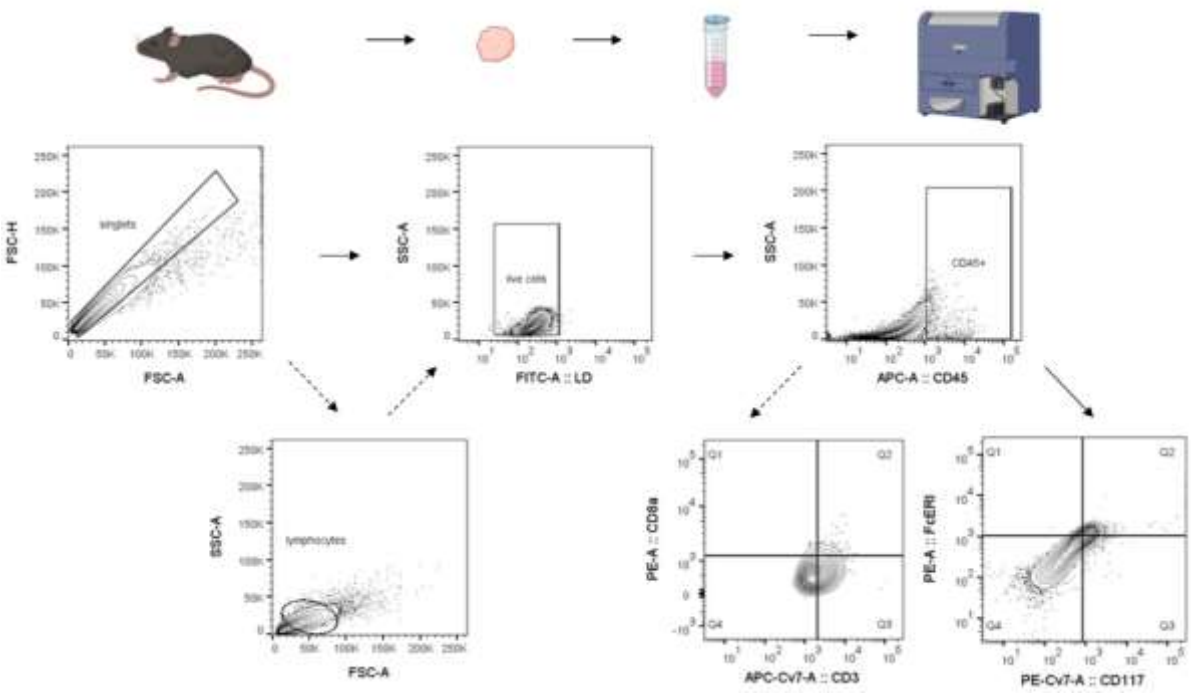

Figura 6: Estratégias de gating para análise de citometria de fluxo. O esquema ilustrativo demonstra que os tumores alográficos foram coletados e digeridos para a análise de citometria de fluxo. A estratégia de gating aplicada levou em consideração as células únicas (singlets), vivas (LD-) e $CD45^+$. Os linfócitos T CD8 foram caracterizados como células $CD45^+CD8a^+CD3^+$ e os MCs determinados como $CD45^+Fc\varepsilon RI^+CD117^+$.

4.13 Extração de RNA e PCR em tempo real (qRT-PCR)

Para a extração de RNA, o RNeasy Mini Kit (Ref. 74104; QIAGEN, Alemanha) foi utilizado segundo as recomendações do fabricante. A etapa de lise das amostras foi realizada por meio de maceração do tecido com nitrogênio líquido, evitando a degradação do RNA. A checagem da integridade e qualidade do RNA extraído foi verificada através da eletroforese em gel de agarose desnaturante. A amostra foi considerada íntegra quando observado as bandas referentes à subunidade 18S e 28S do RNA ribossômico. A síntese de cDNA (DNA complementar) foi realizada com o kit SuperScript® III Reverse Transcriptase

(Thermo Fisher, EUA) de acordo as instruções do fabricante. Brevemente, a técnica utiliza o primer Oligo(dT)20 (Ref 18418020; Thermo Fisher, EUA) que possui complementariedade à cauda poliA presente somente nas moléculas de RNA mensageiro (mRNA) e a transcriptase reversa para sintetizar o DNA fita simples complementar ao RNA.

Para as reações de qRT-PCR foram utilizadas sondas e primers descritos nas tabelas 5 e 6. As reações foram realizadas pelo método de Taqman (Ref PB20.21-05; qPCRbio Probe Mix; PCR Biosystems, EUA) ou utilizando o SYBRgreen (Ref PB20.12-05; qPCRbio Probe Mix; PCR Biosystems, EUA). Os dados foram coletados e analisados usando o sistema Eppendorf Mastercycler® RealPlex2 (Eppendorf, Alemanha). O cálculo dos resultados foi realizado através do método $2^{-\Delta\Delta Ct}$ (*Gapdh* como gene controle endógeno).

Tabela 5: Sondas utilizadas para a quantificação por Taqman.

Sondas	Códigos de referência
Ctnnb1	Mm00483039
Ki67	Mm01278617
Mgmt	Mm00485014
Gapdh	Mm99999915

Tabela 6: Primers utilizados para a quantificação por Syber green.

Primer	Foward	Reverse
Cd11c	TCTTCTGCTGTTGGGGTTTG	CAGTTGCCTGTGTGATAGCC
Cd3	ATGCGGTGGAACACTTTCTG G	GCACGTCAACTCTACACTGGT
Cd4	TCTGGCAACCTGACTCTGAC	TCATCACCACCAGGTTCACT
Cd68	TGTCTGATCTTGCTAGGACC G	GAGAGTAACGGCCTTTTTGTG A
Cd8	CAGAGACCAGAAGATTGTCG	TGATCAAGGACAGCAGAAGG
Foxp3	GGCCCTTCTCCAGGACAGA	GCTGATCATGGCTGGGTTGT
Mcpt1	TTCCAGGTCTGTGTGGGAAG	TCCAGGGCACATATGCAGAG

Mcpt4	TCACCACTGAGAGAGGGTTCA	CATGAGCTCCAAGGGTGACA
Mcpt6	ACGTTGCCCTGCTGGAGCTT	CAGCACGATGTCCCTGGGGG
Gapdh	TGGTGAAGGTCGGTGTGAAC	GACAAGCTTCCCATTCTCGG

4.14 Sequenciamento de nova geração (RNAseq)

Para a realização do sequenciamento de nova geração, o RNA das amostras de tumor e cólon foram extraídas e tratadas DNase (79254, Qiagen, Alemanha) para a eliminação de DNA genômico (**Figura 7A**). A integridade do RNA foi avaliada usando o Agilent Bioanalyzer RNA 6000 Nano kit (Ref 5067-1511). Para a construção das bibliotecas de cDNA foram utilizados o painel QIAseq Target RNAseq Mouse Immuno- Oncology (Ref. 333005, Qiagen, Alemanha) e o kit QIAseq Targeted RNA 96-Index I (Ref. 333117; Qiagen, Alemanha) (**Figura 7B**). A qualidade e tamanho da biblioteca foram avaliadas com o Agilent Bioanalyzer DNA 1000 (Ref 5067-1504) e quantificadas com por qPCR usando o QIAseq Library Quant Assay (Ref 333314, Qiagen, Alemanha). As amostras foram normalizadas e um pool de 10pM preparado para o sequenciamento no MiSeq Sequencing (Illumina, EUA), usando o Illumina MiSeq Reagent Kit v3 de 150 ciclos (Ref 15043894, Illumina, EUA).

A qualidade das reads Fastq foram checadas e alinhadas com o genoma de referência (NCBI.p3/mm9). A contagem das reads foi feita usando o software GeneGlobe Data Analysis Center (Qiagen, Alemanha). Os dados foram normalizados utilizando o pacote DESeq2 do R (**Figura 7C**). Para avaliar a distribuição das amostras, foi plotado um gráfico do tipo PCA. Esse tipo de gráfico demonstra se as amostras dentro dos grupos avaliados possuem um

perfil de expressão semelhante. Os genes com o valor de p < 0,05 e fold change de log2 foram selecionados. O gráfico do tipo *volcano plot* foi utilizado para a visualização da quantidade de genes positivamente ou negativamente regulados (dados não apresentados nos resultados). Os gráficos do tipo heatmap demonstram de forma visual, os níveis de expressão gênica, no qual quanto maior a expressão, mais próximo de cores quentes, como o vermelho. Os pacotes utilizados durante a análise foram: DESeq2, ComplexHeatmap, gplots e Parallel. Todos os arquivos do sequenciamento foram submetidos ao GEO (GSE 146786).

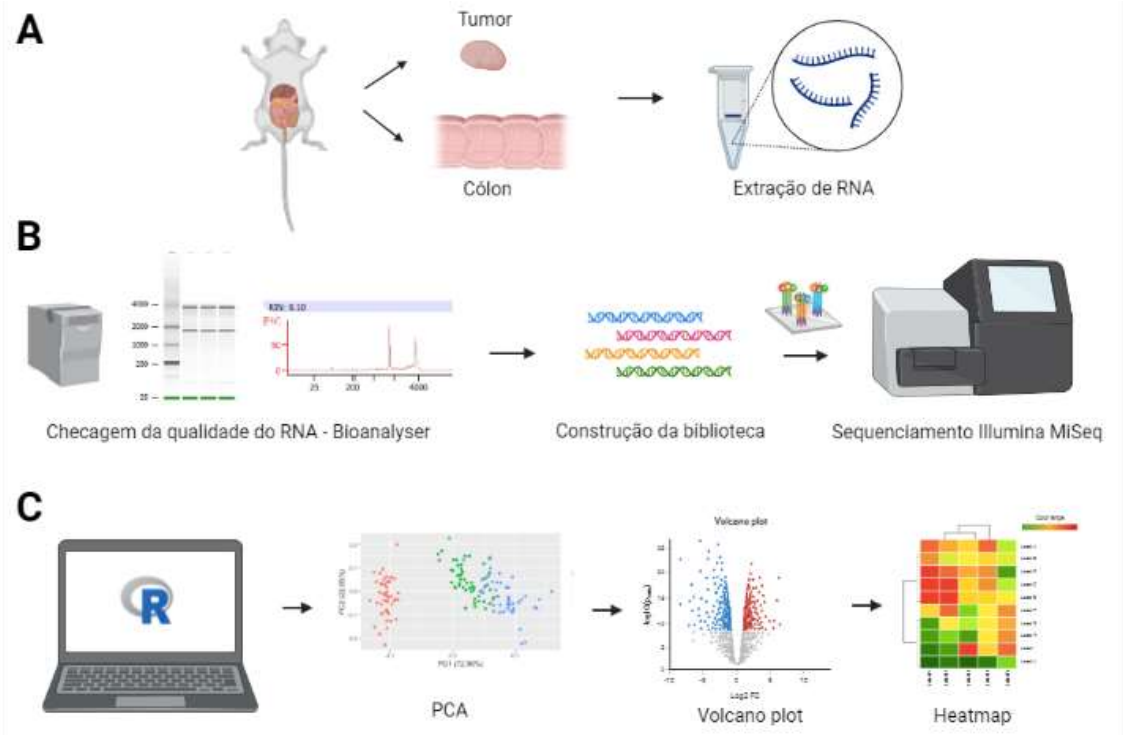

Figura 7: Esquema ilustrativo demonstrando as etapas do RNAseq. **A**: Os tumores ou amostras de cólon foram coletadas dos animais e o RNA extraído. **B**: A qualidade do RNA foi verificada utilizando o Bioanalyser e a biblioteca construída e sequenciada no Illumina MiSeq. **C**: A etapa de análise do sequenciamento foi realizada utilizando o Rstudio.

4.15 Análise estatística

As análises imunogênicas baseadas no TCGA foram realizadas no *software* R. O teste t (two-tailed) foi usado para analisar a frequência de células imunes e/ou assinaturas imunes entre as amostras de CCR com baixa (LMCA) ou alta (HMCA) frequência de MCs ativados.

O *software* R também foi utilizado para analisar os dados de RNAseq. Após a normalização (pacote DESeq2), a expressão diferencial foi calculada considerando o valor de p ajustado (padj) < 0,05. O teste t foi utilizado para análise comparativa de dois grupos, enquanto o One-way-ANOVA (pós teste de Benjamini-Hochberg) foi utilizado para analizar mais que dois grupos ao mesmo tempo.

Todas as análises foram realizadas com o *software* GraphPad Prism 5.0 (Graph Pad Software Inc., San Diego, Califórinia, EUA). O teste de Mann Whitney foi aplicado para analisar experimentos com dois grupos distintos. A one-way ANOVA (pós-teste de Kruskal-Wallis) foi utilizada para analisar experimentos com mais de dois grupos. A two-way ANOVA (pós-teste de Bonferroni) foi aplicada para analisar diferentes parâmetro categóricos independentes em uma variável dependente. A probabilidade de $p<0,05$ foi considerada estatisticamente significante. Todos os dados são apresentados com média ± desvio padrão (STD).

5. Resultados

5.1 A atividade dos mastócitos altera a população de linfócitos em casos de CCR em humanos

A análise das amostras pareadas (cólon saudável e a área tumoral) do mesmo paciente revelou que o número de MCs contendo heparina e histamina (detectada pela coloração de azul de toluidina) e triptase (detectada por reações de IHC) variava dentro dos casos analisados. Parte dos pacientes apresentaram um aumento no número de MCs na região tumoral com relação ao tecido saudável, enquanto outra parte dos pacientes não apresentaram alteração na quantidade de MCs (**Figura 8A**, **B**).

Além disso, quando foi realizada uma meta-análise de 604 amostras de CCR disponíveis no TCGA, foi possível observar que os MCs podem se apresentar na forma ativada (**Figura 8C** à esquerda) ou em repouso (**Figura 8C** à direita). Interessantemente, os casos que apresentaram a população de MCs ativados foram correlacionados negativamente com o processo de infiltração linfocitária ($r = -0,26$; $p = 9,9^{-11}$). Por outro lado, os casos de CCR que possuíam a população de MCs em repouso apresentaram uma correlação positiva para o processo de infiltração linfocitária (**Figura 8C**, painéis inferiores; $r = 0,14$; $p = 3,3^{-3}$).

De forma a refinar a análise, os casos de CCR que apresentaram os MCs ativados foram subdivididos de acordo com o grau de ativação dessas células em: amostras contendo alta frequência de MCs ativados (HMCA; vermelho) e amostras com baixa frequência de MCs ativados (LMCA; azul) (**Figura 8D**). Interessantemente, o número de linfócitos estava aumentado nas amostras LMCA ($p<0,05$; **Figura 8D** gráfico superior). Refinando ainda mais a análise, foi

possível observar que o alto número de MCs está relacionado com uma redução dos linfócitos T CD8 (**Figura 8D**; gráfico inferior).

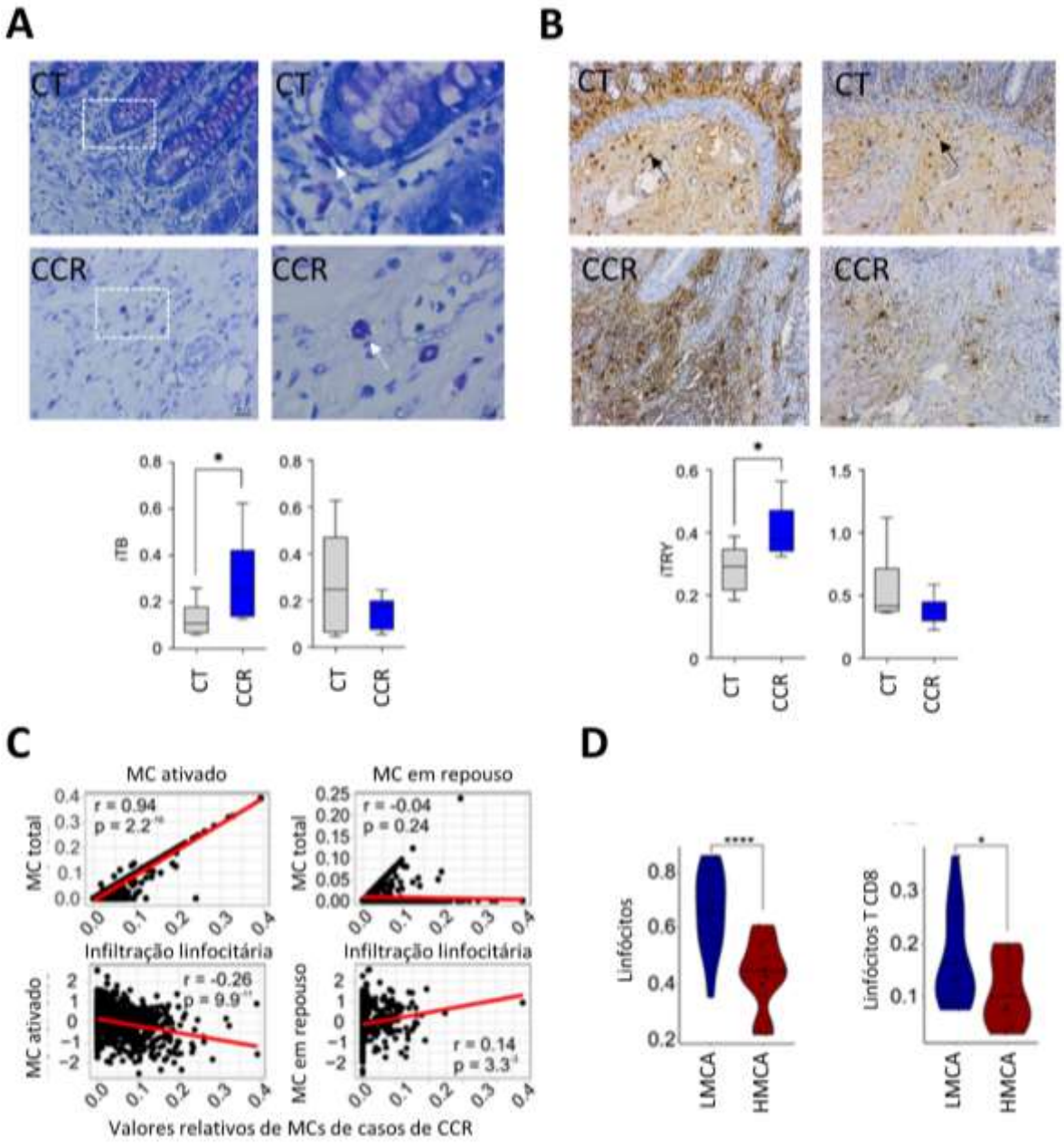

Figura 8: A população de mastócitos varia em casos de carcinoma colorretal (CCR) em humanos. **A**: Amostras combinadas de pacientes coradas com azul de toluidina (iTB) demonstra que parte dos pacientes apresenta um aumento da população de mastócitos (MC, gráfico à esquerda), enquanto parte dos pacientes não apresenta alteração em seu número. **B**: Reações de IHC-P contra triptase validam os dados da coloração de TB. As células positivas para triptase estão apresentam coloração marrom e estão apontadas na seta. **C**: Meta-análise

de 604 amostras indica que parte dos casos de CRC apresenta uma população de MCs ativados (à esquerda), e estas amostras apresentam uma correlação negativa ($r = -0,26$; $p = 9,9^{-11}$) com o processo de infiltração linfocitária. As amostras que possuíam a população de MCs em repouso (à direita), apresentaram uma correlação positiva ($r = 0,14$; $p = 3,3^{-3}$) para a infiltração linfocitária. **D**: A população de MCs ainda pôde ser dividida em altamente altivadas (HMCA, vermelho) e baixamente ativadas (LMCA, azul). O grupo HMCA apresentou uma redução da expressão de linfócitos (gráfico superior) e de linfócitos T CD8 (gráfico inferior). As imagens histológicas foram tiradas no aumento de 40x e 100x. O valor de p foi considerado significativo quando <0,05.

5.2 Mastócitos alteram o processo proliferativo das células tumorais *in vitro*

Uma vez que foram descobertas uma possível relação entre a ativação dos MCs e a ativação linfocitária, buscou-se investigar a ação dos MCs de forma isolada. O modelo escolhido para isso foi a co-cultura a partir do isolamento dos MCs do lavado peritoneal de um camundongo (C57BL/6) previamente exposto às células tumorais (**Figura 9A**).

Após 48 horas da exposição das células MC38 aos MCs, as células tumorais apresentaram uma redução do processo proliferativo (**Figura 9B**). A exposição aos MCs também fez com que as células MC38 apresentassem um aumento de células em apoptose e uma redução da viabilidade celular (**Figura 9C, D**).

A análise do ensaio clonogênico demonstrou que a atividade dos MCs previamente sensibilizados sobre as células tumorais reduziu o número de colônias formadas (**Figura 9E, F**).

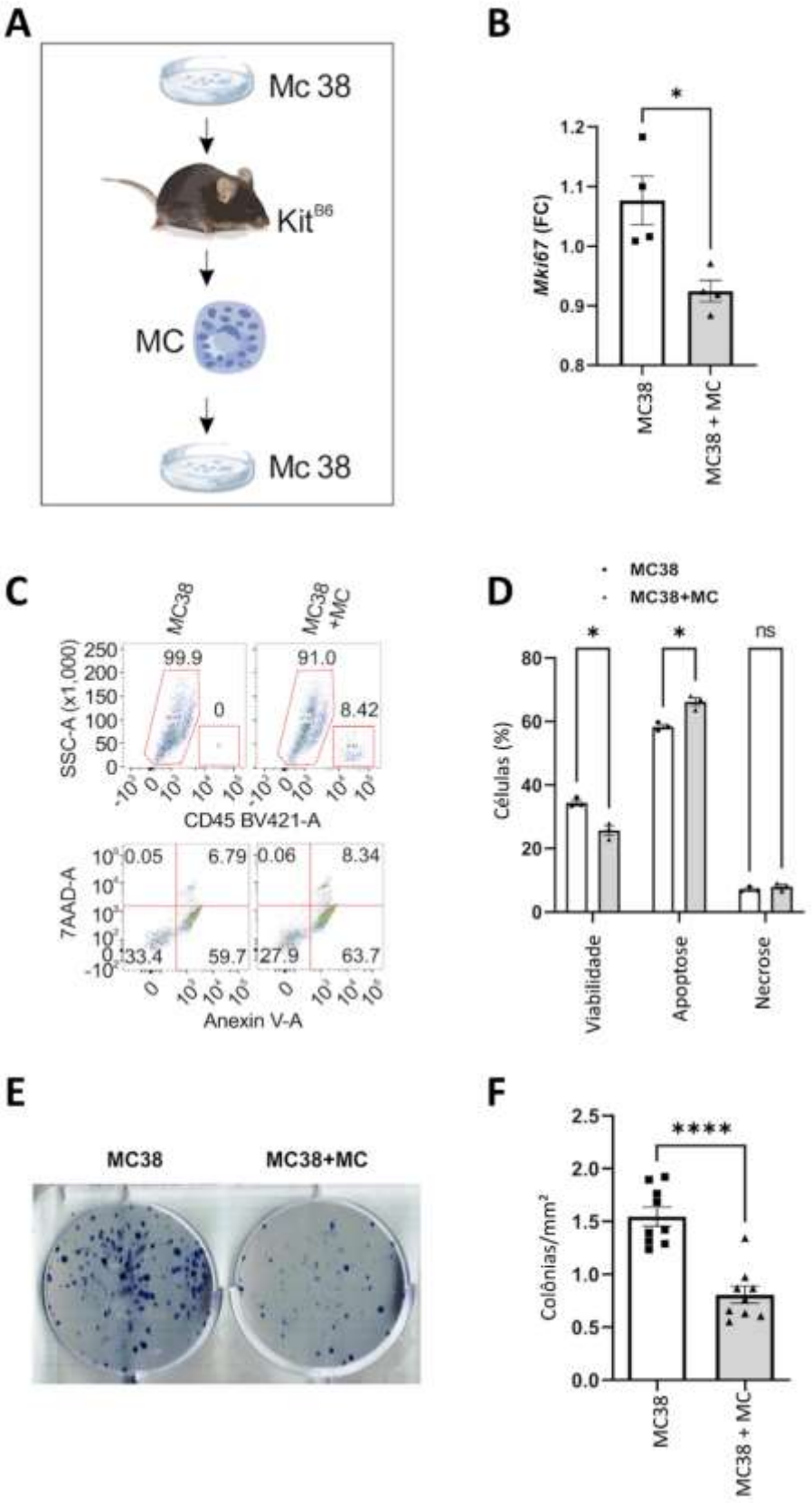

Figura 9: Mastócitos (MCs) alteram a viabilidade das células tumorais in vitro. **A**: Os MCs foram isolados da cavidade peritoneal de um camundongo C57BL/6 (Kit^{B6}) previamente exposto às células MC38. **B**: As células MC38 co-cultivadas com os MCs isolados apresentaram uma redução da proliferação celular

analisada por qRT-PCR para Mki67 ($p<0,05$). **C** e **D**: Análise por citometria de fluxo da viabilidade celular e apoptose. Os MCs foram confirmados através da marcação para $CD45^+$ e a apoptose e necrose avaliados utilizando Anexina V e 7AAD. Os gráficos representam a porcentagem de células positivas para a análise ($p<0,05$). **E** e **F**: Ensaio clonogênico demonstrou que os MCs foram capazes de inibir a formação de colônias tumorais. O número total de colônias foi contado e normalizados pela área da placa ($p<0,05$).

5.3 A atividade dos mastócitos impacta no desenvolvimento de tumores colorretais esporádicos e associados à colite em camundongos

Para explorar mecanisticamente a ação dos MCs durante o desenvolvimento do CCR, camundongos $Kit^{W/sh}$ e C57BL/6 (Kit^{B6}) foram submetidos à tumorigênese associada à colite, ou à tumorigênese esporádica.

No modelo associado à colite, a deficiência de MCs reduziu a formação dos tumores colorretais (**Figura 10A**). A análise desses tumores revelou que, a redução do número de tumores foi acompanhada de um aumento da expressão de *CD8* nos animais KO para MCs (**Figura 10B**). O aumento de CD8 também foi confirmado por IHC (**Figura 10B**).

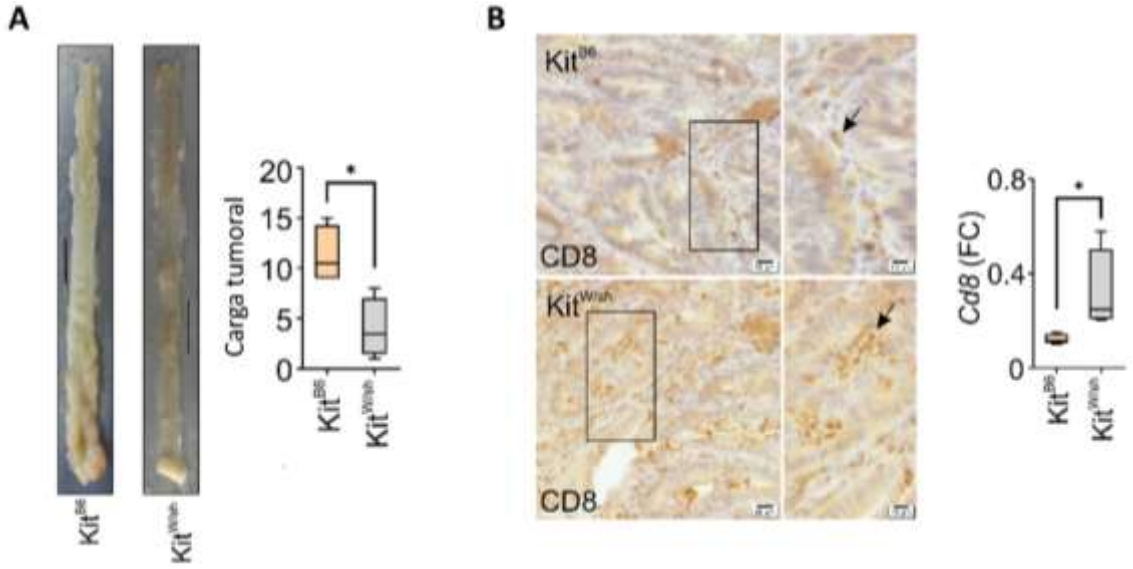

Figura 10: A deficiência de mastócitos (KitW/sh) protege o epitélio colônico contra o desenvolvimento de tumores associados à colite. **A**: Imagens representativas dos tumores associados à colite em camundongos C57BL/6 (Kit^{B6}) e knockout para MCs ($Kit^{W/sh}$). Escala corresponde à 1 cm. Gráficos demonstram o número de tumores por camundongo (n = 8; *p = 0,0286). **B**: Expressão gênica de CD8 (p = 0,0286). Imagens representativas da análise por imunohistoquímica (IHC) para o anticorpo anti-CD8 (40x à esquerda e 100x à direita). As setas indicam as células positivas para CD8. Os dados estão representados como mediana, com os valores mais altos e mais baixos. Os valores de p foram calculados usando o teste two-tailed Mann-Whitney's.

Por outro lado, no modelo do CCR esporádico, a deficiência de MCs promoveu o desenvolvimento dos tumores colorretais (**Figura 11A**). Apesar do aumento da expressão de *CD8* no CCR associado à colite, os tumores esporádicos não apresentaram diferença significativa no infiltrado dessas células (**Figura 11B, D**). A análise da proliferação celular também não se apresentou alterada entre os tumores com deficiência para MCs e o grupo controle (**Figura 11B, C**).

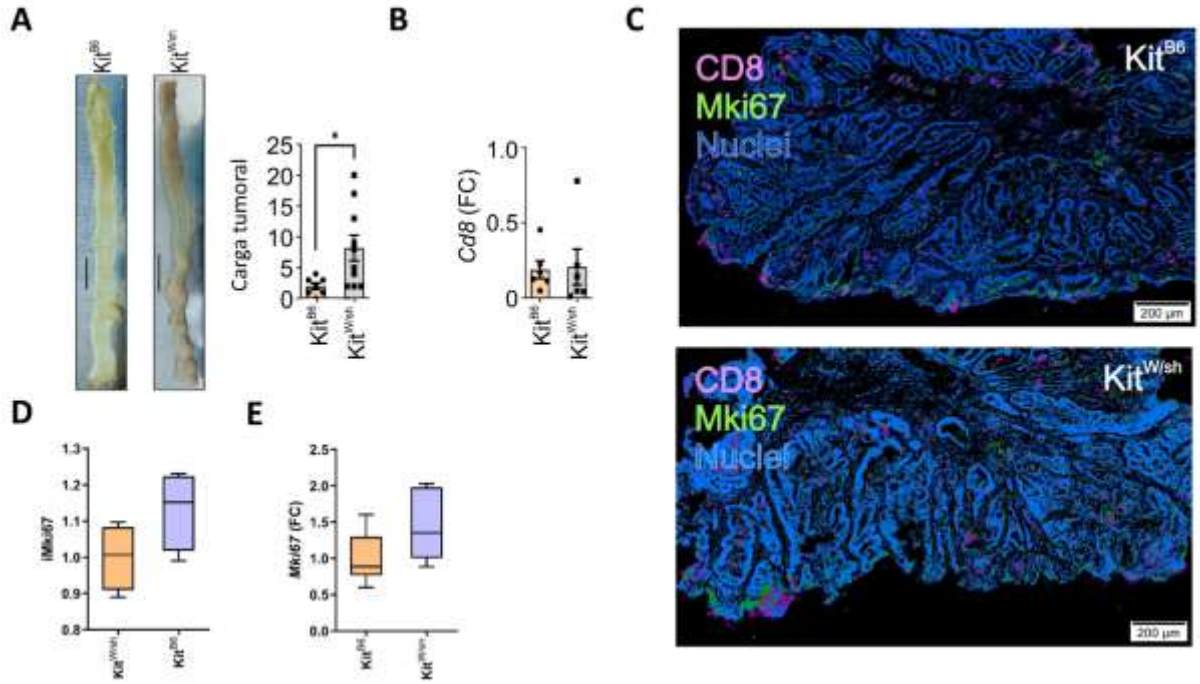

Figura 11: A atividade dos mastócitos protege contra o desenvolvimento dos tumores colorretais esporádicos. **A**: Imagens representativas de tumores induzidos no modelo da CCR esporádica. Escala corresponde à 1 cm. Gráficos demonstram o número de tumores por camundongo (n = 17; *p = 0,0164). **B**: Análise da expressão gênica para CD8 por qRT-PCR (n = 17; p >0,05). **C**: Imagens representativas de IHC multiplex para os linfócitos CD8 e Mki67 (200µm). As células $CD8^+$ estão marcadas em rosa e as células $Mki67^+$ em verde. O nucleo está corado e representado em azul. **D**: Gráficos da quantificação das células positivas para Mki67. As células foram contadas e normalizadas pela área tecidual. **E**: Gráfico da expressão gênica (FC) de Mki67 para validação dos resultados. Não houve diferença na proliferação cellular entre os grupos (p >0,05). Os dados estão representados como mediana, com os valores mais altos e mais baixos. Os valores de p foram calculados usando o teste two-tailed Mann-Whitney's.

Para explorar os resultados do CCR esporádico, foi realizado um painel imune (RNAseq) com o intuito de investigar as principais alterações imunes nos tumores desses animais. A análise da expressão diferencial revelou 83 genes com valor de p < 0,05 entre os grupos (**Tabela 7; Figura 12A**). A deficiência de MCs alterou diversas respostas imunes representadas no *heatmap* (**Figura 12B; Tabela 7**). Dentre as principais vias de sinalização alteradas observadas no software *Database for Annotation, Visualization and Integrated Discovery*

(DAVID), a deficiência de MCs aumentou a expressão dos genes envolvidos nas interações entre receptores citocinas-citocinas ($p = 9{,}8^{-11}$; **Tabela 8**). Além disso, as análises revelaram que a ausência de MCs promoveu uma correlação positiva entre o fator de transcrição *Kit* e os genes associados com a exaustão de células T e apresentação de antígenos tumorais (**Figura 12C**; **Tabela 9**). As análises também revelaram que o fator de transcrição *Nfkb1* apresentou correlação positiva com os genes associados a assinatura imune regulatória (**Figura 12D**; **Tabela 9**). Esses resultados sugerem que a atividade dos MCs varia de acordo com vários fatores, induzindo o desenvolvimento de tumores colorretais, com efeitos opostos nos modelos associados à colite e esporádicos.

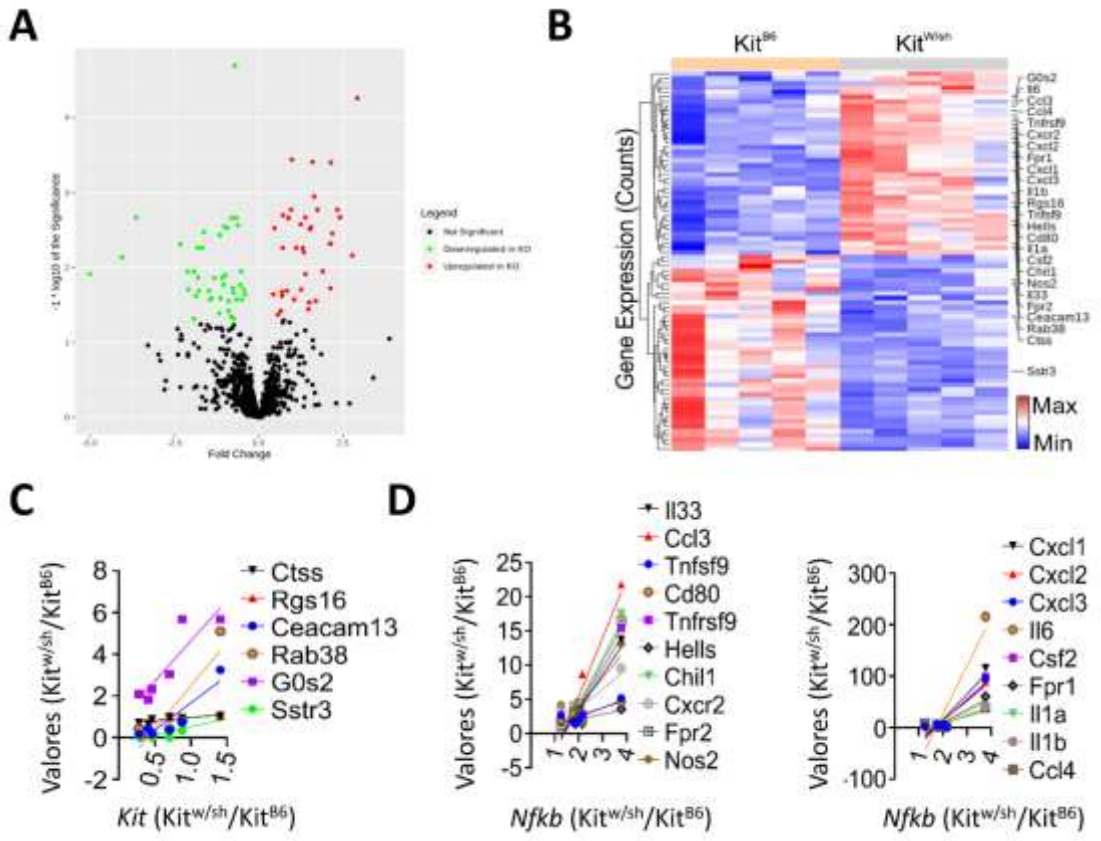

Figura 12: Mastócitos (MCs) possuem ação opostas no desenvolvimento do CCR associado à colite e esporádico. **A**: Gráfico volcano plot dos dados de RNAseq das amostras de tumor colorretal esporádico em animais C57BL/6

(Kit^{B6}) e $Kit^{W/sh}$. O gráfico indica de forma visual a quantidade de genes com expressão aumentada (vermelho), diminuída (verde) ou não alterada (preto) nos animais $Kit^{W/sh}$ em comparação com o grupo controle. **B**: Heatmap indicando dos genes diferencialmente expressos (linhas) entre os tumores dos animais Kit^{B6} e $Kit^{W/sh}$ (n = 10). A cor vermelha indica os genes com alta expressão (Max) e a cor azul indica os genes com baixa expressão (Min). **C** – **D**: Análise da regressão linear dos dados de RNAseq. Os gráficos indicam a correlação positiva com a expressão de Kit e Nfkb.

Tabela 7: Genes diferencialmente expressos em tumores colorretais esporádicos em camundongos knockout para mastócitos. Os dados foram obtidos por RNAseq e analisados usando o pacote DESeq2 do R.

Nome	Acrônimo	log2FC	*p*-Adj	*p*-Value
Genes regulados positivamente				
Chemokine (C-X-C motif) ligand 2	*Cxcl2*	2.91762	5.50E-05	1.20E-07
Interleukin 6	*Il6*	2.76768	6.93E-03	2.88E-04
Chemokine (C-X-C motif) ligand 1	*Cxcl1*	2.41013	2.15E-03	3.29E-05
Colony stimulating factor 2	*Csf2*	2.39663	2.15E-03	3.16E-05
Interleukin 1 α	*Il1a*	2.32562	1.70E-03	1.67E-05
Chemokine (C-X-C motif) ligand 3	*Cxcl3*	2.17899	3.52E-03	1.04E-04
Formyl peptide receptor 1	*Fpr1*	2.13251	3.99E-04	2.18E-06
Chemokine (C-C motif) ligand 4	*Ccl4*	2.1307	4.82E-03	1.57E-04
Interleukin 17ª	*Il17a*	2.11911	1.90E-02	1.12E-03
Interleukin 1 β	*Il1b*	2.107	4.82E-03	1.58E-04
Chemokine (C-C motif) ligand 3	*Ccl3*	1.89559	1.13E-02	5.05E-04
Nitric oxide synthase 2, inducible	*Nos2*	1.73595	1.70E-03	1.51E-05
Chemokine (C-C motif) receptor 10	*Ccr10*	1.68575	2.81E-02	2.25E-03
Chemokine (C-X-C motif) receptor 2	*Cxcr2*	1.6386	1.13E-03	7.43E-06
Histidine decarboxylase	*Hdc*	1.59195	3.94E-04	1.72E-06
Regulator of G-protein signaling 16	*Rgs16*	1.54682	2.90E-03	6.99E-05
Chitinase-like 1	*Chil1*	1.50777	3.08E-03	8.43E-05
G0/G1 switch gene 2	*G0s2*	1.49325	2.94E-02	2.41E-03
Tumor necrosis factor receptor superfamily, member 9	*Tnfrsf9*	1.47377	3.63E-02	3.01E-03
Arginase 2	*Arg2*	1.38296	2.15E-03	2.75E-05
Formyl peptide receptor 2	*Fpr2*	1.38215	1.22E-02	6.10E-04
Tumor necrosis factor (ligand) superfamily, member 9	*Tnfsf9*	1.33416	6.27E-03	2.54E-04
Interleukin 33	*Il33*	1.29891	5.47E-03	2.05E-04
CD80 antigen	*Cd80*	1.25429	1.97E-02	1.19E-03
Selectin, platelet	*Selp*	1.2436	2.66E-03	5.53E-05
Granzyme B	*Gzmb*	1.10501	5.47E-03	2.15E-04
Inositol polyphosphate-4-phosphatase, type II	*Inpp4b*	1.04564	2.68E-02	2.09E-03
Serine hydroxymethylTransferase 2 (mitochondrial)	*Shmt2*	0.97879	3.63E-04	1.19E-06
Nuclear factor of kappa light polypeptide gene enhancer in B cells inhibitor, α	*Nfkbia*	0.96189	1.70E-03	1.39E-05

CD14 antigen	*Cd14*	0.87987	2.19E-03	3.82E-05
Helicase, lymphoid specific	*Hells*	0.87468	2.19E-03	4.01E-05
Cell division cycle 7	*Cdc7*	0.83777	2.05E-02	1.31E-03
Tumor necrosis factor receptor superfamily, member 1b	*Tnfrsf1b*	0.71521	2.02E-03	2.20E-05
Serine/arginine-rich splicing factor 7	*Srsf7*	0.71185	5.47E-03	2.09E-04
BORA Aurora Kinase A Activator	*Bora*	0.69255	2.40E-02	1.73E-03
Activating transcription factor 4	*Atf4*	0.68931	2.12E-02	1.41E-03
Dystrobrevin, beta	*Dtnb*	0.65154	3.81E-02	3.25E-03
Regulatory factor X-associated protein	*Rfxap*	0.56539	4.28E-02	3.74E-03
Sphingomyelin synthase 1	*Sgms1*	0.46723	2.99E-03	7.83E-05
DEAD (Asp-Glu-Ala-Asp) box polypeptide 17	*Ddx17*	0.43006	2.29E-02	1.58E-03
Genes regulados negativamente				
Serine (or cysteine) peptidase inhibitor, clade A, member 1D	*Serpina1d*	-5.0011	1.22E-02	6.16E-04
Somatostatin receptor 3	*Sstr3*	-4.0509	7.35E-03	3.14E-04
Carboxypeptidase A3, mast cell	*Cpa3*	-3.6243	2.15E-03	3.08E-05
Chromogranin B	*Chgb*	-2.3208	4.90E-03	1.66E-04
Endothelin 2	*Edn2*	-2.1053	1.14E-02	5.22E-04
Monoamine oxidase B	*Maob*	-2.0844	1.97E-02	1.21E-03
Collagen, type VIII, alpha 2	*Col8a2*	-1.9191	4.87E-02	4.38E-03
Carcinoembryonic antigen-related cell adhesion molecule 13	*Ceacam13*	-1.9147	1.14E-02	5.49E-04
RAR-related orphan receptor gamma	*Rorc*	-1.9034	1.14E-02	5.49E-04
Vitamin D receptor	*Vdr*	-1.8635	2.40E-02	1.72E-03
Chemokine (C motif) ligand 1	*Xcl1*	-1.8057	5.47E-03	2.08E-04
Solute carrier family 24 (sodium/potassium/calcium exchanger), member 3	*Slc24a3*	-1.7958	1.37E-02	7.17E-04
Hydroxyprostaglandin dehydrogenase 15 (NAD)	*Hpgd*	-1.7713	2.05E-02	1.35E-03
Kit oncogene	*Kit*	-1.6707	5.47E-03	2.11E-04
Fibroblast growth factor 18	*Fgf18*	-1.6239	3.35E-03	9.53E-05
RAB38, member RAS oncogene Family	*Rab38*	-1.4745	2.05E-02	1.34E-03
Myosin XVB	*Myo15b*	-1.4343	2.68E-02	2.07E-03
MHC I like leukocyte 2	*Mill2*	-1.4073	2.58E-02	1.92E-03
SH3 domain and tetratricopeptide repeats 1	*Sh3tc1*	-1.3104	1.38E-02	7.41E-04
Glucosaminyl (N-acetyl) transferase 1, core 2	*Gcnt1*	-1.1739	4.10E-02	3.54E-03

Myocyte enhancer factor 2C	*Mef2c*	-1.1546	3.68E-03	1.13E-04
Melanophilin	*Mlph*	-1.1311	2.58E-02	1.89E-03
KN motif and ankyrin repeat domains 2	*Kank2*	-1.0783	1.38E-02	7.55E-04
Prostaglandin-endoperoxide synthase 1	*Ptgs1*	-1.0425	1.71E-02	9.74E-04
Inositol polyphosphate-4-phosphatase, type II	*Inpp4b*	-1.0258	2.84E-03	6.53E-05
Epithelial membrane protein 1	*Emp1*	-0.9828	1.26E-02	6.50E-04
Erb-b2 receptor tyrosine kinase 2	*Erbb2*	-0.9277	2.99E-03	7.84E-05
Interleukin 15	*Il15*	-0.8982	3.80E-02	3.21E-03
Avian musculoaponeurotic fibrosarcoma oncogene homolog	*Kank2*	-0.888	2.81E-02	2.27E-03
RNA binding motif protein 3	*Rbm3*	-0.8148	4.50E-02	3.99E-03
Zinc finger E-box binding homeobox 1	*Zeb1*	-0.8086	2.19E-03	4.21E-05
ATPase Phospholipid Transporting 9A (Putative)	*Atp9a*	-0.7628	1.88E-02	1.09E-03
Serine (or cysteine) peptidase inhibitor, clade B, member 6ª	*Serpinb6a*	-0.7483	2.19E-02	1.48E-03
Cathepsin S	*Ctss*	-0.7402	4.87E-02	4.42E-03
Glypican 4	*Gpc4*	-0.7059	2.03E-05	2.22E-08
Forkhead box N3	*Foxn3*	-0.6665	2.19E-03	4.31E-05
Sphingomyelin phosphodiesterase 3, neutral	*Smpd3*	-0.6579	2.68E-02	2.10E-03
Proteasome (prosome, macropain) 26S subunit, non-ATPase, 11	*Psmd11*	-0.6125	2.75E-03	6.02E-05
Nuclear mitotic apparatus protein 1	*Numa1*	-0.5496	1.71E-02	9.65E-04
Catalase	*Cat*	-0.5231	1.13E-02	5.07E-04
Protein phosphatase 1, regulatory (inhibitor) subunit 2	*Ppp1r2*	-0.5019	2.68E-02	2.11E-03
von Willebrand factor A domain containing 5ª	*Vwa5a*	-0.4409	1.97E-02	1.23E-03
Inhibitor of kappaB kinase γ	*Ikbkγ*	-0.4047	2.29E-02	1.60E-03

Genes estão representados em ordem descrescente (valores de log2FC).

Tabela 8: Vias de Sinalização alteradas nos tumores colorretais esporádicos deficientes para mastócitos. Os dados foram obtidos por RNAseq e analisados no DAVID (Banco de dados de bioinformática).

Via	*Status*	Valor de *p*	Genes
Interação receptor citocina-citocina	Aumentada	9,80E-11	*Ccl3, Ccl4, Ccr10, Cxcl1, Cxcl2, Cxcr2, Csf2, Il1a, Il1b, Il17a, Il6, Tnfsf9, Tnfrsf1b, Tnfrsf9*
	Diminuída	9,80E-11	*Xcl1, Il15*
Sinalização de Tnf	Aumentada	4,40E-09	*Atf4; Cxcl1, Cxcl2, Cxcl3,Csf2, Il1b, Il6, Nfkbia, Tnfrsf1b*
	Diminuída	4,40E-09	*Ikbkg, Il15*
Sinalização de receptor Toll-like	Aumentada	7,50E-06	*Cd14, Cd80, Ccl3, Ccl4, Il1b, Il6, Nfkbia*
	Diminuída	7,50E-06	*Ikbkg*
Sinalização de quimiocinas	Aumentada	1,00E-05	*Ccl3, Ccl4, Ccr10, Cxcl1, Cxcl2, Cxcl3, Cxcr2, Nfkbia*
	Diminuída	1,00E-05	*Ikbkg, Xcl1*
Sinalização de receptor NOD-like	Aumentada	5,40E-05	*Cxcl1, Cxcl2, Il1b, Il6, Nfkbia*
	Diminuída	5,40E-05	*Ikbkg*
Doença inflamatória instestinal	Aumentada	6,30E-05	*Il1a, Il1b, Il17a, Il6*
DNA citosólico	Aumentada	9,40E-05	*Ccl4, Il1b, Il33, Il6, Nfkbia*
	Diminuída	9,40E-05	*Ikbkg*
Transcrição desrregulada no câncer	Aumentada	1,20E-03	*Cd14, Csf2, Gzmb, Il6*
	Diminuída	1,20E-03	*Maf, Hpgd, Mef2c*
Rede immune intestinal para produção de IgA	Aumentada	3,40E-03	*Cd80, Ccr10, Il15, Il6*

NF-kappa B	Aumentada	5,30E-03	*Cd14, Ccl4, Il1b, Nfkbia*

Tabela 9: Análise de genes do RNAseq correlacionados de forma positiva ou negativa com Kit ou Nfkb1 de tumores colorretais esporádicos de animais $Kit^{W/sh}$.

Correlação positiva	Gene alvo	R^2	Valor de *p*
Nfkb1	*Fpr2*	0.9313	0.0018
Nfkb1	*Chil1*	0.9148	0.0028
Kit	*Ceacam13*	0.9086	0.0121
Kit	*G0s2*	0.8948	0.0160
Nfkb1	*Tnfrsf9*	0.8942	0.0044
Kit	*Rab38*	0.8908	0.0172
Nfkb1	*Fpr1*	0.8736	0.0063
Nfkb1	*Ccl3*	0.8734	0.0063
Kit	*Sstr3*	0.8731	0.0231
Nfkb1	*Il33*	0.8718	0.0065
Nfkb1	*Il6*	0.8688	0.0074
Nfkb1	*Cxcl3*	0.8688	0.0068
Nfkb1	*Cxcl1*	0.8632	0.0074
Nfkb1	*Cxcl2*	0.8610	0.0076
Nfkb1	*Csf2*	0.8519	0.0087
Nfkb1	*Il1a*	0.08437	0.0097
Kit	*Rgs16*	0.8356	0.0383
Kit	*Ctss*	0.8356	0.0382
Nfkb1	*Il1b*	0.7967	0.0167
Nfkb1	*Cxcr2*	0.7768	0.0203
Nfkb1	*Ccl4*	0.7568	0.0243
Nfkb1	*Cd80*	0.7276	0.0349
Nfkb1	*Tnfsf9*	0.7112	0.0349
Nfkb1	*Hells*	0.6832	0.0425
Nfkb1	*Nos2*	0.6748	0.0450
Nfkb1	*Fpr2*	0.9	0.001

Genes estão representados em ordem decrescente (valores de R^2). Os significados dos acrônimos estão descritos na Tabela 5.

5.4 A interação entre os mastócitos e linfócitos impactam no desenvolvimento dos eventos carcinogênicos iniciais no cólon

Considerando que a deficiência de MCs pode promover alterações significantes no MAT, foi explorada a hipótese de que os MCs possuem um papel essencial na construção desse microambiente nas etapas iniciais do CCR.

Para isso, foram determinadas quais alterações linfocitárias ocorrem em resposta ao dano de DNA provocado pelo AOM. A exposição ao carcinógeno provocou um aumento do recrutamento da população de linfócitos T $CD8^+$ (**Figura 13A**, **B**), enquanto a população de linfócitos T $CD4^+$ e $CD4^+Foxp3^+$ não sofreu alterações significativas (**Figura 13 C-D**).

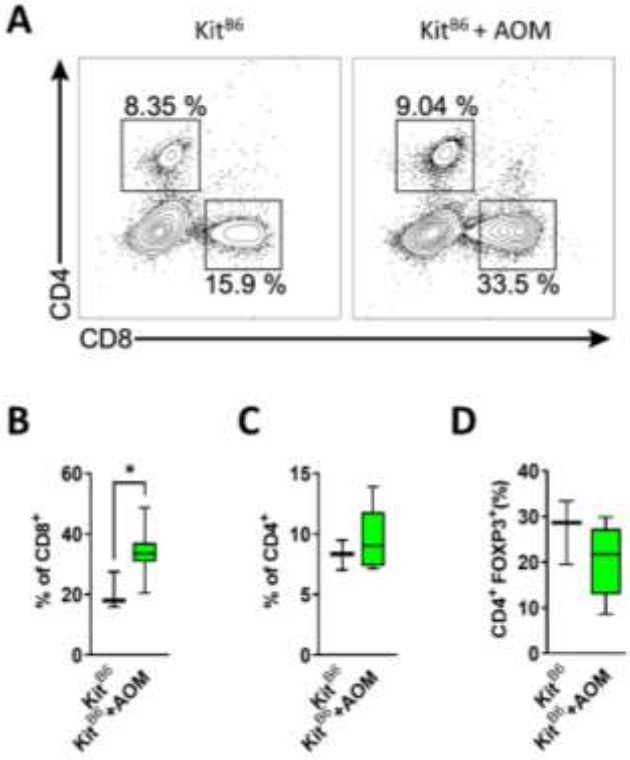

Figura 13: Exposição ao carcinógeno altera a população de linfócitos T CD8 no cólon. **A**: Gráfico representativo da citometria para os linfócitos $CD4^+$ e $CD8^+$, sendo todas essas $CD45^+$, células vivas e únicas. **B**-**D**: Os gráficos demonstram

as porcentagens de linfócitos T CD8+ em animais C57BL/6 (Kit^{B6}) (**B**), CD4+ (**C**) e $CD4^{+}Foxp3^{+}$ (**D**) isoladas do cólon de animais expostos ao carcinógeno. Os dados estão representados como mediana, com os valores mais altos e mais baixos. Os valores de p foram calculados usando o teste two-tailed Mann-Whitney's.

A partir desse resultado, buscou-se investigar se a atividade do sistema MHCI impactaria diretamente na população de linfócitos e MCs (KOLLER BH, *et al.;* 1990). Os animais KO para MHCI (*B2m* KO) quando expostos às 6 doses do carcinógeno apresentaram uma redução da expressão gênica de *Cd8* (**Figura 14A**). Essa redução foi acompanhada de um aumento da expressão gênica dos biomarcadores de MCs (*Mcpt1* (MCs epiteliais) e *Mcpt4* (MCs estromais); **Figura 14B-D**).

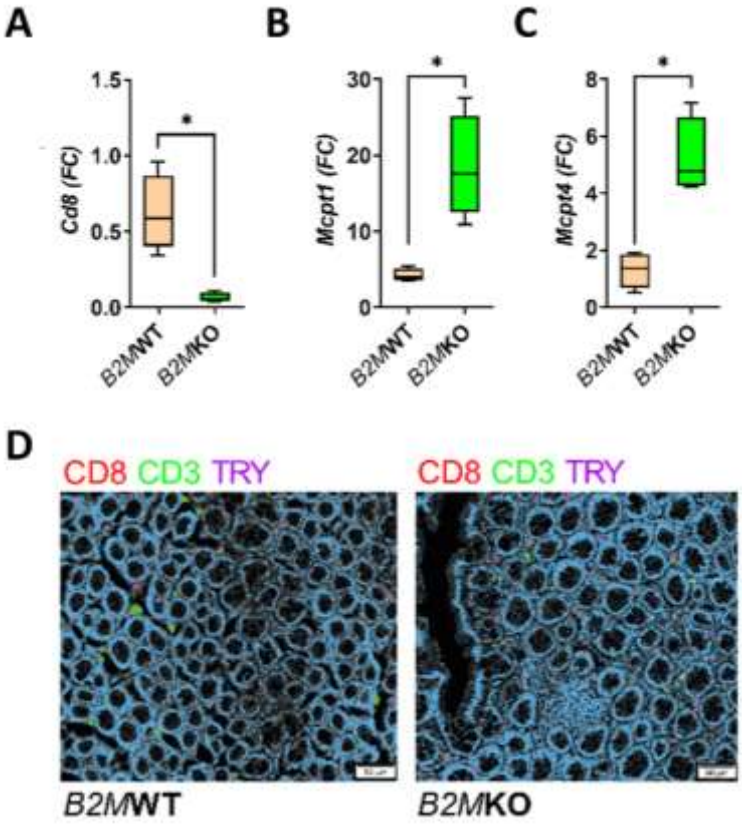

Figura 14: Camundongos MHCI knockout (B2MKO) expostos à 6 doses de AOM e avaliados após 1 semana. A: Os animais B2MKO apresentaram uma redução

na expressão gênica para Cd8 (n = 8, *p =0,02). **B**: Expressão gênica para os marcadores de mastócitos (Mcpt1 n = 8, *p =0,02) e **C**: (Mcpt4 n = 8, *p =0,02). **D**: Imagens representativas da IHC multiplex contra CD8, CD3 e Triptase (TRY) (magnitude de 50 µm). Os dados estão representados como mediana, com os valores mais altos e mais baixos. Os valores de p foram calculados usando o teste two-tailed Mann-Whitney's.

Já os animais KO para o sistema MHCII (*Ciita* KO), apresentaram uma redução na expressão dos marcadores de MCs (**Figura 15A-B**) e não apresentação alterações na expressão de *Cd8* (**Figura 15C-D**).

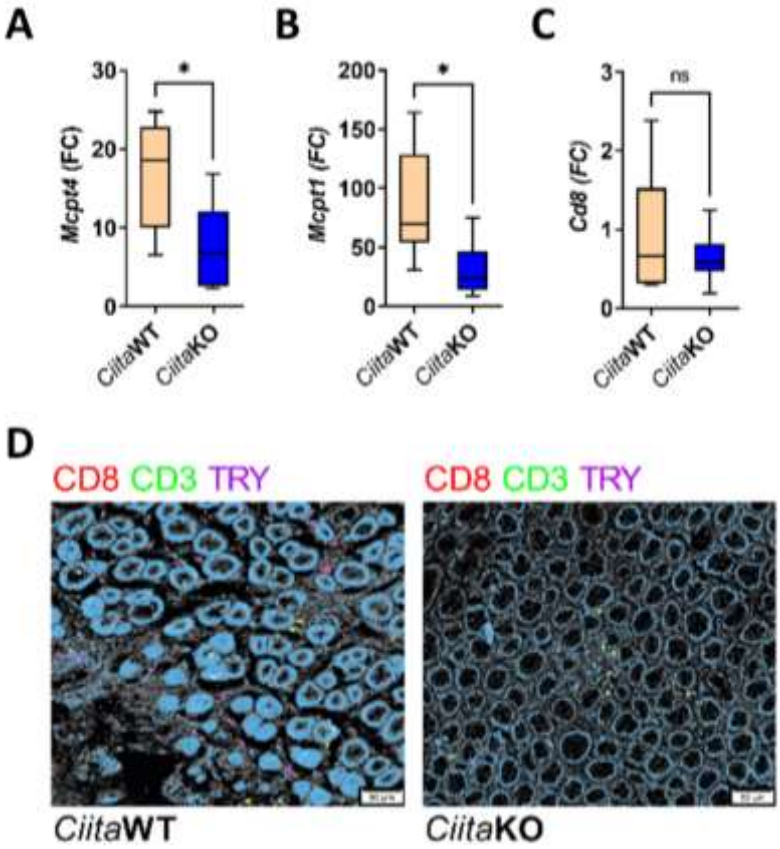

Figura 15: A deleção do sistema MHCI (CiitaKO) altera a população de mastócitos. **A**: Análise da expressão gênica para o marcador de mastócitos Mcpt4 (n = 13, *p =0,02) e Mcpt1 (**B**; n = 13, *p =0,02). **C**: Os animais CiitaKO também apresentaram uma redução da expressão de Cd8 com relação aos animias controle. **D**: Imagens representativas da IHC multiplex contra CD8, CD3 e Triptase (TRY) (magnitude de 50 µm). Os dados estão representados como

mediana, com os valores mais altos e mais baixos. Os valores de p foram calculados usando o teste two-tailed Mann-Whitney's.

Considerando que foram encontrados altos níveis de Il33 nos tumores de animais deficientes para MCs (**Figura 12B, D**; **Tabela 7**), os animais KO para o receptor de Il33 (Il33r KO) também foram expostos às 6 doses de AOM e avaliados no período de 7 dias. A deficiência de Il33r reduziu os marcadores relacionados à CCR (**Figura 16A, B**). Essa condição aumentou os biomarcadores de MCs (**Figura 16C-D**, **F**), mas reduziu o recrutamento de linfócitos T CD8 (**Figura 16E**-**F**).

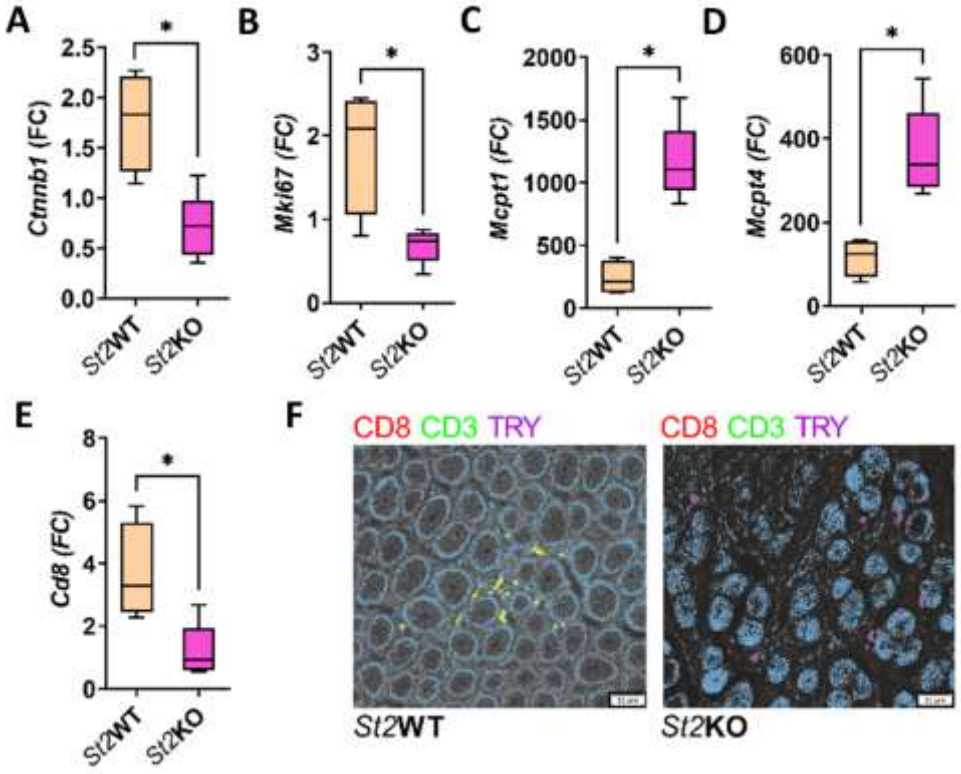

Figura 16: Animais knockout para o receptor da interleucina 33 (Il33r; St2KO) apresentaram alterações na composição do microambiente em resposta ao carcinógeno (6AOM e avaliados após 1 semana). Os animais St2KO apresentaram redução da expressão gênica para os biomarcadores do CCR (**A**, Ctnnb1; n = 9, *p =0,03 e **B**: Mki67 (L, *p =0,03)). **C** e **D**: A expressão dos marcadores de mastócitos (Mcpt1 e Mcpt4) estavam aumentados nos animais

St2KO (n = 9, *p =0,01). **E**: Expressão gênica para Cd8 revelou uma redução nos animais KO (n = 9, *p =0,03). **F**: Imagens representativas da IHC multiplex contra CD8, CD3 e Triptase (TRY) (magnitude de 50 µm). Os dados estão representados como mediana, com os valores mais altos e mais baixos. Os valores de p foram calculados usando o teste two-tailed Mann-Whitney's.

Para confirmar que as etapas iniciais do CCR são dependentes de uma resposta imune para se desenvolver, foram introduzidos na análise animais imunossuprimidos (NOD-*scidγ*). Esse experimento demonstrou que a imunossupressão reduziu o desenvolvimento das lesões preneoplásicas (PL) iniciais (**Figura 17A**). Essa redução foi acompanhada de uma menor taxa de proliferação celular (**Figura 17B**) e uma diminuição na população de MCs positivas para triptase (**Figura 17C**).

A inteleucina 6 (Il6) é outro fator importante no microambiente tumoral devido à sua ação pró-inflamatória (HEICHLER *et al*., 2020). Buscou-se investigar se a deficiência de Il6 alteraria o risco para o desenvolvimento do CCR e impactaria na população de MCs. Os animais Il6 KO apresentaram uma redução no desenvolvimento das PL iniciais e um menor recrutamento de MCs (**Figura 17D-E**).

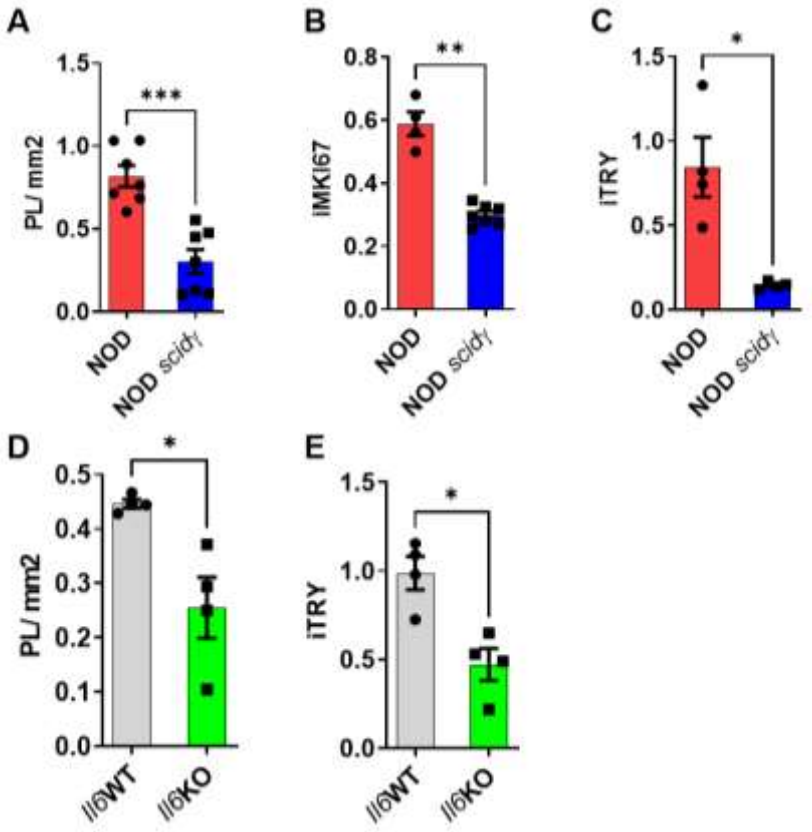

Figura 17: Resposta inflamatória altera a população de mastócitos (MC) e os eventos iniciais da carcinogênese colorretal. (**A**-**E**) Análises histológicas para as lesões preneoplásicas inicias (**A**; n = 14, *p=0,0006; **D**, n = 8; *p=0,002); proliferação celular (**B**, n = 14, *p=0,006) e número de MCs (**C**, n = 14, *p=0,02, **E**, n = 8, *p=0,02) em amostras de animais NOD-scidγ e Il6 KO. Os dados estão representados como media ± desvio padrão. Os valores de p foram calculados usando o teste two-tailed Mann-Whitney's.

Também foi possível demonstrar que a interação entre os MCs e os linfócitos impacta no desenvolvimento das lesões tumorigênicas iniciais no cólon. Animais deficientes para MCs receberam 6 doses de AOM e foram eutanasiados após 6 semanas para avaliação do desenvolvimento dos FCA (**Figura 18A**). Este experimento revelou que a atividade de MCs reduziu o desenvolvimento dos FCA (**Figura 18B**), bem como os níveis de *Cd4* e *Cd11c* (**Figura 18C**-**D**).

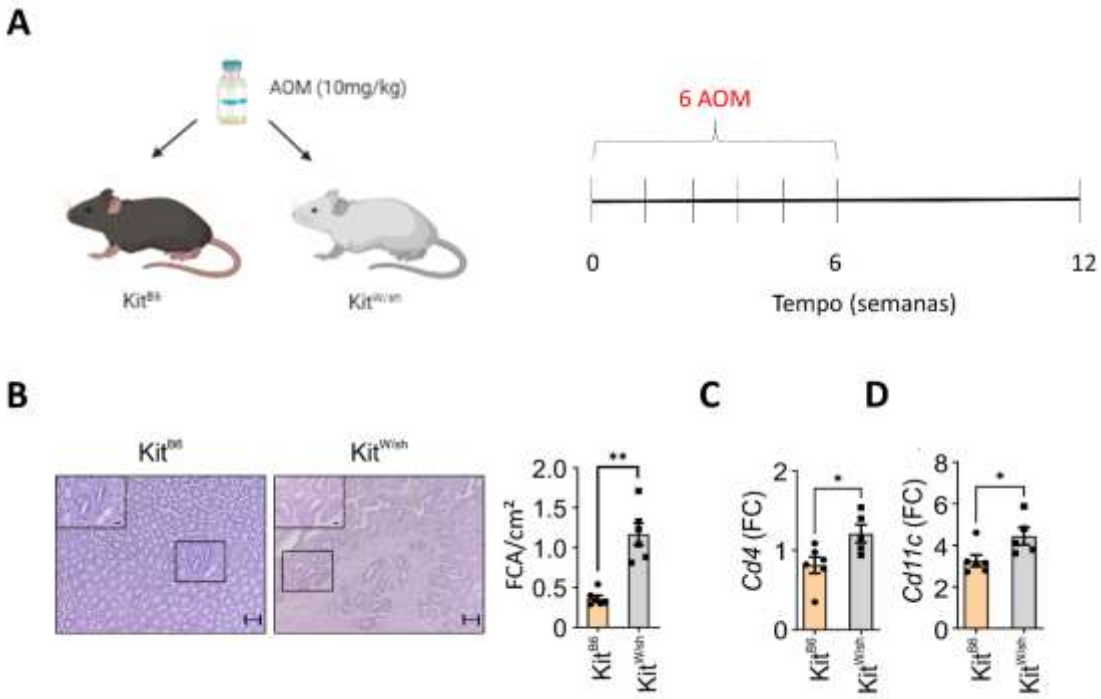

Figura 18: Atividade dos mastócitos (MCs) protege o epitélio colônico das etapas iniciais da tumorigenese colorretal. **A**: Imagens ilustrativas do desenho experimental, no qual camundongos Kit^{B6} (C57BL/6) e $Kit^{W/sh}$ (knockout para mastócitos) receberam 6 doses do carcinógeno (AOM) e foram eutanasiados após 6 semanas. **B**: Imagens representativas (10x e 40x; Escala = 20 μm) das lesões preneoplásicas avançadas (APL). A deficiência de MCs aumentou o número de APL em camundongos (n = 11; *p =0,004). **C-D**: Análise da expressão gênica para Cd4 (n = 11; *p =0,03) e Cd11c (*p = 0,03) de amostras de colon (6AOM+6 semanas). Os dados estão representados como media ± desvio padrão. Os valores de p foram calculados usando o teste two-tailed Mann-Whitney's.

Resultados similares também foram encontrados após uma semana da alta exposição ao carcinógeno (**Figura 19A**). Os animais KitW/sh apresentaram um aumento na expressão de *Cd4* e *Cd11c* (**Figura 19C-D**). Além disso, a deficiência de MCs reduziu a expressão de *Mgmt*, um gene essencial no mecanismo de reparo de dano de DNA contra os adutos (*O^6-methylguanine-DNA-methyltransferase*) (**Figura 19E**).

Com o intuito de investigar o papel dos MCs durante o dano de DNA nas lesões iniciais, os animais deficientes para MCs foram analisados após 72 horas

da 3ª exposição ao AOM (**Figura 19B**). A ausência de MCs não alterou os níveis de dano de DNA (γH2AX), mas aumentou a expressão de *Cd11c* (**Figura 19F-G**).

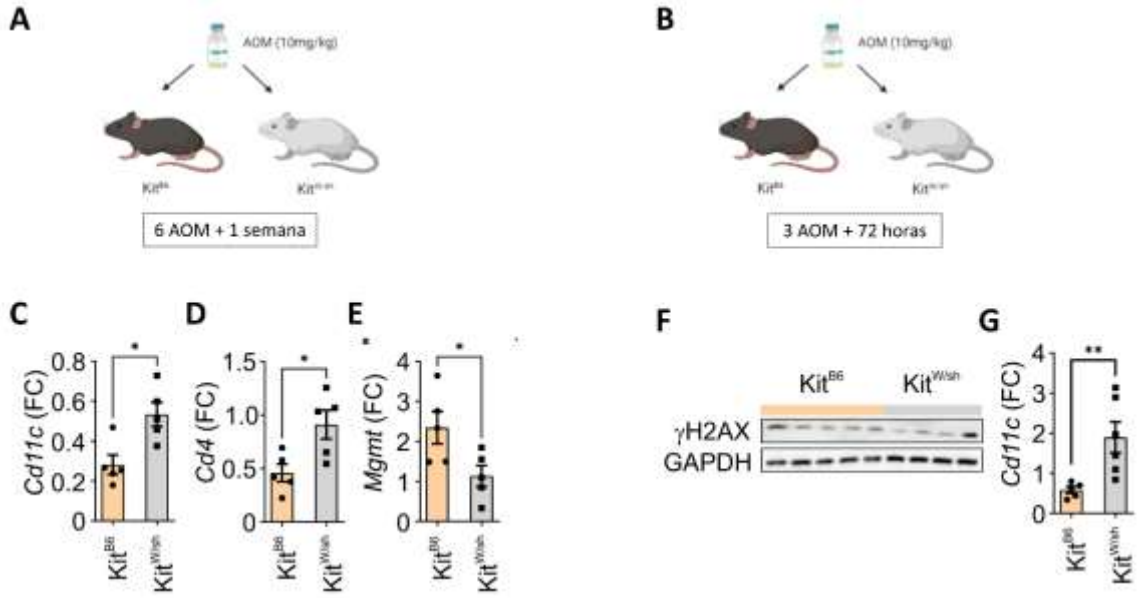

Figura 19: A atividade dos mastócitos (MCs) em resposta ao dano de DNA indutor da tumorigênese colorretal. **A**: Ilustração do desenho experimental utilizado para estudar as alterações dos MCs em resposta à um intenso dano de DNA (6AOM (10mg/kg/semana) + 1 semana). **B**: Ilustração dos animais C57BL/6 (Kit^{B6}) e $Kit^{W/sh}$ (knockout para MCs) que receberam 3 doses de AOM e foram avaliados após 72 horas. **C**-**E**: Análise da expressão gênica para Cd11c (n = 10; *p =0,01), Cd4 (*p =0,02), e Mgmt (n = 11; *p =0,04) de animais expostos à 6AOM e avaliados após 7 dias. **F**: Western blotting contra γH2AX e GADPH em amostras de colon de camundongos após 3 dias da 3ª dose de AOM. **G**: Expressão gênica para Cd11c em amostras de colon de camundongos após 3 dias da 3ª dose de AOM (n = 9; p =0;003). Os dados estão representados como media ± desvio padrão. Os valores de p foram calculados usando o teste two-tailed Mann-Whitney's.

Para explorar as reações imunológicas envolvidas no desenvolvimento das PL iniciais, foram realizadas análises do painel immune por RNAseq das amostras de cólon de animais C57BL/6 e $Kit^{W/sh}$ expostos à 3 doses de AOM e eutanasiados após 3 semanas. Foram identificados 103 diferencialmente

expressos, considerando o valor de p < 0,05 (**Tabela 10**, **Figura 20A-B**). Dentre as diversas reações imunológicas alteradas (**Tabela 11**), a deficiência de MCs impactou significativamente a via de sinalização das doenças inflamatórias intestinais (p= 3,40E-08). Além disso, foram encontradas correlações positivas entre Kit e Stat3 com genes associados com a exaustão de células T e assinaturas imune estimulatórias (**Figura 20C-D**; **Tabela 12**).

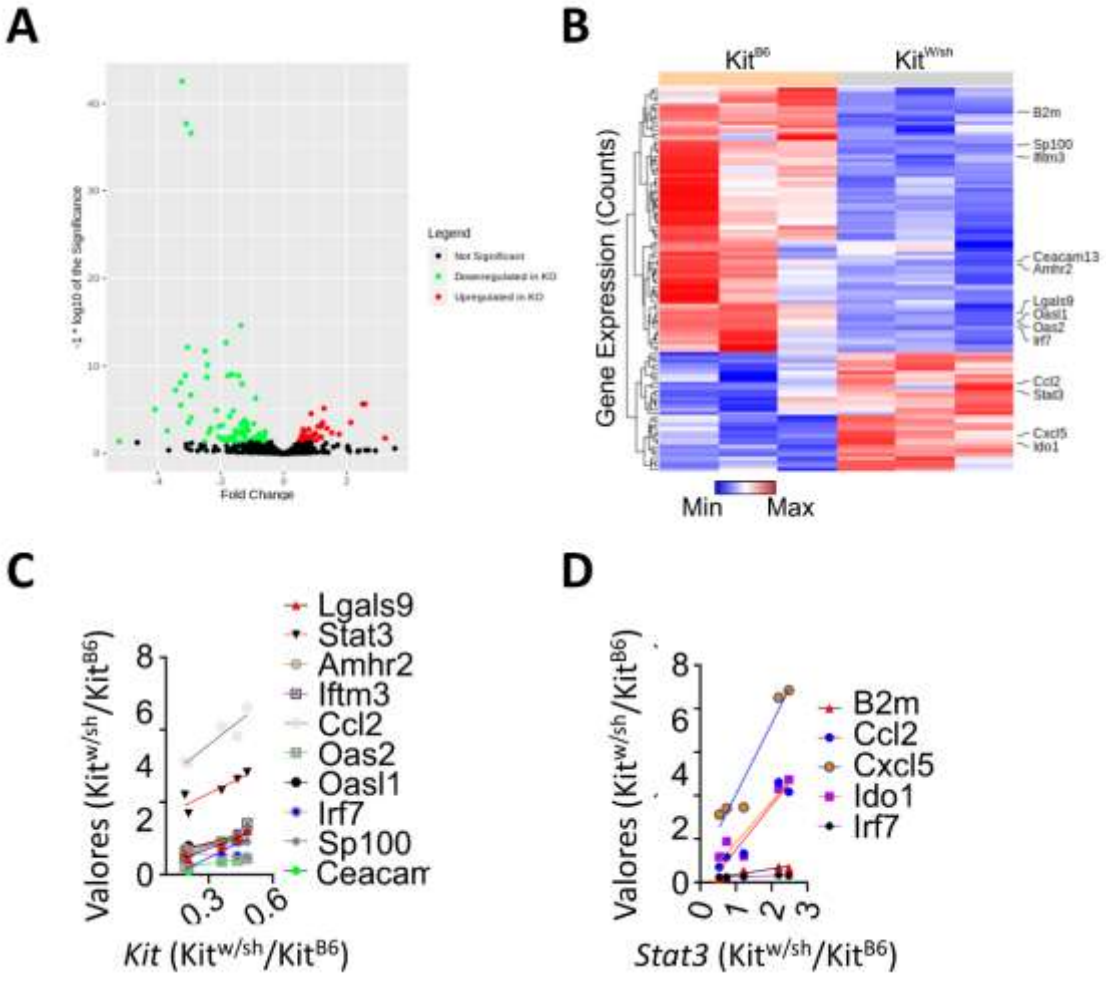

Figura 20: A deficiência em mastócitos (MCs) alterou diversas reações imunes nas fases iniciais da tumorigênese colorretal. **A**: Gráfico volcano plot das amostras do cólon de animais C57BL/6 e $Kit^{w/sh}$ expostos à 3 doses de carcinógeno e eutanasiados após 3 semanas para avaliação das lesoes preneoplásicas iniciais. O gráfico indica de forma visual a quantidade de genes com expressão aumentada (vermelho), diminuída (verde) ou não alterada (preto) nos animais $Kit^{W/sh}$ em comparação com o grupo controle. **B**: Heatmap gerado a

partir dos dados de RNAseq indicam os genes diferencialmente expressos entre as amostras de cólon dos animais C57BL/6 (Kit^{B6}) e animais KO para MCs ($Kit^{W/sh}$) 3 semanas após a 3ª dose do AOM (n = 6). **C**-**D**: Análise de regressão linear dos dados gerados no RNAseq (Tabela 10). Foram analisados correlações positivas com os genes Kit (C) e Stat3 (D). Os dados estão representados como media ± desvio padrão. Os valores de p foram calculados usando o teste two-tailed Mann-Whitney's.

Tabela 10: Lista de genes diferencialmente expressos obtida a partir da análise de RNAseq de amostras de cólon de camundongos C57BL/6 e KitW/sh expostos à 3 doses de carcinógeno e avaliados após 3 semanas da última exposição.

Nome	Acrônimo	log2FC	*p*-Adj	Valor de *p*
Genes regulados positivamente				
Chemokine (C-X-C motif) ligand 5	*Cxcl5*	3.22413	1.82E-02	1.62E-03
Chemokine (C-X-C motif) ligand 13	*Cxcl13*	2.58874	2.24E-06	4.79E-08
Chemokine (C-X-C motif) receptor 5	*Cxcr5*	2.51089	2.29E-06	5.14E-08
Z-DNA binding protein 1	*Zbp1*	2.1316	3.00E-04	1.11E-05
Interferon-induced protein with tetratricopeptide repeats 3	*Ifit3*	1.76255	6.40E-03	4.42E-04
Interleukin 18	*Il18*	1.52986	4.68E-03	3.00E-04
Chemokine (C-C motif) receptor 6	*Ccr6*	1.37639	1.35E-03	6.35E-05
Epithelial membrane protein 1	*Emp1*	1.28044	7.14E-06	1.77E-07
Histocompatibility 2, class II antigen A, β 1	*H2-Ab1*	1.23486	3.00E-04	1.11E-05
Interleukin 21 receptor	*Il21r*	1.21134	5.61E-04	2.27E-05
Tumor necrosis factor receptor superfamily, member 10b	*Tnfrsf10b*	1.19788	1.50E-02	1.28E-03
Nuclear factor of kappa light polypeptide gene enhancer in B cells inhibitor, α	*Nfkbia*	1.1736	8.73E-04	3.81E-05
Guanylate binding protein 2b	*Gbp2b*	1.15584	1.28E-02	1.03E-03
Anti-Mullerian hormone type 2 receptor	*Amhr2*	1.08817	8.73E-04	3.82E-05
Selectin, platelet (p-selectin) ligand	*Selplg*	1.02693	3.21E-02	3.35E-03
Mucosal vascular addressin cell adhesion molecule 1	*Madcam1*	1.01299	4.93E-03	3.21E-04
TRAF3 interacting protein 3	*Traf3ip3*	0.93662	1.10E-02	8.53E-04
Cytidine deaminase	*Cda*	0.9289	6.94E-03	4.99E-04
2'-5' oligoadenylate synthetase 1ª	*Oas1a*	0.87346	2.94E-05	8.59E-07
Histocompatibility 2, class II antigen E β2	*H2-Eb2*	0.83882	1.43E-02	1.21E-03

Chemokine (C-C motif) ligand 19	*Ccl19*	0.80013	1.84E-03	9.30E-05
Histocompatibility 2, class II antigen A, α	*H2-Aa*	0.70998	8.82E-03	6.54E-04
Lymphotoxin B	*Ltb*	0.70568	2.76E-02	2.76E-03
RAB27A, member RAS oncogene family	*Rab27a*	0.69102	2.03E-02	1.89E-03
Guanylate binding protein 2	*Gbp2*	0.65227	2.63E-02	2.58E-03
Endothelin 1	*Edn1*	0.6305	2.63E-03	1.54E-04
Transmembrane and immunoglobulin domain containing 1	*Tmigd1*	0.62949	2.04E-03	1.08E-04
Interferon regulatory factor 7	*Irf7*	0.61944	1.94E-03	1.00E-04
Heparan sulfate (glucosamine) 3-O-sulfotransferase 3B1	*Hs3st3b1*	0.56872	9.59E-03	7.22E-04
SMAD family member 3	*Smad3*	0.53498	2.51E-02	2.42E-03
Nuclear antigen Sp100	*Sp100*	0.48685	4.98E-02	5.66E-03
Genes regulados negativamente				
Complement receptor 2	*Cr2*	-5.2193	4.19E-02	4.57E-03
Metallothionein 2	*Mt2*	-4.0879	9.89E-06	2.56E-07
Chemokine (C-C motif) ligand 2	*Ccl2*	-3.6923	2.63E-03	1.53E-04
CD2 antigen	*Cd2*	-3.4363	6.10E-08	1.10E-09
Phospholipase A2, group VII (platelet-activating factor acetylhydrolase, plasma)	*Pla2g7*	-3.2754	8.39E-09	1.32E-10
Cytochrome b-245, beta polypeptide	*Cybb*	-3.2693	3.25E-06	7.67E-08
2'-5' oligoadenylate synthetase 3	*Oas3*	-3.2321	2.98E-43	3.35E-46
Histocompatibility 2, M region locus 3	*H2-M3*	-3.1173	1.28E-09	1.44E-11
Tumor necrosis fator	*Tnf*	-3.0967	2.07E-38	4.66E-41
Carcinoembryonic antigen-related cell adhesion molecule 13	*Ceacam13*	-3.0565	7.45E-13	5.02E-15
Bone marrow stromal cell antigen 1	*Bst1*	-3.0226	3.00E-04	1.08E-05
CD48 antigen	*Cd48*	-2.9478	2.17E-07	4.15E-09

2'-5' oligoadenylate synthetase-like 1	*Oasl1*	-2.9434	2.68E-37	9.03E-40
Chemokine (C-X-C motif) ligand 1	*Cxcl1*	-2.9432	8.20E-05	2.58E-06
SMAD family member 2	*Smad2*	-2.5089	4.98E-02	5.73E-03
Histone cluster 1, H1c	*Hist1h1c*	-2.4994	1.96E-12	1.54E-14
Chemokine (C-X-C motif) ligand 2	*Cxcl2*	-2.4367	1.95E-09	2.85E-11
Fucosyltransferase 4	*Fut4*	-2.4197	8.04E-11	7.23E-13
CD177 antigen	*Cd177*	-2.3846	4.40E-03	2.72E-04
Carbonic anhydrase 4	*Car4*	-2.3158	1.39E-03	6.86E-05
B lymphoid kinase	*Blk*	-2.1328	1.23E-05	3.32E-07
Lymphocyte antigen 75	*Ly75*	-2.0604	8.95E-04	4.12E-05
Histocompatibility 2, T region locus 24	*H2-T24*	-2.0561	1.29E-02	1.07E-03
CD74 antigen	*Cd74*	-1.9534	5.91E-04	2.46E-05
T cell receptor associated transmembrane adaptor 1	*Trat1*	-1.9484	3.03E-02	3.07E-03
Carboxypeptidase A3, mast cell	*Cpa3*	-1.8726	1.90E-02	1.73E-03
Kit oncogene	*Kit*	-1.8279	2.24E-13	1.26E-15
Lymphocyte transmembrane adaptor 1	*Lax1*	-1.8135	3.12E-02	3.19E-03
Kynureninase (L-kynurenine hydrolase)	*Kynu*	-1.7685	1.34E-09	1.81E-11
Interferon induced transmembrane protein 3	*Ifitm3*	-1.7126	6.18E-05	1.87E-06
Interferon regulatory factor 1	*Irf1*	-1.7119	2.69E-02	2.66E-03
CD22 antigen	*Cd22*	-1.6939	1.26E-02	1.00E-03
B and T lymphocyte associated	*Btla*	-1.6385	9.68E-10	9.78E-12
CD69 antigen	*Cd69*	-1.6102	1.48E-05	4.15E-07
Malic enzyme 1, NADP(+)-dependent, cytosolic	*Me1*	-1.5944	1.90E-02	1.71E-03
DEAD (Asp-Glu-Ala-Asp) box polypeptide 58	*Ddx58*	-1.5393	2.30E-03	1.27E-04
Beta-2 microglobulin	*B2m*	-1.5158	4.51E-03	2.84E-04

Spi-B transcription factor (Spi-1/PU.1 related)	*Spib*	-1.4302	1.34E-09	1.69E-11
Glypican 4	*Gpc4*	-1.4035	4.95E-02	5.56E-03
CD52 antigen	*Cd52*	-1.3942	5.39E-03	3.58E-04
2'-5' oligoadenylate synthetase 1G	*Oas1g*	-1.3506	4.18E-04	1.64E-05
Three prime repair exonuclease 1	*Trex1*	-1.3436	2.29E-03	1.23E-04
Optineurin	*Optn*	-1.3247	1.25E-08	2.11E-10
Apolipoprotein D	*Apod*	-1.2874	6.43E-03	4.55E-04
Myocyte enhancer factor 2C	*Mef2c*	-1.2523	1.53E-04	5.00E-06
Lectin, galactose binding, soluble 9	*Lgals9*	-1.2305	1.06E-02	8.10E-04
2'-5' oligoadenylate synthetase 1B	*Oas1b*	-1.2252	3.00E-03	1.79E-04
Signal transducer and activator of transcription 3	*Stat3*	-1.2118	3.33E-02	3.52E-03
DnaJ heat shock protein family (Hsp40) member B1	*Dnajb1*	-1.1764	3.00E-04	1.08E-05
LPS-responsive beige-like anchor	*Lrba*	-1.1744	8.80E-04	3.95E-05
Myelin and lymphocyte protein, T cell differentiation protein	*Mal*	-1.1117	4.98E-02	5.76E-03
Immunoglobulin kappa constant	*Igkc*	-1.1016	2.44E-03	1.37E-04
Interferon Induced Transmembrane Protein 3	*Ifitm3*	-1.1015	2.44E-03	1,37E-04
Serine (or cysteine) preptidase inhibitor, clade A, member 1B	*Serpina1b*	-0.9767	1.92E-02	1.77E-03
Acid phosphatase, prostate	*Acpp*	-0.9537	4.04E-04	1.54E-05
Membrane-spanning 4-domains, subfamily A, member 1	*Ms4a1*	-0.9392	3.14E-02	3.24E-03
B cell scaffold protein with ankyrin repeats 1	*Bank1*	-0.8961	5.07E-07	1.03E-08
Indoleamine 2,3-dioxygenase 1	*Ido1*	-0.8774	1.63E-02	1.43E-03
2'-5' oligoadenylate synthetase 2	*Oas2*	-0.8606	2.10E-02	1.99E-03
Protein tyrosine phosphatase, receptor type, C	*Ptprc*	-0.8081	1.63E-02	1.43E-03
Transient receptor potential cation channel, subfamily V, member 6	*Trpv6*	-0.7858	6.26E-03	4.22E-04
IKAROS family zinc finger 2	*Ikzf2*	-0.7351	6.40E-03	4.46E-04

Histocompatibility 2, O region alpha locus	*H2-Oa*	-0.6812	1.28E-02	1.05E-03
Carcinoembryonic antigen-related cell adhesion molecule 12	*Ceacam12*	-0.6733	4.92E-02	5.48E-03
Zinc and ring finger 1	*Znrf1*	-0.6444	3.93E-02	4.24E-03
Regulator of G-protein signaling 16	*Rgs16*	-0.6152	7.96E-03	5.82E-04
Paired box 5	*Pax5*	-0.5946	2.49E-02	2.38E-03
CD19 antigen	*Cd19*	-0.5853	3.25E-03	1.97E-04
Bone marrow stromal cell antigen 2	*Bst2*	-1.582	4.19E-02	4.61E-03
CD72 antigen	*Cd72*	-1.565	1.11E-02	8.72E-04
Lysophosphatidylcholine acyltransferase 4	*Lpcat4*	-1.355	2.42E-15	1.09E-17
Protein tyrosine phosphatase, receptor type, J	*Ptprj*	-1.196	1.37E-03	6.61E-05

Genes estão representados em ordem descrescente (valores de log2FC).

Tabela 11: Vias de Sinalização alteradas nas lesões preneoplásicas iniciais de camundongos deficientes para mastócitos. Os dados foram obtidos por RNAseq e analisados no DAVID (Banco de dados de bioinformática).

Via	Status	Valor de *p*	Genes
Síndrome inflamatória intestinal	Aumentada	3.40E-08	*Smad3, H2-Aa, H2-Ab1, Il18, Il21r*
	Diminuída	3.40E-08	*Smad2, H2-Oa, Stat3, Tnf*
Interação receptor citocina-citocina	Aumentada	1.20E-07	*Amhr2, Ccl19, Ccr6, Cxcl13, Cxcl5, Cxcr5, Il18, Il21r, Ltb, Tnfrsf10b*
	Diminuída	1.20E-07	*Ccl2, Cxcl1, Cxcl2, Tnf*
Apresentação e processamento de antígenos	Aumentada	6.30E-06	*H2-Aa, H2-Ab1*
	Diminuída	6.30E-06	*Cd74, B2m, H2-M3, H2-Oa, H2-T24, Tnf*
Moléculas de adesão (CAMs)	Aumentada	9.80E-06	*H2-Aa, H2-Ab1, Madcam1, Selplg*
	Diminuída	9.80E-06	*Cd2, Cd22, H2-M3, H2-Oa, H2-T24, Ptprc*
Sinalização de quimiocinas	Aumentada	4.50E-05	*Ccl19, Ccr6, Cxcl13, Cxcl5, Cxcr5, Nfbia*
	Diminuída	4.50E-05	*Ccl2, Cxcl1, Cxcl2, Stat3*
Receptores NOD-like	Diminuída	1.30E-04	*Ccl2, Cxcl1, Cxcl2, Tnf*
Sinalização de DNA citosólico	Aumentada	2.20E-04	*Zbp1, Irf7, Il18, Nfkbia*
	Diminuída	2.20E-04	*Ddx58, Trex1*
Sinalização de TNF	Diminuída	2.50E-03	*Ccl2, Cxcl1, Cxcl2, Tnf*
Receptor de células B	Diminuída	3.10E-03	*Cd19, Cd22, Cd72, Cr2*
TGF-beta	Aumentada	3.80E-02	*Smad3, Amhr2*
	Diminuída	3.80E-02	*Smad2, Tnf*

Tabela 12: Análise de genes do RNAseq correlacionados de forma positiva ou negativa com Kit ou Nfkb1 de tumores colorretais esporádicos de animais $Kit^{W/sh}$.

Correlação positiva	Gene alvo	R^2	Valor de *p*
Kit	*Oas2*	0.9796	0.0012
Stat3	*Cxcl5*	0.9307	0.0079
Stat3	*Ccl2*	0.9257	0.0088
Kit	*Lgals9*	0.9209	0.0097
Stat3	*Irf7*	0.8860	0.0169
Stat3	*Ido1*	0.8782	0.0188
Kit	*Amhr2*	0.8670	0.0215
Kit	*Ccl2*	0.8663	0.0217
Stat3	*B2m*	0.8603	0.0232
Kit	*Irf7*	0.8458	0.0270
Kit	*Iftm3*	0.8451	0.0272
Kit	*Oasl1*	0.8199	0.0344
Kit	*Sp100*	0.7935	0.0426
Kit	*Stat3*	0.7813	0.0466
Kit	*Ceacam13*	0.7720	0.0498

Genes estão representados em ordem decrescente (valores de R^2). Os significados dos acrônimos estão descritos na Tabela 8.

Para validar esses resultados, foi realizado um transplante de medulla óssea (BMT) nos animais $Kit^{W/sh}$ e C57BL/6 antes de iniciar o protocolo de indução das PL iniciais (**Figura 21A-B**). Esse experimento revelou que o resgate da população de MCs nos camundongos $Kit^{W/sh}$ aumentou a taxa de proliferação cellular nos animais após as aplicações de AOM (*Mki67* [FC], Kit^{B6}BMT – 1,3±0,1; $Kit^{W/sh}$ BMT – 2,9±0,5; p =0,006). Interessantemente, o resgate da atividade dos MCs aumentou os níveis do marcador de MCs estromais (*Mcpt4*), e não alterou os marcadores de MCs epiteliais (*Mcpt1*) (**Figura 21C-D**). O resgate da população de MCs nos animias KO também foi acompanhado de uma redução na expressão gênica de *Cd11c* (**Figura 21E**). Por outro lado, não houve

alteração na expressão gênica para *Cd4* e *Cd8* (**Figura 21F-G**). Esses resultados demonstram que os MCs impactam e são impactados por outras reações imunes ao longo do desenvolvimento das etapas iniciais do CCR.

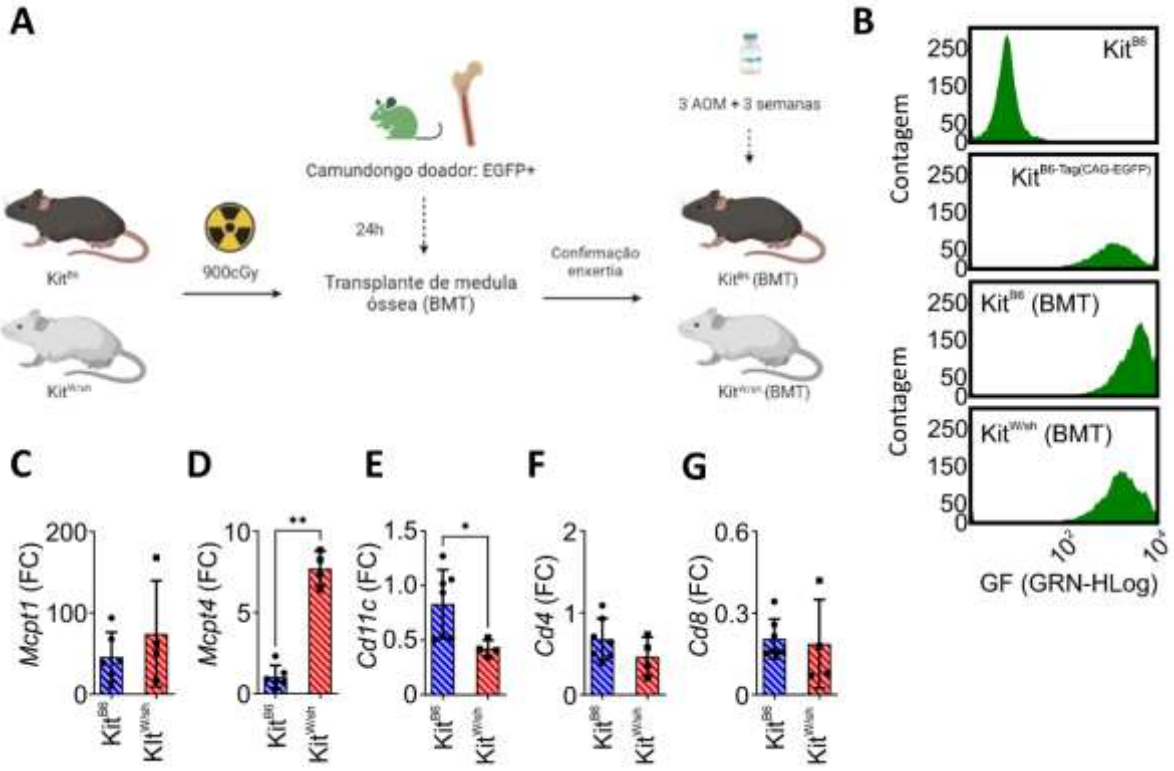

Figura 21: Os animais C57BL/6 (Kit^{B6}) e $Kit^{W/sh}$ (knockout para mastócitos (MCs)) receberam transplante de medula óssea (BMT) para validação dos resultados. **A**: Esquema ilustrativo do procedimento de BMT. Os animais receberam uma alta dose de irradiação ionizante (900cGy) e foram transplantados após 24 horas. O camundongo doador utilizado era EGFP+ para controle da enxertia. Após a confirmação do BMT, os animais receberam 3 doses de carcinógeno (AOM) e foram eutanasiados após 3 semanas. **B**: Histogramas representativos do protocolo de BMT realizado nos animais Kit^{B6} e $Kit^{W/sh}$. Os gráficos representam a intensidade de fluorescencia das células $EGFP^{+}$ (GF; eixo x) e a contagem cellular (eixo y). **C**-**G**: Análise da expressão gênica para Mcpt1 (n = 10; p >0,05), Mcpt4 (*p =0,004), Cd11c (*p =0,01), Cd4 (p >0,05), e Cd8 (p >0,05) nas amostras de cólon 3 semanas após a 3ª exposição ao AOM (procedimento realizado após a confirmação do BMT). Os dados estão representados como media ± desvio padrão. Os valores de p foram calculados usando o teste two-tailed Mann-Whitney's.

5.5 Mastócitos como alvo contra as lesões CCR

Os resultados até o momento demonstraram que a população de MCs pode promover eventos específicos em diferentes estágios do desenvolvimento do CCR. Com base nesses achados, foi utilizado o fármaco cromoglicato dissódico (CA; 25mg/kg/dia; WARGOVICH MJ, *et al*.; 1996) para inibir a atividade dos MCs em diferentes etapas do desenvolvimento das PL iniciais (3 doses de AOM e avaliação após 3 semanas do último *hit* de dano de DNA) (**Figura 22A**). Embora o tratamento com o CA não alterou os níveis de dano de DNA no tecido colônico (**Figura 22B**), a inibição da atividade dos MCs juntamente com as aplicações de AOM, aumentaram o número de PL (**Figura 22C; barra vermelha**). De forma oposta, a administração do CA somente nas semanas posteriores às administrações do AOM foi capaz de inibir a formação dessas lesões inicias (**Figura 22C; barra azul**). A inibição dos MCs concomitante ao AOM também aumentou o processo de proliferação celular (*Mki67*; **Figura 22D**), e os níveis da expressão de *Cd4*, *Foxp3*, *Cd8* (**Figura 22F-H**) e *Cd3* (*Cd3* [FC], AOM – 1,3±0,1; AOM+CA – 3,0±0,3; AOM-CA – 2,3±0,7; AOM vs AOM+CA, p =0,03). A expressão de *Cd11c* permaneceu inalterada (**Figura 22E**).

A análise do RNAseq desses grupos experimentais revelou que a inibição dos MCs com o CA provocou importantes alterações nos processos inflamatórios (**Figura 22I**; **Tabela 13** e **14**). Dentre as diversas alterações imunológicas, o tratamento com o CA posterior à exposição ao AOM inibiu os elementos chave para a via de adesão celular (p=1.2E-8; **Tabela 15**). A análise dos dados de RNAseq dessas amostras também revelou uma correlação positiva entre *Hey1* e os marcadores para células dendríticas (**Figura 22J**; **Tabela 16**). Esse

tratamento também alterou a correlação entre *Pax5* com os biomarcadores do sistema MHC (**Figura 22K**, **Tabela 16**). Já a inibição da atividade dos MCs concomitante à exposição ao carcinógeno (AOM+CA) reduziu a via de sinalização da apresentação de antígenos tumorais (p=1.2E-5; **Tabela 17**). Além disso, promoveu uma correlação positiva entre *Birc5* e *Pax5* com os biomarcadores de antígenos tumorais e células B e T (**Figura 22M**, **N**; **Tabela 18**).

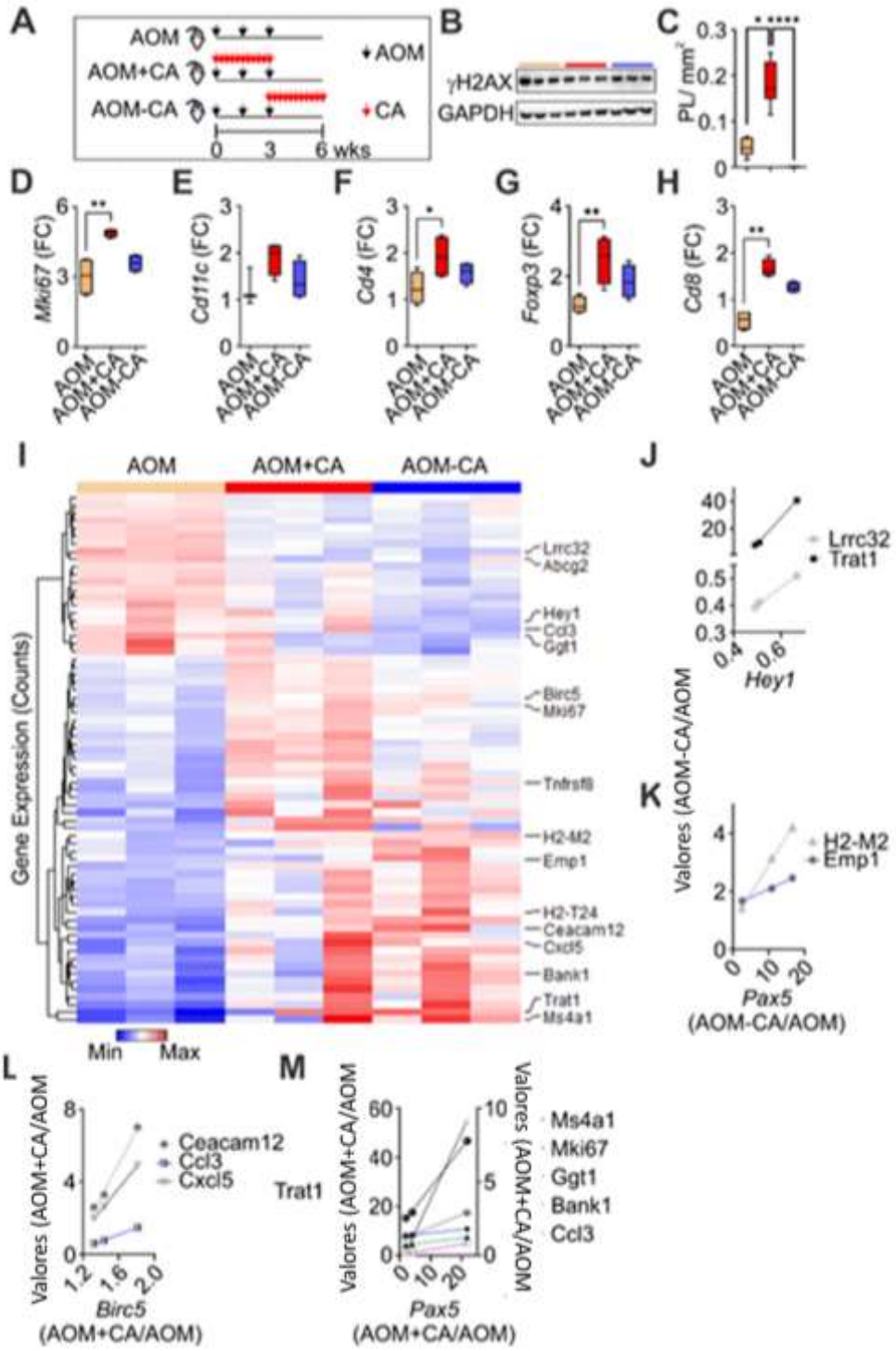

Figura 22: A atividade dos mastócitos (MCs) impacta o desenvolvimento das lesões iniciais do CCR e pode ser utilizada como alvo terapêutico. **A**: Linha do tempo demonstrando os diferentes grupos experimentais. As setas vermelhas indicam os tratamentos com cromoglicato dissódico (CA) e as setas pretas indicam as aplicações de carcinógeno (AOM) ao longo das 6 semanas de experimento. **B**: Análise de dano de DNA através de Western blotting para γH2AX e GAPDH nas amostras de cólon. **C**: Gráfico demonstrando o número de

lesões preneoplásicas no cólon dos animais que receberam os diferentes tratamentos (n = 24; *p =0,042, ****p <0,0001). **D-H**: Análise da expressão gênica para Mki67 (n = 24; *p <0,01; AOM vs AOM+CA), Cd11c (p >0,05), Cd4 (*p <0,05; AOM vs AOM+CA), Foxp3 (*p <0,01; AOM vs AOM+CA), e Cd8 (*p <0,01; AOM vs AOM+CA). Os valores de p foram calculados usando o teste ANOVA (Kruskal-Walli's). **I**: Heatmap gerado a partir dos dados de RNAseq indicam os genes diferencialmente expressos (n=12). **J-M**: Análise de regressão linear dos dados de RNAseq. **J-K** correspondem às correlações obtidas a partir da razão dos dados de AOM-CA por AOM. **M-N** correspondem às correlações obtidas a partir da razão dos dados de AOM+CA por AOM.

Tabela 13: Mastócitos podem ser alvos farmacológicos alterando o desenvolvimento de lesões preneoplásicas inicias no cólon (AOM vs AOM+CA). Os dados foram obtidos por RNAseq.

Nome	Acrônimo	log2FC	*p*-Adj	Valor de *p*
Genes regulados positivamente				
ATP-binding cassette, sub-family G (WHITE), member 2	*Abcg2*	0.94418	1.38E-03	1.15E-05
CDC14 cell division cycle 14A	*Cdc14a*	0.6245	7.49E-03	1.34E-04
Frizzled class receptor 2	*Fzd2*	0.54644	4.26E-02	1.87E-03
Caspase 1	*Casp1*	0.46988	4.26E-02	1.77E-03
Abhydrolase domain containing 2	*Abhd2*	0.46076	4.64E-02	2.10E-03
Nedd4 family interacting protein 1	*Ndfip1*	0.45897	1.95E-02	5.34E-04
Chemokine (C-X-C motif) ligand 12	*Cxcl12*	0.44735	2.23E-02	7.68E-04
Genes regulados negativamente				
Chemokine (C-C motif) ligand 19	*Ccl19*	-3.5472	6.04E-04	3.59E-06
Interleukin 13	*Il13*	-3.4608	4.91E-02	2.40E-03
T cell receptor associated transmembrane adaptor 1	*Trat1*	-2.8763	2.23E-02	7.54E-04
Membrane-spanning 4-domains, subfamily A, member 1	*Ms4a1*	-2.3658	4.91E-02	2.34E-03
Complement receptor 2	*Cr2*	-2.3086	4.90E-03	7.57E-05
CD19 antigen	*Cd19*	-1.9972	1.29E-03	9.18E-06
Carcinoembryonic antigen-related cell adhesion molecule 12	*Ceacam12*	-1.9074	1.53E-02	3.81E-04
Chemokine (C-X-C motif) ligand 5	*Cxcl5*	-1.794	8.22E-03	1.63E-04
Nitric oxide synthase 2, inducible	*Nos2*	-1.7376	4.26E-02	1.83E-03
Ubiquitin D	*Ubd*	-1.5843	3.95E-04	1.88E-06
CD22 antigen	*Cd22*	-1.5688	2.08E-02	5.93E-04
Dual specificity phosphatase 2	*Dusp2*	-1.5562	4.90E-03	7.42E-05
Granzyme A	*Gzma*	-1.5448	1.12E-02	2.40E-04

Suppressor of cytokine signaling 1	*Socs1*	-1.4443	1.38E-02	3.21E-04
Spi-B transcription factor	*Spib*	-1.4357	2.23E-02	7.69E-04
Chemokine (C-C motif) receptor 6	*Ccr6*	-1.3625	4.71E-02	2.19E-03
Zeta-chain associated protein kinase	*Zap70*	-1.1181	2.25E-02	8.01E-04
CD72 antigen	*Cd72*	-1.0918	3.63E-02	1.38E-03
Serine peptidase inhibitor, clade A, member 3N	*Serpina3n*	-1.0806	1.38E-02	3.27E-04
Proteasome subunit, beta type 9	*Psmb9*	-1.0404	1.91E-06	2.27E-09
Chemokine (C-C motif) ligand 5	*Ccl5*	-1.0292	1.58E-04	5.63E-07
Z-DNA binding protein 1	*Zbp1*	-0.964	3.60E-03	4.70E-05
Natural killer cell group 7 sequence	*Nkg7*	-0.8674	2.32E-03	2.21E-05
Transporter 1, ATP-binding cassette, sub-family B	*Tap1*	-0.8594	8.22E-03	1.66E-04
CD74 antigen	*Cd74*	-0.7109	4.47E-05	1.06E-07
Centromere protein F	*Cenpf*	-0.705	1.64E-02	4.28E-04
Histocompatibility 2, class II antigen A, β 1	*H2-Ab1*	-0.7036	6.03E-03	1.00E-04
Antigen identified by monoclonal antibody Ki 67	*Mki67*	-0.6661	2.39E-02	8.81E-04
Baculoviral IAP repeat-containing 5	*Birc5*	-0.6435	2.23E-02	7.02E-04
Histocompatibility 2, Q region locus 4	*H2-Q4*	-0.624	2.22E-02	6.60E-04
Histocompatibility 2, class II antigen A, α	*H2-Aa*	-0.5918	2.86E-03	3.40E-05
Histocompatibility 2, class II antigen E β	*H2-Eb1*	-0.5903	2.86E-03	3.20E-05
Histocompatibility 2, M region locus 3	*H2-M3*	-0.5693	3.97E-02	1.56E-03
Proteasome subunit, beta type 10	*Psmb10*	-0.4267	3.99E-02	1.61E-03

Genes estão representados em ordem descrescente (valores de log2FC).

Tabela 14: Mastócitos podem ser alvos farmacológicos alterando o desenvolvimento de lesões preneoplásicas inicias no cólon (AOM vs AOM→CA). Os dados foram obtidos por RNAseq.

Nome	Acrônimo	log2FC	*p*-Adj	Valor de *p*
Genes regulados positivamente				
γ-glutamyltransferase 1	*Ggt1*	2.69378	4.80E-02	2.10E-03
Chemokine (C-C motif) ligand 3	*Ccl3*	1.53774	4.76E-02	2.00E-03
Leucine rich repeat containing 32	Lrrc32	1.29369	2.59E-02	6.35E-04
CD36 antigen	*Cd36*	1.083	2.87E-02	7.37E-04
Interleukin 15	*Il15*	1.04341	4.90E-02	2.23E-03
Hairy/enhancer-of-split related with YRPW motif 1	*Hey1*	1.00961	4.76E-02	1.96E-03
Alanyl (membrane) aminopeptidase	*Anpep*	0.83758	3.15E-02	1.06E-03
Spondin 2. extracellular matrix protein	Spon2	0.80936	1.41E-02	1.97E-04
Cysteine-rich secretory protein LCCL domain containing 2	*Crispld2*	0.7985	2.38E-02	4.99E-04
CD34 antigen	*Cd34*	0.79222	1.23E-02	1.20E-04
Collagen. type III. alpha 1	*Col3a1*	0.61973	2.10E-02	3.91E-04
Frizzled class receptor 2	*Fzd2*	0.6149	2.16E-02	4.28E-04
Vascular endothelial growth factor C	Vegfc	0.59837	4.80E-02	2.13E-03
Acid phosphatase. Prostate	*Acpp*	0.59654	4.44E-02	1.76E-03
Insulin-like growth factor binding protein 5	*Igfbp5*	0.56027	3.11E-02	9.31E-04
Chemokine (C-X-C motif) ligand 12	*Cxcl12*	0.54604	6.64E-03	3.87E-05
CDC14 cell division cycle 14ª	*Cdc14a*	0.536	3.11E-02	9.68E-04
Genes regulados negativamente				
Chemokine (C-C motif) ligand 19	*Ccl19*	-4.111	4.56E-05	5.32E-08
T cell receptor associated transmembrane adaptor 1	Trat1	-3.2211	1.23E-02	1.58E-04
Cochlin	*Coch*	-3.1581	4.44E-02	1.74E-03

Carcinoembryonic antigen-related cell adhesion molecule 12	*Ceacam12*	-2.6061	2.15E-04	7.51E-07
Membrane-spanning 4-domains. subfamily A. member 1	Ms4a1	-2.5536	3.11E-02	1.01E-03
Chemokine (C-C motif) receptor 7	*Ccr7*	-2.3446	1.23E-02	1.56E-04
Complement receptor 2	*Cr2*	-2.3063	1.06E-02	7.38E-05
CD19 antigen	*Cd19*	-2.2856	1.40E-04	3.26E-07
Cystatin F (leukocystatin)	*Cst7*	-2.2784	4.95E-02	2.31E-03
Histocompatibility 2. class II antigen E β2	*H2-Eb2*	-1.8299	2.55E-02	5.95E-04
CD22 antigen	*Cd22*	-1.7512	1.23E-02	1.18E-04
Histocompatibility 2. O region α locus	*H2-Ao*	-1.7194	3.56E-02	1.25E-03
B cell scaffold protein with ankyrin repeats 1	*Bank1*	-1.5358	2.55E-02	5.92E-04
Chemokine (C-X-C motif) ligand 5	*Cxcl5*	-1.5001	4.42E-02	1.65E-03
Chemokine (C-C motif) receptor 6	*Ccr6*	-1.4843	2.91E-02	7.79E-04
Dual specificity phosphatase 2	*Dusp2*	-1.4269	1.70E-02	2.77E-04
Spi-B transcription factor	Spib	-1.4116	3.11E-02	9.09E-04
Nuclear receptor subfamily 4. group A. member 2	Nr4a2	-1.3889	1.55E-02	2.35E-04
Tumor necrosis factor receptor superfamily. member 8	Tnfrsf8	-1.2221	4.99E-02	2.40E-03
Histocompatibility 2. T region locus 24	*H2-T24*	-1.1875	4.42E-02	1.64E-03
Histocompatibility 2. M region locus 2	*H2-M2*	-1.1742	4.99E-02	2.44E-03
Z-DNA binding protein 1	Zbp1	-0.9897	6.06E-03	2.82E-05
Epithelial membrane protein 1	*Emp1*	-0.9596	1.92E-02	3.36E-04
Melanophilin	Mlph	-0.936	1.23E-02	1.56E-04
Protein tyrosine phosphatase. receptor type. C	Ptprc	-0.8487	3.11E-02	9.96E-04
Centromere protein F	*Cenpf*	-0.705	1.64E-02	4.28E-04
Histocompatibility 2, class II antigen A, β 1	*H2-Ab1*	-0.7036	6.03E-03	1.00E-04
Antigen identified by monoclonal antibody Ki 67	*Mki67*	-0.6661	2.39E-02	8.81E-04

Baculoviral IAP repeat-containing 5	*Birc5*	-0.6435	2.23E-02	7.02E-04
Histocompatibility 2, Q region locus 4	*H2-Q4*	-0.624	2.22E-02	6.60E-04
Histocompatibility 2, class II antigen A, α	*H2-Aa*	-0.5918	2.86E-03	3.40E-05
Histocompatibility 2, class II antigen E β	*H2-Eb1*	-0.5903	2.86E-03	3.20E-05
Histocompatibility 2, M region locus 3	*H2-M3*	-0.5693	3.97E-02	1.56E-03
Proteasome subunit, beta type 10	*Psmb10*	-0.4267	3.99E-02	1.61E-03

Genes estão representados em ordem descrescente (valores de log2FC).

Tabela 15: Vias de Sinalização alteradas nas lesões preneoplásicas iniciais de camundongos tratados farmacologicamente com cromoglicato dissódico (CA) após a indução carcinogênica (AOM vs AOM→CA). Os dados foram obtidos por RNAseq e analisados no DAVID (Banco de dados de bioinformática).

Via	*Status*	Valor de *p*	Genes
Moléculas de adesão celular	Diminuída	1.2E-8	*Cd34, H2-M2, H2-M3, H2-Oa, H2-T24, H2-Ab1, H2-Aa, H2-Eb1, Ptprc*
Rede immune intestinal para produção de IgA	Diminuída	6.9E-7	*H2-Oa, H2-Aa, H2-Ab1, H2-Eb1*
	Aumentada	6.9E-7	*Cxcl12, Il15*
Apresentação e processamento de antígenos	Diminuída	8.9E-7	*H2-M2, H2-M3, H2-Oa, H2-T24, H2-Ab1, H2-Aa, H2-Eb1*
Interação receptor citocina-citocina	Aumentada	4.8E-5	*Ccl3, Il15, Cxcl12*
	Diminuída	4.8E-5	*Ccl19, Ccr6, Ccr7, Cxcl5, Tnfrsf8*
Sinalização de quimiocinas	Aumentada	1.2E-3	*Ccl9, Ccl3, Cxcl12*
	Diminuída	1.2E-3	*Ccr6, Ccr7, Cxcl5*
Receptor de célula B	Diminuída	3.4E-2	*Cd19, Cd22, Cr2*

Os significados dos acrônimos estão descritos nas Tabelas 13 e 14.

Tabela 16: Genes positivamente correlacionados com Pax5 e Hey1 durante o desenvolvimento das lesões preneoplásicas iniciais de camundongos tratados com o cromoglicato dissódico (CA) após a exposição carcinogênica (AOM vs AOM→CA).

Correlação positiva	Gene alvo	R^2	Valor de *p*
Pax5	*H2-M2*	0.9995	0.0203
Hey1	*Trat1*	0.9992	0.0262
Pax5	*Emp1*	0.9979	0.0403
Hey1	*Lrrc32*	0.9977	0.0429

Genes estão representados em ordem decrescente (valores de R^2). Os significados dos acrônimos estão descritos nas Tabelas 11 e 12.

Tabela 17: Vias de Sinalização alteradas nas lesões preneoplásicas iniciais de camundongos tratados farmacologicamente com cromoglicato dissódico (CA) concomitante à indução carcinogênica (AOM vs AOM+CA). Os dados foram obtidos por RNAseq e analisados no DAVID (Banco de dados de bioinformática).

Via	*Status*	Valor de *p*	Genes
Apresentação e processamento de antígenos	Diminuída	1.2E-5	*Cd74, H2-M3, H2-Aa, H2-Ab1, H2-Eb1, Tap1*
Rede immune intestinal para produção de IgA	Diminuída	5.0E-4	*H2-Aa, H2-Ab1, H2-Eb1*
Síndrome inflamatória intestinal	Diminuída	1.4E-3	*H2-Aa, H2-Ab1, H2-Eb1, Il13*
Interação receptor citocina-citocina	Diminuída	1.9E-3	*Ccl19, Ccl5, Ccr6, Cxcl5, Il13*
Receptor de células B	Diminuída	2.2E-3	*Cd19, Cd22, Cd72, Cr2*
Moléculas de adesão celular (CAMs)	Diminuída	3.0E-3	*Cd22, H2-M3, H2-Aa, H2-Ab1, H2-Eb1*
Sinalização de quimiocinas	Diminuída	5.9E-3	*Ccl19, Ccl5, Ccr6, Cxcl5*
NF-kappa B	Diminuída	5.1E-2	*Ccl19, Zap70*

Os significados dos acrônimos estão descritos nas Tabelas 13 e 14.

Tabela 18: Genes positivamente correlacionados com Pax5 e Birc5 durante o desenvolvimento das lesões preneoplásicas iniciais de camundongos tratados com o cromoglicato dissódico (CA) concomitantemente à exposição carcinogênica (AOM vs AOM+CA).

Correlação positiva	Gene alvo	R^2	Valor de *p*
Pax5	*Ggt1*	1.0000	0.0030
Birc5	*Cxcl5*	0.9997	0.0165
Pax5	*Ccl3*	0.9997	0.0104
Pax5	*Ms4a1*	0.9991	0.0192
Pax5	*Mki67*	0.9989	0.0208
Birc5	*Ccl3*	0.9985	0.0346
Pax5	*Bank1*	0.9975	0.0317
Birc5	*Ceacam12*	0.9969	0.0498

Genes estão representados em ordem decrescente (valores de R^2). Os significados dos acrônimos estão descritos nas Tabelas 13 e 14.

A capacidade do CA de inibir o desenvolvimento das PL iniciais após a exposição ao AOM revelou que a inibição dos MCs poderia alterar o desenvolvimento dos tumores alográficos. Para testar está hipótese, os animais KitW/sh e C57BL6 (KitB6) receberam o implante subcutâneo das células MC38 (**Figura 23A**). A análise do crescimento em camundongos revelou que a deficiência para MCs ($Kit^{W/sh}$) foi capaz de bloquear o desenvolvimento dos tumores alográficos sem alterar a atividade proliferativa (**Figura 23B**, **D**). De forma interessante, a deficiência de MCs aumentou os níveis de expressão de *Cd4* e *Cd8* nos tumores alográficos (**Figura 23E, F**). Este aumento na expressão de *Cd8* foi acompanhado do infiltrado de linfócitos T CD8 (**Figura 23C**).

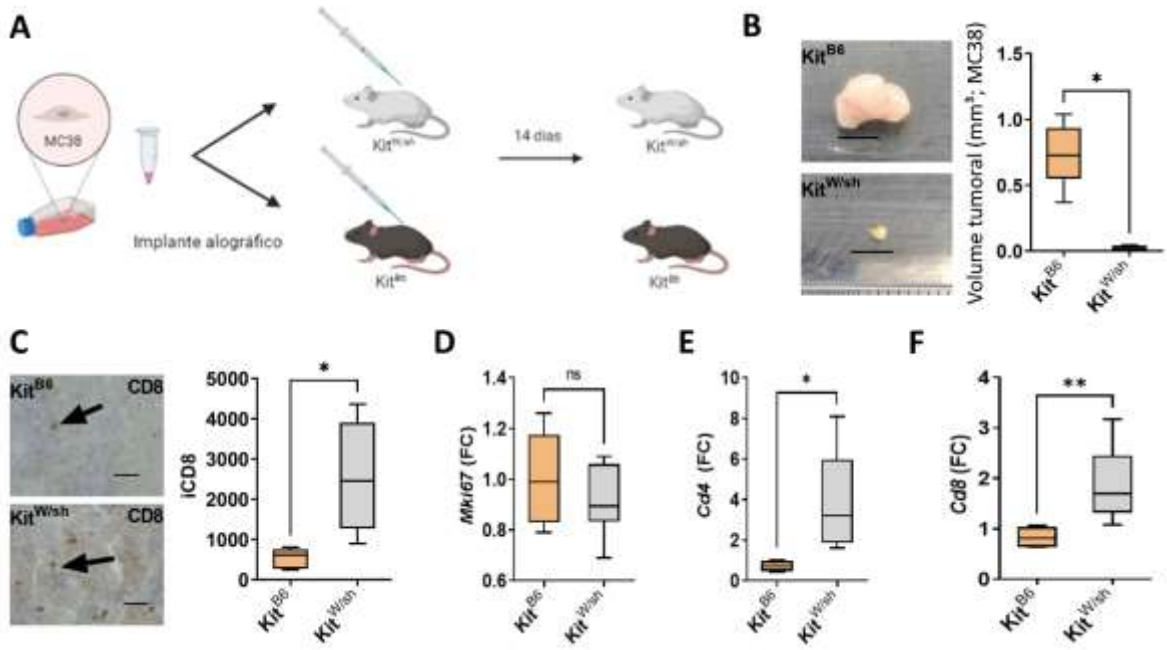

Figura 23: Atividade dos mastócitos (MCs) por ser usada como alvo terapêutico contra o CCR em camundongos. **A**: Ilustração demonstrando o desenho experimental. As células MC38 foram cultivadas e implantadas de forma subcutânea nos animais C57BL/6 (Kit^{B6}) e $Kit^{W/sh}$. Os tumores alográficos foram avaliados após 14 dias do implante. **B**: Imagens representativas dos tumores colorretais alográficos (Escala = 1 cm) de camundongos C56BL/6 (KitB6) e knockout para MCs (KitW/sh). O volume do tumor foi analisado após 14 dias do implante subcutâneo (n = 9; *p=0,01).**B**: Imagens representativas de células positivas para $CD8^+$ em reações de imunohistoquímica (IHC). A deficiência de MCs promoveu uma infiltração de células $CD8^+$ nos tumores (n = 9; *p=0,01). Escala = 0,3 µm. **C**-**E**: Análise da expressão gênica para Mki67 (n = 9; p>0,05),Cd4 (*p=0,01) e Cd8 (*p=0,009). Os dados estão representados como mediana, com os valores mais altos e mais baixos. O valor de p foi calculado usando o teste two-tailed Mann-Whitney.

A análise do RNAseq desses tumores alográficos desenvolvidos em animais $Kit^{W/sh}$ revelou que a deficiência de MCs regulou negativamente a via de sinalização dos proteossomos (p=8.6E-10) e positivamente os elementos chave para o processamento e apresentação de antígenos (p=3.1E-5) (**Figura 24A**; **Tabela 19** e **20**). Também foi possível observar que a deficiência de MCs promoveu uma correlação positiva entre *Batf* e *Maf* com os biomarcadores da

interação entre receptores de citocinas e regulação negativa com os marcadores do receptor de células T e macrófagos do tipo 2 (M2) (**Figura 24B-C**; **Tabela 21**).

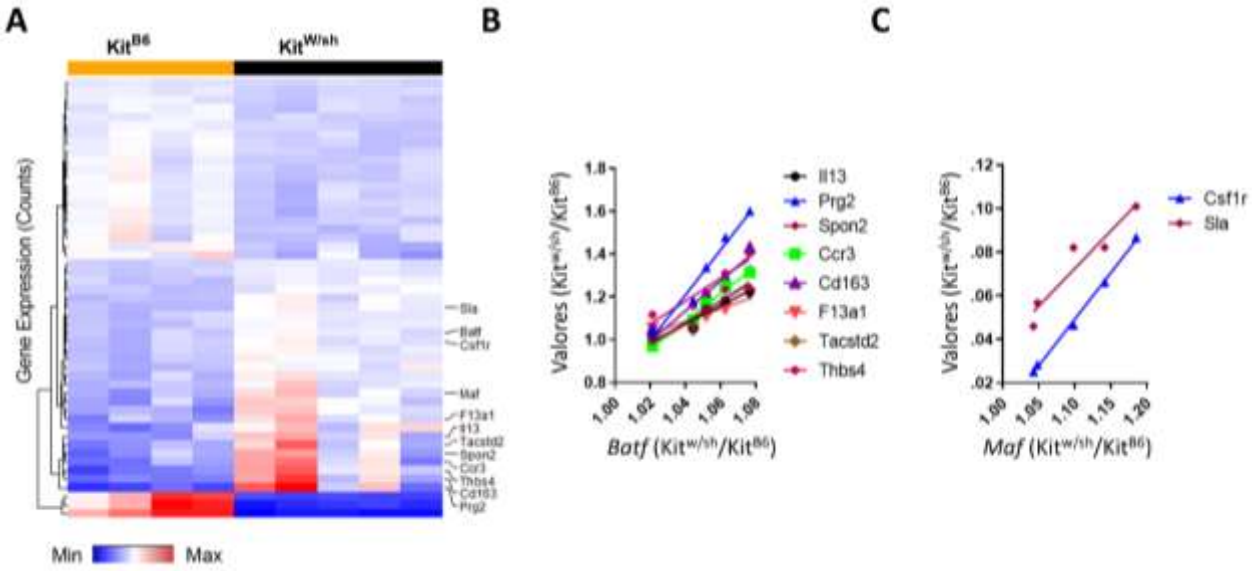

Figura 24: Análise de painel imune por RNAseq revelou 51 genes diferencialmente expressos entre os tumores alográficos desenvolvidos em camundongos C57BL/6 (Kit^{B6}) e knockout para mastósticos ($Kit^{W/sh}$). **A**: Heatmap gerado a partir dos dados de RNAseq indicando os genes diferencialmente expressos (n = 9). **C**, **D**: Análise de regressão linear dos dados coletados por RNAseq de tumores colorretais alográficos de camundongos C57BL/6 (Kit^{B6}) e knockout para MCs ($Kit^{W/sh}$).

Tabela 19: Lista de genes diferencialmente expressos em tumores colorretais alográficos desenvolvidos em animais C57BL/6 e $Kit^{W/sh}$. Os dados foram coletados por RNAseq e normalizados pelo pacote DESeq2 do software R.

Nome	Acrônimo	log2FC	*p*-Adj	Valor de *p*
Genes regulados positivamente				
RNA binding motif protein 3	*Rbm3*	8.39E+14	1.37E+14	1.77E+09
Cell adhesion molecule 1	*Cadm1*	8.37E+14	1.18E+14	3.38E+14
Proteasome (prosome, macropain) subunit, alpha type 2	*Psma2*	8.01E+14	7.53E+14	1.79E+14
Proteasome (prosome, macropain) subunit, beta type 7	*Psmb7*	7.85E+14	1.44E+14	4.74E+14
Proteasome (prosome, macropain) inhibitor subunit 1	*Psmf1*	7.58E+14	4.88E+14	3.53E+14
Caspase 1	*Casp1*	7.57E+14	1.63E+14	2.56E+09
Tryptase alpha/beta 1	*Tpsab1*	7.50E+14	1.07E+02	3.07E-01
Proteasome (prosome, macropain) subunit, beta type 5	*Psmb5*	7.13E+14	4.49E+14	2.70E+14
Carboxypeptidase A3, mast cell	*Cpa3*	6.78E+14	6.11E-26	8.74E-29
Interferon induced transmembrane protein 3	*Ifitm3*	6.53E+14	1.18E+14	3.31E+14
Tryptase beta 2	*Tpsb2*	6.49E+14	1.57E+03	6.75E+00
Proteasome (prosome, macropain) activator subunit 1 (PA28 alpha)	*Psme1*	6.39E+13	2.00E+14	8.02E+14
Proteasome (prosome, macropain) 26S subunit, non-atpase, 6	*Psmd6*	6.13E+14	3.25E+14	1.48E+14
Proteasome (prosome, macropain) subunit, alpha type 4	*Psma4*	5.97E+14	3.47E+14	1.74E+14
Lectin, galactose binding, soluble 9	*Lgals9*	5.50E+14	4.88E+14	3.10E+14
Chemokine (C-C motif) receptor 5	*Ccr5*	5.50E+14	1.58E+14	5.87E+14
Vascular cell adhesion molecule 1	*Vcam1*	5.10E+14	3.47E+14	1.71E+14
Macrophage scavenger receptor 1	*Msr1*	4.89E+14	4.88E+14	3.30E+14

Proteasome (prosome, macropain) activator subunit 2 (PA28 beta)	*Psme2*	4.84E+14	1.84E+14	7.09E+14
Catalase	*Cat*	4.55E+14	4.46E+14	2.62E+14
Regulator of G-protein signaling 2	*Rgs2*	4.49E+14	4.36E+14	2.43E+14
Hepatitis A virus cellular receptor 2	*Havcr2*	4.38E+14	4.88E+14	3.37E+13
Beta-2 microglobulin	*B2m*	3.92E+14	4.18E+14	2.16E+14
Chemokine (C motif) ligand 1	*Xcl1*	1.00E+14	2.56E+13	1.09E+14
Genes regulados negativamente				
Basic leucine zipper transcription factor, ATF-like	*Batf*	-5.87E+14	4.88E+14	3.56E+14
Chemokine (C-C motif) receptor 3	*Ccr3*	-2.03E+14	2.56E+13	1.10E+14
CD163 antigen	*Cd163*	-3.19E+12	5.71E+14	5.72E+08
CD5 antigen	*Cd5*	-1.27E+13	1.18E+14	3.34E+14
Class II transactivator	*Ciita*	-8.39E+14	1.91E+14	3.27E+09
C-type lectin domain family 10, member A	*Clec10a*	-1.99E+14	7.53E+14	1.83E+14
Colony stimulating factor 1 receptor	*Csf1r*	-6.71E+14	4.27E+14	2.32E+14
Dual specificity phosphatase 5	*Dusp5*	-8.73E+14	4.27E+14	2.32E+14
Coagulation factor XIII, A1 subunit	*F13a1*	-1.34E+14	1.46E+14	5.09E+14
Histocompatibility 2, class II antigen A, beta 1	*H2-Ab1*	-6.65E+14	9.83E+14	1.12E+09
Histocompatibility 2, class II antigen E beta	*H2-Eb1*	-8.66E+14	3.16E+14	2.71E+08
Histone cluster 1, h1c	*Hist1h1c*	-8.62E+14	3.25E+14	1.49E+14
Interleukin 13	*Il13*	-1.89E+14	4.88E+14	3.56E+14
K(lysine) acetyltransferase 6[a]	*Kat6a*	-5.78E+13	1.23E+14	3.78E+14
Leptin receptor overlapping transcript	*Leprot*	-8.37E+14	1.63E+14	2.50E+09
MAP-kinase activating death domain	*Madd*	-7.40E+14	4.44E+14	2.54E+14
Avian musculoaponeurotic fibrosarcoma oncogene homolog	*Maf*	-1.22E+14	1.46E+14	5.23E+13
Nuclear factor of kappa light polypeptide gene enhancer in B cells 1, p105	*Nfkb1*	-4.57E+14	6.19E+14	1.24E+13

Nudix (nucleoside diphosphate linked moiety X)-type motif 9	*Nudt9*	-6.03E+14	1.23E+14	3.87E+14
Programmed cell death 1 ligand 2	*Pdcd1lg2*	-1.56E+14	6.66E+14	1.43E+14
Proteoglycan 2, bone marrow	*Prg2*	-4.22E+14	2.19E+14	4.07E+09
Solute carrier family 15 (H+/peptide transporter), member 2	*Slc15a2*	-8.60E+13	1.67E+14	1.20E+08
Solute carrier family 7 (cationic amino acid transporter, y+ system), member 8	*Slc7a8*	-6.46E+14	4.83E+14	2.97E+14
Suppressor of cytokine signaling 1	*Socs1*	-5.57E+14	3.47E+14	1.65E+14
Spondin 2, extracellular matrix protein	*Spon2*	-1.61E+14	4.88E+14	3.28E+13
Tumor-associated calcium signal transducer 2	*Tacstd2*	-2.22E+13	4.88E+14	3.56E+14
Thrombospondin 4	*Thbs4*	-2.78E+14	3.85E+09	2.20E+07

Genes estão representados em ordem descrescente (valores de log2FC).

Tabela 20: Vias de Sinalização alteradas nos tumores colorretais alográficos desenvolvidos em camundongos C57BL/6 e $Kit^{W/sh}$. Os dados foram obtidos por RNAseq e analisados no DAVID (Banco de dados de bioinformática).

Via	*Status*	Valor de *p*	Genes
Proteossomo	Diminuída	8.6E-10	*Psmd6, Psme1, Psme2, Psmf1, Psma2, Psma4, Psmb5, Psmb7*
Processamento e apresenção de antígenos	Aumentada	3.1E-5	*Ciita, H2-Ab1, H2-Eb1*
	Diminuída	3.1E-5	*B2m, Psme1, Psme2*
Síndrome inflamatória intestinal	Aumentada	1.4E-4	*Maf, H2-Ab1, H2-Eb1, Il13, Nfkb1*
Móleculas de adesão celular	Aumentada	6.0E-3	*H2-Ab1, H2-Eb1, Pdcd 1lg2*
	Diminuída	6.0E-3	*Cadm1, Vcam1*
Interação receptor citocina-citocina	Diminuída	2.3E-2	*Ccr5, Xcl1*
	Aumentada	2.3E-2	*Ccr3, Csf1r, Il13*
Sinalização de quimiocinas	Diminuída	5.9E-2	*Xcl1, Ccr5*
	Aumentada	5.9E-2	*Ccr3, Nfkb1*

Os significados dos acrônimos estão descritos nas Tabelas 19.

Tabela 21: Genes positivamente correlacionados com Maf e Batf nos tumores colorretais alográficos desenvolvidos em camundongos C57BL/6 e $Kit^{W/sh}$. Os dados foram gerados através do RNAseq.

Correlação positiva	Gene alvo	R^2	Valor de *p*
Maf	*Csf1r*	0.9974	0.001538
Maf	*Sla*	0.9086	0.007703
Batf	*Ccr3*	0.9861	0.0007
Batf	*F13a1*	0.8799	0.0184
Batf	*Cd163*	0.8905	0.0159
Batf	*Il13*	0.9396	0.0064
Batf	*Prg2*	0.9637	0.0030
Batf	*Spon2*	0.9207	0.0097
Batf	*Tacstd2*	0.8619	0.05175
Batf	*Thbs4*	0.9101	0.04024

Os significados dos acrônimos estão descritos nas Tabelas 19.

Com base no resultado anterior, buscou-se explorar se a inibição dos MCs com o CA mimetizaria os achados dos animais deficientes para MCs (**Figura 23A**). No 7º dia após o implante das células de adenocarcinoma colônico, os animais começaram a ser tratados diariamente com salina ou CA (**Figura 25A).** O tratamento com o CA apresentou resultados positivos para a terapia contra o CCR, uma vez que foi capaz bloquear o desenvolvimento dos tumores colorretais alográficos ao longo do experimento (**Figura 25B**-**C**).

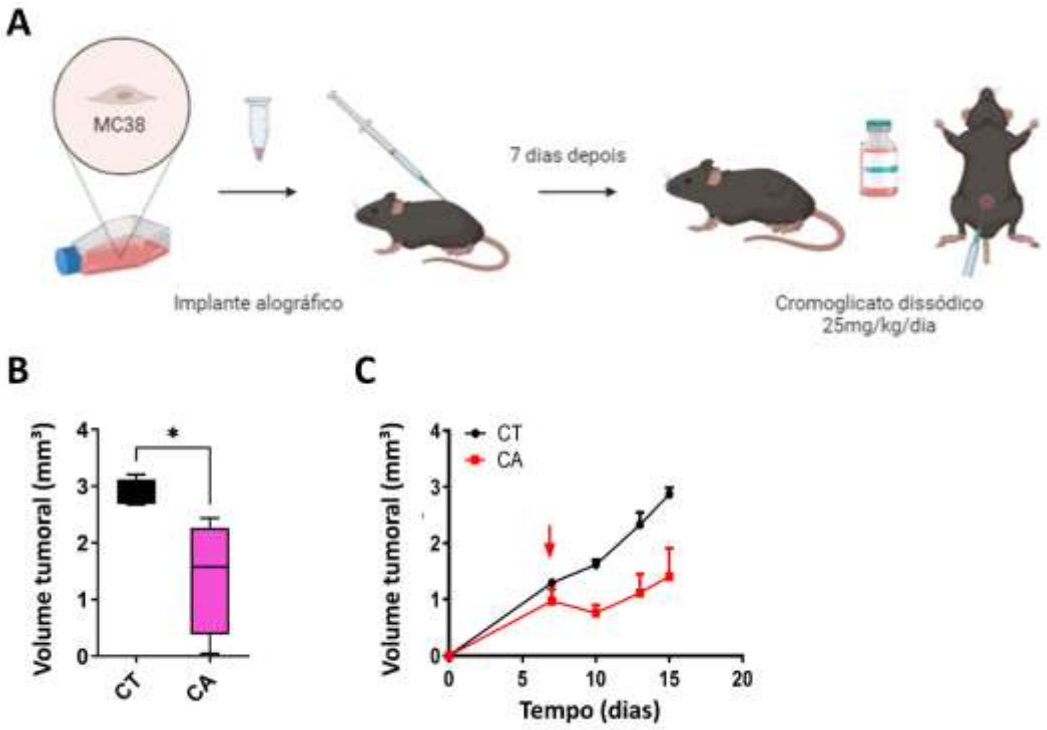

Figura 25: Modelo de implante alográfico para testar o potencial terapeutico dos mastócitos. **A**: Ilustração representativa do modelo de implante alográfico. As células de adenocarcinoma colorretal fora implantadas de forma subcutânea em camundongos C57BL/6, e após 7 dias, os animais foram tratados ou não com cromoglicato dissódico (CA; 25mg/kg/dia) por 17 dias. **B**: Volume tumoral (colorretal) relativo de camundongos tratados com cromoglicato dissódico (CA) e não tratados (CT) após 15 dias de experimento (n= 8; *p=0,02). **C**: Crescimento relativo dos tumores ao longo do tempo (eixo x). O experimento teve duração de 15 dias e foi dividido em grupo tratado com cromoglicato dissódico (CA 25mg/kg/dia; vermelho) e controle não tratado (CT; preto) (n = 8).

Para explorar o potencial terapêutico do bloqueio da atividade dos MCs, o CA foi testado para o tratamento contra tumores alográficos de melanoma.De forma semelhante ao tumor colorretal, o CA foi capaz de prevenir o crescimento das células de melanoma (**Figura 26A-B**). Além disso, o tratamento com CA nos tumores de melanoma reduziu a população de linfócitos T $CD8^{+}CD3^{+}$ sem alterar a população de MCs (**Figura 26C-E**).

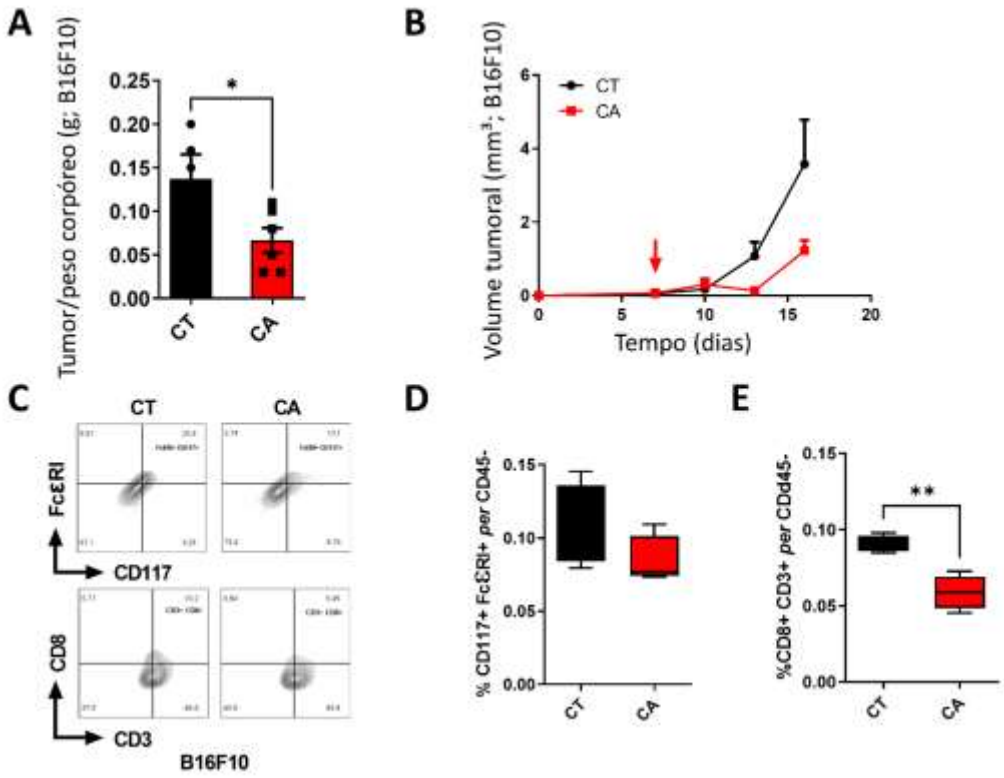

Figura 26: A atividade dos mastócitos (MCs) pode ser terapeuticamente explorada em casos de melamona em camundongos. **A**: Volume tumoral relativo (células de melanoma – B16F10) de camundongos tratados com cromoglicato dissódico (CA) e não tratados (CT) após 15 dias de experimento (n= 11; *p=0,04). **B**: Crescimento relativo entre os tumores com células de melanoma (B16F10) tratados com cromoglicato dissódico (CA; vermelho) e não tratados (CT; preto) por 15 dias (n = 11). **C**: Gráficos representativos das gates utilizadas na análise da citometria de fluxo para MCs ($CD45^+$ $CD117^+FcεRI^+$) e linfócitos T CD8 ($CD45^+$ $CD3^+CD8^+$) de células isoladas dos tumores B16F10. **D-E**: Gráficos demonstrando a porcentagem e MCs ($CD45^+CD117^+FcεRI^+$) e linfócitos T CD8 ($CD45^+CD8^+CD3^+$) isolados das amostras de tumor (n = 8; *p=0,002). Os dados estão mostrados como mediana, com os valores mais altos e mais baixos. Os valores de p foram calculados usando o teste t two-tailed Mann-Whitney.

A partir desses resultados, buscou-se investigar se a inibição da atividade dos MCs possuiria a mesma ação em tumores corretais alográficos em estágios mais avançados. Assim, os tumores começaram a ser tratados 14 dias após o implante, 7 dias posterior ao tratamento usual. Os tumores tratados com CA apresentaram uma diferença significativa do volume tumoral ao longo do experimento, sem alterar o peso corporal dos animais (**Figura 27A-C**). A redução

do volume tumoral foi acompanhada de um aumento da população de linfócitos T $CD8^+CD3^+$ sem alterar o número de MCs (**Figura 27D-F**).

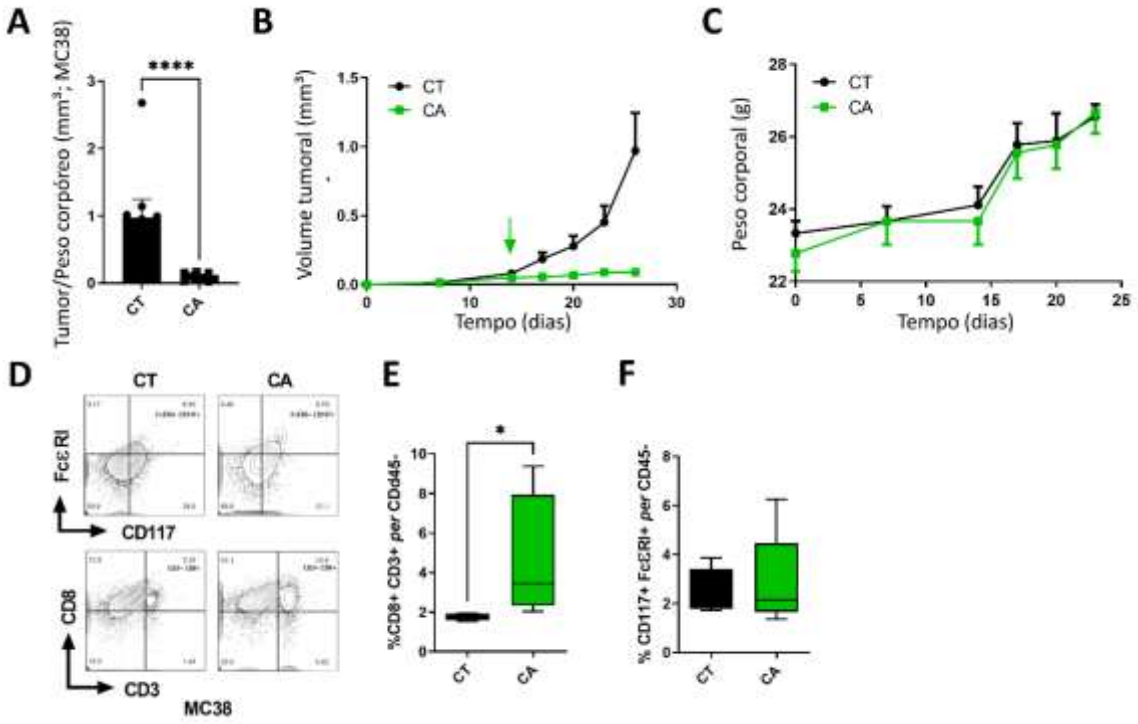

Figura 27: A atividade dos mastócitos pode ser usada como alvo da terapia contra os tumores colorretais em camundongos. **A**: Razão do volume tumoral relativo de tumores colorretais pelo peso corpóreo do animal tratado com CA ou não após 26 dias do início do experimento (n = 17; ****p<0,0001). **B**: Crescimento relativo dos tumores colorretais avançados em camundongos. O grupo tratado com cromoglicato dissódico (CA; 25mg/kg/dia; verde) apresentou menor crescimento quando comparado com o grupo não tratado (CT; preto) (n = 17; 26 dias de experimento). **C**: Gráfico demonstrando o acompanhamento do peso corporal dos animais durante os tratamentos. Os dados estão representados como média ± desvio padrão. **D**: Gráficos demonstrando a estratégia de gates para a avaliação do número de células $CD45^+$ $CD3^+CD8^+$ e $CD45^+FcεRI^+CD117^+$ isoladas de amostras de tumores colorretais avançados. **E**: Gráficos demonstrando a porcentagem de células $CD45^+$ $CD3^+CD8^+$ isoladas de amostras de tumores colorretais avançados (n = 8; *p=0,02). **F**: Gráfico demonstrando a porcentagem de MCs ($CD45^+CD117^+FcεRI^+$) isolada das amostras de tumor (n = 17). Os dados estão representados como mediana, com os valores mais baixos e mais altos e o desvio padrão. O valore de p foi calculado usando o teste t two-tailed Mann-Whitney.

Com o intuito de verificar se a atividade terapêutica do CA estava associada à uma maior atividade linfocitária, foi utilizado o modelo animal RAG-1. Os animais foram divididos em dois grupos: RAG-1 tratado com salina, e RAG-1 tratado com CA. Os tratamentos tiveram início 3 dias antes do implante e foram mantidos durante todo o experimento (**Figura 28A**). Neste modelo experimental, a inibição da atividade dos MCs em conjunto com uma resposta ineficiente dos linfócitos T, não foi capaz de conter o crescimento dos tumores (**Figura 28B-D**). Esses dados demonstram que a atividade do CA é dependente de uma resposta linfocitária efetiva.

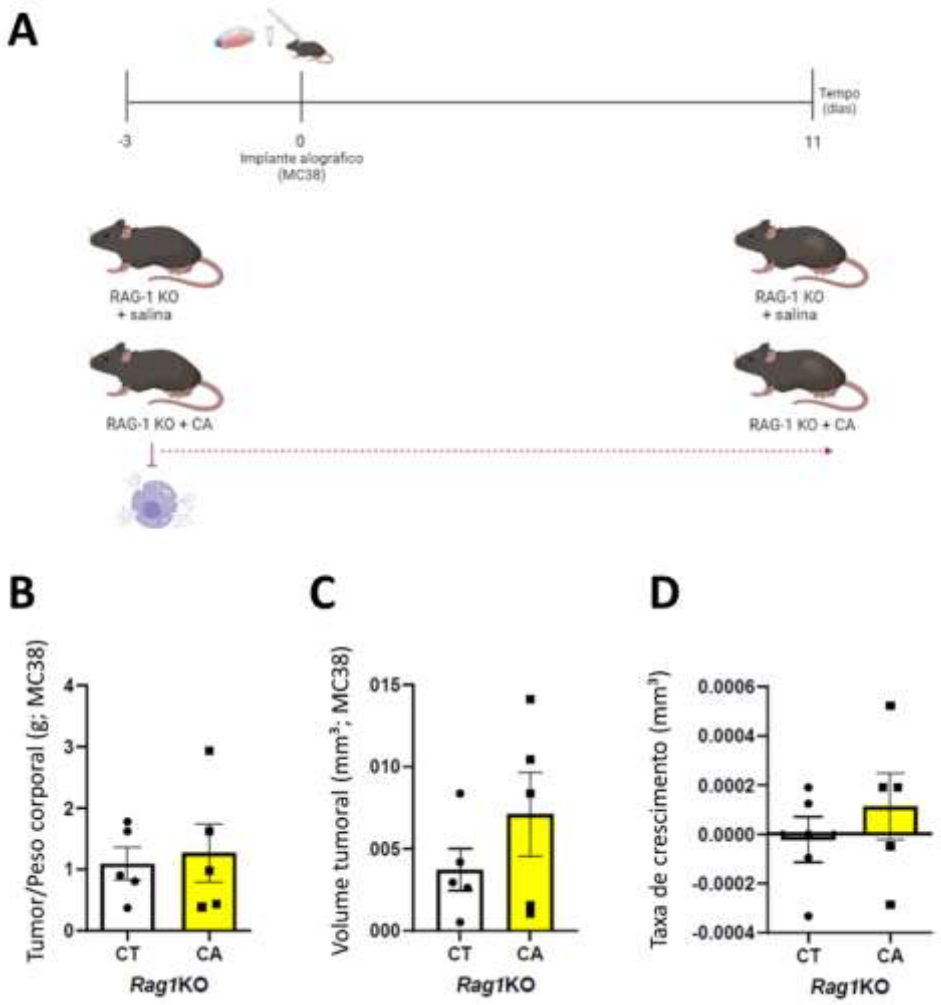

Figura 28: Inibição da atividade dos mastócitos (MCs) com o cromoglicato dissódico (CA) em animais sem linfócitos T maduros (RAG-1) não possui efeito anti-câncer. **A**: Desenho experimental utilizando o CA para criar um microambiente sem ativação dos MCs e dos linfócitos T. Os animais receberam o implante alográfico com as células de adenocarcinoma colorretal (MC38) após 3 dias do início do tratamento. Os tumores foram avaliados após 11 dias da data do implante. **B**: Relação entre o tamanho dos tumores pelo peso do animal não apresentou diferença entre os tratamentos aplicados (n=10; p > 0,05). **C**: Volume tumoral no 14º dia de experimento. O tratamento com CA não apresentou resultados significativos (n=10; p > 0,05). **D**: Taxa de crescimento calculada considerando o volume final e inicial do tumor, e o tempo de experimento (n=10; p > 0,05). Os dados estão representados como pontos individuais com média ± desvio padrão. Os valores de p foram calculados usando o two-tailed Mann Whitney's teste.

Esses dados demonstraram que a atividade dos MCs pode ser um alvo com potencial terapêutico. Assim, buscou-se investigar se o CA poderia ser

combinado com o tratamento padrão ouro no tratamento do CCR. O tratamento dos tumores alográficos com a combinação do 5-FU com o CA potencializou os efeitos do quimioterápico (**Figura 29A-B**). Além disso, essa combinação de tratamentos revelou ser comparável com a associação do 5-FU com os anticorpos imunoterápicos padrões (anti-Pd1) (**Figura 29C**). Todos esses resultados demonstram que os MCs impactam no desenvolvimento do CCR e podem ser importantes alvos farmacológicos para essa doença.

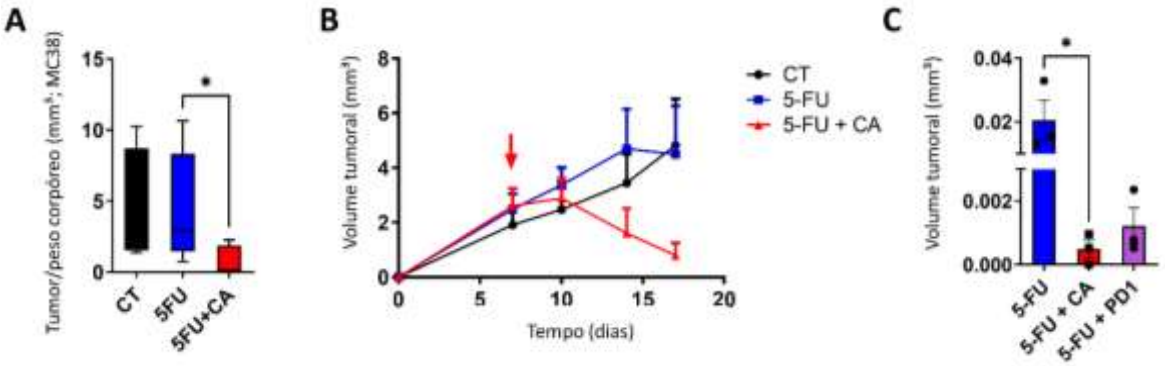

Figura 29: Associação do cromoglicato dissódico (CA) com o 5-FU potencializa o efeito do quimioterápico. **A**: Volume dos tumores tratados com 5-FU, não tratados e a combinação de 5-FU com CA por 17 dias (n = 15; *p=0,04). **B**: Crescimento relativo dos tumores ao longo do tempo (eixo x). O experimento teve duração de 17 dias e os grupos experimentais estão descritos como CT (preto); 5-FU (70mg/kg; azul); e combinação de 5-FU com CA (vermelho). Os dados estão representados como média ± desvio padrão. **C**: Volume dos tumores tratados com 5-FU, não tratados e a combinação de 5-FU com anti-Pd1 por 17 dias (n = 9; *p=0,04). Os dados estão representados com mediana, com os valores mais altos e mais baixos; ou pontos individuais com média ± desvio padrão (K). Os valores de p foram calculados usando o teste two-tailed Mann Whitney's test e o teste ANOVA (Kruskal-Wallis').

6. Discussão de resultados

6.1 A possível interação entre MCs e LTCs em pacientes diagnosticados com CRC

Os MCs são células imunes complexas e desenvolvem um papel essencial na homeostasia intestinal através da interação com a resposta imune inata e adaptativa (BULFONE-PAUS, BAHRI, 2015). Sua ação no desenvolvimento da carcinogênese já demonstrou ser benéfica ou prejudicial (RIGONI *et al*., 2015; TANAKA, ISHIKAWA, 2013; MEHDAWI *et al.*, 2016).

Inicialmente, nosso estudo investigou se diferentes níveis de biomarcadores de MCs seriam detectados entre um tecido colônico normal ou maligno em pacientes diagnosticados com CCR. Uma vez que os MCs podem estar ativados ou não em pacientes com CCR (MEHDAWI *et al.*, 2016; FLORES *et al.*, 2020; ZHAO *et al.*, 2022), nós decidimos desenvolver um estudo meta-analítico com mais de 600 casos de CRC para verificar sugestões previas de um possível eixo MC-LTC atuante no desenvolvimento de tumores (BODDULURI *et al.*, 2018; MAO *et al*. 2018). Nossos resultados confirmam que a ativação de MCs parece alterar a densidade da população tumoral de LTC. Isto revelou a existência de um possível eixo MC-LTC modulando o desenvolvimento de CRC.

Outros trabalhos também investigaram a ação dos MCs em amostras de pacientes com CCR. Tan e colabores relataram que uma baixa contagem de MCs se correlacionava com tumores mais invasivos, aumento do número de lesões metastáticas e redução da sobrevida dos pacientes em 5 anos (TAN *et al.*, 2005). Um outro estudo com 72 casos de CCR demonstrou que uma alta densidade de MCs poderia promover a sobrevida global e reduzir o risco de malignidade relacionados com a doença (MEHDAWI *et al*., 2016). Um estudo

randomizado com 82 casos de metástases hepáticas colorretais demonstrou que a densidade de MCs aumentava após a quimioterapia. Este estudo também demonstrou que números elevados de MCs se correlacionam com regressão tumoral e sobrevida livre de progressão (TANIS *et al*. 2015). Em trabalhos mais recentes, a avaliação dos MCs em amostras de sangue periférico de pacientes com CCR revelou que tais células não estavam associadas à progressão dos tumores (ZHAO *et al.*, 2022).

Por outro lado, Malfettone e colaboradores demonstraram que a redução na população de MCs melhora o prognóstico de pacientes com CCR, enquanto o aumento dessa densidade celular piora o desfecho da doença (MALFETTONE *et al*, 2013). Outro grupo de pesquisa também demonstrou que os mastócitos ativados estavam positivamente correlacionados com os tumores colorretais metastáticos (FLORES *et al.*, 2020).

Um trabalho publicado em 2018 demonstrou que, apesar de uma alta contagem de MCs estar associado à uma baixa sobrevida geral do paciente, a ação dessas células imunes era dependente do estágio do CCR (MAO *et al*., 2018). Mao e colaboradores também demonstraram uma possível associação entre a população de MCs com os linfócitos T CD8 infiltrados no tumor (MAO *et al*., 2018).

Assim, nosso trabalho confirma que um possível eixo MC-LTC pode modular o desenvolvimento da CRC.

6.2 A possível interação entre MCs e LTCs altera o desenvolvimento de tumores colorretais esporádicos ou aqueles associados à colite

Nossos experimentos demonstram que os MCs podem agir diretamente ou indiretamente sobre o desenvolvimento da tumorigênese colorretal. É interessante observar que após os MCs serem previamente expostos a células CCR, eles parecem reconhecer e induzir estas células malignas à morte. Contudo, nosso estudo também demonstra que os MCs podem agir diferencialmente durante o desenvolvimento da tumorigênese colorretal; ou seja, MCs podem promover o desenvolvimento de tumores colorretais relacionados a colite, ou agir de forma protetora contra aqueles eventos esporádicos. Estes eventos também impactaram o infiltrado linfocitário tumoral.

Um estudo prévio demonstrou que camundongos deficientes em MCs são menos suscetíveis à tumorigênese colorretal associada a inflamação (TANAKA *et al.*, 2013). Em contrapartida, outros pesquisadores observaram que a deficiência de MC aumentou o número de lesões malignas no cólon (RIGONI *et al.*, 2015). Um outro grupo de pesquisa relatou que a deficiência de MCs ($Kit^{W/w-v}$) reduziu a carga de tumores colorretais esporádicos (WEDEMEYER, GALLI, 2005). Porém, a cepa de camundongos utilizada em nosso trabalho ($Kit^{W/sh}$) e a cepa $Kit^{W/w-v}$ apresentam algumas diferenças apesar de ambas serem deficientes para MCs. Os animais $Kit^{W/w-v}$ apresentam outras alterações genéticas, como anemia profunda e infertilidade, resultando em outras alterações no MAT (GRIMBALDESTON *et al*., 2005). Essas alterações da linhagem $Kit^{W/w-v}$ interferem nos resultados, demonstrando efeitos opostos aos observados após a mesma exposição carcinogênica (**Figura 20** e **Figura suplementar 3**).

Utilizando o modelo animal $Apc^{Min/+}$, outros trabalhos corroboram com os resultados do CCR esporádico, demonstrando que a atividade dos MCs bloqueou o desenvolvimento dos tumores (SINNAMON *et al*., 2008; BODDULURI *et al.*, 2018). Bodduluri e colaboradores (2018) demonstraram também que a atividade dos MCs estava relacionada com o recrutamento de células T $CD8^+$ (BODDULURI *et al.*, 2018).

Nosso estudo biomolecular sugere que MCs podem alterar a ação de importantes fatores de transcrição e efetores da sinalização imune em tumores colorretais. Parece possível que alterações no fator de transcrição *Kit* influenciem a expressão de antígenos tumorais e a ativação imune. A atividade de MCs também parece influenciar as funções de *Nfkb1*, resultando na apresentação de uma assinatura gênica imuno regulatória que altera o desenvolvimento tumorigênico no cólon. Também é plausível que os MCs regulem a resposta inflamatória relacionada ao desenvolvimento tumoral, uma vez que sua deficiência promoveu uma ativação de receptores Toll-like e a sinalização induzida por Tnf-α. Assim, considerando que alterações na atividade de MCs promoveram um microambiente pró-inflamatório favorável para o desenvolvimento tumoral, é possível que modulações induzidas por MCs sobre a densidade de LTCs precedam a detecção macroscópica de lesões tumorais. Desta forma, não é possível desconsiderar a hipótese de que uma ativação imune exarcebada via uma desregulação da atividade de MCs possa induzir a exaustão de LTCs, facilitando o desenvolvimento tumoral.

Além disso, o aumento de IL6 e IL33 sob a ativação de *Nfkb1* podem estar relacionadas a um maior desenvolvimento de CCR (MAYWALD *et al*., 2015; DESAI *et al.*, 2016; HE *et al*., 2017). Sorrentino e colaboradores (2021)

demonstraram que a exaustão de células T, B e *natural killer* estão associados com um pior prognóstico para o paciente diagnosticados com CCR (SORRENTINO *et al*., 2021). Esses resultados, associados com a influência de *Kit* sobre a expressão de antígenos tumorais e a ativação imune sugerem que os MCs estejam envolvidos no processo de imune edição do câncer.

Os nossos resultados demonstram que o eixo MC-LTC não interfere diretamente neste estágio da carcinogênese colorretal esporádica, sendo possível que este module as etapas precedentes à detecção macroscópica de tumores. Assim, as alterações na população de MCs podem estar envolvidas na formação de um microambiente pró-inflamatório e no processo de seleção imune das células tumorais.

6.3 Diferentes fatores imunes podem atuar sobre o eixo MC-LTC durante o desenvolvimento inicial de lesões tumorigênicas no cólon

Uma vez que a deficiência de MCS não altera o infiltrado linfocitário em lesões tumorais esporádicas, nós investigamos se o eixo MC-LTC poderia ser modulado nas fases iniciais do desenvolvimento tumoral por meio de outros elementos imunológicos diversos. Desde que a exposição carcinogênica promoveu uma maior densidade de linfócitos CD8, a deleção de MHCI parece negativamente alterar esta população celular, apesar de promover um aumento na densidade de MCs. Do contrário, a ausência de MHCII reduziu a densidade de MCs sem alterar o infiltrado linfocitário. Surpreendentemente, a deleção do receptor da IL33 promoveu uma maior densidade de MCs, e reduziu a expressão de marcadores tumorais e de linfócitos CD8. Estas descobertas sugerem que o

desenvolvimento de eventos iniciais da tumorigênese colorretal requer a desregulação de diversos elementos da resposta imunológica, que por conseguinte, desregula a atividade do eixo MC-LTC facilitando a expansão de lesões pré-tumorais em tumorais macroscópicas.

Já havia sido relatado que os aloanticorpos anti-MHC são capazes de modular a atividade dos MCs (LE BOUTEILLER *et al*., 1976). Além disso, Malbec e colaborades (2016) descreveram mecanimos de inibição, da proliferação ativada por oncogenes em mastocitomas (MALBEC *et al.*, 2016). Eles revelaram que o reconhecimento de antígeno por IgG ligado a FcγR em MCs poderia mediar a trans-inibição sem a formação de co-agrupamento com a ligação de FcεRI a anticorpos IgE (MALBEC *et al.*, 2016). Adicionalmente, estudos demonstraram que os MCs parecem ser capazes de expressar MHCII em cultura de células, mas que o mesmo não ocorre no modelo *in vivo* (KAMBAYASHI et al., 2009; CHATTERJEE, GASHEV, 2014). Dudeck e colaborares (2017) demonstraram que as proteínas MHCII podiam ser transferidas entre células do sistema imune inato, como de uma célula dendrítica para os MCs, através de ligações semelhantes às sinapses (DUDECK *et al*., 2017).

Outros trabalhos também sugerem que Il33r seja necessário para o processo de expansão celular no CCR (O'DONNELL *et al*., 2016). A deficiência de Il33 também demonstrou inibir a carga tumoral, reduzir a densidade de MCs e a liberação de proteases e citocinas (MAYWALD *et al*., 2015; HE *et al*., 2017). Além disso, a sinalização de Il11 induzida por Il33 derivada de tumor é capaz de ativar os MCs e promover o desenvolvimento de câncer gástrico em camundongos. A deleção genética de Il33r também bloqueou o recrutamento

dependente de MCs e macrófagos que limitam o crescimento tumoral (EISSMANN *et al.*, 2019).

A atividade de MCs também demonstrou ser modulada de acordo com os estímulos inflamatórios presentes no estroma reativo à iniciação da tumorigênese colorretal. Os resultados dos animais imunodeficientes sugerem que a atividade imune inflamatória pode estimular o desenvolvimento das lesões precursoras do CCR esporádico por meio da pressão seletiva. A redução nos níveis de IL6 também demonstrou modular a atividade dos MCs e influenciar no desenvolvimento das PLs.

Desai e colaboradores corroboram com estes resultados demonstrando que a liberação de Il6 expande a população de MCs e promove sua reatividade (DESAI *et al.*, 2016). Também já havia sido demonstrado que o estímulo de Il6 nas células $CD34^{+}$ de cordão umbilical foi responsável por aumentar os níveis de quimase e histamina (CONTI *et al.*, 2002). Tanto no CRC humano quanto na polipose de camundongos, os MCs demonstraram ser capazes de modular e serem modulados pelos níveis de Il10, Il6, Il17 e Il2, pelos quais recrutam os linfócitos Treg promovendo o desenvolvimento do CRC (BLATNER *et al*., 2010).

Assim, nós demonstramos por meio de diversos modelos animais, que alterações em diversos componentes imunes podem atuar no eixo MC-LTC e alterar o desenvolvimento das lesões precursoras do CCR. De forma adicional, nossos resultados reforçam a hipótese de que os MCs estão envolvidos no processo de imune seleção das células tumorais.

6.4 Ação do eixo MC-LTC sobre o desenvolvimento de lesões tumorigênicas inicias

Nossos experimentos demonstram que a ação de MCs sobre a densidade do infiltrado linfocitário e sobre o desenvolvimento de lesões tumorigênicas iniciais é independente da indução de dano genômico. De fato, os MCs parecem ser essenciais para a promoção de um ambiente pró-inflamatório, facilitando assim a expansão de lesões tumorigênicas. Neste contexto, é interessante observar que a desregulação da atividade de MCs facilitou um maior infiltrado linfocitário e maior densidade de lesões pré-tumorais. Estas observações parecem ocorrer em conjunto com alterações no processamento de antígenos tumorais e resposta inflamatória exacerbada. É possível que este processo esteja relacionado a ação de *Stat3*, *Cxcl5*, *Ccl2* e *Ido1*, uma vez que isso facilitaria a expansão de células tumoralmente transformadas (BOLLRATH *et al*. 2009; THAKER *et al.*, 2013). Esses resultados, reforçam a hipótese de que as alterações na atividade dos MCs influenciam no processo de imune edição do câncer através do reconhecimento e proliferação das células tumorais.

A inibição da atividade dos MCs em diferentes pontos da tumorigênese torna mais clara os efeitos do eixo MC-LTC sobre este processo. Este experimento permitiu demonstrar que MCs podem agir de forma protetora durante o dano de DNA indutor das lesões tumorigênicas. Nesta condição, os animais apresentaram um aumento no desenvolvimento das CAB, infiltrado linfocitário, e alterações do processamento e apresentação de antígenos tumorais. A ação imune regulatória de MCs também fica evidente por meio da redução das vias de sinalização de citocinas, quimiocinas, células B, e Nfkb. Isto

ocorreu em conjunto com alterações no fator de transcrição *Pax5* como ponto determinante para modulações sobre marcadores de proliferação celular (*Mki67*) e células B (*Ms4a1* e *Bank1*), sugerindo uma maior atividade da resposta imune humoral.

Em contrapartida, a inibição da ação dos MCs após a indução do dano de DNA teve efeitos anti-tumorigênicos. Apesar de não alterar as populações de linfócitos ou os níveis de dano de DNA, o tratamento com o CA foi capaz de impedir completamente o desenvolvimento das lesões tumorigênicas iniciais. Dentre os processos envolvidos na proteção contra o desenvolvimento das CABs, a inibição da atividade dos MCs demonstrou alterar positivamente as moléculas de adesão celular no epitélio colônico.

Esses dados demonstram que os MCs são elementos importantes na manutenção do equilíbrio da ativação e recrutamento da reposta imune, afetando diretamente o risco de desenvolvimento do CCR.

6.5 O eixo MC-LTC pode ser um alvo terapêutico anti-tumoral em potencial.

A deficiência dos MCs promoveu a infiltração das populações de linfócitos T CD4 e CD8, em conjunto com a inibição do desenvolvimento dos tumores alográficos. O aumento da expressão de *Batf*, fator de transcrição envolvido na regulação da resposta Th17 (PUNKENBURG *et al*., 2016), estava associada com genes marcadores de células dendríticas (*F13a1* e *Tactsd2*). Além disso, o aumento da expressão de *Maf* associado com o aumento de *Sla* e *Csf1r* também

indicam que, a ausência dos MCs promoveu uma maior ativação dos linfócitos Treg por meio da ação das células dendríticas. Uma vez que a atividade dos MCs promoveu o crescimento dos tumores alográficos, a inibição da atividade dessas células poderia ser uma boa alterativa terapêutica contra o CCR.

A inibição farmacológica da atividade dos MCs com o CA bloqueou o crescimento dos tumores alográficos de melanoma e CCR em diferentes estágios de desenvolvimento. A menor taxa de crescimento foi acompanhada de uma maior infiltração e atividade dos linfócitos T CD8. Esses resultados reforçam a idéia de que a atividade de MCs altera diretamente o efeito de LTCs sobre células e lesões tumorais. Essa hipótese foi explorada mecanisticamente em animais imunodeficientes sob uma inibição farmacológica da atividade de MCs. Este experimento demonstrou que sem a atividade de LTCs a inibição de MCs não reduziu o desenvolvimento de CCR.

A partir destas observações, aventamos a hipótese de que a inibição da atividade de MCs poderia ser combinada com um quimioterápico. A investigação desta hipótese demonstrou que a inibição farmacológica da atividade de MCs poderia potencializar a atividade anti-tumoral de um quimioterápico a um nível comparável ao de um imunoterápico anti-PD1.

A inibição farmacológica da atividade de MCs já havia sido demonstrada uma estratégia anti-tumoral eficazes contra diferentes tipos de tumores (ARUMUGAM, RAMACHANDRAN, LOGSDON, 2006; WROBLEWSKI, 2017). A inibição dos MCs tem sido combinada com gencitabina, diminuindo o crescimento de tumores de pâncreas (ARUMUGAM, RAMACHANDRAN, LOGSDON, 2006). Outros trabalhos também demonstraram que a associação terapia antiangiogênica com a inibição da atividade dos MCs para tratar linfoma

murino e câncer de pâncreas (WROBLEWSKI, 2017). Somasundaram e colaboradores (2021) demonstraram que a combinação de fármacos que inibem a atividade de MCs melhoram os resultados da terapia anti-PD1 em melanomas (SOMASUNDARAM *et al;* 2021).

Esses fatos ilustram que MCs são alvos terapêuticos que podem potencializar os efeitos anti-tumorais das terapias atuais. No entanto, uma limitação potencial do presente estudo é que, além de inibir a atividade dos MCs, o CA já foi relatado afetando a sinalização e a sobrevivência das células cancerígenas, bem como outras respostas imunes (MOTAWI *et al*., 2014; PUZZOVIO *et al;* 2022). Contudo, o fato de o CA bloquear o crescimento de tumores CCR em desenvolvimento com ou sem a combinação com o 5-FU fortalece a ideia de que pacientes com CCR podem se beneficiar de terapias baseadas nos MCs.

7. Conclusão

Este trabalho demonstrou que os MCs são células imunes de ação complexa, porém modulável durante o desenvolvimento do CCR (**Figura 30**). Sua ação é dependente do estímulo indutor da tumorigenese, podendo ela potencializar a resposta inflamatória criando um microambiente propício para o crescimento do tumor, ou ser responsável pela ativação equilibrada da resposta imune diante do dano de DNA inicial. Foi possível explorar e demonstrar que a atividade dos MCs altera e é alterada por modificações na resposta imune, fato que afeta diretamente o eixo MC-LTC. Por meio dos diversos modelos experimentais, foi demonstrado que a atividade dos MCs reduziu a infiltração das células T CD8, e que esta relação é inversamente proporcional.

Essa relação entre MCs e linfócitos T CD8 ganha maior peso na terapia contra o CCR. O bloqueio da atividade dos MCs demonstrou ser uma terapia alternativa eficaz contra o CCR promovendo um maior infiltrado de células T CD8. A associação do CA com um quimioterápico padrão também demonstrou ter efeitos benéficos no tratamento do CCR esporádico.

Dessa forma, demonstramos que o eixo MC-LTC altera significativamente o desenvolvimento de CCR e tem o potencial de ser explorado terapeuticamente contra esta malignidade.

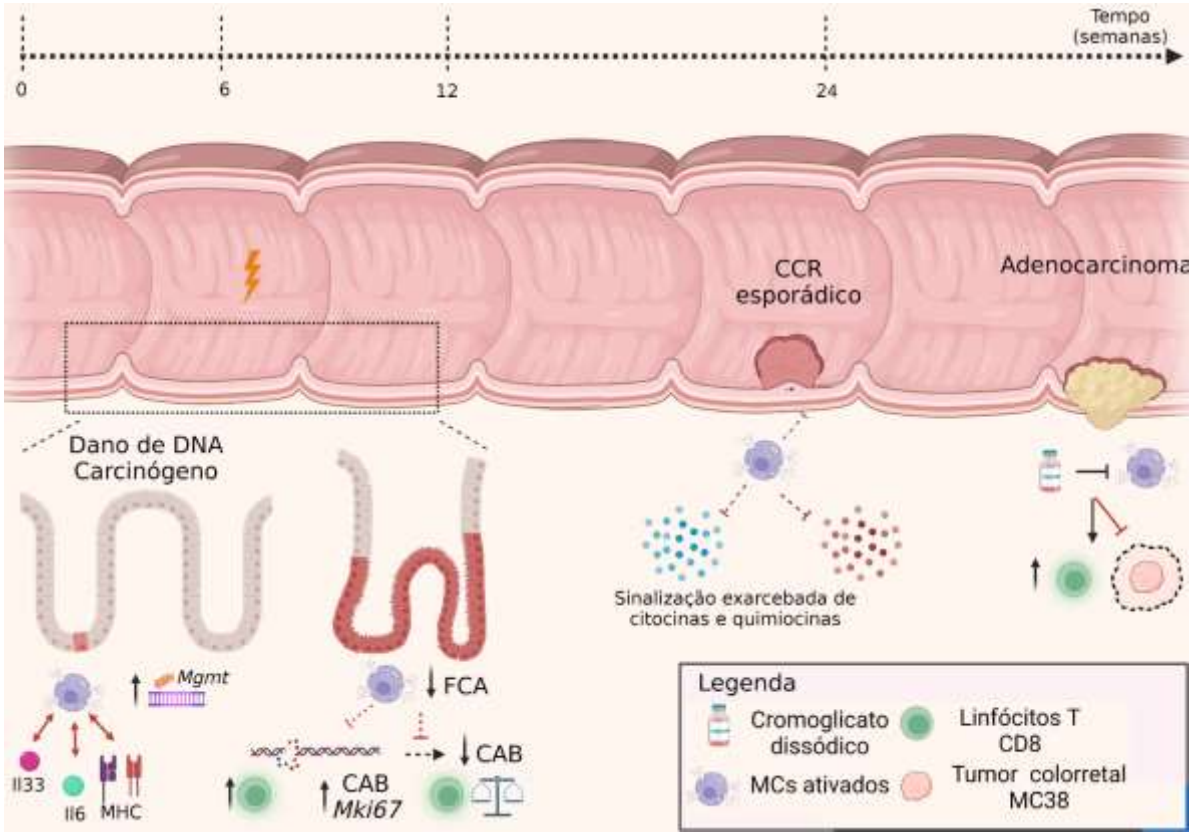

Figura 30: Ilustração demonstrando a ação dos mastócitos (MCs) durante toda a etapa de desenvolvimento do câncer colorretal (CCR). A ação dos MCs demonstrou associação com a atividade dos linfócitos T CD8, além de ser um potencial alvo terapêutico contra o CCR.

8. Referências bibliográficas

ABONIA JP, *et al*. Constitutive homing of mast cell progenitors to the intestine depends on autologous expression of the chemokine receptor CXCR2. **Blood**; v.105, n.11, p: 4308-13; 2005. Disponível em: <https://www.ncbi.nlm.nih.gov/pmc/articles/PMC1895025/>.

ABRAHAM SN, ST JOHN AL. Mast cell-orchestrated immunity to pathogens. **Nat Rev Immunol**. V.10, n.6, p.440-452, Jun 2010. Disponível em: < https://www.ncbi.nlm.nih.gov/pmc/articles/PMC4469150/>.

ALBERT-BAYO M, *et al*. Intestinal Mucosal Mast Cells: Key Modulators of Barrier Function and Homeostasis. **Cells**; v.8; n.2; p:135; 2019. Disponível em: < https://pubmed.ncbi.nlm.nih.gov/30744042/>.

ARAI H, *et al*. The Landscape of Alterations in DNA Damage Response Pathways in Colorectal Cancer. **Clin Cancer Res**., v. 27, n.11, p: 3234-3242; 2021. Disponível em: < https://aacrjournals.org/clincancerres/article/27/11/3234/671475/The-Landscape-of-Alterations-in-DNA-Damage>.

ARUMUGAM T, RAMACHANDRAN V, LOGSDON CD. Effect of cromolyn on S100P interactions with RAGE and pancreatic cancer growth and invasion in mouse models. **J Natl Cancer Inst**., v.98, p:1806-18; 2006. Disponível em: < https://www.ncbi.nlm.nih.gov/pmc/articles/PMC4461034/>.

BARKER, N. et al. Crypt stem cells as the cells-of-origin of intestinal cancer. **Nature,** v. 457, n. 7229, p. 608-11, Jan 2009. ISSN 1476-4687. Disponível em: < https://www.ncbi.nlm.nih.gov/pubmed/19092804 >.

BARNES PJ. Histamine receptors in the lung. **Agents Actions Suppl,** v. 33; p103-122, 1992. Disponível em: < https://pubmed.ncbi.nlm.nih.gov/1647126/>.

BAUMGARTH, N. The double life of a B-1 cell: Self-reactivity selects for protective effector functions. **Nat. Rev. Immunol,** v.11, 34-46; 2011. Disponível em: https://www.nature.com/articles/nri2901>.

BIRD RP. Observation and quantification of aberrant crypts in the murine colon treated with a colon carcinogen: preliminary findings. **Cancer Lett**, v.37, n(2), p:147-51; 1987. Disponível em: < https://www.sciencedirect.com/science/article/pii/0304383587901571?via=ihub >.

BIRD RP. Role of aberrant crypt foci in understanding the pathogenesis of colon cancer. **Cancer Lett**; v.93; n(1); p:55-71; 1995. Disponível em: < https://www.sciencedirect.com/science/article/pii/030438359503788X?via%3Dihub>.

BISCHOFF, S.C. Role of mast cells in allergic and non-allergic immune responses: Comparison of human and murine data. **Nat. Rev. Immunol**., v.7, p93:104; 2007. Disponível em: < https://www.nature.com/articles/nri2018>.

BLATNER NR, *et al*. In colorectal cancer mast cells contribute to systemic regulatory T-cell dysfunction. **Proc Natl Acad Sci**, v.107, p:6430-5; 2010. Disponível em: < https://www.ncbi.nlm.nih.gov/pmc/articles/PMC2851977/>.

BLOKZIJL, F. et al. Tissue-specific mutation accumulation in human adult stem cells during life. Nature 538, 260–264 (2016).

BODDULURI SR, *et al*. Mast Cell-Dependent CD8(+) T-cell Recruitment Mediates Immune Surveillance of Intestinal Tumors in Apc(Min/+) Mice. **Cancer Immunol Res**., v.6, p:332-347; 2018.

BOOTH C., POTTEN C.S. Gut instincts: thoughts on intestinal epithelial stem cells. **J Clin Invest**. 2000;105(11):1493-1499. Disponível em : <https://doi.org/10.1172/JCI10229 >.

BOWCUTT, R. *et al*. Heterogeneity across the murine small and large intestine. **World J Gastroenterol,** v. 20, n. 41, p. 15216-32, 2014. ISSN 2219-2840. Disponível em: < https://www.ncbi.nlm.nih.gov/pubmed/25386070 >.

BULFONE-PAUS S, BAHRI R. Mast Cells as Regulators of T Cell Responses. **Front Immunol**; v.6:394; 2015. Disponível em: < https://www.ncbi.nlm.nih.gov/pmc/articles/PMC4528181/>.

CAMUSSI, G.; *et al*. Exosomes/microvesicles as a mechanism of cell-to-cell communication. **Kidney Int.**, v.78, p:838–848; 2010. Disponível em: < https://pubmed.ncbi.nlm.nih.gov/20703216/>.

CHATTERJEE V, GASHEV AA. Mast cell-directed recruitment of MHC class II positive cells and eosinophils towards mesenteric lymphatic vessels in adulthood and elderly. **Lymphat Res Biol**., v.12,p:37-47; 2014. Disponível em: < https://www.ncbi.nlm.nih.gov/pmc/articles/PMC3961842/>.

CHENG H, LEBLOND CP. Origin, differentiation and renewal of the four main epithelial cell types in the mouse small intestine. V. Unitarian Theory of the origin of the four epithelial cell types. **Am J Anat**., v.141, n. 4, p. 537-61; 1974. Disponível em < https://pubmed.ncbi.nlm.nih.gov/4440635>.

CONTI P, *et al*. Interleukin-6 and mast cells. **Allergy Asthma Proc**., v.23; p:331-5; 2002. Disponível em: < https://pubmed.ncbi.nlm.nih.gov/12476543/>.

CORRIGAN, F., *et al*. Neurogenic inflammation after traumatic brain injury and its potentiation of classical inflammation. **J Neuroinflammation** 13, 264; 2016. Disponível em: <https://doi.org/10.1186/s12974-016-0738-9>.

DE PALMA M, BIZIATO D, PETROVA TV. Microenvironmental regulation of tumour angiogenesis. **Nat Rev Cancer.**, v.17, n.8, p:457–474; 2017. Disponível em: <https://doi.org/10.1038/nrc.2017.51>.

De ROBERTIS M, *et al*. The AOM/DSS murine model for the study of colon carcinogenesis: From pathways to diagnosis and therapy studies. **J Carcinog**. 2011; 10:9. Disponível em: < https://pubmed.ncbi.nlm.nih.gov/21483655/>.

DESAI A, *et al*. IL-6 promotes an increase in human mast cell numbers and reactivity through suppression of suppressor of cytokine signaling 3. **J Allergy Clin Immunol.**, v.137; p:1863-1871 e6; 2016. Disponível em: < https://www.ncbi.nlm.nih.gov/pmc/articles/PMC4899186/>.

DETORAKI A, *et al*. Vascular endothelial growth factors synthesized by human lung mast cells exert angiogenic effects. **J Allergy Clin Immunol**., v. 123, n.5, p:1142–1149; 2009. Disponível em: <https://doi.org/10.1016/j.jaci.2009.01.044>.

DINARVAND P, *et al*. Familial Adenomatous Polyposis Syndrome: An Update and Review of Extraintestinal Manifestations. **Arch Pathol Lab Med**., v.143, n.11, p:1382-1398. May, 2019. Disponível em: < https://pubmed.ncbi.nlm.nih.gov/31070935/>.

DONG H, *et al*. Suppression of Brain Mast Cells Degranulation Inhibits Microglial Activation and Central Nervous System Inflammation. **Mol Neurobiol**.; v.54, n.2; p:997-1007; 2017. Disponível em: < https://pubmed.ncbi.nlm.nih.gov/29792730/>.

DUDECK J, *et al*. Mast cells acquire MHCII from dendritic cells during skin inflammation. **J Exp Med**, v214, p:3791-3811, 2017. Disponível em: < https://pubmed.ncbi.nlm.nih.gov/29084819/>.

DVORAK HF. Tumors: wounds that do not heal. Similarities between tumor stroma generation and wound healing. **N Engl J Med**; v.315, p:1650–1659, 1986. Disponível em: <https://pubmed.ncbi.nlm.nih.gov/3537791/>.

DVORAK, AM, *et al*. IgE-mediated anaphylactic degranulation of isolated human skin mast cells. **Blood**, v.77, p: 569–578; 1991. Disponível em: < https://www.sciencedirect.com/science/article/pii/S0006497120830687?via%3 Dihub>.

DVORAK, AM, *et al*. Ultrastructural evidence for piecemeal and anaphylactic degranulation of human gut mucosal mast cells in vivo. **Int. Arch. Allergy Immunol.**, v.99, 74–83; 1992. Disponível em: < https://pubmed.ncbi.nlm.nih.gov/1483068/>.

DWYER DF, BARRETT NA, AUSTEN KF; Immunological Genome Project Consortium. Expression profiling of constitutive mast cells reveals a unique identity within the immune system. **Nat Immunol**.. v.17, n.7, p:878-87; Jun 2016. Disponível em: < https://pubmed.ncbi.nlm.nih.gov/27135604/>.

EHRLICH P: Beiträge zur Kenntniss der Anilinfärbungen und ihrer Verwendung in der mikroskopischen Technik *Archiv. f. mikrosk. Anat*, v.13, p.263–277; 1877.

EISSMANN MF, *et al*. IL-33-mediated mast cell activation promotes gastric cancer through macrophage mobilization. **Nat Commun**., v.10; p:2735; 2020. Disponível em: < https://pubmed.ncbi.nlm.nih.gov/31227713/>.

ELLIS H, MAHADEVAN V. Anatomy of the caecum, appendix and colon. Surgery (Oxford), v32, n4, p155-158; 2014. Disponível em: <https://www.sciencedirect.com/science/article/pii/S0263931914000210>.

FLORES DE LOS RIOS PA, *et al*. Differential expression of mast cell granules in samples of metastatic and non-metastatic colorectal cancer in patients. Acta Histochem, v.122, n.7, p:151618; 2020. Disponível em: < https://pubmed.ncbi.nlm.nih.gov/33066840/>.

FODDE R. The APC gene in colorectal cancer. **Eur J Cancer**, v.38, n.7, p:867-71; 2002. Disponível em: < https://pubmed.ncbi.nlm.nih.gov/11978510/>.

FORSYTHE P. Mast Cells in Neuroimmune Interactions. **Trends Neurosci.**; v.42, n.1; p:43-55; 2019. Disponível em: <https://pubmed.ncbi.nlm.nih.gov/30293752/>.

FUKATA M, Chen A, Vamadevan AS, Cohen J, Breglio K, Krishnareddy S, et al. Toll-like receptor-4 promotes the development of colitis-associated colorectal tumors. **Gastroenterology**, v.133, p:1869–1881, 2007. Disponível em: < https://pubmed.ncbi.nlm.nih.gov/18054559/>.

GALLI SJ, GRIMBALDESTON M, Tsai M. Immunomodulatory mast cells: negative, as well as positive, regulators of immunity. **Nat Rev Immunol**., v. 8, n.6, p:478-86, 2008. Disponível em: < https://pubmed.ncbi.nlm.nih.gov/18483499/ >

GEHART H, CLEVERS H. Tales from the crypt: new insights into intestinal stem cells. **Nat Rev Gastroenterol Hepatol**; 16, n. 1, p. 19-34; 2019. Disponível em: < https://pubmed.ncbi.nlm.nih.gov/30429586/>.

GENDRIN, C., *et al*. Mast cell chymase decreases the severity of group B Streptococcus infections. **J. Allergy Clin. Immunol**.; v.142, p.120–129; 2018. Disponível em: < https://www.ncbi.nlm.nih.gov/pmc/articles/PMC5847414/>.

GOLDBERG MT, BLAKEY DH, BRUCE WR. Comparison of the effects of 1,2-dimethylhydrazine and cyclophosphamide on micronucleus incidence in bone marrow and colon. **Mutat Res**; v.109, n(1); p:91-8; 1983. Disponível em: <https://www.sciencedirect.com/science/article/pii/0027510783900982?via%3Dihub>.

GORZALCZANY Y, *et al*. Mast cells are directly activated by contact with cancer cells by a mechanism involving autocrine formation of adenosine and autocrine/paracrine signaling of the adenosine A3 receptor. **Cancer Lett**; v.397; p23–32; 2017. Disponíel em: < https://doi.org/10.1016/j.canlet.2017.03.026>.

GRIMBALDESTON MA, *et al*. Mast cell-deficient W-sash c-kit mutant Kit W-sh/W-sh mice as a model for investigating mast cell biology in vivo. **Am J Pathol**., n.167; p:835-48; 2005. Disponível em: < https://www.ncbi.nlm.nih.gov/pmc/articles/PMC1698741/>.

GRONKE, K., *et al*. Interleukin-22 protects intestinal stem cells against genotoxic stress. **Nature,** v.566, p. 249–253; 2019. Disponível em: <https://doi.org/10.1038/s41586-019-0899-7>.

GROSCHWITZ KR, *et al*. Mast cells regulate homeostatic intestinal epithelial migration and barrier function by a chymase/Mcpt4-dependent mechanism. **Proc Natl Acad Sci**; v.106, n(52); p:22381-6; 2009. Disponível em: < https://www.pnas.org/doi/abs/10.1073/pnas.0906372106>.

GRUJIC M, *et al*. The combined action of mast cell chymase, tryptase and carboxypeptidase A3 protects against melanoma colonization of the lung. **Oncotarget**, v.8, n(15), p:25066-25079; 2017. Disponível em: < https://www.ncbi.nlm.nih.gov/pmc/articles/PMC5421910/>.

GRUJIC M, *et al*. Protective role of mouse mast cell tryptase Mcpt6 in melanoma. **Pigment Cell Melanoma Res**, v.33, n4, p:579-590; 2020. Disponível em: < https://www.ncbi.nlm.nih.gov/pmc/articles/PMC7317424/>.

GUO X, *et al.* Mast cell tryptase contributes to pancreatic cancer growth through promoting angiogenesis via activation of angiopoietin-1. **Int J Mol Sci,** v.17, n.6; p:834; 2016. Disponível em: < https://doi.org/10.3390/ijms17060834>.

GUPTA K, HARVIMA IT. Mast cell-neural interactions contribute to pain and itch. **Immunol Rev**; v.282(1):168-187; 2018. Disponível em: < https://www.ncbi.nlm.nih.gov/pmc/articles/PMC5812374/>.

HAGEMAN, JH *et al*. Intestinal Regeneration: Regulation by the Microenvironment. **Dev Cell**, v.54, n. 4, p. 435-446; 2020. Disponível em: < https://pubmed.ncbi.nlm.nih.gov/32841594/>.

HE Z, *et al*. Epithelial-derived IL-33 promotes intestinal tumorigenesis in Apc (Min/+) mice. **Sci Rep**., v.7; p:5520; 2017. Disponível em: < https://pubmed.ncbi.nlm.nih.gov/28710436/>.

HEICHLER C, *et al*. STAT3 activation through IL-6/IL-11 in cancer-associated fibroblasts promotes colorectal tumour development and correlates with poor prognosis. **Gut**; v.69, n(7):1269-1282; 2020. Disponível em: <https://gut.bmj.com/content/69/7/1269.long>.

HEINIMANN K. Erblicher Darmkrebs: Klinik. Hereditary Colorectal Cancer: Clinics, Diagnostics and Management]. **Ther Umsch**, v.75, n.10, p:601-606; 2018. Disponível em: < https://pubmed.ncbi.nlm.nih.gov/31232663/ >.

HILL SJ. Multiple histamine receptors: properties and functional characteristics. **Biochem Soc Trans**., v. 20, p:122–5; 1992. Disponível em: < https://pubmed.ncbi.nlm.nih.gov/1321744/ >.

HUGENHOLTZ F, DE VOS WM. Mouse models for human intestinal microbiota research: a critical evaluation. **Cell Mol Life Sci**; v.75, n(1); p:149-160; 2018. Disponível em: < https://www.ncbi.nlm.nih.gov/pmc/articles/PMC5752736/>.

HUMPHRIES A, Wright NA. Colonic crypt organization and tumorigenesis. **Nat Rev Cancer**, 8, n. 6, p.415-24; 2008. Disponível em: < https://pubmed.ncbi.nlm.nih.gov/18480839/ >.

ITZKOWITZ SH, YIO X. Inflammation and cancer IV. Colorectal cancer in inflammatory bowel disease: the role of inflammation. **Am Physiol J Gastrointest Liver Physiol**; 287:G7–17; 2004. Disponível em: <https://pubmed.ncbi.nlm.nih.gov/15194558/>.

JASSO GJ, *et al*. Colon stroma mediates an inflammation-driven fibroblastic response controlling matrix remodeling and healing. **PLoS Biol**. ; v.20(1):e3001532; 2022.

JEN J, *et al*. Molecular determinants of dysplasia in colorectal lesions. **Cancer Res**; v.54, n(21); p:5523-6; 1994. Disponível em: < https://aacrjournals.org/cancerres/article/54/21/5523/500546/Molecular-Determinants-of-Dysplasia-in-Colorectal>.

KAMBAYASHI T, KORETZKY GA. Proximal signaling events in Fc epsilon RI-mediated mast cell activation. **J Allergy Clin Immunol**; v.119(3):544-52; quiz 553-4; 2007. Disponível em: < https://www.jacionline.org/article/S0091-6749(07)00179-0/fulltext>.

KAMBAYASHI T, *et al*. Inducible MHC class II expression by mast cells supports effector and regulatory T cell activation. **J Immunol**., v.182, p:4686-95, 2009. Disponível em: < https://www.ncbi.nlm.nih.gov/pmc/articles/PMC2922395/>.

KANAGARATHAM C, *et al*. IgE and IgG Antibodies as Regulators of Mast Cell and Basophil Functions in Food Allergy. **Front Immunol**; v.11:603050; 2020. Disponível em: < https://www.ncbi.nlm.nih.gov/pmc/articles/PMC7759531/>.

KANNEN V, *et al*. Antiproliferative effects of fluoxetine on colon cancer cells and in a colonic carcinogen mouse model. **PLoS One**; v;7(11):e50043. Erratum in: **PLoS One**. 2013;8(6); 2012. Disponível em: < https://journals.plos.org/plosone/article?id=10.1371/journal.pone.0050043>

KANNEN V, *et al*. Colon preneoplasia after carcinogen exposure is enhanced and colonic serotonergic system is suppressed by food deprivation. **Toxicology**; v.312; p:123-31; 2013. Disponível em: < https://www.sciencedirect.com/science/article/abs/pii/S0300483X13002333?via%3Dihub>.

KARARLI TT. Comparison of the gastrointestinal anatomy, physiology, and biochemistry of humans and commonly used laboratory animals. **Biopharm Drug Dispos**; v16(5):351-80; 1995. Disponível em: < https://pubmed.ncbi.nlm.nih.gov/8527686/>.

KEUM, N.; GIOVANNUCCI, E. Global burden of colorectal cancer: Emerging trends, risk factors and prevention strategies. **Nat. Rev**. Gastroenterol. Hepatol., v.16, p. 713–732, 2019. Disponível em: < https://www.nature.com/articles/s41575-019-0189-8>.

KINZLER KW, VOGELSTEIN B. Lessons from hereditary colorectal cancer. **Cell**; v.87(2):159-70; 1996. Disponível em: < https://www.cell.com/fulltext/S0092-8674(00)81333-1>.

KITAMURA Y, GO S, HATANAKA K: Decrease of mast cells in W/Wv mice and their increase by bone marrow transplantation. **Blood**; v.52; p: 447– 452; 1978. Disponível em: < https://www.sciencedirect.com/science/article/pii/S000649712068288X>.

KNIGHT PA, *et al*. Aberrant mucosal mast cell protease expression in the enteric epithelium of nematode-infected mice lacking the integrin alphavbeta6, a transforming growth factor-beta1 activator. **Am J Pathol**; v.171(4):1237-48; 2007. Disponível em: < https://ajp.amjpathol.org/article/S0002-9440(10)62387-5/fulltext>.

KOLLER BH, *et al.* Normal development of mice deficient in beta 2M, MHC class I proteins, and CD8+ T cells. **Science**.; v.248; p:1227-30; 1990. Disponível em: < https://www.science.org/doi/10.1126/science.2112266?cookieSet=1>.

KOMI, D.E.A., REDEGELD, F.A. Role of Mast Cells in Shaping the Tumor Microenvironment. **Clinic Rev Allerg Immunol**, v.58, p:313–325; 2020. Disponível em: < https://pubmed.ncbi.nlm.nih.gov/31256327/>.

KONDO, N. et al. DNA damage induced by alkylating agents and repair pathways. **J Nucleic Acids,** v. 2010, p. 543531, Nov 2010. ISSN 2090-021X. Disponível em: < https://www.ncbi.nlm.nih.gov/pubmed/21113301 >.

JUTEL M, AKDIS CA. Histamine as an immune modulator in chronic inflammatory responses. **Clin Exp Allergy,** v.37; p:308–10, 2007. Disponível em: < doi:10.1111/j.1365-2222.2007.02666.x>.
LIU, C.; CRAWFORD, J.M. O trato gastrointestinal. IN: ROBBINS & COTRAN. Patologia – Bases patológicas das doenças. Elsevier, 2005.

LE BOUTEILLER P, *et al*. An ultrastructural study of two different responses of mouse mast cells to transplantation antibodies directed against the same transplantation antigens. **Eur J Immunol**., v.6, p:326-32, 1976. Disponível em: < https://pubmed.ncbi.nlm.nih.gov/186271/>.

LYNCH HT, CHAPELLE A. Hereditary Colorectal Cancer. **N Engl J Med**; v.348, p919-932; 2003. Disponível em: < https://pubmed.ncbi.nlm.nih.gov/12621137/>.

LYON MF, GLENISTER PH. A new allele sash (Wsh) at the W-locus and a spontaneous recessive lethal in mice. **Genet Res**, v.39, n.3, p:315-22; 1982. Disponível em: < https://pubmed.ncbi.nlm.nih.gov/7117838/>.

MALBEC O, *et al*. Trans-inhibition of activation and proliferation signals by Fc receptors in mast cells and basophils. **Sci Signal**., v.9, p:126; 2016. Disponível em: < https://www.science.org/doi/abs/10.1126/scisignal.aag1401?doi=10.1126/scisignal.aag1401>.

MALFETTONE A, *et al*. High density of tryptase-positive mast cells in human colorectal cancer: a poor prognostic factor related to protease-activated receptor 2 expression. **J Cell Mol Med**., v.17; p:1025-37; 2013. Disponível em: < https://www.ncbi.nlm.nih.gov/pmc/articles/PMC3780541/>.

MARTIN FL, Morais CLM, Sakita JY, Uyemura SA, Kannen V. Age-Related and Gender-Related Increases in Colorectal Cancer Mortality Rates in Brazil Between 1979 and 2015: Projections for Continuing Rises in Disease. **J Gastrointest Cancer**; v.52(1):280-288; 2021. Disponível em: < https://www.ncbi.nlm.nih.gov/pmc/articles/PMC7900022/>.

MARTINEZ, R.; *et al*. Anatomia do Tupo Digestivo, p. 61 -88. In: **Sistema Digestório: Integração Básico-Clínica**. São Paulo: Blucher, 2016. Disponível em: < https://hi.br1lib.org/book/13147716/467ff6>.

MAO Y, *et al*. Low tumor infiltrating mast cell density confers prognostic benefit and reflects immunoactivation in colorectal cancer. **Int J Cancer**., v.143; p:2271-2280; 2018. Disponível em: < https://pubmed.ncbi.nlm.nih.gov/29873076/>.

MAYWALD RL, *et al.* IL-33 activates tumor stroma to promote intestinal polyposis. **Proc Natl Acad Sci**; v.112; p:E2487-96; 2015. Disponível em: < https://pubmed.ncbi.nlm.nih.gov/25918379/>.

MCLELLAN EA, BIRD RP. Aberrant crypts: potential preneoplastic lesions in the murine colon. **Cancer Res**; v.48; n(21), p:6187-92; 1988. Disponível em: < https://pubmed.ncbi.nlm.nih.gov/3167865/>.

MEHDAWI L, OSMAN J, TOPI G, *et al.* High tumor mast cell density is associated with longer survival of colon cancer patients. **Acta Oncol**; v.55; p:1434-1442; 2016. Disponível em: < https://pubmed.ncbi.nlm.nih.gov/27355473/>.

MEKORI, YA; *et al*. Integrating innate and adaptive immune cells: Mast cells as crossroads between regulatory and effector B and T cells. **Eur. J. Pharmacol**., v.778, p.84–89; 2016. Disponível em: < https://pubmed.ncbi.nlm.nih.gov/25941086/>.

MITTAL A, *et al*. Mast Cell Neural Interactions in Health and Disease. **Front Cell Neurosci**; v.13:110; 2019. Disponível em: < https://www.ncbi.nlm.nih.gov/pmc/articles/PMC6435484/>.

MÖLLERHERM, H.; von KÖCKRITZ-BLICKWEDE, M.; BRANITZKI-HEINEMANN, K. Antimicrobial activity of mast cells:Role and relevance of extracellular DNA traps. **Front. Immunol**., v.7, 265; 2016. Disponível em: < https://www.ncbi.nlm.nih.gov/pmc/articles/PMC4947581/>.

MOTAWI TM, *et al*. Evaluation of naproxen and cromolyn activities against cancer cells viability, proliferation, apoptosis, p53 and gene expression of survivin and caspase-3. **J Enzyme Inhib Med Chem**. V.29; p:153-61; 2014. Disponível em: <https://pubmed.ncbi.nlm.nih.gov/23368763/>.

MOTAWI TK, *et al*. Cromolyn chitosan nanoparticles as a novel protective approach for colorectal cancer. **Chem Biol Interact**, v.275; p:1-12; 2017. Disponível em: < https://pubmed.ncbi.nlm.nih.gov/28732690/>.

NAGLE DL, *et al*. Physical mapping of the Tec and Gabrb1 loci reveals that the Wsh mutation on mouse chromosome 5 is associated with an inversion. **Hum Mol Genet**, v.4; n.11; p:2073-9; 1995. Disponível em: < https://pubmed.ncbi.nlm.nih.gov/8589683/>.

NAKANO T, *et al*. Different repopulation profile between erythroid and nonerythroid progenitor cells in genetically anemic W/Wv mice after bone marrow transplantation. **Blood**, v74 (5), p:1552-6; 1989. Disponível em: < https://www.sciencedirect.com/science/article/pii/S0006497120756648?via%3Dihub>.

NEUFERT C, BECKER C, NEURATH MF. An inducible mouse model of colon carcinogenesis for the analysis of sporadic and inflammation-driven tumor progression. **Nat Protoc**., v:2; n(8), p:1998-2004; 2007. Disponível em: < https://www.nature.com/articles/nprot.2007.279>.

NEWMAN AM, *et al*. Robust enumeration of cell subsets from tissue expression profiles. Nat Methods., v.12; p:453-7; 2015. Disponível em: < https://www.nature.com/articles/nmeth.3337>

NIELSEN HJ, *et al*. Independent prognostic value of eosinophil and mast cell infiltration in colorectal cancer tissue. **J Pathol**, v.189; p:487-95; 1999. Disponível em: < https://pubmed.ncbi.nlm.nih.gov/10629548/>.

O'DONNELL C, *et al*. An antitumorigenic role for the IL-33 receptor, ST2L, in colon cancer. **Br J Cancer**., v.114; p:37-43; 2016. Disponível em: < https://pubmed.ncbi.nlm.nih.gov/26679377/>.

OKAYASU, I. *et al*. A novel method in the induction of reliable experimental acute and chronic ulcerative colitis in mice. **Gastroenterology,** v. 98, 694–702; 1990. Disponível em: < https://www.sciencedirect.com/science/article/abs/pii/001650859090290H>.

OVERMAN EL, RIVIER JE, MOESER AJ. CRF induces intestinal epithelial barrier injury via the release of mast cell proteases and TNF-α. **PLoS One**;

v.7(6):e39935; 2012. Disponível em: < https://www.ncbi.nlm.nih.gov/pmc/articles/PMC3386952/>.

PAWANKAR R.; *et al*. Nasal mast cells in perennial allergic rhinitics exhibit increased expression of the Fc epsilonRI, CD40L, IL-4, and IL-13, and can induce IgE synthesis in B cells. **J. Clin. Invest**, v.99, 1492–1499; 1997. Disponível em: <https://www.ncbi.nlm.nih.gov/pmc/articles/PMC507968/>.

POWELL SM, *et al*. APC mutations occur early during colorectal tumorigenesis. **Nature**; v.359, n.6392, p:235-7; 1992. Disponível em: < https://www.nature.com/articles/359235a0>.

PRETLOW, TP, *et al*. Aberrant crypts: putative preneoplastic foci in human colonic mucosa. Cancer Res., 51, 1564-1567; 1991. Disponível em: < https://aacrjournals.org/cancerres/article/51/5/1564/497456/Aberrant-Crypts-Putative-Preneoplastic-Foci-in>.

PUNKENBURG E, *et al*. Batf-dependent Th17 cells critically regulate IL-23 driven colitis-associated colon cancer. **Gut**; v.65(7):1139-50; 2016. Disponível em: < https://gut.bmj.com/content/65/7/1139.long>.

PUZZOVIO PG, *et al*. Cromolyn Sodium differentially regulates human mast cell and mouse leukocyte responses to control allergic inflammation. **Pharmacol Res**., v.178; p:106172; 2022. Disponível em: < https://pubmed.ncbi.nlm.nih.gov/35278626/>.

RONCUCCI, I. Early events in human colorectal carinogenesis. Aberrant crypts and microadenoma, **Ital. J. Gastroenterol**., v.24, n(9), p:498-501; 1992. Disponível em: < https://pubmed.ncbi.nlm.nih.gov/1489980/>.

RONCUCCI, L. et al. Aberrant crypt foci in colorectal carcinogenesis. Cell and crypt dynamics. **Cell Prolif,** v. 33, n. 1, p. 1-18, Feb 2000. ISSN 0960-7722. Disponível em: < https://www.ncbi.nlm.nih.gov/pubmed/10741640 >.

SAKITA, JY. *et al.* A critical discussion on diet, genomic mutations and repair mechanisms in colon carcinogenesis. **Toxicol Lett,** v. 265, p. 106-116, Jan 2017. ISSN 1879-3169. Disponível em: < https://www.ncbi.nlm.nih.gov/pubmed/27908614 >.

SAKITA JY, *et al*. Serotonin synthesis protects the mouse colonic crypt from DNA damage and colorectal tumorigenesis. **J Pathol**; v.249(1):102-113; 2019. Disponível em: < https://onlinelibrary.wiley.com/doi/10.1002/path.5285>.

SAMOSZUK M, TAN J, CHORN G. Clonogenic growth of human breast cancer cells co-cultured in direct contact with serum-activated fibroblasts. **Breast Cancer Res**., v.7; p:274-83; 2005. Disponível em: < https://pubmed.ncbi.nlm.nih.gov/15987422/>.

SANDIG H, BULFONE-PAUS S. TLR signaling in mast cells: common and unique features. **Front Immunol**; v.3:185; 2012. Disponível em: < https://www.ncbi.nlm.nih.gov/pmc/articles/PMC3389341/>.

SINNAMON MJ, Carter KJ, Sims LP, et al. A protective role of mast cells in intestinal tumorigenesis. **Carcinogenesis**, v.29; p:880-6; 2008. Disponível em: < https://pubmed.ncbi.nlm.nih.gov/18258601/>.

SCHNEIDER, LA; *et al*. Molecular mechanism of mast cell mediated innate defense against endothelin and snake venom sarafotoxin. **J. Exp. Med.**, v.204, p:2629–2639; 2007. Disponível em: < https://www.ncbi.nlm.nih.gov/pmc/articles/PMC2118486/>.

SHAH SC, ITZKOWITZ SH. Colorectal Cancer in Inflammatory Bowel Disease: Mechanisms and Management. **Gastroenterology**, v.162, n.3, p:715-730.e3; 2022. Disponível em: < https://pubmed.ncbi.nlm.nih.gov/34757143/>.

SHEFLER I, *et al*. T cell-derived microvesicles induce mast cell production of IL-24: relevance to inflammatory skin diseases. **J Allergy Clin Immunol.**; v.133(1):217-24.e1-3; 2014. Disponível em: <https://pubmed.ncbi.nlm.nih.gov/23768573/>.

SHIH, IM.; *et al*. Top-down morphogenesis of colorectal tumors. **Proc Natl Acad Sci,** v.98, n. 5, p. 2640-2645, 2001. Disponível em: < https://pubmed.ncbi.nlm.nih.gov/11226292/>.

SHIN JS, GAO Z, ABRAHAM SN. Involvement of cellular caveolae in bacterial entry into mast cells. **Science**; v.289, n.5480; p:785-8; 2000. Disponível em: < https://pubmed.ncbi.nlm.nih.gov/10926542/>.

SHIN, K.; *et al*. Mouse mast cell tryptase mMCP-6 is a critical link between adaptive and innate immunity in the chronic phase of Trichinella spiralis infection. **J. Immunol**., v.180, 4885–4891; 2008. Disponível em: < https://www.ncbi.nlm.nih.gov/pmc/articles/PMC2969178/>.

SINNAMON MJ, Carter KJ, Sims LP, et al. A protective role of mast cells in intestinal tumorigenesis. **Carcinogenesis**. V.29, p:880-6; 2008. Disponível em: < https://pubmed.ncbi.nlm.nih.gov/18258601/>.

SOMASUNDARAM, R., *et al*. Tumor-infiltrating mast cells are associated with resistance to anti-PD-1 therapy. **Nat Commun** 12, 346; 2021. Disponível em: <https://doi.org/10.1038/s41467-020-20600-7>.

SONG M. Global epidemiology and prevention of colorectal cancer. **Lancet Gastroenterol Hepatol**., v.7, p:588-590; 2022. Disponível em: <https://www.thelancet.com/journals/langas/article/PIIS2468-1253(22)00089-9/fulltext>.

SORRENTINO C, *et al*. Colorectal Cancer-Associated Immune Exhaustion Involves T and B Lymphocytes and Conventional NK Cells and Correlates With

a Shorter Overall Survival. **Front Immunol**; v.12; p:778329; 2021. Disponível em: <https://www.frontiersin.org/articles/10.3389/fimmu.2021.778329/full>.

SRINIVAS US, *et al*. ROS and the DNA damage response in cancer. **Redox Biol**., v.25, p:101084, 2019. Disponível em: < https://pubmed.ncbi.nlm.nih.gov/30612957/ >.

SUNG H., *et al*. Global Cancer Statistics 2020: GLOBOCAN estimates of incidence and mortality worldwide for 36 cancers in 185 countries. **CA Cancer J Clin**, v.71: 209-249; 2021. Disponível em: < https://pubmed.ncbi.nlm.nih.gov/33538338/>.

TAMMA R,*et al*. Spatial distribution of mast cells and macrophages around tumor glands in human breast ductal carcinoma. **Exp Cell Res**. V. 359, n.1, p:179–184; 2017. Disponível em: < https://doi.org/10.1016/j.yexcr.2017.07.033>.

TAN SY, *et al*. Prognostic significance of cell infiltrations of immunosurveillance in colorectal cancer. **World J Gastroenterol.**, v.11, p:1210-4, 2005. Disponível em: < https://www.ncbi.nlm.nih.gov/pmc/articles/PMC4250716/>.

TANIS E, *et al*. Prognostic impact of immune response in resectable colorectal liver metastases treated by surgery alone or surgery with perioperative FOLFOX in the randomised EORTC study 40983. **Eur J Cancer**., v.51; p:2708-17, 2015. Dispoível em: < https://pubmed.ncbi.nlm.nih.gov/26342674/>.

THAKER AI, *et al*. IDO1 metabolites activate β-catenin signaling to promote cancer cell proliferation and colon tumorigenesis in mice. **Gastroenterology**; v.145(2), p:416-25.e1-4; 2013. Disponível em: < https://www.ncbi.nlm.nih.gov/pmc/articles/PMC3722304/>.

TRAINA G.. The role of mast cells in the gut and brain. **J. Integr. Neurosci**., v.20(1), p: 185–196; 2021. Disponível em: <https://doi.org/10.31083/j.jin.2021.01.313>.

TSAI M, *et al*. Mast cells derived from embryonic stem cells: a model system for studying the effects of genetic manipulations on mast cell development, phenotype, and function in vitro and in vivo. **Int J Hematol** v.75, 345–349; 2002. Disponível em: < https://doi.org/10.1007/BF02982122>.

RAJAMÄKI K, *et al*. Genetic and epigenetic characteristics of inflammatory bowel disease-associated colorectal cancer. **Gastroenterology**; v.161; p:592–607; 2021. Diponível em: < https://pubmed.ncbi.nlm.nih.gov/33930428/>.

Ravindran A, *et al*. An Optimized Protocol for the Isolation and Functional Analysis of Human Lung Mast Cells. **Front Immunol**., v.9; p:2193; 2018. Disponível em: < https://www.frontiersin.org/articles/10.3389/fimmu.2018.02193>.

RECKLINGHAUSEN, F. Ueber Eiter- und Bindegewebskörperchen. **Archiv f. pathol. Anat**. 28, 157–197; 1863. Disponível em: < https://doi.org/10.1007/BF01930779>.

RIBATTI D, CRIVELLATO E. Mast cells, angiogenesis, and tumour growth. **Biochim Biophys Acta,** v.1822; n.1; p:2–8; 2012. Disponível em? < https://doi.org/10.1016/j.bbadis.2010.11.010>.

RIBATTI D, RANIERI G. Tryptase, a novel angiogenic factor stored in mast cell granules. **Exp Cell Res**, v.332, n.2, p:157–162; 2015. Disponível em: < https://doi.org/10.1016/j.yexcr.2014.11.014>.

RIGONI A, *et al*. Mast Cells Infiltrating Inflamed or Transformed Gut Alternatively Sustain Mucosal Healing or Tumor Growth. **Cancer Res**, v.75; p:3760-70; 2015. Disponível em: < https://pubmed.ncbi.nlm.nih.gov/26206557/>.

ROBLES AI, *et al*. Whole-exome sequencing analyses of inflammatory bowel diseaseassociated colorectal cancers. **Gastroenterology**, v.150; p:931–943; 2016. Disponível em: < https://pubmed.ncbi.nlm.nih.gov/26764183/>.

ROSENBERG, D. W.; GIARDINA, C.; TANAKA, T. Mouse models for the study of colon carcinogenesis. **Carcinogenesis**, v. 30, n. 2, p. 183-96, Feb 2009. ISSN 1460-2180. Disponível em: < https://www.ncbi.nlm.nih.gov/pubmed/19037092 >.

TANAKA T, ISHIKAWA H. Mast cells and inflammation-associated colorectal carcinogenesis. **Semin Immunopathol**., v.35; p:245-54; 2013. Disponível em: < https://pubmed.ncbi.nlm.nih.gov/22993030/>.

THANGAM EB, *et al*. The Role of Histamine and Histamine Receptors in Mast Cell-Mediated Allergy and Inflammation: The Hunt for New Therapeutic Targets. **Front Immunol**, v.9:1873; 2018. Disponível em: < https://pubmed.ncbi.nlm.nih.gov/30150993/>.

TREUTING PM, ARENDS MJ, DINTZIS SM. Comparative anatomy and histology: Lower gastrointestinal tract. **Elsevier Inc**; v2; p213-228. Disponível em: < http://dx.doi.org/10.1016/B978-0-12-802900-8.00012-9>.

TRIGGIANI M, *et al*. Lung mast cells are a source of secreted phospholipases A2. **J Allergy Clin Immunol**.; v.124(3):558-65, 565.e1-3; 2009. Disponível em: <https://www.ncbi.nlm.nih.gov/pmc/articles/PMC2788562/>.

VALITUTTI, S.; ESPINOSA, E. Cognate interactions between mast cells and helper T lymphocytes. **Self Nonself**, v.1, p:114–122; 2010. Disponível em: < https://www.ncbi.nlm.nih.gov/pmc/articles/PMC3065669/>.

VAN DIEST SA, *et al*. Relevance of mast cell-nerve interactions in intestinal nociception. **Biochim Biophys Acta**, v.1822; n.1; p:74-84; 2012. Disponível em: < https://doi.org/10.1016/j.bbadis.2011.03.019>.

VANUYTSEL T, *et al*. Psychological stress and corticotropin-releasing hormone increase intestinal permeability in humans by a mast cell-dependent mechanism. **Gut**; v.63(8):1293-9; 2014. Disponível em: < https://gut.bmj.com/content/63/8/1293.long>.

VESELY MD, *et al*. Natural innate and adaptive immunity to cancer. **Annu Rev Immuno**l, v.29, p:235-71; 2011. Disponível em: < https://pubmed.ncbi.nlm.nih.gov/21219185/ >

VISCIANO C, *et al.* Mast cells induce epithelial-to-mesenchymal transition and stem cell features in human thyroid cancer cells through an IL-8-Akt-Slug pathway. **Oncogene**, v.34, n.40, p:5175–5186; 2015. Disponível em: <https://doi.org/10.1038/onc.2014.441>.

VOGELSTEIN B, KINZLER KW. The Path to Cancer --Three Strikes and You're Out. **N Engl J Med**; v.373, n.20, p:1895-8; 2015. Disponível em: < https://pubmed.ncbi.nlm.nih.gov/26559569/>.

XING W, *et al*. Protease phenotype of constitutive connective tissue and of induced mucosal mast cells in mice is regulated by the tissue. **Proc Natl Acad Sci**, v.108:14210-5; 2011. Disponível em: < https://www.ncbi.nlm.nih.gov/pmc/articles/PMC3161524/>.

YAEGER R, *et al*. Genomic alterations observed in colitis-associated cancers are distinct from those found in sporadic colorectal cancers and vary by type of inflammatory bowel disease. **Gastroenterology**; v.151; p:278–287.e6; 2016. Disponível em < https://pubmed.ncbi.nlm.nih.gov/27063727/>.

YU Y, Blokhuis B, Derks Y. Human mast cells promote colon cancer growth via bidirectional crosstalk: studies in 2D and 3D coculture models. **Oncoimmunology**, v.7, n.11; e1504729; 2018. Disponível em: < https://doi.org/10.1080/2162402x.2018.1504729>.

WARGOVICH MJ, *et al*. Aberrant crypts as a biomarker for colon cancer: evaluation of potential chemopreventive agents in the rat. **Cancer Epidemiol Biomarkers Prev**.; v.5:355-60; 1996. Disponível em: < https://pubmed.ncbi.nlm.nih.gov/9162301/>.

WECHSLER, JB; *et al*. Histamine drives severity of innate inflammation via histamine 4 receptor in murine experimental colitis. **Mucosal. Immunol**., v.11, p:861–870; 2018. Disponível em: < https://www.nature.com/articles/mi2017121>.

WERNERSSON S, PEJLER G. Mast cell secretory granules: armed for battle. **Nat Rev Immunol**, v.14, n.7, p:478-94; 2014. Disponível em: < https://pubmed.ncbi.nlm.nih.gov/24903914/>.

WEST PW; BULFONE-PAUS S. Mast cell tissue heterogeneity and specificity of immune cell recruitment. **Front. Immunol**, v.13; p:932090; 2022. Disponível em: < https://pubmed.ncbi.nlm.nih.gov/35967445/>.

WEDEMEYER J, GALLI SJ. Decreased susceptibility of mast cell-deficient Kit(W)/Kit(W-v) mice to the development of 1, 2-dimethylhydrazine-induced

intestinal tumors. **Lab Invest**, v.85; p:388-96; 2005. Disponível em: < https://pubmed.ncbi.nlm.nih.gov/15696191/>.

WOOD JD. Neuropathophysiology of functional gastrointestinal disorders. **World Journal of Gastroenterology**; v.13: 1313; 2007. Disponível em: <https://www.ncbi.nlm.nih.gov/pmc/articles/PMC4146914/>.

WROBLEWSKI M, *et al*. Mast cells decrease efficacy of anti-angiogenic therapy by secreting matrix-degrading granzyme B. **Nat Commun**., v.8; p:269; 2017. Disponível em: < https://www.nature.com/articles/s41467-017-00327-8>.

ZHAO P, *et al*. Levels of circulating mast cell progenitors and tumour-infiltrating mast cells in patients with colorectal cancer. **Oncol Rep**.; v.47; n.5; p:89; 2022. Disponível em: < https://pubmed.ncbi.nlm.nih.gov/35293596/>.

9. Anexos

9.1 Figuras suplementares

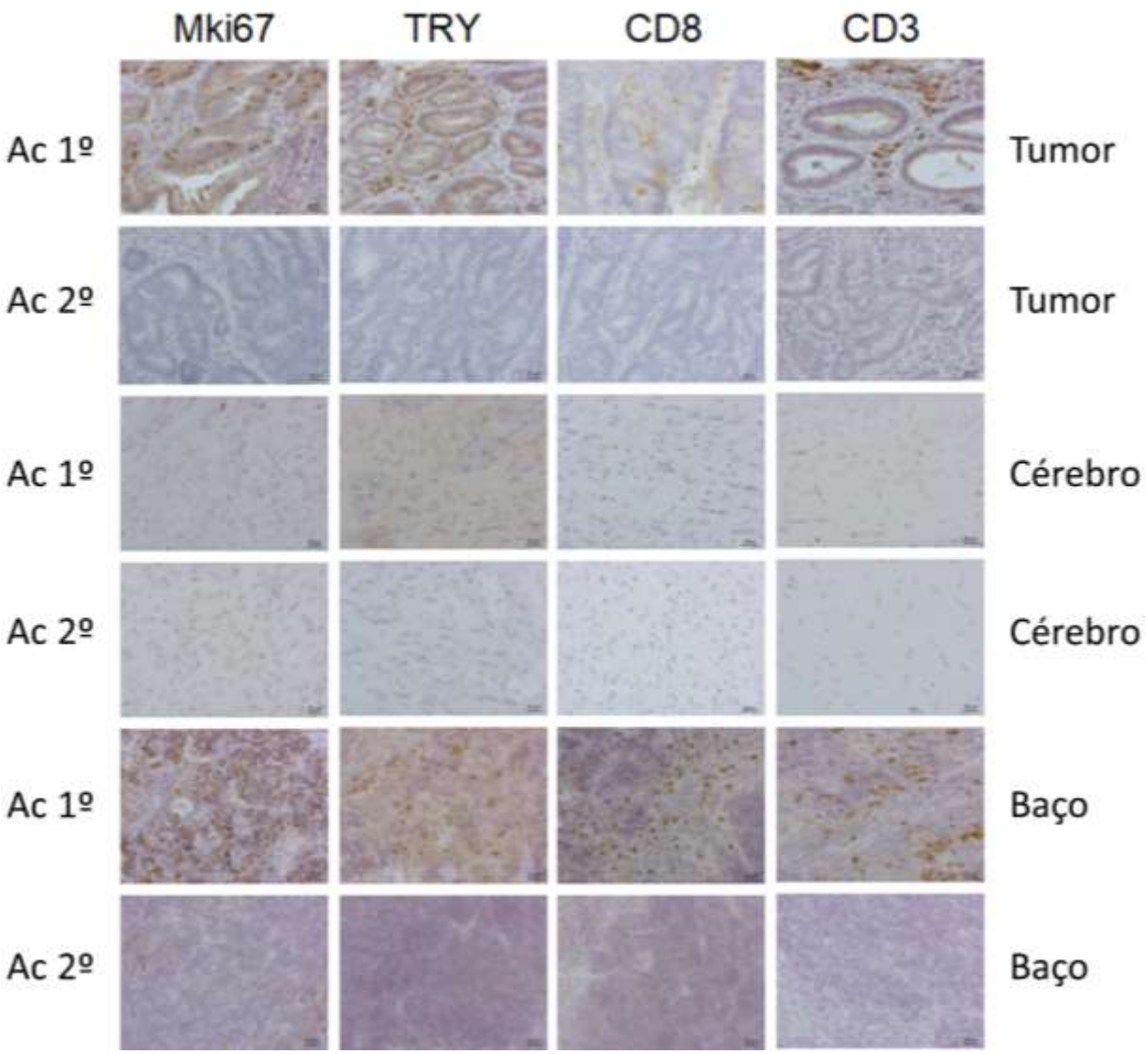

Figura suplementar 1: Reações e tecidos utilizados como controle de imunohistoquímica (IHC). Como controle negativo da reação, foram utilizados somente o anticorpo secundário e o cromógeno. Além disso, foram utilizadas amostras para o controle positivo (baço) e negativo (cérebro).

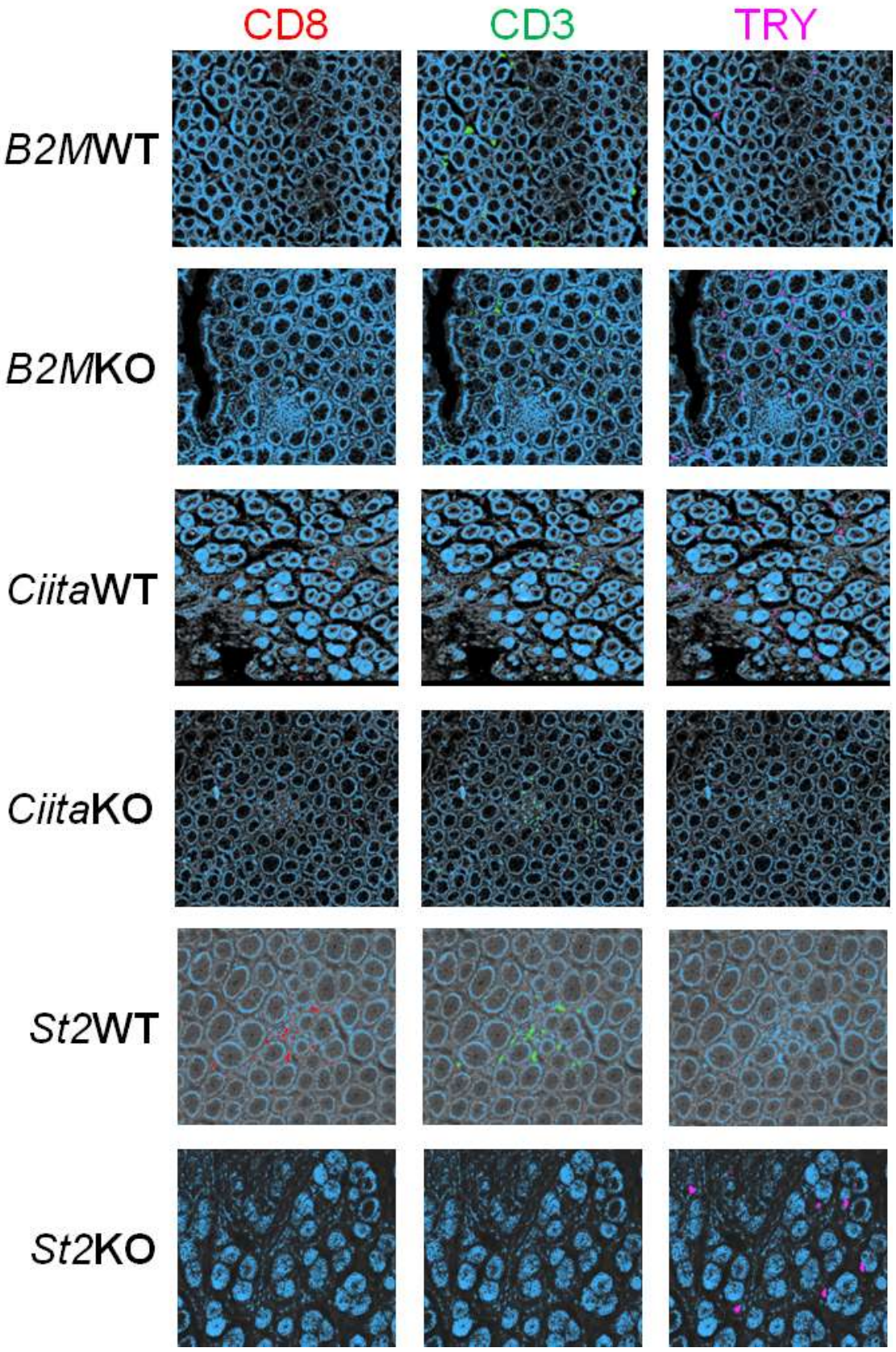

Figura suplementar 2: Reações de IHC-multiplex separadas e pseudo-coloridas para os anticorpos anti-CD8, anti-CD3 e anti-triptase (anti-TRY). As imagens estão reprentadas em 50µm.

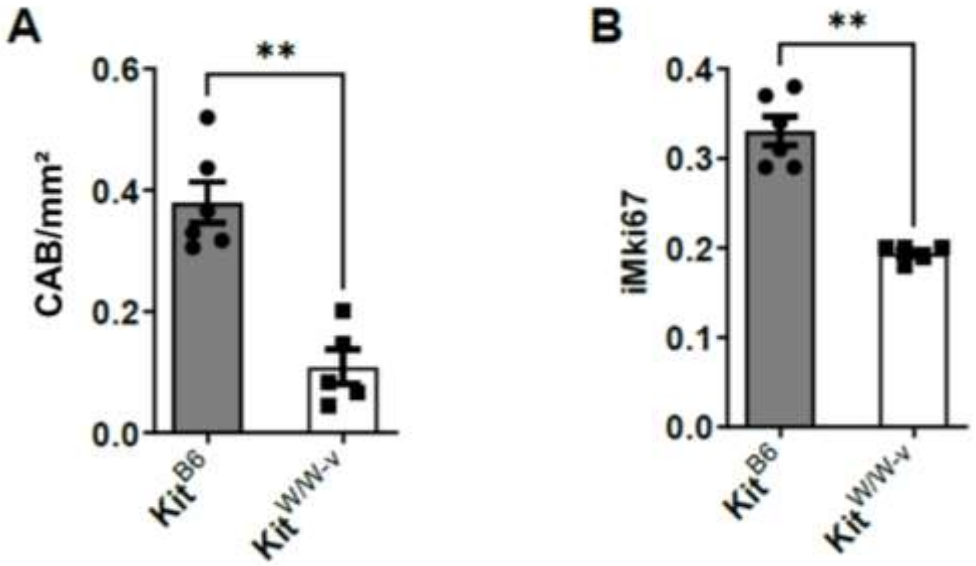

Figura suplementar 3: Modelo animal $Kit^{W/wv}$ altera o desenvolvimento das criptas aberrantes (CAB) na tumorigênese colorretal esporádica. **A**: Análise histopatológica das AC em animais C57BL/6 (Kit^{B6}) e $Kit^{W/wv}$ no cólon de animais expostos à 3 doses de AOM e avaliados após 3 semanas (n = 11; **p = 0,004). **B**: Análise da proliferação celular a partir de reações de IHC para Mki67 nos animais C57BL/6 (Kit^{B6}) e $Kit^{W/wv}$ (n = 11; **p = 0,002). Os dados estão representados como pontos individuais com média ± desvio padrão. O valor de p foi calculado utilizando o two-tailed Mann-Whitney teste.

9.2 Autorizações Comitê de Ética

HOSPITAL DAS CLÍNICAS DA FACULDADE DE MEDICINA
DE RIBEIRÃO PRETO DA UNIVERSIDADE DE SÃO PAULO

FMRP-USP
RIBEIRÃO PRETO

Ribeirão Preto, 02 de outubro de 2014

Ofício nº 3630/2014
CEP/FC

PROCESSO HCRP nº 12873/2014

Prezados Pesquisadores,

O trabalho intitulado **"A ATIVIDADE DOS SISTEMA NERVOSO ENTÉRICO NO DESENVOLVIMENTO DA CARCINOGENESE DE CÓLON" – Versão 2 de 06/06/2014,** foi analisado pelo Comitê de Ética em Pesquisa, em sua 395ª Reunião Ordinária realizada em 29/09/2014, e enquadrado na categoria: **APROVADO,** bem como a solicitação de dispensa do Termo de Consentimento Livre e Esclarecido.

Este Comitê segue integralmente a Conferência Internacional de Harmonização de Boas Práticas Clínicas (IGH-GCP), bem como a Resolução nº 466/2012 CNS/MS.

Lembramos que devem ser apresentados a este CEP, o Relatório Parcial e o Relatório Final da pesquisa. De acordo com Carta Circular nº 003/2011/CONEP/CNS, datada de 21/03/2011, o sujeito de pesquisa ou seu representante, quando for o caso, deverá rubricar todas as folhas do Termo de Consentimento Livre e Esclarecido – TCLE – apondo sua assinatura na última do referido Termo; o pesquisador responsável deverá da mesma forma, rubricar todas as folhas do Termo de Consentimento Livre e Esclarecido – TCLE – apondo sua assinatura na última página do referido Termo.

Atenciosamente.

PROF. DR. FABIO CARMONA
Vice-Coordenador do Comitê de Ética em
Pesquisa do HCRP e da FMRP-USP

Ilustríssimos Senhores
DR. VINICIUS KANNEN CARDOSO
PROF. DR. SERGIO BRITTO GARCIA/DRª MARIANGELA BRUNALDI
Depto. de Patologia e Medicina Legal

UNIVERSIDADE DE SÃO PAULO

Faculdade de Ciências Farmacêuticas de Ribeirão Preto

COMISSÃO DE ÉTICA NO USO DE ANIMAIS

A U T O R I Z A Ç Ã O

Certificamos que a proposta intitulada "Ação de mastócitos durante a carcinogênese colorretal esporádica", registrada sob nº 22.1.233.60.2, sob a responsabilidade de Juliana Yumi Sakita e Sergio Akira Uyemura, que envolve a manutenção e utilização de animais pertencentes ao filo Chordata, subfilo Vertebrata (exceto o homem) para fins de pesquisa científica encontra-se de acordo com os preceitos da Lei nº 11.794, de 8 de outubro de 2008, do Decreto º 6.899, de 15 de julho de 2009, e com as normas editadas pelo Conselho Nacional de Controle da Experimentação Animal (CONCEA), foi aprovada em 08/08/2022 pela Comissão de Ética no Uso de Animais da Faculdade de Ciências Farmacêuticas de Ribeirão Preto (CEUA FCFRP).

Lembramos da obrigatoriedade de apresentação do relatório de atividades, em modelo da CEUA, para emissão do certificado, como disposto nas Resoluções Normativas do CONCEA.

Colaborador: Vinicius Kannen Cardoso

Finalidade	( ) Ensino (x) Pesquisa Científica				
Vigência da Autorização	01/09/2020 a 29/02/2024				
Espécie/Linhagem/Raça	Cam. Isogênico C57BL/6	Cam. *Knockout* ST2	Cam. *Knockout* BM2	Cam. *Knockout* CIITA	Cam. *Knockout* Kit $^{W/sh}$
Nº de animais	109	6	6	6	30
Peso/Idade	21 g / 8 semanas				
Sexo	Macho				
Origem	Biotério Central da PUSP-RP	Biotério de Animais Especiais da FMRP-USP			

Ribeirão Preto, 8 de agosto de 2022.

Ana Patrícia Yatsuda Natsui
Vice-Coordenadora da CEUA-FCFRP

Journal for ImmunoTherapy of Cancer

Decision Letter (jitc-2022-004653.R2)

From: info.jitc@bmj.com

To: vkannen@usp.br

CC:

Subject: Your submission to Journal for ImmunoTherapy of Cancer has been accepted

Body: 07-Sep-2022
jitc-2022-004653.R2 - The mast cell-T cell axis alters development of colitis-dependent and -independent colorectal tumours: potential for therapeutically targeting via mast cell inhibition

Dear Dr. Kannen:

We are pleased to accept your article for publication in Journal for ImmunoTherapy of Cancer.

Within 2-3 working days, you will receive an email with payment options and instructions from BMJ's e-commerce partner, Copyright Clearance Center. You will be able to choose either to pay by credit card or invoice. If you are not making the payment yourself, you may forward the email to the person or organisation that will be paying on your behalf. Your article will not be processed by production until you have paid the article processing charge or requested an invoice. For more details on open access publication please visit our Author Hub: https://authors.bmj.com/open-access/.

Please note, that if your institution is part of one of BMJ's Publish and Read or prepay agreements your request for funding will be automatically processed based on this acceptance and you will only receive an email accepting or denying your funding request. To find out if your institution is part of a Publish and Read or prepay agreement visit BMJ's open access agreements page: https://authors.bmj.com/open-access/institutional-programme/.

Once payment is confirmed and your article is sent to Production, copyediting and typesetting will be completed. We will email you a proof to check via our online tool usually within 10-15 days of this time; please check your junk mail folder.

The proof is your opportunity to check for typesetting errors and the completeness and accuracy of the text; including author names and affiliations, tables and figures; including legends, numerical, mathematical, or other scientific expressions. We ask that you only make minor corrections at this stage. Please provide any comments within 48 hours. There will be no further opportunities to make corrections prior to publication.

See https://authors.bmj.com/after-submitting/accepted/ for more information about what to expect once your article has been accepted.

We publish most articles online in their final form around three weeks after acceptance. See https://authors.bmj.com/after-submitting/online-publication/ for more information about online publication. BMJ will deposit your article in all indexes affiliated with the journal.

Any final comments from the reviewer(s) are included at the foot of this email. The comments are for your information only, but in the case of minor requests (e.g. typos) these can be corrected when you receive your proof.

If your article is selected for press release by BMJ's Press Office you will be informed as soon as possible.

If you have any questions, please contact the Editorial Office.

Thank you for your contribution, and we hope that you will continue to submit to the journal in future.

Kind regards,

Pedro J. Romero, MD
Editor-in-Chief
Journal for ImmunoTherapy of Cancer

Reviewer(s)' Comments to Author (if any):

Reviewer: 2

Comments to the Author
The Authors have addressed this reviewer's comments.

Date Sent: 07-Sep-2022

Close Window

Journal for ImmunoTherapy of Cancer

The mast cell-T cell axis alters development of colitis-dependent and -independent colorectal tumours: potential for therapeutically targeting via mast cell inhibition

Journal:	*Journal for ImmunoTherapy of Cancer*
Manuscript ID	jitc-2022-004653.R2
Article Type:	Original research
Date Submitted by the Author:	28-Aug-2022
Complete List of Authors:	Sakita, Juliana; University of Sao Paulo Faculty of Pharmaceutical Sciences of Ribeirao Preto Elias-Oliveira, Jefferson; Universidade de Sao Paulo Faculdade de Medicina de Ribeirao Preto Carlos, Daniela; University of Sao Paulo, Department of Biochemistry and Immunology de Souza Santos, Emerson; University of Sao Paulo, Department of Toxicology, Bromatology, and Clinical Analysis Almeida, Luciana Yamamoto; University of Sao Paulo, Department of Clinical Medicine Malta, Tathiane M; University of Sao Paulo, Department of Toxicology, Bromatology, and Clinical Analysis Brunaldi, Mariângela O; University of Sao Paulo, Department of Pathology Albuquerque, Sergio; University of Sao Paulo, Department of Toxicology, Bromatology, and Clinical Analysis Araújo Silva, Cleide Lúcia; University of Sao Paulo, Department of Biochemistry and Immunology Andrade, Marcus V.; Federal University of Minas Gerais, Department of Clinical Medicine Garcia, Sergio Britto; University of Sao Paulo, Department of Pathology Cunha, Fernando; Universidade de Sao Paulo Faculdade de Medicina de Ribeirao Preto Cebinelli, Guilherme Cesar Martelossi; University of Sao Paulo, Department of Pharmacology Martins, Ronaldo; Universidade de Sao Paulo Faculdade de Medicina de Ribeirao Preto Bonato, Vania; Universidade de Sao Paulo Faculdade de Medicina de Ribeirao Preto Matthews, Jason; University of Toronto, Pharmacology and Toxicology; University of Oslo, Nutrition Colli, Leandro; University of Sao Paulo, Medical Imaging, Hematology, and Oncology Martin, Francis L; Biocel Ltd Uyemura, Sergio A; University of Sao Paulo, Department of Toxicology, Bromatology, and Clinical Analysis Kannen, Vinicius; University of Sao Paulo, Department of Genetics; University of Toronto, Pharmacology and Toxicology
Keywords:	CD8-Positive T-Lymphocytes, Immune Evation, Immunotherapy, Tumor

	Microenvironment, Tumor Escape

I, the Submitting Author has the right to grant and does grant on behalf of all authors of the Work (as defined in the below author licence), an exclusive licence and/or a non-exclusive licence for contributions from authors who are: i) UK Crown employees; ii) where BMJ has agreed a CC-BY licence shall apply, and/or iii) in accordance with the terms applicable for US Federal Government officers or employees acting as part of their official duties; on a worldwide, perpetual, irrevocable, royalty-free basis to BMJ Publishing Group Ltd ("BMJ") its licensees and where the relevant Journal is co-owned by BMJ to the co-owners of the Journal, to publish the Work in this journal and any other BMJ products and to exploit all rights, as set out in our licence.

The Submitting Author accepts and understands that any supply made under these terms is made by BMJ to the Submitting Author unless you are acting as an employee on behalf of your employer or a postgraduate student of an affiliated institution which is paying any applicable article publishing charge ("APC") for Open Access articles. Where the Submitting Author wishes to make the Work available on an Open Access basis (and intends to pay the relevant APC), the terms of reuse of such Open Access shall be governed by a Creative Commons licence – details of these licences and which Creative Commons licence will apply to this Work are set out in our licence referred to above.

Other than as permitted in any relevant BMJ Author's Self Archiving Policies, I confirm this Work has not been accepted for publication elsewhere, is not being considered for publication elsewhere and does not duplicate material already published. I confirm all authors consent to publication of this Work and authorise the granting of this licence.

The mast cell-T cell axis alters development of colitis-dependent and -independent colorectal tumours: potential for therapeutically targeting *via* mast cell inhibition

Juliana Y. Sakita[1], Jefferson Elias-Oliveira[2], Daniela Carlos[2], Emerson de Souza Santos[3], Luciana Y. Almeida[4], Tathiane M. Malta[3], Mariângela O. Brunaldi[5], Sergio Albuquerque[3], Cleide L. A. Silva[6], Marcus V. Andrade[7], Vânia L. D. Bonato[2], Sergio B. Garcia[5], Fernando Q. Cunha[8], Guilherme C. M. Cebinelli[8], Ronaldo B. Martins[9], Jason Matthews[10,11], Leandro Colli[12], Francis L. Martin[13,14], *Sergio A. Uyemura[3], *Vinicius Kannen[1,10]

[1]Department of Genetics, University of Sao Paulo, Ribeirao Preto, Brazil; [2]Department of Biochemistry and Immunology, University of São Paulo, Ribeirao Preto, Brazil; [3]Department of Toxicology, Bromatology, and Clinical Analysis, University of Sao Paulo, Ribeirao Preto, Brazil; [4]Department of Clinical Medicine, University of Sao Paulo, Ribeirao Preto, Brazil; [5]Department of Pathology and Forensic Medicine, University of Sao Paulo, Ribeirao Preto, Brazil; [6]Hemotherapy Center of Ribeirao Preto, Brazil; [7]Department of Clinical Medicine, Federal University of Minas Gerais, Belo Horizonte, Brazil; [8]Department of Pharmacology, University of Sao Paulo, Ribeirao Preto, Brazil; [9]Department of Cell and Molecular Biology, Virology Research Center, University of Sao Paulo, Ribeirao Preto, Brazil; [10]Department of Pharmacology and Toxicology, University of Toronto, Toronto, Canada; [11]Department of Nutrition, Institute of Basic Medical Sciences, University of Oslo, Oslo, Norway; [12]Department of Medical Imaging, Hematology, and Oncology, Ribeirao Preto Medical School, University of Sao Paulo, Ribeirao Preto, Brazil; [13]Biocel Ltd., Hull, HU10 7TS, UK; [14]Department of Cellular Pathology, Blackpool Teaching Hospitals NHS Foundation Trust, Whinney Heys Road, Blackpool FY3 8NR, UK.

*These authors are joint senior authors

Running title: Mast cells activity in colorectal tumorigenesis

Conflicts of interest: The authors declare no conflicts of interest.

Corresponding author: Vinicius Kannen, Ph.D., University of Toronto, Department of Pharmacology and Toxicology, 1 King's College Cir, M5S 1A8, Toronto-ON, Canada; Phone: +1416 946 0851; E-mail: vinicius.kannen@utoronto.ca

Abstract

Background Colorectal cancer (CRC) has a high mortality rate and can develop in either colitis-dependent (CA-CRC) or -independent (sCRC) manner. There has been a significant debate about whether mast cells (MCs) promote or inhibit the development of CRC. Herein we investigated mast cell (MC) activity throughout the multi-stepped development of CRC in both human patients and animal models.

Methods We analysed human patient matched samples of healthy colon *versus* CRC tissue alongside conducting a TCGA-based immunogenomic analysis and multiple experiments employing genetically engineered mouse (GEM) models.

Results Analysing human CRC samples revealed that MCs can be active or inactive in this disease. An activated MC population decreased the number of tumour-residing CD8 T cells. In mice, MC deficiency decreased the development of CA-CRC lesions, while it increased the density of tumour-based CD8 infiltration. Furthermore, co-culture experiments revealed that tumour-primed MCs promote apoptosis in CRC cells. In MC-deficient mice, we found that MCs inhibited the development of sCRC lesions. Further exploration of this with several GEM models confirmed that different immune responses alter and are altered by MC activity, which directly alters colon tumorigenesis. Since rescuing MC activity with bone marrow transplantation in MC-deficient mice or pharmacologically inhibiting MC effects impacts the development of sCRC lesions, we explored its therapeutic potential against CRC. MC activity promoted CRC cell engraftment by inhibiting CD8+ cell infiltration in tumours, pharmacologically blocking it inhibits the ability of allograft tumours to develop. This therapeutic strategy potentiated the cytotoxic activity of fluorouracil chemotherapy.

Conclusion Therefore, we suggest that MCs have a dual role throughout CRC development and are potential druggable targets against this disease.

Keywords: Colitis; tumours; immune system; mast cell-lymphocyte axis; azoxymethane

What is already known on this topic – The role of MCs in CRC is controversial as they can either promote or inhibit it. Studying this issue may reveal druggable targets for oncostatic therapies.

What this study adds – Our study shows that an MC-lymphocyte axis alters the development of both CA-CRC and sCRC. However, several immune mechanisms can also change MCs' function and CRC development. Moreover, pharmacologically inhibiting MC activity blocks the growth of CRC and melanoma tumours. This therapeutic strategy can be combined with a chemotherapeutic compound.

How this study might affect research, practice or policy – Our findings define specific conditions in which MCs can promote or block CRC development. They also highlight MCs as a versatile druggable target against melanoma and CRC.

Introduction

Mast cells (MCs) have been suggested to play a pivotal yet complex role in several immune-mediated reactions in the body [1-3]. Bone marrow releases immature MCs that migrate towards their patrolling sites that are then activated according to immediate region-specific needs. Also, MCs synthesize inflammatory factors towards antigens binding to the Fc region of immunoglobulin E (IgE) coating their membrane [2-4].

In human colorectal cancer (CRC), a reduced MC population has been associated with a good prognosis, whilst elevated numbers appear to be associated with poorer disease outcomes [5, 6]. Conversely, there have also been reports suggesting that increased MC numbers in tumours promote patient survival rates [7, 8]. In carcinogen-exposed animal models, which resemble the development of sporadic CRC (sCRC), MC deficiency reduced tumour burden [9]. Pharmacologically inhibiting MCs' activity decreased CRC risk also [10].

Other research groups have suggested that MCs promote the development of colitis-associated CRC (CA-CRC) in mice [11, 12]. Haribabu and colleagues reported that MC deficiency promotes the development of colon tumours in mice carrying a heterozygous mutation in the *adenomatous polyposis coli* ($Apc^{Min/+}$) gene; thus, MCs might orchestrate an anticancer immunological reaction during the development of intestinal tumorigenesis [13]. Sinnamon *et al.* demonstrated similar observations that MC deficiency increases tumour numbers in $Apc^{Min/+}$ mice [14].

Whether the MC activity can differentially alter the development of CA-CRC and sCRC lesions remains unknown. We have thus challenged the hypothesis that MC activity alters and can be altered by different immune reactions. Our findings not only confirm that a MC-T cell axis alters the development of CA-CRC and sCRC tumours but that its

potential can be pharmacologically harnessed to treat CRC in combination with a standard chemotherapeutic compound.

Materials and Methods

Human samples and immunogenomic analysis

The Research Ethics Committee of the Clinical Hospital of the Ribeirao Preto School of Medicine of the University of São Paulo approved the use of matching malignant and healthy human tissue samples of nineteen CRC cases (38 samples in total; 19 healthy colon tissues and 19 CRC tissues) from the surgical tissue bank (12873/2014). According to the Declaration of Helsinki for the research use of previously collected human biospecimens in minimal risk studies, this Research Ethics Committee waived the patient informed consent. None of the patients underwent chemotherapy or radiotherapy prior to sample collection. Coded tissue samples ensured patient confidentiality.

Also, we performed an immunogenomic analysis based on 604 CRC cases from The Cancer Genome Atlas (TCGA). It investigated the immune cell population estimated by CIBERSORT [15], and the immune features that our previous report described [16]. Additionally, we selected the TCGA CRC samples classified as "genome stable subtype" and divided them in two groups based on the frequency of activated MC by setting up a dichotomy comparing the top quarter (high MC activated frequency, HMCA) against the bottom quarter (low MC activated frequency, LMCA). The samples with intermediary frequency were excluded from the analysis.

Mouse experiments

The Research Ethics Committee for Animal Use of the School of Pharmaceutical Sciences of Ribeirao Preto of the University of Sao Paulo approved the current study

(22.1.233.60.2). The following mouse strains were purchased from the Jackson Laboratories (USA): $Kit^{W/sh}$ (#012861), $Kit^{W/W-v}$ (#100410), *B2m* knockout (KO; #002087), *Ciita* KO (#003239), *Il6* KO (#002650), NOD (#001976), NOD-*scid*γ (#005557), C57BL/6J (#000664; named herein Kit^{B6}, *B2m*WT, or *Ciita*WT), BALB/cJ (#000651; named herein *St2*WT), C57BL/6-Tg(CAG-EGFP)131Osb/LeySopJ (#006567; named herein $Kit^{B6\text{-}Tag(CAG\text{-}EGFP)}$), and *Rag1* KO (#002216). The *St2*KO mouse strain was developed and donated by Dr Andrew McKenzie [17].

Cell culture, co-culture, and allograft CRC model

A murine CRC cell line (MC38) was cultured (±95% humidity; 37°C; 5% CO_2) in Dulbecco's Modified Eagle Medium (D5030; 10% foetal bovine serum, 12103C; 100U/ml penicillin-streptomycin, P0781; 10mM sodium pyruvate, P5280; Sigma-Aldrich, US).

To harvest tumour-primed MCs, Kit^{B6} mice were intraperitoneally (i.p.) injected with MC38 cells (1×10^6). Following 7 days from this procedure, MCs were isolated from the peritoneal cavity according to our previous description [18]. Tumour-primed MCs were co-cultured with MC38 cells at a ratio of 1:10.

MC38 cells ($2x10^6$) were subcutaneously injected to induce allograft tumours in both $Kit^{W/sh}$ and Kit^{B6} mice. Tumours grew for 14 days and were monitored with a caliper. Treatments started from the 7th day onwards. Treatments were saline, cromolyn (CA; Sigma-Aldrich; C0399; 25 mg/ kg/ day; [19]), and fluorouracil (5-FU; Libbs Farmaceutica Ltda, Sao Paul, Brazil; 70 mg/ kg once every 3 days; [20]).

Colon tumorigenic mouse models

The CA-CRC protocol consisted of a single i.p. injection of azoxymethane (AOM; 10 mg/kg; Sigma-Aldrich; A5486) followed by three cycles of 2% dextran sulphate sodium (DSS; Sigma-Aldrich; 42867; [21]). Experiments were ended in a CO_2 chamber (10^{th} week).

The sCRC protocol consisted of 6 i.p. injections of AOM throughout 6 weeks. Tumours were detected after other 18 weeks [21]. Early tumorigenic lesions (APL) were detected after 6 weeks from the 6^{th} AOM exposure. DNA damage can be studied after 3 days and single APLs (PL) after 1 week from the 6^{th} AOM injection. Our protocol of 3 i.p. AOM injections followed by 3 days or 3 weeks was also applied [22].

Bone marrow transplantation

To rescue MC deficiency, $Kit^{W/sh}$ mice and their counterparts underwent a single lethal dose of whole-body irradiation (IR; RS-2000 Biological Research Irradiator [Rad Source, Kansas City, MO, US]; 7 Gy). After 12 h, IR-exposed mice received 1×10^7 freshly isolated mouse bone marrow cells expressing enhanced green fluorescent protein (EGFP) from $Kit^{B6\text{-}Tag(CAG\text{-}EGFP)}$ mice [23]. After other 6 weeks, bone marrow transplantation (BMT) was confirmed by counting EGFP cells in flow cytometry (Guava easyCyte 8HT [MerkMillipore, Burlington, MA, USA]; InCyte 2.7 software). Then, mice underwent sCRC protocol.

qPCR

The RNeasy Mini Kit (74104; Qiagen, DE) was used to prepare RNA samples. Then, cDNA synthesis followed the manufacture's guideline for the SuperScript® III Reverse Transcriptase kit (Thermo Fisher Scientific, USA; 18080093). **Suppl Tab 1** and **Suppl Tab 2** show probes and primers, respectively. Data were collected and analysed using an

Eppendorf Mastercycler® RealPlex2 system (Eppendorf, DE). The fold-change (FC) between reaction control, experimental control, and target groups was calculated using the $2^{-\Delta\Delta Ct}$ method (*Gapdh* as a housekeeping gene).

Flow cytometry

According to the manufacturer's guideline (Thermo Fisher Scientific, USA), the Annexin V/ 7AAD kit (#88-8006-74) was used to analyse viability and apoptosis. Also, colonic lymphocytes, tumour immune cellular populations, and tumour cells were isolated as we have described previously [24, 25]. Then, samples were incubated with antibodies against CD45-FITC (1:250), CD45-APC (1:250), CD45-BV421 (1:300), CD117-PE-Cy7 (1:250), FcεRI-PE (1:250), CD8a-PE (1:300), CD3-FITC (1:250), CD4-FITC (1:250), and FOXP3-APC (1:300; **Suppl Tab 3**). Cellular viability was checked by 7AAD (#A1310; Thermo Fisher Scientific) or FVS-APC Cy-7 (#565388; BD Biosciences). The data acquisition was performed on FACSVerse (BD Biosciences) and analysis carried out by the FlowJo software (FlowJo LLC, USA). Lymphocytes were determined as $CD4^+$, $CD4^+$FOXP3+, $CD8^+$, and $CD8^+CD3^+$ gated from singlet viable $CD45^+$ cells. MCs were determined as CD45+FcεRI+CD117+ cells. Values are given as percentage.

Clonogenic assay

For decades the clonogenic assay has been used to test the number of cancer cell colonies in different experimental settings [26]. It can also be applied in co-culturing systems [27]. After tumour-primed MCs were co-cultured with MC38 cells for 5 days, colonies were fixed and stained with 0.2% crystal violet solution. The well area normalized the number of colonies.

Histopathological analysis and multiplex immunohistochemistry

As previously reported [28], 4-µm paraffin-embedded tissue sections were stained with toluidine blue (TB; Sigma-Aldrich; 89640) before determining the density of MCs *per* sample area (iTB; Axio Imager M2 [Carl-Zeiss, DE]). To validate this analysis (iTRY), immunohistochemistry (IHC; Picture-Max Dab Kit; Thermo Fisher Scientific, USA; 878983) stained samples following manufacturer's instructions (anti-MC tryptase [TRY; 1:100; ab2378], ABCAM, USA;).

Following our previous description [22], tumours and preneoplastic tissue samples underwent H&E staining and analysis (lesions *per* mm^2). IHC stained samples with primary antibodies (**Suppl Tab 3**) for analysis (number of positive *per* crypt).

A multiplex IHC was performed following our protocol [22]. Reactivity to primary antibodies (**Suppl Tab 3; Suppl Fig 1**) was determined by a Vector AEC Substrate kit (Vector Laboratories, USA; SK-4200). Stained tissue slides were scanned using an Aperio ImageScope AT system (Leica Biosystems, DE). Image processing and visualization were carried out using ImageScope software (Leica Biosystems).

RNAseq panel analysis

To prepare RNA samples, we used Qiagen RNeasy (#74106) and Qiagen RNase-free DNase kits (#79254). The RNA integrity was analysed by Agilent Bioanalyzer RNA 6000 Nano kit (Agilent Technologies, USA; #5067–1511). The cDNA libraries were built with QIAseq Targeted RNAseq Mouse Immuno-Oncology panel (#333005) and QIAseq Targeted RNA 96-Index I kits (#333117). The Agilent Bioanalyzer DNA 1000 Assay (#5067–1504) assessed libraries quality and size. The QIAseq Library Quant Assay Kit (#333314) quantified libraries before the Illumina MiSeq Reagent Kit v3 (150 cycles;

Illumina Inc., USA; #15043894) was applied for sequencing them in a MiSeq Sequencing System. Datasets (GSE 146786) were analysed with the R package DESeq2 [29].

Immunoblotting analysis

According to our previous report [22], immunoblotting analyses were performed. Following cold protein extraction (RIPA Buffer, R0278; phosphatase inhibitors, P0044; protease inhibitor, P2714; Sigma-Aldrich), protein concentration was determined (Pierce BCA Protein Assay Kit, 23225; Thermo Fisher Scientific). Any kD™ Mini-PROTEAN® TGX Stain-Free™ Protein Gels (#4568123; Bio-Rad Laboratories, USA) were used for electrophoresis. Then, we used the Bio-Rad Trans-Blot® Turbo™ Mini Nitrocellulose Transfer Packs (#1704158) together with the Bio-Rad Trans-Blot® Turbo™ Transfer System. Next, membranes were incubated at 4°C overnight with primary antibodies (**Suppl Tab 3**).

Statistical analysis

The R software was applied for the TCGA-based immunogenomic analysis [30]. Also, we computed the Pearson correlation between immune features and MC populations. A two-tailed T-test was used to analyse the frequency of immune cell populations/signatures between CRC samples with low (LMCA) and high MC activated (HMCA) frequencies.

The R software was also applied for analysing the RNAseq datasets. After the data normalization by DESeq2, the differential expression was calculated (p-value adjust <0.05). Test t was used to analyse only two groups, while the One-way ANOVA (post-hoc test Benjamini–Hochberg) was used to analyse more than two groups. The libraries used were: DESeq2, ComplexHeatmap, gplots and parallel.

Other datasets were analysed in the GraphPad Prism 9.3 software (Graph Pad Software Inc., USA). The two-tailed Mann-Whitney's test analysed probabilities between two different groups. The One-way ANOVA test (Kruskal-Wallis' post-hoc test) was applied to analyse experiments with more than two groups. The Two-way ANOVA test (with Bonferroni's post-hoc test) was applied to analyse different categorical independent endpoints with one dependent variable. A probability of $p < 0.05$ was considered to be statistically significant.

Results

The mast cell activity alters the lymphocyte population in human CRC cases

Analysing matching samples of normal colon and CRC tissues reveals that MC numbers might increase or remain unchanged in this pathological condition when compared with normal colon tissue from the same patient (**Fig 1A, B**). Furthermore, TCGA-based immunogenomic analysis of 604 CRC cases shows that MCs reside in tumours as either active or inactive units (**Fig 1C**). We also observed that activated MCs negatively correlated with lymphocyte infiltration in CRC cases, whereas dormant MCs positively correlated with these cells (**Fig 1C**). We further verified these observations by studying CRC cases in which activated MCs were present in either low (LMCA) or high numbers (HMCA). An HMCA appeared to decrease the number of tumour-residing CD8 T cells (**Fig 1D**). Our observations confirm previous reports that MCs may alter the CRC development and CD8 T cell density in those lesions.

The mast cell activity impacts the development of colitis-dependent or -independent tumours in mice

To test the idea that MCs can directly affect CRC cells, we first harvested high-MC numbers from Kit^{B6} mice bearing MC38 cell-induced ascites (**Fig 2A**). Peritoneal MCs from MC38-bearing mice reduced proliferation of CRC cells in a co-culture model (**Fig 2B**). MCs also promoted apoptosis in MC38 cells (**Fig 2C-D**). Moreover, MCs decreased the number of MC38 colonies in a long-term co-culturing system (**Fig 2E-F**).

To mechanistically explore MC activity throughout the multi-stage development of CRC, tumorigenesis was induced in mice in either a colitis-dependent (CA-CRC) or a colitis-independent fashion (sCRC) [21]. Induction of CA-CRC in MC-deficient mice ($Kit^{W/sh}$) reduced tumour burden compared to counterparts, even with high-*Cd8* expression levels in those tumours (**Fig 3A-B**). However, this experimental condition did not alter *Cd3* expression levels (Kit^{B6} – 1.0±0.1; $Kit^{W/sh}$ – 1.3±0.2; p =0.38). Histopathological analysis confirmed that MC-deficiency promoted a higher number of CD8+ cells in CA-CRC lesions (**Fig 3B**). MC deficiency did not alter the *Cd11c* (Kit^{B6} – 0.6±0.08; $Kit^{W/sh}$ – 0.4±0.17; p =0.48) and *Cd4* levels (Kit^{B6} – 1.8±0.2; $Kit^{W/sh}$ – 2.5±0.6; p =0.48).

After mice underwent the sCRC induction protocol, we observed that MC deficiency promoted the development of sporadic colorectal tumours (**Fig 3C**). In sCRC lesions, unlike the CA-CRC ones, MC deficiency did not alter the *Cd8* expression levels, nor the tumour infiltration of CD8 lymphocytes (**Fig 3D, E; Suppl Fig 2A**). However, it decreased tumour *Cd3* expression levels (Kit^{B6} – 1.0±0.1; $Kit^{W/sh}$ – 0.6±0.1; p =0.04). By analysing a proliferation biomarker, we observed proliferative rates did not change, significantly (**Fig 3E; Suppl Fig 2A – C**).

To explore these findings, we performed an RNAseq analysis to investigate that MC deficiency alters several inflammatory responses (**Fig 3F**; **Suppl Tab 4**). MC deficiency up-regulated the cytokine-cytokine receptor interaction pathway (p =9.8^{-11};

Suppl Tab 5). Our findings suggest that MC activity varies according to the various factors inducing the development of colorectal tumours, as opposing results between CA-CRC and sCRC models demonstrate.

The mast cell-lymphocyte axis impacts the development of early tumorigenic events in the colon

Considering that MC deficiency may promote significant changes in the tumour microenvironment, we explored the hypothesis that MCs play a pivotal role in building this tumour microenvironment from the early tumorigenic steps onwards. First, we observed that the sCRC protocol increased the colonic CD8 T cell population during the development of the early tumorigenic steps in the colon (**Fig 4A**; **Suppl Fig 3**). This finding led us to rationalize that major histocompatibility complex class I (MHCI) activity directly impacts the lymphocyte population [31]. When we induced early tumorigenic lesions in a MHCI deficiency model (*B2m* KO), we observed reduced *Cd8* expression levels but increased levels of MC biomarkers (mast cell protease 1, *Mcpt1* [epithelial]; *Mcpt4* [stromal]; [32]; **Fig 4B-E**; **Suppl Fig 4**). Conversely, MHCII deficiency decreased the expression of *Mcpt1* and *Mcpt4* in the colon of AOM-exposed mice (**Fig 4F-I**; **Suppl Fig 4**). To confirm that these early tumorigenic steps required a specific immune response to develop, they were induced in NOD-scidγ immunosuppressed mice. This experiment revealed that immunosuppression decreases the development of early tumorigenic lesions, epithelial cellular proliferation, and the number of MCs (**Suppl Fig 5A-C**).

As MC-deficient sCRC tumours had low *Il6* expression levels (**Fig 3F**), a mouse Il6 deficiency model underwent induction of early tumorigenic lesions. This colonic Il6 deficient microenvironment decreased the development of early tumorigenic lesions and MC numbers (**Suppl Fig 5D-E**). Considering that we found that high-*Il33* levels occurs

in MC deficient sCRC lesions (**Fig 3F**) and a previous study has shown that the interleukin 33 receptor (*Il33r*) modulated MC-related tumorigenic effects [11], we induced early colon tumorigenic lesions in an *Il33r* deficiency model. The *Il33r* deficiency reduced CRC-related biomarkers in carcinogen-exposed mice (**Fig 4J, L**). This condition up-regulated expression levels of MC biomarkers but downregulated the gene encoding *Cd8* (**Fig 4M-P**; **Suppl Fig 4**).

We further confirmed that an MC-lymphocyte axis impacts the development of early tumorigenic lesions in the colon. Thus, these lesions were induced in MC deficient mice and analysed after 6 weeks from the 6th carcinogenic exposure. This experiment revealed that MC activity reduces the development of early tumorigenic lesions and the levels of *Cd4* and *Cd11c* (**Fig 5A-C**). We further confirmed that increased *Cd4* and *Cd11c* levels were occurring just a week from the 6th carcinogenic exposure (**Fig 5D-E**). Moreover, MC deficiency decreased the expression of a gene associated to an essential DNA damage repair (DDR) mechanism against AOM-related DNA adducts known as O^6-methylguanine-DNA-methyltransferase (*Mgmt)* (**Fig 5F**).

To further investigate the MC role in these early colon tumorigenic events, we applied our previous reported strategy to study DNA damage and single early tumorigenic events [22]. DNA damage was analysed following 72 h from the 3rd carcinogenic exposure to reveal that MC deficiency did not alter the γH2AX levels in the colon while increasing the *Cd11c* expression (**Fig 5G-H**). To study the earliest immunological reactions activated by MC deficiency, we performed transcriptomic analyses in the colon of mice at the 3rd week from the 3rd carcinogenic exposure. Out of several immunological reactions (**Fig 5I; Suppl Tab 6**), MC deficiency significantly impacted the inflammatory bowel disease pathway (**Suppl Tab 7**).

We next validated these findings by performing BMT in $Kit^{W/sh}$ mice before inducing the development of single early colon tumorigenic lesions in them (**Fig 5J**). This experiment revealed that restoring MCs into previously MC deficient mice increased proliferation in the carcinogen-exposed colon (*Mki67* [FC], Kit^{B6}BMT – 1.3±0.1; $Kit^{W/sh}$ BMT – 2.9±0.5; p =0.006). Interestingly, rescuing MC activity in MC deficient mice before the development of single early colon tumorigenic lesions increased the Mcpt4 levels while blocking the expression of *Cd11C* (**Fig 5K, L**). These results illustrate that MCs impact and are impacted by other immune reactions activated throughout the development of early colon tumorigenic lesions.

Targeting mast cells against CRC lesions

Since our observations suggested that the MC population could promote specific effects in different stages of CRC development, we treated Kit^{B6} mice with CA to inhibit MC activity throughout the 3 weeks of carcinogenic exposure or following this period (**Fig 6A**). Although CA treatment did not alter DNA damage levels (**Fig 6B**), inhibiting MC activity throughout the carcinogenic exposure increased sCRC risk, whereas mice given CA post-carcinogen induction did not develop early tumorigenic lesions (**Fig 6C**). This time-related MC inhibition that promoted the development of early tumorigenic lesions also increased proliferation and up-regulated the expression levels of *Cd4*, *Foxp3*, *Cd8*, and *Cd3* (*Cd3* [FC], AOM – 1.3±0.1; AOM+CA – 3.0±0.3; AOM-CA – 2.3±0.7; AOM *vs* AOM+CA, p =0.03; **Fig 6D, F-H**).

We then performed transcriptomic studies to clarify significant changes in inflammatory reactions promoted by pharmacologically inhibiting the MC activity (**Fig 6I**; **Suppl Tab 8 – 9**). Out of several immunological changes that the CA treatment induces, it inhibited key elements of the cell adhesion pathway (**Fig 6I**; **Suppl Tab 10**).

Conversely, when CA treatment and carcinogenic exposure are given together, it down-regulates the antigen processing and presentation pathway (**Suppl Tab 11**).

These findings led us to verify how much MCs could impact the engraftment potential of CRC cells. This experiment revealed that MC deficiency blocks the development of CRC allograft tumours without altering their proliferative activity (**Fig 7A; Suppl Fig 6A**). Interestingly, this MC deficiency significantly up-regulates the tumour *Cd4* and *Cd8* expression levels (**Suppl Fig 6B-C**). Moreover, it increased the tumour infiltration of CD8 lymphocytes (**Fig 7B**). When we performed an RNAseq analysis to explore potential immune reactions associated with MC deficient tumours, it showed a down-regulation of the proteasome pathway and up-regulation of key elements of the antigen processing and presentation mechanism (**Fig 7C; Suppl. Tab. 12, 13**).

Once we tested the therapeutic potential of MC inhibition against CRC development, it revealed that inhibiting MC activity significantly blocks the development of allograft colorectal tumours (**Fig 7D; Suppl Fig 7A**). To further explore the anticancer therapeutic potential of MC activity blockade, we observed that CA treatment prevented the growth of melanoma tumour allografts (**Fig 7E; Suppl Fig 8A-B**). Surprisingly, blocking MC activity in melanoma reduced the $CD8^{+}CD3^{+}$ T cell population without altering the MC one (**Fig 7F; Suppl Fig 8C-D**). Encouraged by these findings, we blocked MC activity in colorectal tumours 14 days after cancer implantation (**Suppl Fig 9A-B**). Again, CA treatment inhibited colorectal tumour development and increased the $CD8^{+}CD3^{+}$ T cell population without altering the MC numbers (**Fig 7G-I; Suppl Fig 9C**). To challenge the idea that inhibiting MC activity would enhance anticancer response by cytotoxic lymphocytes, we treated CD3-deficient mice with CA for 3 days before implanting MC38 cancer cells. We then monitored the tumour growth for other 11 days.

It revealed that without an effective T cell-based response CA treatment did not reduce tumour growth (**Suppl Fig 11**).

This observation led to testing whether this drug could be combined with a gold-standard chemotherapy in CRC treatment. We found that CA potentialized the anticancer effects of 5-FU (**Fig 7J; Suppl Fig 7B**). Nevertheless, the results of this combination therapy seem to be comparable to the association of chemotherapy with a standard immunotherapeutic antibody (**Fig 7K**). Our data demonstrate that MCs impact the multistage development of CRC and are a druggable target against this disease.

Discussion

In this study, we have shown that MCs play an intricate role in CRC development in human patients. Tan *et al.* reported that a low MC counting correlates with more invasive tumours, increased number of metastatic lesions, and reduced 5-year survival rates [33]. Another study with 72 cases of CRC showed that a high MC density could promote overall survival and reduce the risk of malignancy-related deaths [7]. A randomized study with 82 cases of colorectal liver metastases has shown that chemotherapy increases MC density. This study also demonstrated that high MC numbers correlates with tumour regression and progression free survival [34].

Contrary, Malfettone *et al.* have shown that a reduced MC population improves the prognosis of CRC patients while increasing this cell density worsens the outcome of the disease [5]. Also, Nielsen *et al.* reported that increased MC numbers in a tumour might be related to better patient survival rates [8]. Mao *et al.* also showed in 854 subjects that a high MC counting may lead to poor overall patient survival. However, the authors also found that a high MC number may improve the patient survival in cases of stages II and III not receiving adjuvant chemotherapy. They further showed that MC density alters the

CD8 T cell population [6]. Our findings suggest that MC populations closely interacts with tumour-infiltrating lymphocytes.

Our mouse-based dataset provides significant evidence that MCs could either promote or inhibit the development of colon tumours. Although tumour-primed MCs seemed to have some anticancer activity in a co-culture system, our *in vivo* experiments suggest that the MC effects can vary according to the type of stimuli promoting CRC. Whereas MCs would inhibit CD8 cell density but promote inflammation-related CRC (CA-CRC), they may be protective against the DNA damage-related form of this disease (sCRC). In a *Kit* mutant mouse strain other than the $Kit^{W/sh}$ one (differences described by Grimbaldeston *et al.* [35]), Wedemeyer *et al.* reported that MC deficiency reduced carcinogen-induced colorectal tumour burden [9]. We have also observed that $Kit^{W/sh}$ and $Kit^{W/W\text{-}v}$ respond differently to the same carcinogen exposure (**Fig 3A**, **5A** and **Suppl Fig 11**).

Sinnamon *et al.* reported that deleting adenomatous polyposis coli (*Apc*) in mice promotes TRY expression in tumours. By ablating the MC population in $Apc^{Min/+}$ mice, they found that MC activity blocked tumour development [14]. Bodduluri *et al.* have also shown that chemokine-mediated MC recruitment initiates MC-derived leukotriene-regulated CD8+ T-cell homing and antitumor immunity reducing intestinal tumour burden in $Apc^{Min/+}$ mice [13]. In the CA-CRC model, Tanaka *et al.* reported that MC deficient mice are less susceptible to inflammation-associated colorectal tumours [12]. Rigoni *et al.* also observed that MC deficiency increased the number of malignant lesions in the colon [11].

We further demonstrated that MC activity alters pivotal immune mechanisms and vice-versa. Whether MC density seemed to determine the growth potential of carcinogen-induced lesions (**Figs. 3, 5, 6**), an effect completely reversed in cancer (**Fig. 7**), essential

immune factors also changed the MC activity. The balance between MHCI and MHCII levels altered MC-related chemokines release in our study. Le Bouteiller *et al*. found that anti-MHC alloantibodies modulate MC activity [36]. When MCs were stimulated by antibody bipolar bridging, Daeron and Voisin showed that MHC-I reverse signalling modulates MC activity [37, 38]. Moreover, Malbec *et al*. revealed that antigen recognition by FcγR-bound IgG on MCs could mediate trans-inhibition without co-clustering with FcεRI binding to IgE antibodies, a mechanism inhibiting oncogen-induced proliferation in mastocytoma[39]. Furthermore, MCs seem able to express MHCII in cell culture but not *in vivo* [1, 40]. Then, Dudeck *et al*. showed that innate-to-innate synapse-like contacts enable DC-to-MC molecule transfers including MHCII proteins and subsequent T cell priming[41].

The Il6-related and Il33r-related signalling promoted opposing effects on MC activity during the early colon tumorigenic steps. Desai *et al* have shown that Il6 stimulation expands MC population and promotes its reactivity [42]. It has been demonstrated that that differentiating CD34+ human cord blood cells into MCs requires stem cell factor stimulation but adding IL6 increases cell size and intracellular levels of chymase and histamine[43]. In both human CRC and mouse polyposis, MCs can modulate and be modulated by Il10, Il6, Il17, and Il2 levels, by which they recruit Treg and promote Treg-induced suppression of host-vs-graft rejection responses or render the Treg proinflammatory role furthering CRC development [44]. Interestingly, Il33r seems required for CRC cellular expansion[45], while Il33 deficiency inhibited intestinal tumour burden and reduced intra-tumour MC density and MC-derived proteases and cytokines release [46, 47]. Moreover, Il11-induced tumour-derived Il33 signalling activates MCs and promotes gastric cancer development in mice. Genetically ablating Il33r blocks MC-dependent recruitment of macrophages limiting tumour growth [48].

We further explored the idea that MCs are druggable targets against CRC. Pharmacologically inhibiting MC activity blocks tumour growth and can be combined with standard chemotherapy strategies. Pharmacologically inhibiting MCs activity has been shown an effective anticancer strategy against different types of tumours [10, 49-51]. Moreover, drug-based MC inhibition has been combined with gemcitabine, decreasing pancreatic cancer's tumour growth [50]. Also, it has also been associated with anti-angiogenic therapy to treat murine lymphoma and pancreatic cancer [51]. These facts illustrate that MCs are a druggable target that can potentialize the anticancer effects of current therapies. However, a potential limitation of our study is that in addition to inhibiting MC activity CA can impact cancer cell signalling and survival as well as other immune responses [52, 53]. The fact that CA treatment requires T lymphocytes to block tumour growth and can be combined with 5-FU strengthens the idea that CRC patients may can benefit from MC-based therapies.

Therefore, we suggest that MC activity can significantly impact CRC development in either a beneficial or harmful fashion; this effect seems to be substantially determined during the early stages of this disease. Moreover, this MC activity appears to be a druggable target with significant potential for anti-CRC therapeutic strategies.

Acknowledgements

The authors disclose receipt of the following financial support for the development of this investigation: Sao Paulo Research Foundation (FAPESP; 2014/06428-5). The funder had no role in the study design, data collection, analysis, decision to publish, or preparation of the manuscript.

Contributorship statement

Study concept and design: VK; Acquisition of data: JYS, JEO, LYA, ESS, MOB, TMM, SA, CLAS, DC, MVA, VLD, SBG, FQC, GCMC, RBM, LMC, FLM, SAU, VK; Statistical analysis: JYS, JEO, TMM, GCMC, VK; Analysis and interpretation of data: All; Drafting the first version of the manuscript: JYS and VK; Critical revision of the manuscript: All; Obtained funding: DC, TMM, MOB, VLDB, FQC, JM, LMC, FLM, SAU, VK; Technical and material support: LYA, MOB, SA, CLAS, DC, VLDB, RBM, MAV, SBG, FQC, JM, LMC, SAU, VK; Study supervision: SAU, VK.

References

1. Chatterjee V, Gashev AA. Mast cell-directed recruitment of MHC class II positive cells and eosinophils towards mesenteric lymphatic vessels in adulthood and elderly. *Lymphat Res Biol*. 2014;12:37-47.

2. Villa I, Skokos D, Tkaczyk C, et al. Capacity of mouse mast cells to prime T cells and to induce specific antibody responses in vivo. *Immunology*. 2001;102:165-72.

3. Frandji P, Tkaczyk C, Oskeritzian C, et al. Exogenous and endogenous antigens are differentially presented by mast cells to CD4+ T lymphocytes. *Eur J Immunol*. 1996;26:2517-28.

4. Dimitriadou V, Mecheri S, Koutsilieris M, et al. Expression of functional major histocompatibility complex class II molecules on HMC-1 human mast cells. *J Leukoc Biol*. 1998;64:791-9.

5. Malfettone A, Silvestris N, Saponaro C, et al. High density of tryptase-positive mast cells in human colorectal cancer: a poor prognostic factor related to protease-activated receptor 2 expression. *J Cell Mol Med*. 2013;17:1025-37.

6. Mao Y, Feng Q, Zheng P, et al. Low tumor infiltrating mast cell density confers prognostic benefit and reflects immunoactivation in colorectal cancer. *Int J Cancer*. 2018;143:2271-2280.

7. Mehdawi L, Osman J, Topi G, et al. High tumor mast cell density is associated with longer survival of colon cancer patients. *Acta Oncol*. 2016;55:1434-1442.

8. Nielsen HJ, Hansen U, Christensen IJ, et al. Independent prognostic value of eosinophil and mast cell infiltration in colorectal cancer tissue. *J Pathol*. 1999;189:487-95.

9. Wedemeyer J, Galli SJ. Decreased susceptibility of mast cell-deficient Kit(W)/Kit(W-v) mice to the development of 1, 2-dimethylhydrazine-induced intestinal tumors. *Lab Invest*. 2005;85:388-96.

10. Motawi TK, El-Maraghy SA, ElMeshad AN, et al. Cromolyn chitosan nanoparticles as a novel protective approach for colorectal cancer. *Chem Biol Interact*. 2017;275:1-12.

11. Rigoni A, Bongiovanni L, Burocchi A, et al. Mast Cells Infiltrating Inflamed or Transformed Gut Alternatively Sustain Mucosal Healing or Tumor Growth. *Cancer Res*. 2015;75:3760-70.

12. Tanaka T, Ishikawa H. Mast cells and inflammation-associated colorectal carcinogenesis. *Semin Immunopathol*. 2013;35:245-54.

13. Bodduluri SR, Mathis S, Maturu P, et al. Mast Cell-Dependent CD8(+) T-cell Recruitment Mediates Immune Surveillance of Intestinal Tumors in Apc(Min/+) Mice. *Cancer Immunol Res*. 2018;6:332-347.

14. Sinnamon MJ, Carter KJ, Sims LP, et al. A protective role of mast cells in intestinal tumorigenesis. *Carcinogenesis*. 2008;29:880-6.

15. Newman AM, Liu CL, Green MR, et al. Robust enumeration of cell subsets from tissue expression profiles. *Nat Methods*. 2015;12:453-7.

16. Thorsson V, Gibbs DL, Brown SD, et al. The Immune Landscape of Cancer. *Immunity*. 2019;51:411-412.

17. Townsend MJ, Fallon PG, Matthews DJ, et al. T1/ST2-deficient mice demonstrate the importance of T1/ST2 in developing primary T helper cell type 2 responses. *J Exp Med*. 2000;191:1069-76.

18. Carlos D, Sa-Nunes A, de Paula L, et al. Histamine modulates mast cell degranulation through an indirect mechanism in a model IgE-mediated reaction. *Eur J Immunol*. 2006;36:1494-503.

19. Wargovich MJ, Chen CD, Jimenez A, et al. Aberrant crypts as a biomarker for colon cancer: evaluation of potential chemopreventive agents in the rat. *Cancer Epidemiol Biomarkers Prev*. 1996;5:355-60.

20. Kubota T, Fujita S, Kodaira S, et al. Antitumor activity of fluoropyrimidines and thymidylate synthetase inhibition. *Jpn J Cancer Res*. 1991;82:476-82.

21. Neufert C, Becker C, Neurath MF. An inducible mouse model of colon carcinogenesis for the analysis of sporadic and inflammation-driven tumor progression. *Nat Protoc*. 2007;2:1998-2004.

22. Sakita JY, Bader M, Santos ES, et al. Serotonin synthesis protects the mouse colonic crypt from DNA damage and colorectal tumorigenesis. *J Pathol*. 2019;249:102-113.

23. Finnberg NK, Hart LS, Dolloff NG, et al. High-resolution imaging and antitumor effects of GFP(+) bone marrow-derived cells homing to syngeneic mouse colon tumors. *Am J Pathol*. 2011;179:2169-76.

24. Leite CA, Mota JM, de Lima KA, et al. Paradoxical interaction between cancer and long-term postsepsis disorder: impairment of de novo carcinogenesis versus favoring the growth of established tumors. *J Immunother Cancer*. 2020;8.

25. Ravindran A, Ronnberg E, Dahlin JS, et al. An Optimized Protocol for the Isolation and Functional Analysis of Human Lung Mast Cells. *Front Immunol*. 2018;9:2193.

26. Puck TT, Marcus PI. A Rapid Method for Viable Cell Titration and Clone Production with Hela Cells in Tissue Culture: The Use of X-Irradiated Cells to Supply Conditioning Factors. *Proc Natl Acad Sci U S A*. 1955;41:432-7.

27. Samoszuk M, Tan J, Chorn G. Clonogenic growth of human breast cancer cells co-cultured in direct contact with serum-activated fibroblasts. *Breast Cancer Res*. 2005;7:R274-83.

28. Puebla-Osorio N, Sarchio SNE, Ullrich SE, et al. Detection of Infiltrating Mast Cells Using a Modified Toluidine Blue Staining. *Methods Mol Biol*. 2017;1627:213-222.

29. Love MI, Huber W, Anders S. Moderated estimation of fold change and dispersion for RNA-seq data with DESeq2. *Genome Biol*. 2014;15:550.

30. Computing RFfS. A Language and Environment for Statistical Computing. 2021.

31. Koller BH, Marrack P, Kappler JW, et al. Normal development of mice deficient in beta 2M, MHC class I proteins, and CD8+ T cells. *Science*. 1990;248:1227-30.

32. Xing W, Austen KF, Gurish MF, et al. Protease phenotype of constitutive connective tissue and of induced mucosal mast cells in mice is regulated by the tissue. *Proc Natl Acad Sci U S A*. 2011;108:14210-5.

33. Tan SY, Fan Y, Luo HS, et al. Prognostic significance of cell infiltrations of immunosurveillance in colorectal cancer. *World J Gastroenterol*. 2005;11:1210-4.

34. Tanis E, Julie C, Emile JF, et al. Prognostic impact of immune response in resectable colorectal liver metastases treated by surgery alone or surgery with perioperative FOLFOX in the randomised EORTC study 40983. *Eur J Cancer*. 2015;51:2708-17.

595 35. Grimbaldeston MA, Chen CC, Piliponsky AM, et al. Mast cell-deficient W-sash c-kit
596 mutant Kit W-sh/W-sh mice as a model for investigating mast cell biology in vivo. *Am J*
597 *Pathol*. 2005;167:835-48.
598 36. Le Bouteiller P, Daeron M, Duc HT, et al. An ultrastructural study of two different
599 responses of mouse mast cells to transplantation antibodies directed against the same
600 transplantation antigens. *Eur J Immunol*. 1976;6:326-32.
601 37. Daeron M, Voisin GA. H-2 antigens, on mast cell membrane, as target antigens for
602 anaphylactic degranulation. *Cell Immunol*. 1978;37:467-72.
603 38. Daeron M, Voisin GA. Mast cell membrane antigens and Fc receptors in anaphylaxis.
604 I. Products of the major histocompatibility complex involved in alloantibody-induced
605 mast cell activation. *Immunology*. 1979;38:447-58.
606 39. Malbec O, Cassard L, Albanesi M, et al. Trans-inhibition of activation and
607 proliferation signals by Fc receptors in mast cells and basophils. *Sci Signal*. 2016;9:ra126.
608 40. Kambayashi T, Allenspach EJ, Chang JT, et al. Inducible MHC class II expression by
609 mast cells supports effector and regulatory T cell activation. *J Immunol*. 2009;182:4686-
610 95.
611 41. Dudeck J, Medyukhina A, Frobel J, et al. Mast cells acquire MHCII from dendritic
612 cells during skin inflammation. *J Exp Med*. 2017;214:3791-3811.
613 42. Desai A, Jung MY, Olivera A, et al. IL-6 promotes an increase in human mast cell
614 numbers and reactivity through suppression of suppressor of cytokine signaling 3. *J*
615 *Allergy Clin Immunol*. 2016;137:1863-1871 e6.
616 43. Conti P, Kempuraj D, Di Gioacchino M, et al. Interleukin-6 and mast cells. *Allergy*
617 *Asthma Proc*. 2002;23:331-5.
618 44. Blatner NR, Bonertz A, Beckhove P, et al. In colorectal cancer mast cells contribute
619 to systemic regulatory T-cell dysfunction. *Proc Natl Acad Sci U S A*. 2010;107:6430-5.

45. O'Donnell C, Mahmoud A, Keane J, et al. An antitumorigenic role for the IL-33 receptor, ST2L, in colon cancer. *Br J Cancer*. 2016;114:37-43.

46. Maywald RL, Doerner SK, Pastorelli L, et al. IL-33 activates tumor stroma to promote intestinal polyposis. *Proc Natl Acad Sci U S A*. 2015;112:E2487-96.

47. He Z, Chen L, Souto FO, et al. Epithelial-derived IL-33 promotes intestinal tumorigenesis in Apc (Min/+) mice. *Sci Rep*. 2017;7:5520.

48. Eissmann MF, Dijkstra C, Jarnicki A, et al. IL-33-mediated mast cell activation promotes gastric cancer through macrophage mobilization. *Nat Commun*. 2019;10:2735.

49. Johnson C, Huynh V, Hargrove L, et al. Inhibition of Mast Cell-Derived Histamine Decreases Human Cholangiocarcinoma Growth and Differentiation via c-Kit/Stem Cell Factor-Dependent Signaling. *Am J Pathol*. 2016;186:123-33.

50. Arumugam T, Ramachandran V, Logsdon CD. Effect of cromolyn on S100P interactions with RAGE and pancreatic cancer growth and invasion in mouse models. *J Natl Cancer Inst*. 2006;98:1806-18.

51. Wroblewski M, Bauer R, Cubas Cordova M, et al. Mast cells decrease efficacy of anti-angiogenic therapy by secreting matrix-degrading granzyme B. *Nat Commun*. 2017;8:269.

52. Motawi TM, Bustanji Y, El-Maraghy S, et al. Evaluation of naproxen and cromolyn activities against cancer cells viability, proliferation, apoptosis, p53 and gene expression of survivin and caspase-3. *J Enzyme Inhib Med Chem*. 2014;29:153-61.

53. Puzzovio PG, Bruggemann TR, Pahima H, et al. Cromolyn Sodium differentially regulates human mast cell and mouse leukocyte responses to control allergic inflammation. *Pharmacol Res*. 2022;178:106172.

Figure Legends

Fig. 1. *MC activity effects in human CRC cases.*

(A) Representative images of MCs stained by TB (CRC or normal colon [CT] samples from the same patient; 40× [left-side] and 100× [right-side] magnification; sectioned lines indicate 100× magnified areas; arrows lead to positive cells). (B) Representative images of MCs stained by anti-tryptase antibody (TRY; 20× magnification; increased [upper-left] or unchanged [lower-left] MC numbers) in both CT and CRC samples. (A – B) MC density was found to be increased (A, n = 16, **p* =0.023; B, n = 14, **p* =0.026), or remain unchanged (A, n = 22; B, n = 12; *p* >0.05).

(C) A Immune features (*y* axes; total MCs [upper panels], or leukocyte infiltration [lower panels]) *vs* MC activated (left panels) or resting fractions (right panels; *x* axes) for CRC cases from TCGA.

(D) The CRC cohort positive for a MC activated (MCA) profile was divided in two groups of cases with low (LMCA) or high MCA values (HMCA). Lymphocytes and CD8 T cell levels are shown to be increased in LMCA group (****p =0.000105; *p =0.0284).

Data are shown as the median, highest and lowest values, and upper and lower quartiles. Dots represent individual tumour samples. The Pearson correlation was applied. *P*-values were calculated using two-tailed Mann-Whitney's test.

Fig. 2. *MCs induce apoptosis in murine CRC cells.*

(A) Tumour-primed MCs were isolated 7 days after Kit^{B6} mice received a single i.p. injection of murine CRC cells (MC38). Once purified, tumour-primed MCs were co-cultured with MC38 cells for 2 (B – D) or 5 days (E – F).

(B) Gene expression analysis by qPCR for *Mki67* (p <0.05).

(C – D) Representative dot plots of flow cytometric analysis for gating CD45(-) cells or MC38. It was followed by viability and apoptosis analysis. Graph shows percentages of negative or positive MC38 cells for Anexin V ($p < 0.05$).

(E – F) Representative images of clonogenic assays. Graph shows the relative number of colonies for each group ($p < 0.001$).

Dots represent individual values together with mean ± SEM. *P*-values were calculated using two-tailed Mann-Whitney's and Two-way ANOVA tests (Bonferroni's post-hoc) tests.

Fig. 3. *The dual MC role in colorectal tumorigenesis.*

(A) Representative images of tumours induced by the CA-CRC protocol (Scale bars = 1 cm). Graph shows tumour numbers *per* mice (n = 8; *p =0.0286).

(B) Gene expression analysis for *Cd8* (p =0.0286). Representative images of tumours stained by an anti-CD8 antibody (40× [left-side] and 100× [right-side] magnification; lines indicate 100× magnified areas; arrows lead to positive cells).

(C) Representative images of tumours induced by sCRC protocol (Scale bars = 1 cm). Graph shows tumour numbers *per* mice (n = 17; p =0.0164).

(D) Gene expression analysis for *Cd8* ($p > 0.05$).

(E) Representative images of multiplex IHC staining for CD8 lymphocytes (CD8) and proliferating tumour cells (Mki67; magnification at 200 µm). Data are shown as the median, highest and lowest values, and upper and lower quartiles (A, B), or individual data points with mean ± SEM (C, D). *p*-values were calculated using two-tailed Mann-Whitney's test.

(F) Heatmap of hierarchical clustering indicates differentially expressed genes (rows) between tumour samples from Kit^{B6} and $Kit^{W/sh}$ mice (n = 10). Red indicates up-regulation (Max) and blue indicates down-regulation (Min).

Fig. 4. *The early colorectal tumorigenic steps require complex immune reactions to develop.*

(A) Representative dot plot graphs of CD4+ and CD8+ lymphocytes gated for CD45+, live cells, and singlet.

(B – D, F – G, J – O) Gene expression analysis for *Cd8* (B, n = 8, **p* =0.02; H, n = 13, *p* >0.05; O, n = 9, **p* =0.03), *Mcpt1* (C, n = 8, **p* =0.02; G, n = 13, **p* =0.02; M, n = 9, **p* =0.01), *Mcpt4* (D, n = 8, **p* =0.02; F, n = 13, **p* =0.02; N, n = 9, **p* =0.01), *Ctnnb1* (J, n = 9, **p* =0.03), and *Mki67* (L, **p* =0.03) in *B2M*KO, *Ciita*KO, and *St2*KO mice, and their counterparts.

(E, I, P) Representative images of multiplex IHC staining with anti-CD8, anti-CD3, and anti-TRY antibodies (magnification at 50 μm).

Data are shown as the median, highest and lowest values, and upper and lower quartiles. *p*-values were calculated using a two-tailed Mann-Whitney's test.

Fig. 5. *The MC activity protects against early colorectal tumorigenic steps.*

(A) Representative images (10× and 40× [inset]; Scale bars = 20 μm) of early tumorigenic events preceding the detection of fully grown tumours in the colon. MC deficiency increases the number of them (n = 11; **p* =0.004).

(B – C) Gene expression analysis in colon samples of mice at the 6th week after the 6th carcinogenic exposure for *Cd4* (n = 11; **p* =0.03) and *Cd11c* (**p* =0.03).

(D – F) Gene expression analysis in colon samples of mice at the 1st week after the 6th carcinogenic exposure for *Cd11c* (n = 10; **p* =0.01), *Cd4* (**p* =0.02), and *Mgmt* (n = 11; **p* =0.04).

(G) DNA damage levels by immunoblotting against γH2AX and GADPH in colon samples of mice at the 3rd day after the 3rd carcinogenic exposure.

(H) Gene expression analysis for *Cd11c* in colon samples of mice at the 3rd day after the 3rd carcinogenic exposure (n = 9; *p* =0.003).

(I) Heatmap of hierarchical clustering obtained from RNA-seq data indicates differentially expressed genes between colon samples of Kit^{B6} and $Kit^{W/sh}$ mice at the 3rd week after the 3rd carcinogenic exposure (n = 6).

(J) Representative histograms of the BMT protocol performed in both Kit^{B6} and $Kit^{W/sh}$ mice. Spectral colour represents $EGFP^{+}$ cells by fluorescence intensity (GF; *x* axis) and cell counting (*y* axis) in different experimental conditions.

(K – M) Gene expression analysis for *Mcpt4* (*p =0.004), *Cd11c* (**p* =0.01), and *Cd8* (*p* >0.05) in colon samples of mice at the 3rd week after the 3rd carcinogenic exposure following the BMT procedure.

Data are shown as individual data points with mean ± SEM. *p*-value was calculated using a two-tailed Mann-Whitney's test.

Fig. 6. *The MC activity impacts the development of early tumorigenic lesions in the colon.*

(A) Timeline for different groups treated with CA (red arrows) and AOM (black arrows) throughout 6 weeks.

(B) DNA damage levels by immunoblotting against γH2AX and GADPH in colon samples.

(C) Inhibiting MC activity in specific timepoints of carcinogenic exposure can either promote or inhibit the development early tumorigenic events in the colon (n = 24; *p =0.042, ****p <0.0001).

(D – H) Gene expression analysis for *Mki67* (n = 24; *p <0.01; AOM *vs* AOM+CA), *Cd11c* (p >0.05), *Cd4* (*p <0.05; AOM *vs* AOM+CA), *Foxp3* (*p <0.01; AOM *vs* AOM+CA), and *Cd8* (*p <0.01; AOM *vs* AOM+CA). Data are shown as the median, highest and lowest values, and upper and lower quartiles (C – H). p-values were calculated using ANOVA with a Kruskal-Wallis' post-hoc test.

(I) Heatmap of hierarchical clustering obtained from RNA-seq data indicates differentially expressed genes (n = 12).

Fig. 7. *The MC activity can be therapeutically targeted against CRC in mice.*

(A) Representative images of tumours following harvest (Scale bars = 1 cm). The volume of allograft tumours were analysed after 14 days from their subcutaneous implantation (n = 9; *p =0.01).

(B) Representative images of CD8+ cells stained by anti-CD8 antibody (40× magnification; Scale bars = 30 μm; arrows lead to positive cells). MC deficiency promotes CD8+ cell infiltration in tumours (n = 9, *p =0.01).

(C) Heatmap of hierarchical clustering obtained from RNA-seq data indicates differentially expressed genes (n = 9).

(D) Relative tumour volume between CA-treated (CA) and untreated (CT) mice at the last day of a 15-days experiment (n = 8; *p =0.02).

(E) Relative tumour volume between CA-treated and untreated mice bearing melanoma tumours at the last day of a 15-days experiment (n = 11; *p =0.04).

(F, H) Representative dot plot graphs of MCs (CD45+CD117+FcεRI+) and CD45+CD8+CD3+ T cells isolated from B16F10 tumour samples.

(G) Relative tumour volume between CA-treated and untreated mice bearing CRC tumours at the last day of a 26-days experiment (n = 17; *$p < 0.0001$).

(I) Graphs show percentages of $CD45^{+}CD8^{+}CD3^{+}$ T cells isolated from tumour samples (n = 8; *p =0.02).

(J, K) Relative tumour growth among untreated, 5-FU-treated, and combined treatments with 5-FU for 17 days (J, n = 15; *p =0.04; K, n = 9; *p =0.04).

Data are shown as the median, highest and lowest values, and upper and lower quartiles, or individual data points with mean ± SEM. p-values were calculated using two-tailed Mann-Whitney's test and ANOVA with a Kruskal-Wallis' post-hoc test.

Figure 1

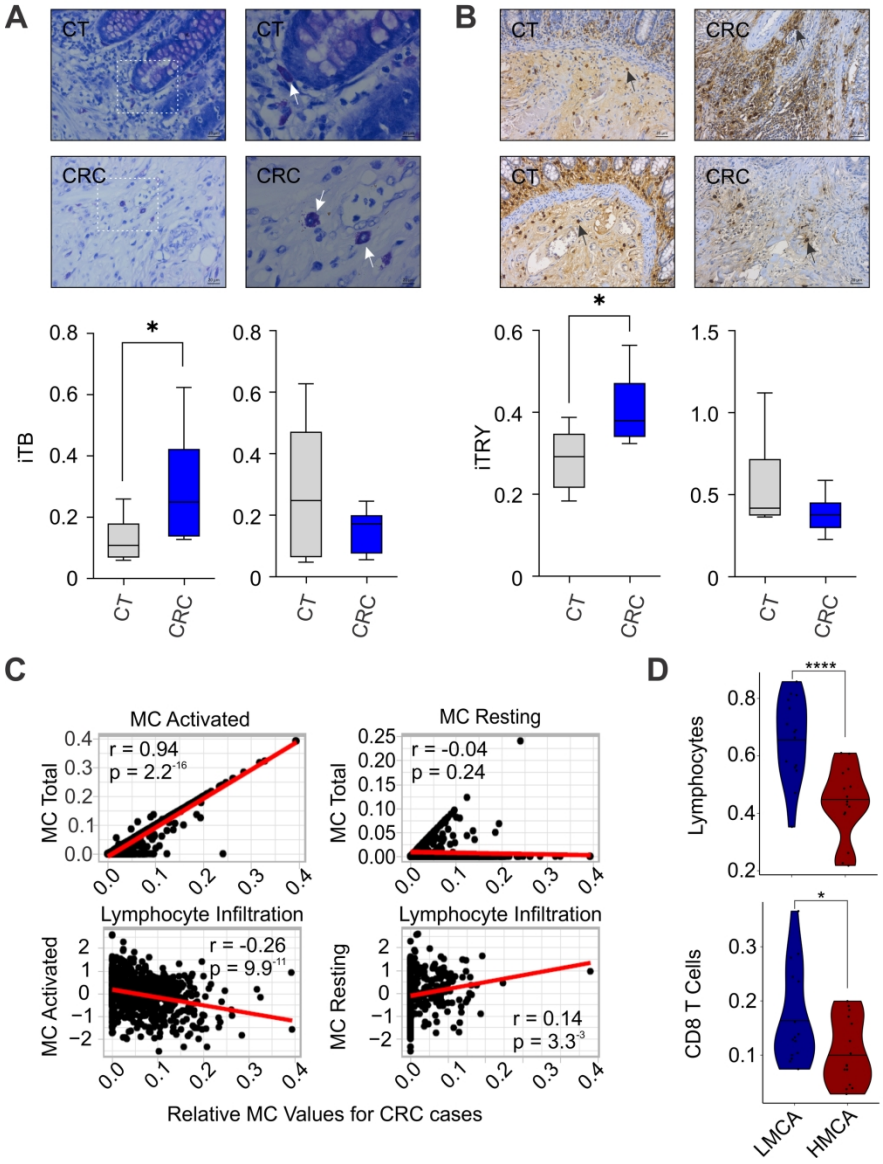

182x249mm (300 x 300 DPI)

Figure 2

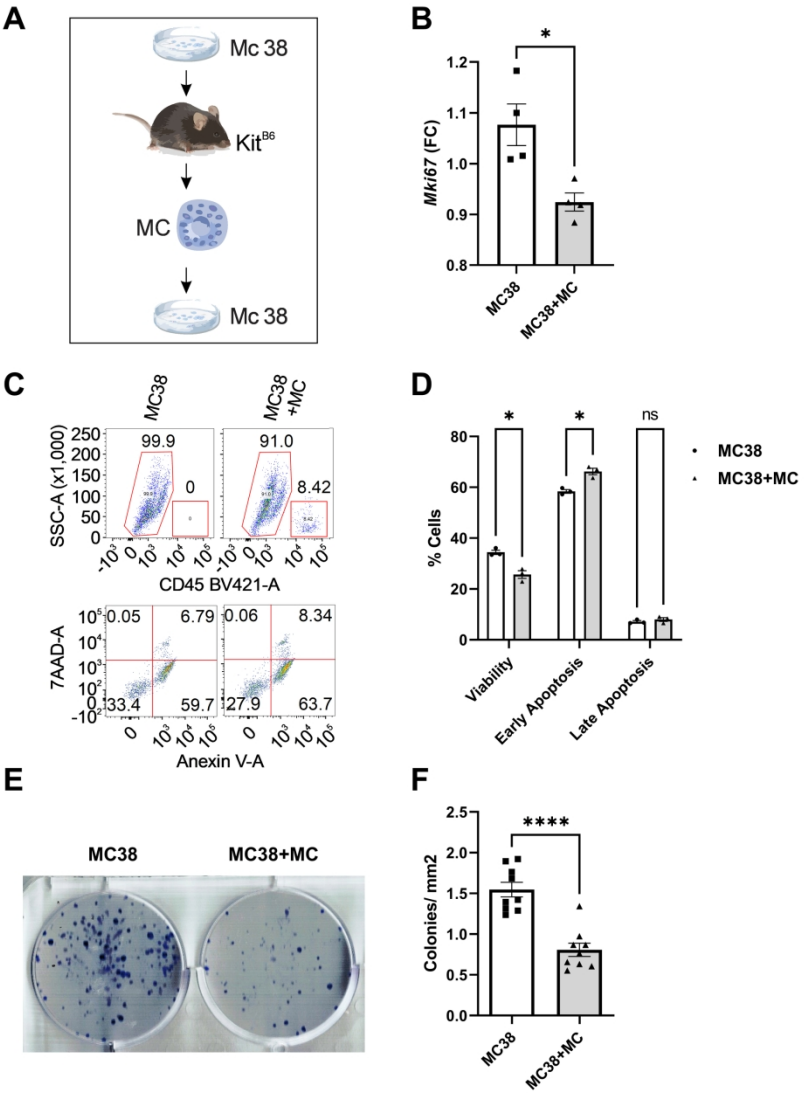

189x269mm (300 x 300 DPI)

Figure 3

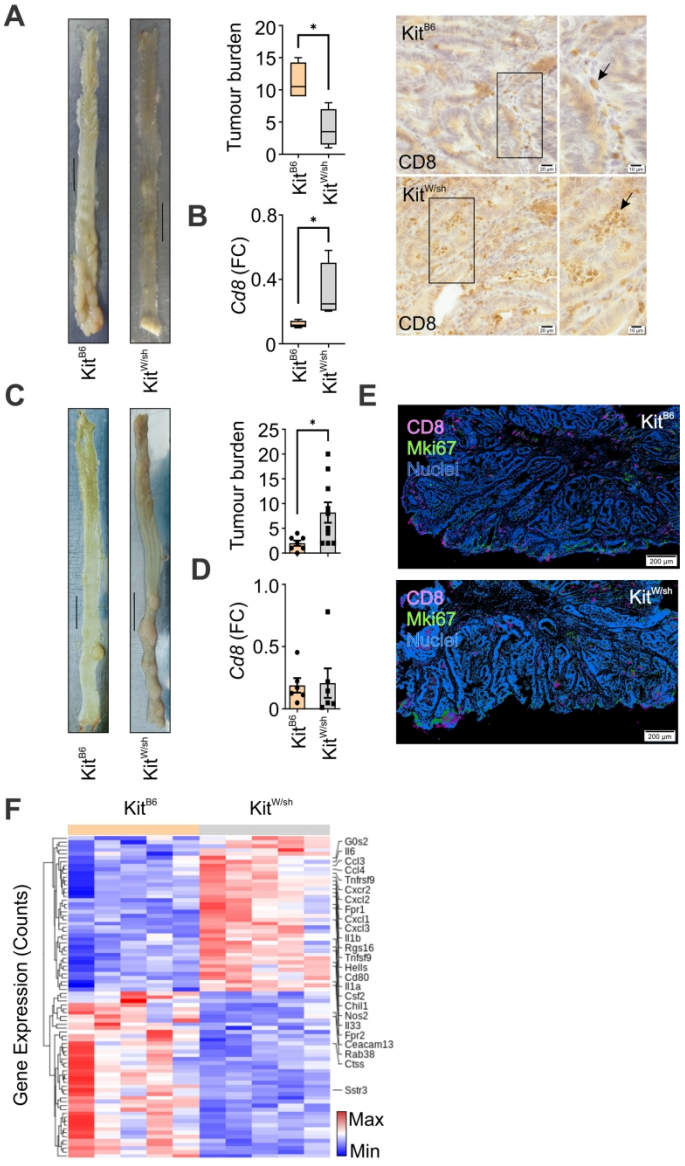

152x270mm (300 x 300 DPI)

Figure 4

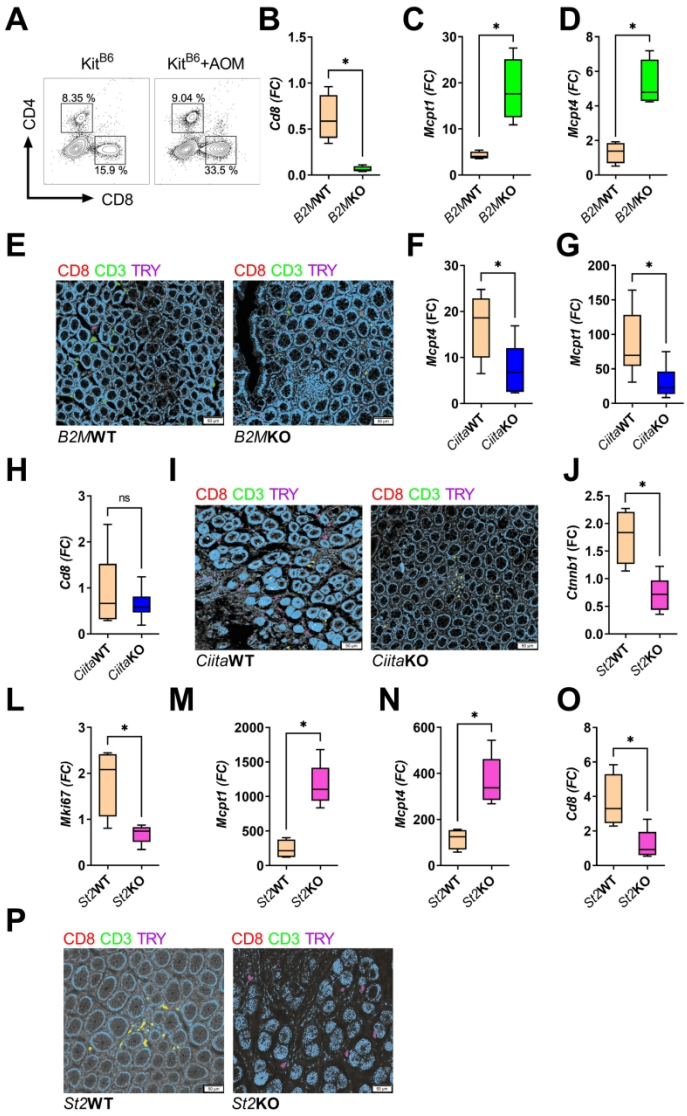

163x261mm (300 x 300 DPI)

Figure 5

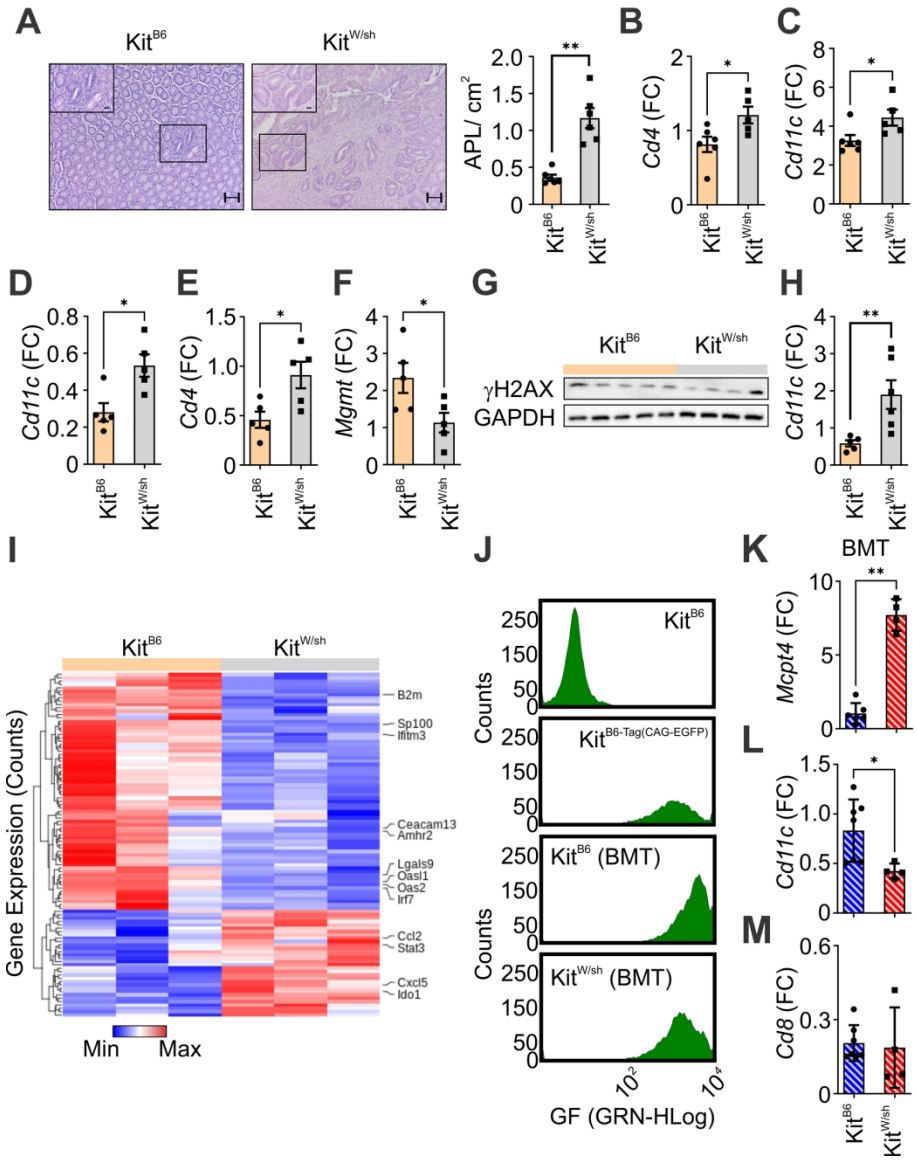

172x223mm (300 x 300 DPI)

Figure 6

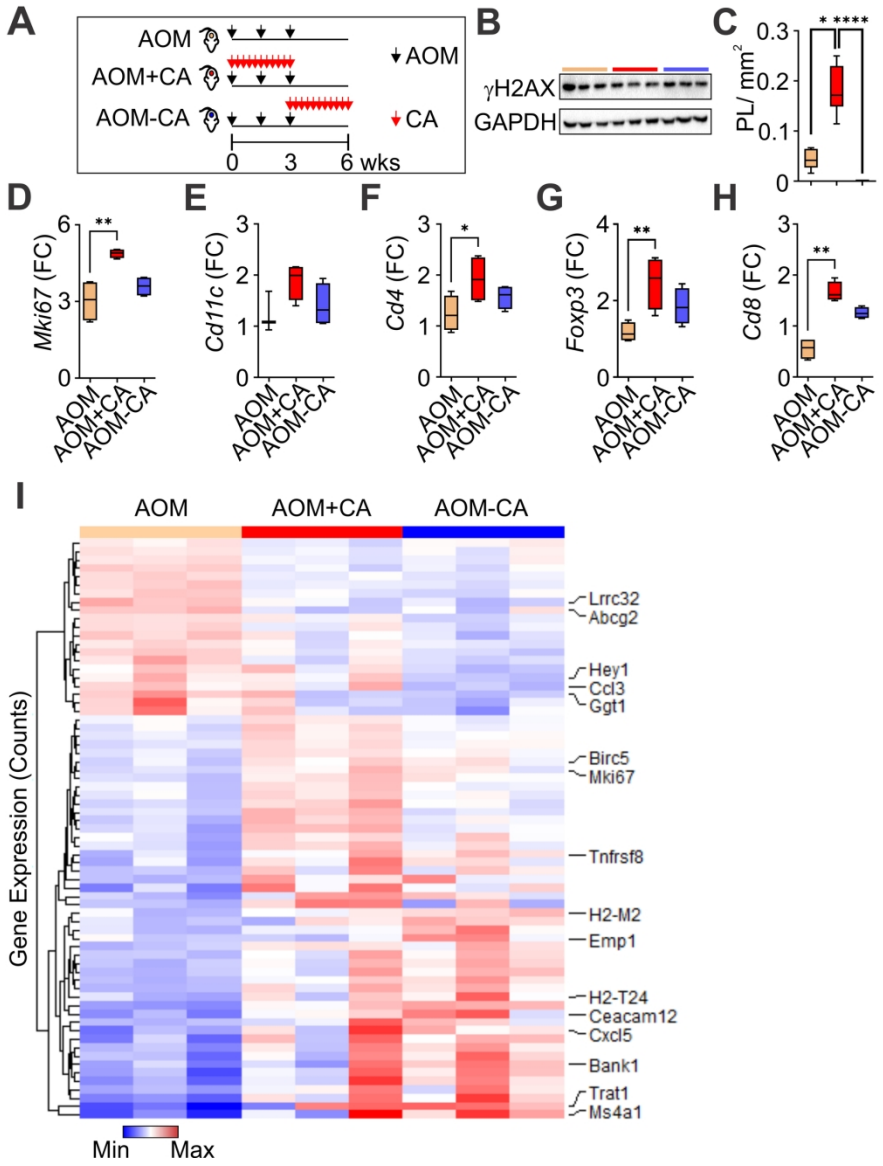

160x216mm (300 x 300 DPI)

Figure 7

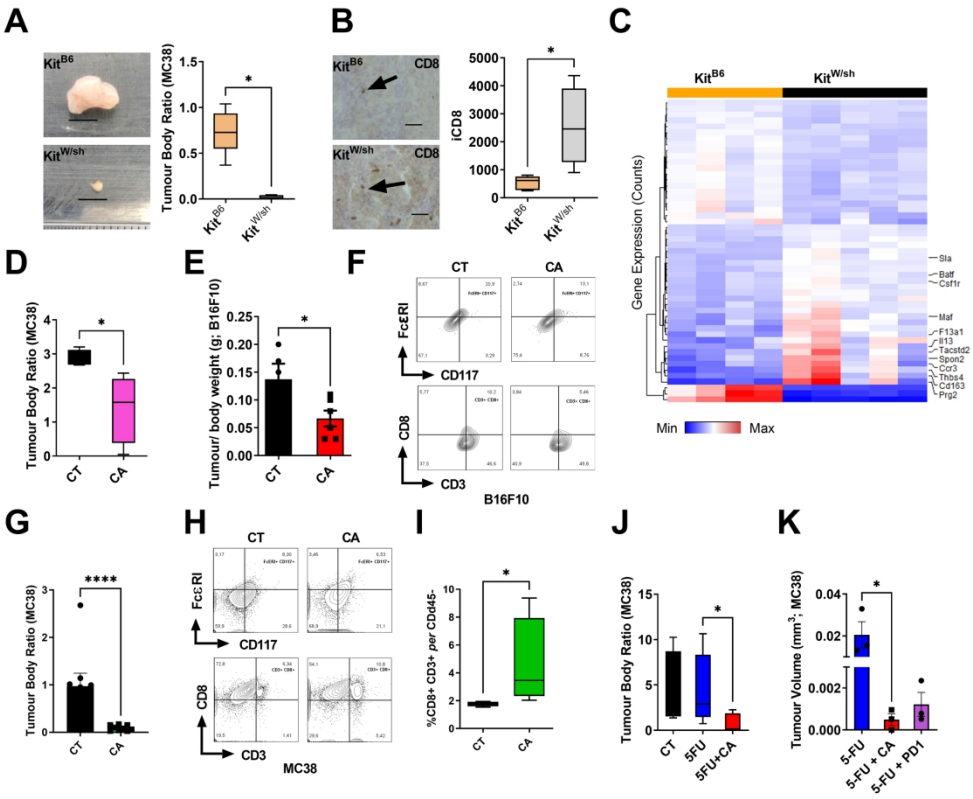

208x187mm (300 x 300 DPI)

Supplementary Figures

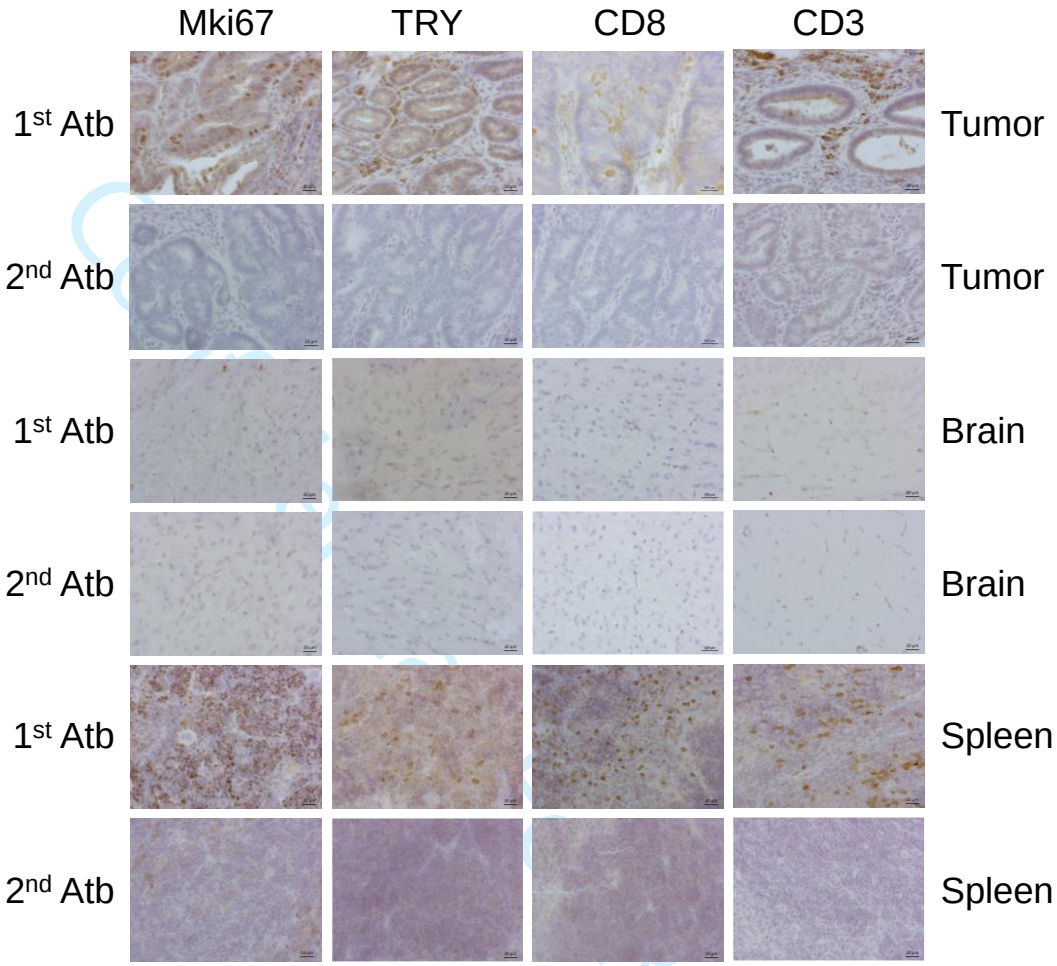

Suppl. Fig. 1. *Testing primary and secondary antibodies against positive and negative tissue samples.* To verify the working condition of our primary and secondary antibodies, we tested different antibodies (Suppl. Tab. 3) against samples from tumour (target tissue), spleen (positive control tissue), and brain (negative control tissue). Antibodies worked according to the manufacturer's guideline.

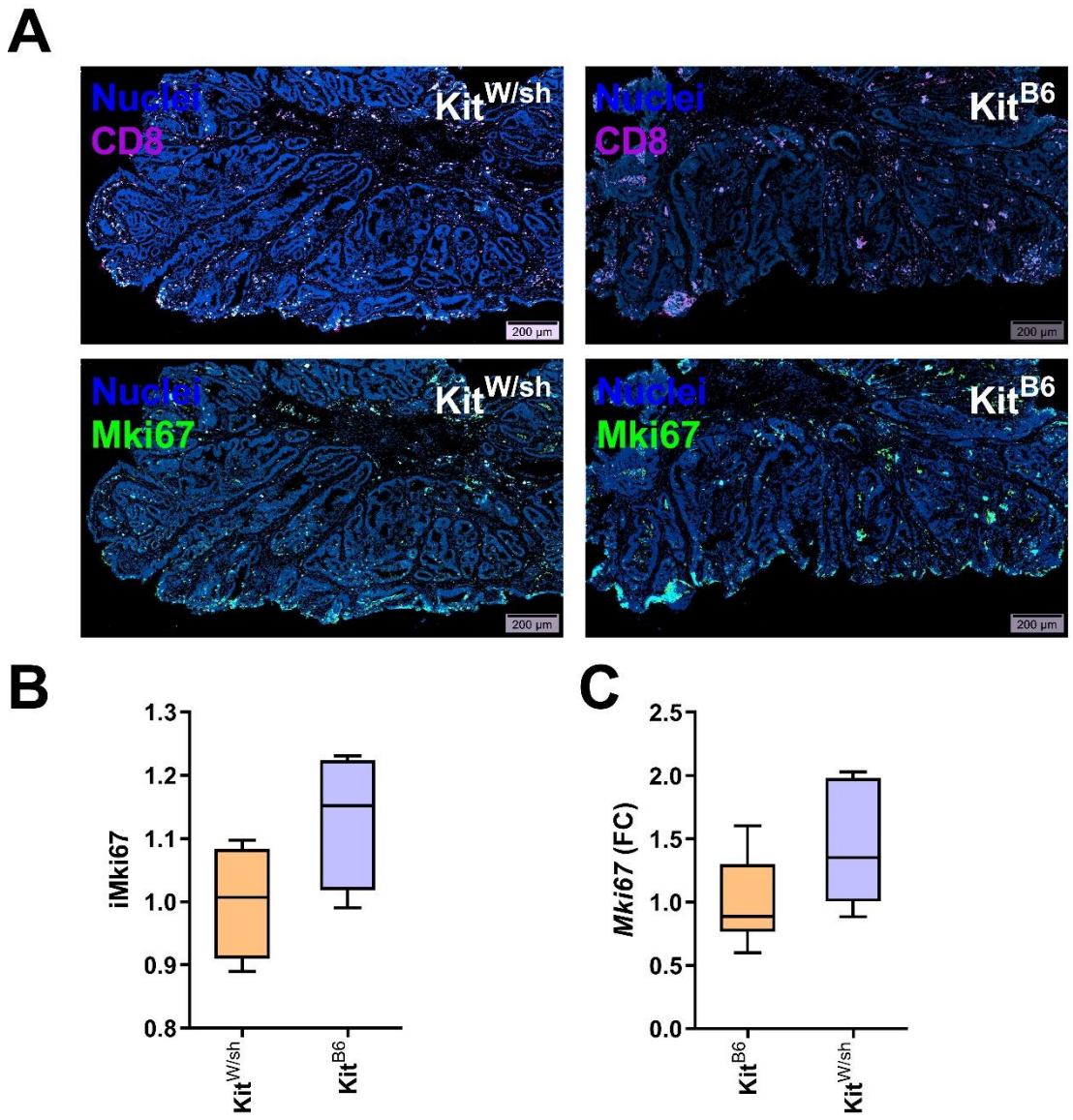

Suppl. Fig. 2. *Representative single images of multiplex IHC staining, and histopathological and gene expression analyses.*
(A) Representative single images of multiplex IHC staining with anti-CD8 and anti-Mki67 antibodies (magnification at 200 µm).
(B, C) Histopathological (n = 8) and gene expression (n = 12) analyses for Mki67 ($p > 0.05$). Data are shown as the median, highest and lowest values, along with upper and lower quartiles. *P*-values were calculated using a two-tailed Mann-Whitney test.

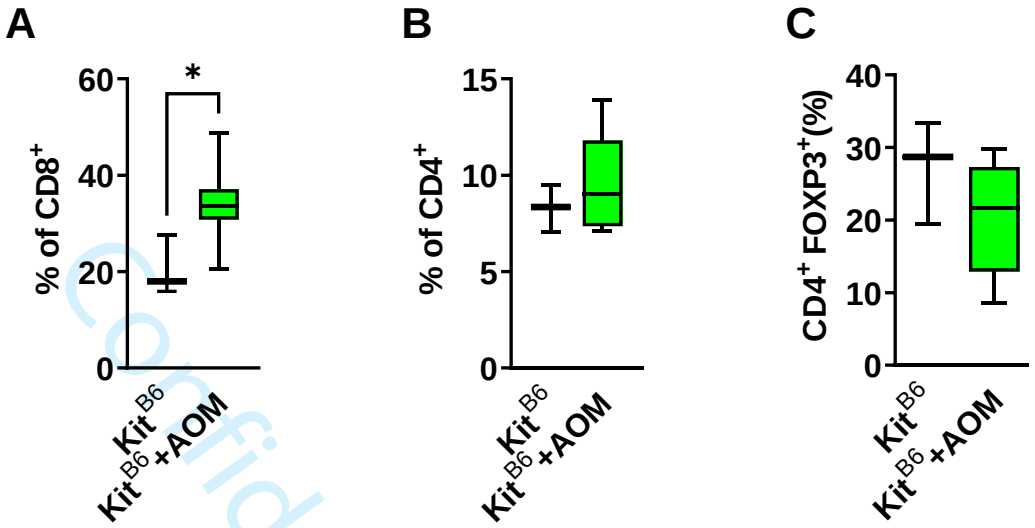

Suppl. Fig. 3. *Carcinogenic exposure alters CD8 T cell population in the colon.*
(A – C) Graphs show percentages of CD8+, CD4+, and CD4+FOXP3+ T cells isolated from colon samples (n = 10; *p =0.03). Data are shown as the median, highest and lowest values, along with upper and lower quartiles. *P*-values were calculated using a two-tailed Mann-Whitney test.

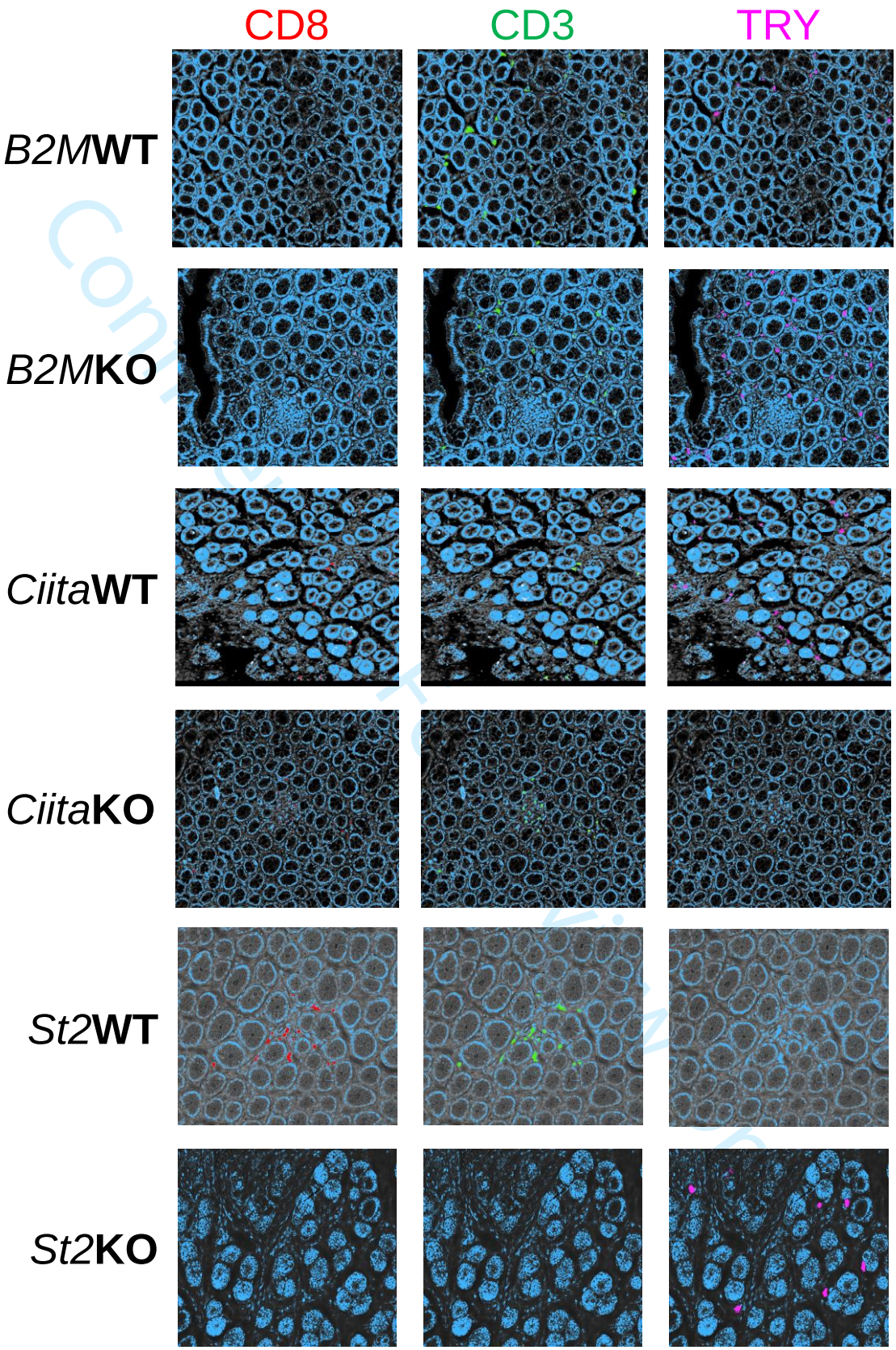

Suppl. Fig. 4. *Multiplex IHC staining*. Representative single images of multiplex IHC staining with anti-CD8, anti-CD3, and anti-TRY antibodies (magnification at 50 µm).

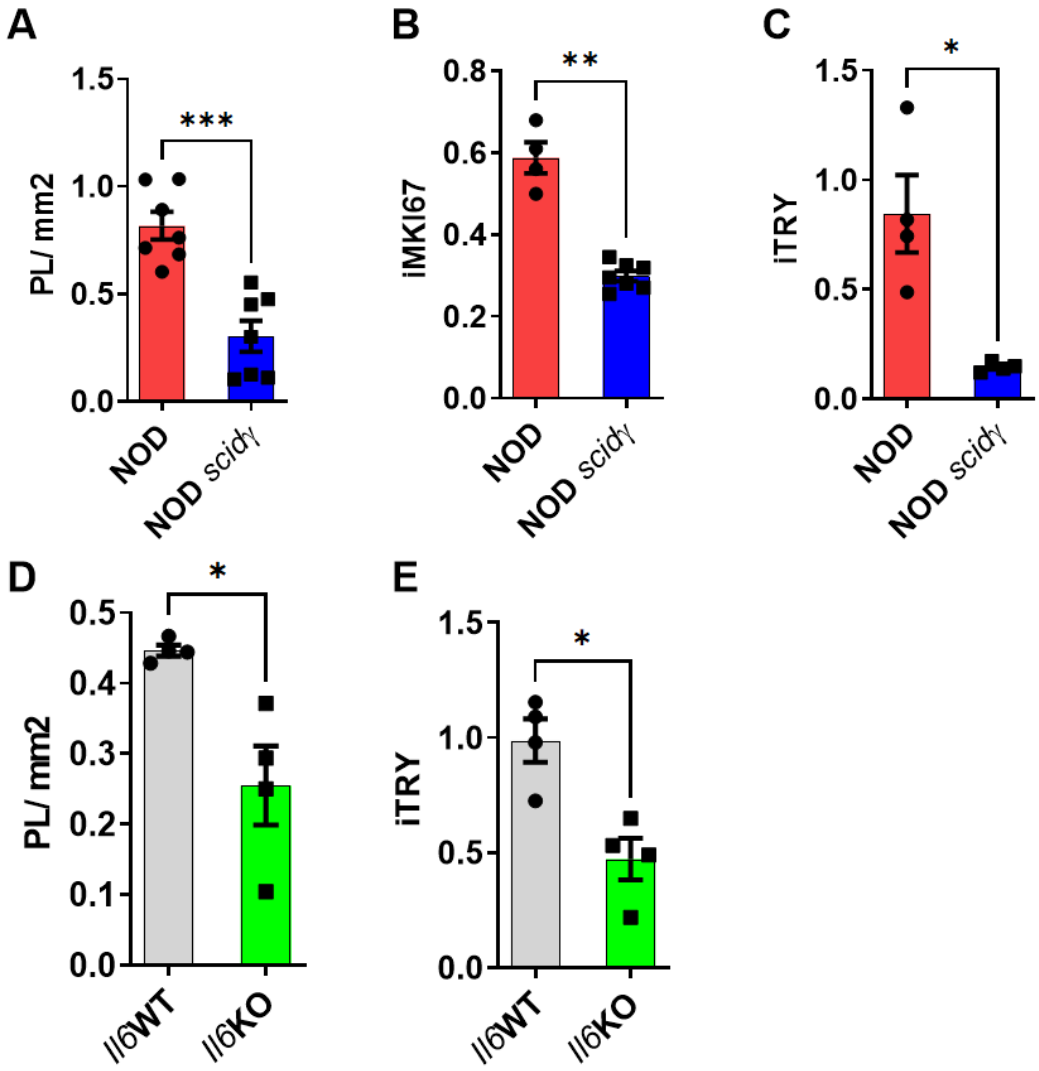

Suppl. Fig. 5. *Inflammatory response alters MC population and colon tumorigenesis since its early steps.*

(A – E) Histopathological analyses for single early tumorigenic lesions (A, n = 14, **p* =0.0006; D, n = 8, **p* =0.02), proliferation (B, n = 11, **p* =0.006), and MC numbers (C, n = 8, **p* =0.02; E, n = 8, **p* =0.02) in colonic samples from NOD *scidγ* and *Il6KO* mice and their counterparts. Data are shown as individual data points with mean ± SEM. p-values were calculated using a two-tailed Mann-Whitney test.

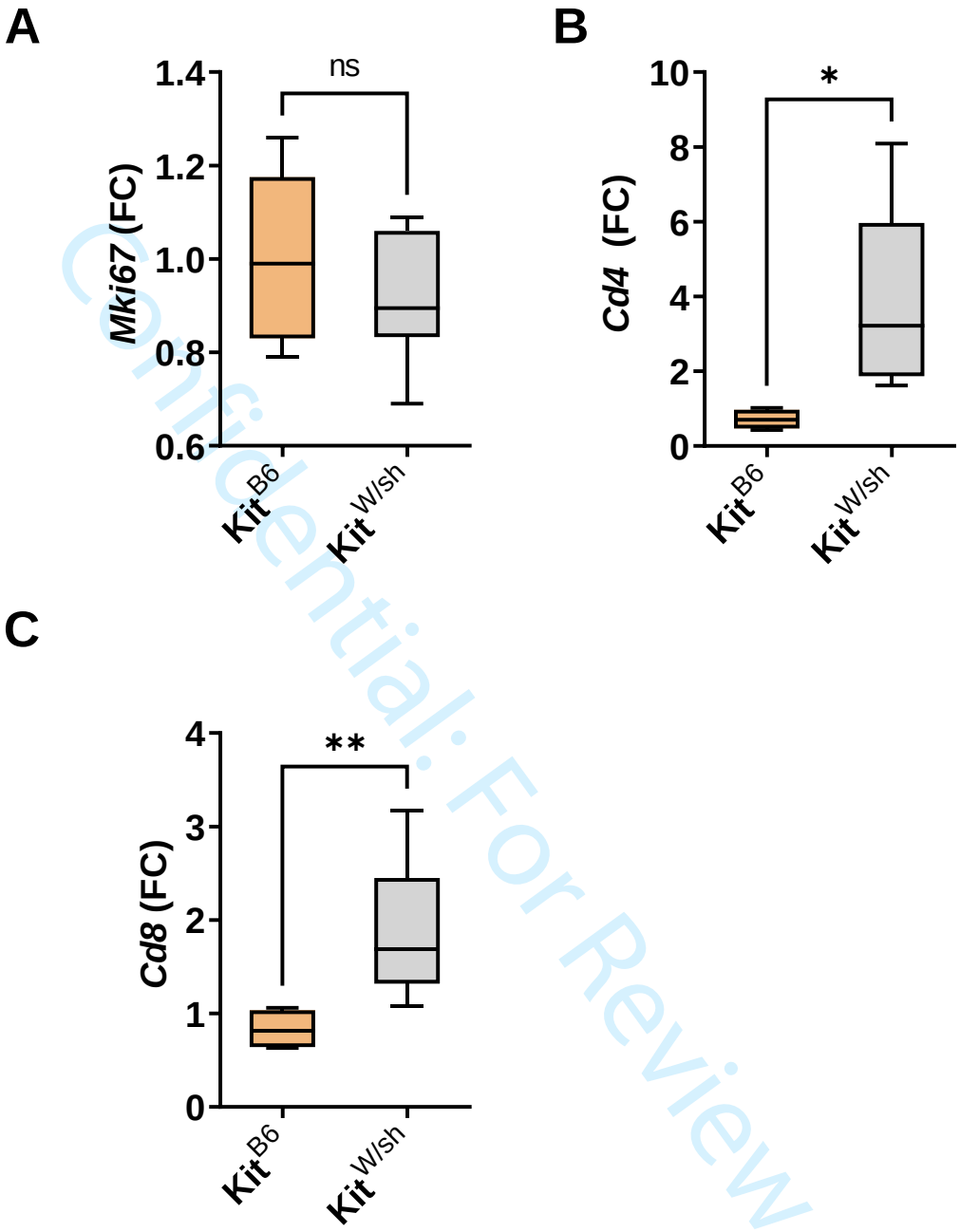

Suppl. Fig. 6. *The MC activity alter the immune response against CRC in mice.*
(A – C) Gene expression analysis for *Mki67* (n = 9; $p > 0.05$), *Cd4* (*$p = 0.01$), and *Cd8* (*$p = 0.009$). Data are shown as the median, highest and lowest values, along with upper and lower quartiles. *P*-values were calculated using a two-tailed Mann-Whitney test.

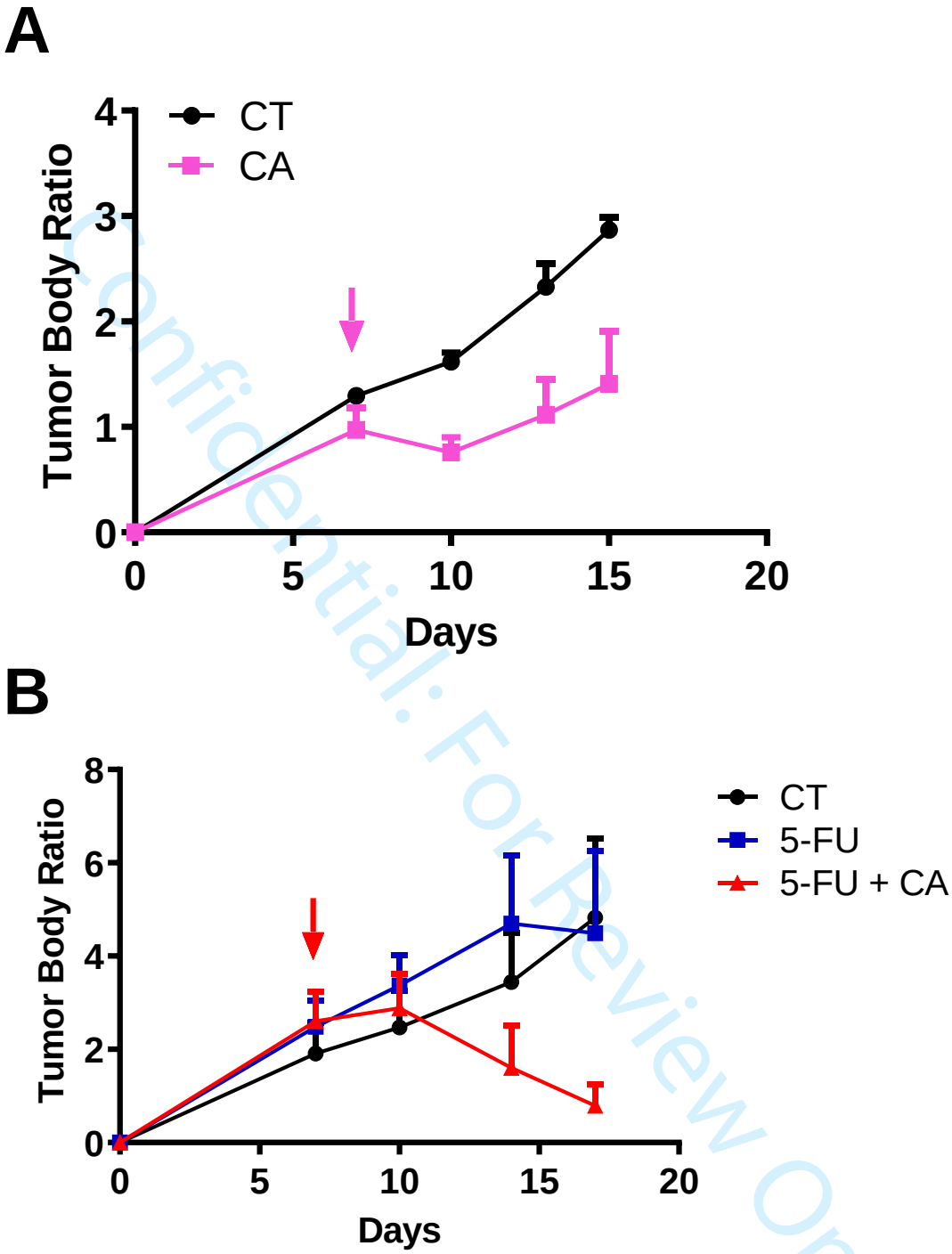

Suppl. Fig. 7. *The MC activity can be therapeutically targeted against CRC in mice.*
(A) Relative tumour growth between CA-treated (CA) and untreated (CT) mice for 15 days (n = 8).
(B) Relative tumour growth among untreated (CT), 5-FU-treated, and combined treatment of 5-FU and CA mice for 17 days (n = 15). Data are shown as mean ± SEM.

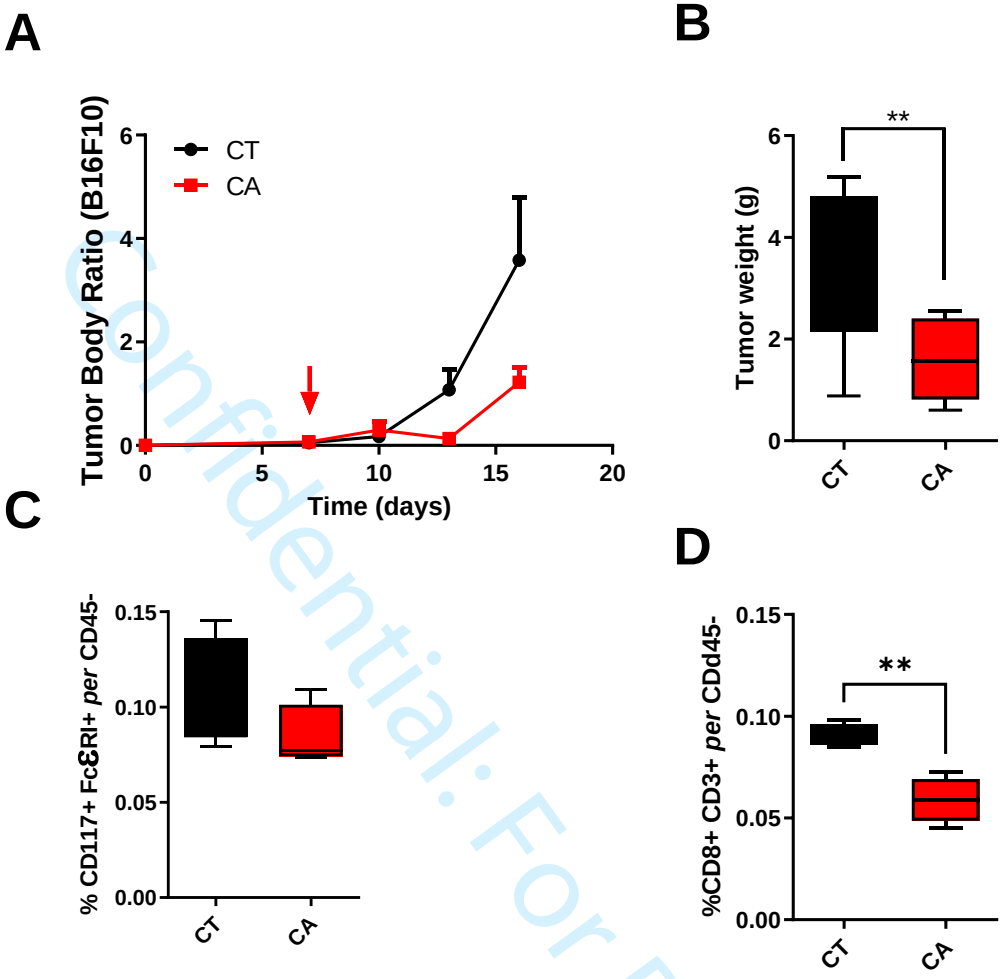

Suppl. Fig. 8. *The MC activity can be therapeutically targeted against melanoma in mice.*
(A) Relative tumour growth between CA-treated (CA) and untreated (CT) mice for 15 days (n = 11). Data are shown as mean ± SEM.
(B) Tumour weight between untreated and treated mice for 15 days (n = 11; **p* =0.03).
(C, D) Graphs show percentages of MCs ($CD45^+CD117^+Fc\varepsilon RI^+$) and $CD45^+CD8^+CD3^+$ T cells isolated from tumour samples (n = 8; **p* =0.002). Data are shown as the median, highest and lowest values, along with upper and lower quartiles. *P*-values were calculated using a two-tailed Mann-Whitney test.

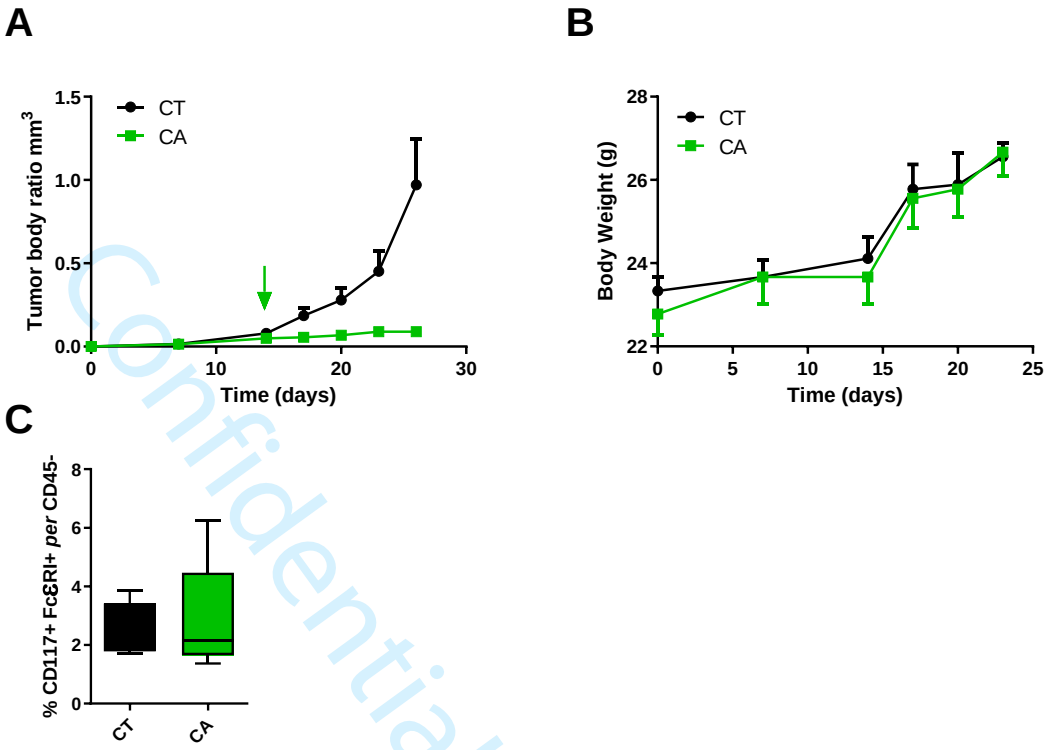

Suppl. Fig. 9. *The MC activity can be therapeutically targeted against colorectal tumours in mice.*

(A, B) Relative tumour growth and body weight between CA-treated (CA) and untreated (CT) mice for 15 days (n = 17). Data are shown as mean ± SEM.

(C) Graphs show percentages of MCs ($CD45^+CD117^+Fc\varepsilon RI^+$) isolated from tumour samples (n = 8). Data are shown as the median, highest and lowest values, along with upper and lower quartiles. *P*-values were calculated using a two-tailed Mann-Whitney test.

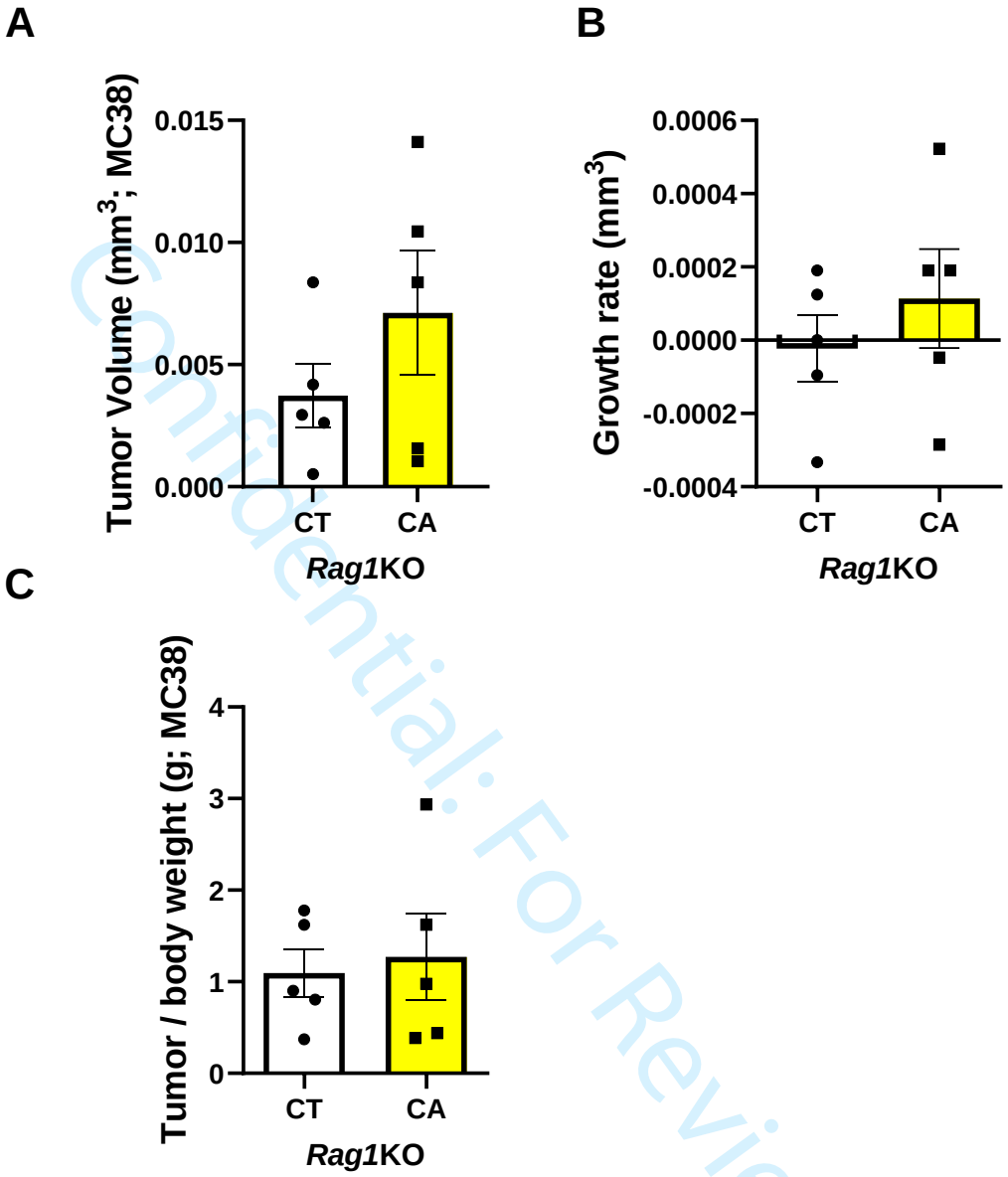

Suppl. Fig. 10. *The anticancer CA effects against colorectal tumours require T lymphocytes activity in mice.*

(A – C) Relative tumour growth in CA treated and untreated Rag1KO mice for 14 days (n = 10; $p > 0.05$). Data are shown as individual data points with mean ± SEM. p-values were calculated using two-tailed Mann Whitney's test.

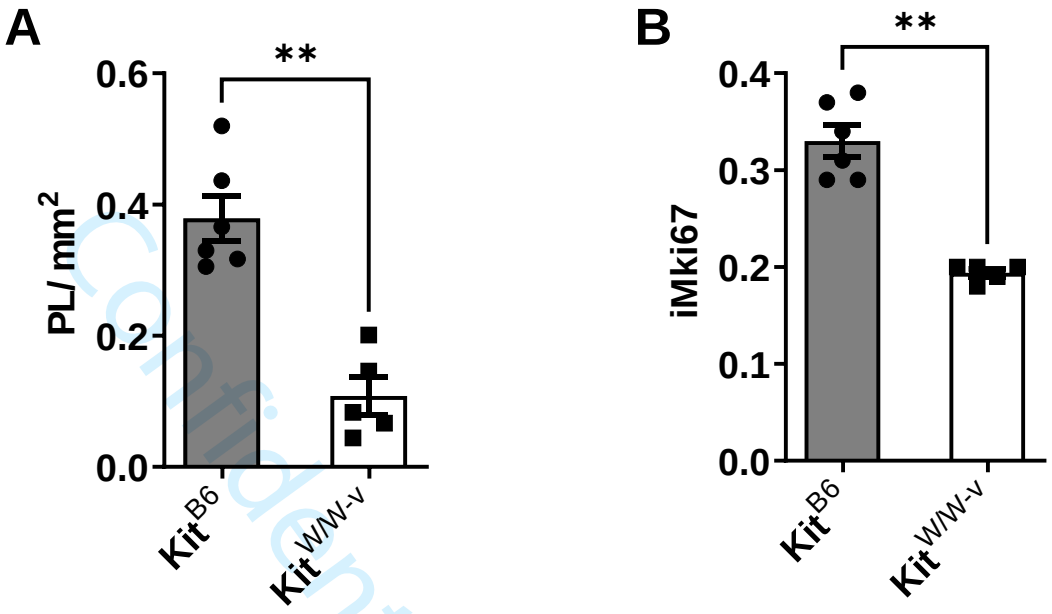

Suppl. Fig. 11. *The MC activity alter colorectal tumorigenesis in mice.*
(A, B) Histopathological analyses for single early tumorigenic lesions (A, n = 11, **p* =0.004), and proliferation (B, n = 11, **p* =0.002) in colonic samples from $Kit^{W/W\text{-}v}$ mice and their counterparts. Data are shown as individual data points with mean ± SEM. p-values were calculated using a two-tailed Mann-Whitney test.

Suppl. Tab. 1. *List of TaqMan Probes used in the study.*

Targets	Probes ID
Ctnnb1	Mm00483039
Gapdh	Mm99999915
Mki67	Mm01278617
Mgmt	Mm00485014

Suppl. Tab. 2. *List of qPCR SYBR rimer sequences used in the study.*

Primers	Sequences
Cd11c F	TCTTCTGCTGTTGGGGTTTG
Cd11c R	CAGTTGCCTGTGTGATAGCC
Cd4 F	TCTGGCAACCTGACTCTGAC
Cd4 R	TCATCACCACCAGGTTCACT
Cd8 F	CAGAGACCAGAAGATTGTCG
Cd8 R	TGATCAAGGACAGCAGAAGG
Cd3 F	ATGCGGTGGAACACTTTCTGG
Cd3 R	GCACGTCAACTCTACACTGGT
Foxp3 F	GGCCCTTCTCCAGGACAGA
Foxp3 R	GCTGATCATGGCTGGGTTGT
Mcpt1 F	TTCCAGGTCTGTGTGGGAAG
Mcpt1 R	TCCAGGGCACATATGCAGAG
Mcpt4 F	TCACCACTGAGAGAGGGTTCA
Mcpt4 R	CATGAGCTCCAAGGGTGACA
Mcpt6 F	ACGTTGCCCTGCTGGAGCTT
Mcpt6 R	CAGCACGATGTCCCTGGGGG
Gapdh F	TGGTGAAGGTCGGTGTGAAC
Gapdh R	GACAAGCTTCCCATTCTCGG

Suppl. Tab. 3. *List of primary antibodies used in the study.*

Antibodies	ID	Concentration
Cd8	Ab203035	1:150
Cd3	Ab5690	1:500
GAPDH	Ab181602	1:10000
Mki67	Ab16667	1:150
Triptase	Ab2378	1:150
γH2AX	Ab81299	1:5000
CD45-FITC	11-0451-82	1:250
Cd45-APC	561873	1:250
CD45-BV421	103133	1:300
CD117-PE-Cy7	55863	1:250
FcεRI-PE	134307	1:250
CD8a-PE	553032	1:300
CD3-FITC	557354	1:250
CD4-FITC	100405	1:300
Foxp3-APC	77-5775-40	1:300

Suppl. Tab. 4. *Significantly altered genes by MC deficiency in sCRC lesions. Data were obtained by RNA-seq.*

Name	Acronym	log2FC	*p*-Adj	*p*-Value
Upregulated genes				
Chemokine (C-X-C motif) ligand 2	*Cxcl2*	2.91762	5.50E-05	1.20E-07
Interleukin 6	*Il6*	2.76768	6.93E-03	2.88E-04
Chemokine (C-X-C motif) ligand 1	*Cxcl1*	2.41013	2.15E-03	3.29E-05
Colony stimulating factor 2	*Csf2*	2.39663	2.15E-03	3.16E-05
Interleukin 1 α	*Il1a*	2.32562	1.70E-03	1.67E-05
Chemokine (C-X-C motif) ligand 3	*Cxcl3*	2.17899	3.52E-03	1.04E-04
Formyl peptide receptor 1	*Fpr1*	2.13251	3.99E-04	2.18E-06
Chemokine (C-C motif) ligand 4	*Ccl4*	2.1307	4.82E-03	1.57E-04
Interleukin 17A	*Il17a*	2.11911	1.90E-02	1.12E-03
Interleukin 1 β	*Il1b*	2.107	4.82E-03	1.58E-04
Chemokine (C-C motif) ligand 3	*Ccl3*	1.89559	1.13E-02	5.05E-04
Nitric oxide synthase 2, inducible	*Nos2*	1.73595	1.70E-03	1.51E-05
Chemokine (C-C motif) receptor 10	*Ccr10*	1.68575	2.81E-02	2.25E-03
Chemokine (C-X-C motif) receptor 2	*Cxcr2*	1.6386	1.13E-03	7.43E-06
Histidine decarboxylase	*Hdc*	1.59195	3.94E-04	1.72E-06
Regulator of G-protein signaling 16	*Rgs16*	1.54682	2.90E-03	6.99E-05
Chitinase-like 1	*Chil1*	1.50777	3.08E-03	8.43E-05
G0/G1 switch gene 2	*G0s2*	1.49325	2.94E-02	2.41E-03
Tumor necrosis factor receptor superfamily, member 9	*Tnfrsf9*	1.47377	3.63E-02	3.01E-03
Arginase 2	*Arg2*	1.38296	2.15E-03	2.75E-05
Formyl peptide receptor 2	*Fpr2*	1.38215	1.22E-02	6.10E-04
Tumor necrosis factor (ligand) superfamily, member 9	*Tnfsf9*	1.33416	6.27E-03	2.54E-04
Interleukin 33	*Il33*	1.29891	5.47E-03	2.05E-04
CD80 antigen	*Cd80*	1.25429	1.97E-02	1.19E-03
Selectin, platelet	*Selp*	1.2436	2.66E-03	5.53E-05
Granzyme B	*Gzmb*	1.10501	5.47E-03	2.15E-04
Inositol polyphosphate-4-phosphatase, type II	*Inpp4b*	1.04564	2.68E-02	2.09E-03
Serine hydroxymethylTransferase 2 (mitochondrial)	*Shmt2*	0.97879	3.63E-04	1.19E-06
Nuclear factor of kappa light polypeptide gene enhancer in B cells inhibitor, α	*Nfkbia*	0.96189	1.70E-03	1.39E-05
CD14 antigen	*Cd14*	0.87987	2.19E-03	3.82E-05
Helicase, lymphoid specific	*Hells*	0.87468	2.19E-03	4.01E-05
Cell division cycle 7	*Cdc7*	0.83777	2.05E-02	1.31E-03

Tumor necrosis factor receptor superfamily, member 1b	*Tnfrsf1b*	0.71521	2.02E-03	2.20E-05
Serine/arginine-rich splicing factor 7	*Srsf7*	0.71185	5.47E-03	2.09E-04
BORA Aurora Kinase A Activator	*Bora*	0.69255	2.40E-02	1.73E-03
Activating transcription factor 4	*Atf4*	0.68931	2.12E-02	1.41E-03
Dystrobrevin, beta	*Dtnb*	0.65154	3.81E-02	3.25E-03
Regulatory factor X-associated protein	*Rfxap*	0.56539	4.28E-02	3.74E-03
Sphingomyelin synthase 1	*Sgms1*	0.46723	2.99E-03	7.83E-05
DEAD (Asp-Glu-Ala-Asp) box polypeptide 17	*Ddx17*	0.43006	2.29E-02	1.58E-03
Downregulated genes				
Serine (or cysteine) peptidase inhibitor, clade A, member 1D	*Serpina1d*	-5.0011	1.22E-02	6.16E-04
Somatostatin receptor 3	*Sstr3*	-4.0509	7.35E-03	3.14E-04
Carboxypeptidase A3, mast cell	*Cpa3*	-3.6243	2.15E-03	3.08E-05
Chromogranin B	*Chgb*	-2.3208	4.90E-03	1.66E-04
Endothelin 2	*Edn2*	-2.1053	1.14E-02	5.22E-04
Monoamine oxidase B	*Maob*	-2.0844	1.97E-02	1.21E-03
Collagen, type VIII, alpha 2	*Col8a2*	-1.9191	4.87E-02	4.38E-03
Carcinoembryonic antigen-related cell adhesion molecule 13	*Ceacam13*	-1.9147	1.14E-02	5.49E-04
RAR-related orphan receptor gamma	*Rorc*	-1.9034	1.14E-02	5.49E-04
Vitamin D receptor	*Vdr*	-1.8635	2.40E-02	1.72E-03
Chemokine (C motif) ligand 1	*Xcl1*	-1.8057	5.47E-03	2.08E-04
Solute carrier family 24 (sodium/potassium/calcium exchanger), member 3	*Slc24a3*	-1.7958	1.37E-02	7.17E-04
Hydroxyprostaglandin dehydrogenase 15 (NAD)	*Hpgd*	-1.7713	2.05E-02	1.35E-03
Kit oncogene	*Kit*	-1.6707	5.47E-03	2.11E-04
Fibroblast growth factor 18	*Fgf18*	-1.6239	3.35E-03	9.53E-05
RAB38, member RAS oncogene family	*Rab38*	-1.4745	2.05E-02	1.34E-03
Myosin XVB	*Myo15b*	-1.4343	2.68E-02	2.07E-03
MHC I like leukocyte 2	*Mill2*	-1.4073	2.58E-02	1.92E-03
SH3 domain and tetratricopeptide repeats 1	*Sh3tc1*	-1.3104	1.38E-02	7.41E-04
Glucosaminyl (N-acetyl) transferase 1, core 2	*Gcnt1*	-1.1739	4.10E-02	3.54E-03
Myocyte enhancer factor 2C	*Mef2c*	-1.1546	3.68E-03	1.13E-04
Melanophilin	*Mlph*	-1.1311	2.58E-02	1.89E-03
KN motif and ankyrin repeat domains 2	*Kank2*	-1.0783	1.38E-02	7.55E-04

Prostaglandin-endoperoxide synthase 1	*Ptgs1*	-1.0425	1.71E-02	9.74E-04
Inositol polyphosphate-4-phosphatase, type II	*Inpp4b*	-1.0258	2.84E-03	6.53E-05
Epithelial membrane protein 1	*Emp1*	-0.9828	1.26E-02	6.50E-04
Erb-b2 receptor tyrosine kinase 2	*Erbb2*	-0.9277	2.99E-03	7.84E-05
Interleukin 15	*Il15*	-0.8982	3.80E-02	3.21E-03
Avian musculoaponeurotic fibrosarcoma oncogene homolog	*Kank2*	-0.888	2.81E-02	2.27E-03
RNA binding motif protein 3	*Rbm3*	-0.8148	4.50E-02	3.99E-03
Zinc finger E-box binding homeobox 1	*Zeb1*	-0.8086	2.19E-03	4.21E-05
ATPase Phospholipid Transporting 9A (Putative)	*Atp9a*	-0.7628	1.88E-02	1.09E-03
Serine (or cysteine) peptidase inhibitor, clade B, member 6a	*Serpinb6a*	-0.7483	2.19E-02	1.48E-03
Cathepsin S	*Ctss*	-0.7402	4.87E-02	4.42E-03
Glypican 4	*Gpc4*	-0.7059	2.03E-05	2.22E-08
Forkhead box N3	*Foxn3*	-0.6665	2.19E-03	4.31E-05
Sphingomyelin phosphodiesterase 3, neutral	*Smpd3*	-0.6579	2.68E-02	2.10E-03
Proteasome (prosome, macropain) 26S subunit, non-ATPase, 11	*Psmd11*	-0.6125	2.75E-03	6.02E-05
Nuclear mitotic apparatus protein 1	*Numa1*	-0.5496	1.71E-02	9.65E-04
Catalase	*Cat*	-0.5231	1.13E-02	5.07E-04
Protein phosphatase 1, regulatory (inhibitor) subunit 2	*Ppp1r2*	-0.5019	2.68E-02	2.11E-03
von Willebrand factor A domain containing 5A	*Vwa5a*	-0.4409	1.97E-02	1.23E-03
Inhibitor of kappaB kinase γ	*Ikbkγ*	-0.4047	2.29E-02	1.60E-03

According to their log2FC values, genes are shown in descending order.

Suppl. Tab. 5: *Pathways significantly altered by MC deficiency in sCRC lesions. Data were obtained by RNA-seq and analysed on DAVID (Bioinformatic Database).*

Pathway	Status	*p*-Value	Genes
Cytokine-cytokine receptor interaction	Upregulated	9,80E-11	*Ccl3, Ccl4, Ccr10, Cxcl1, Cxcl2, Cxcr2, Csf2, Il1a, Il1b, Il17a, Il6, Tnfsf9, Tnfrsf1b, Tnfrsf9*
	Downregulated	9,80E-11	*Xcl1, Il15*
TNF signaling	Upregulated	4,40E-09	*Atf4; Cxcl1, Cxcl2, Cxcl3,Csf2, Il1b, Il6, Nfkbia, Tnfrsf1b*
	Downregulated	4,40E-09	*Ikbkg, Il15*
Toll-like receptor signaling	Upregulated	7,50E-06	*Cd14, Cd80, Ccl3, Ccl4, Il1b, Il6, Nfkbia*
	Downregulated	7,50E-06	*Ikbkg*
Chemokine signaling	Upregulated	1,00E-05	*Ccl3, Ccl4, Ccr10, Cxcl1, Cxcl2, Cxcl3, Cxcr2, Nfkbia*
	Downregulated	1,00E-05	*Ikbkg, Xcl1*
NOD-like receptor signaling	Upregulated	5,40E-05	*Cxcl1, Cxcl2, Il1b, Il6, Nfkbia*
	Downregulated	5,40E-05	*Ikbkg*
Inflammatory bowel disease (IBD)	Upregulated	6,30E-05	*Il1a, Il1b, Il17a, Il6*
Cytosolic DNA-sensing	Upregulated	9,40E-05	*Ccl4, Il1b, Il33, Il6, Nfkbia*
	Downregulated	9,40E-05	*Ikbkg*
Transcriptional dysregulation in cancer	Upregulated	1,20E-03	*Cd14, Csf2, Gzmb, Il6*
	Downregulated	1,20E-03	*Maf, Hpgd, Mef2c*
Intestinal immune network for IgA production	Upregulated	3,40E-03	*Cd80, Ccr10, Il15, Il6*
NF-κβ signaling	Upregulated	5,30E-03	*Cd14, Ccl4, Il1b, Nfkbia*

Acronyms meaning is given in Suppl. Tab. 4.

Suppl. Tab. 6. *Significantly altered genes by MC deficiency in early colon tumorigenic lesions. Data were obtained by RNA-seq.*

Name	Acronym	log2FC	*p*-Adj	*p*-Value
Upregulated genes				
Chemokine (C-X-C motif) ligand 5	*Cxcl5*	3.22413	1.82E-02	1.62E-03
Chemokine (C-X-C motif) ligand 13	*Cxcl13*	2.58874	2.24E-06	4.79E-08
Chemokine (C-X-C motif) receptor 5	*Cxcr5*	2.51089	2.29E-06	5.14E-08
Z-DNA binding protein 1	*Zbp1*	2.1316	3.00E-04	1.11E-05
Interferon-induced protein with tetratricopeptide repeats 3	*Ifit3*	1.76255	6.40E-03	4.42E-04
Interleukin 18	*Il18*	1.52986	4.68E-03	3.00E-04
Chemokine (C-C motif) receptor 6	*Ccr6*	1.37639	1.35E-03	6.35E-05
Epithelial membrane protein 1	*Emp1*	1.28044	7.14E-06	1.77E-07
Histocompatibility 2, class II antigen A, β 1	*H2-Ab1*	1.23486	3.00E-04	1.11E-05
Interleukin 21 receptor	*Il21r*	1.21134	5.61E-04	2.27E-05
Tumor necrosis factor receptor superfamily, member 10b	*Tnfrsf10b*	1.19788	1.50E-02	1.28E-03
Nuclear factor of kappa light polypeptide gene enhancer in B cells inhibitor, α	*Nfkbia*	1.1736	8.73E-04	3.81E-05
Guanylate binding protein 2b	*Gbp2b*	1.15584	1.28E-02	1.03E-03
Anti-Mullerian hormone type 2 receptor	*Amhr2*	1.08817	8.73E-04	3.82E-05
Selectin, platelet (p-selectin) ligand	*Selplg*	1.02693	3.21E-02	3.35E-03
Mucosal vascular addressin cell adhesion molecule 1	*Madcam1*	1.01299	4.93E-03	3.21E-04
TRAF3 interacting protein 3	*Traf3ip3*	0.93662	1.10E-02	8.53E-04
Cytidine deaminase	*Cda*	0.9289	6.94E-03	4.99E-04
2'-5' oligoadenylate synthetase 1A	*Oas1a*	0.87346	2.94E-05	8.59E-07
Histocompatibility 2, class II antigen E β2	*H2-Eb2*	0.83882	1.43E-02	1.21E-03
Chemokine (C-C motif) ligand 19	*Ccl19*	0.80013	1.84E-03	9.30E-05

Histocompatibility 2, class II antigen A, α	*H2-Aa*	0.70998	8.82E-03	6.54E-04
Lymphotoxin B	*Ltb*	0.70568	2.76E-02	2.76E-03
RAB27A, member RAS oncogene family	*Rab27a*	0.69102	2.03E-02	1.89E-03
Guanylate binding protein 2	*Gbp2*	0.65227	2.63E-02	2.58E-03
Endothelin 1	*Edn1*	0.6305	2.63E-03	1.54E-04
Transmembrane and immunoglobulin domain containing 1	*Tmigd1*	0.62949	2.04E-03	1.08E-04
Interferon regulatory factor 7	*Irf7*	0.61944	1.94E-03	1.00E-04
Heparan sulfate (glucosamine) 3-O-sulfotransferase 3B1	*Hs3st3b1*	0.56872	9.59E-03	7.22E-04
SMAD family member 3	*Smad3*	0.53498	2.51E-02	2.42E-03
Nuclear antigen Sp100	*Sp100*	0.48685	4.98E-02	5.66E-03
Downregulated genes				
Complement receptor 2	*Cr2*	-5.2193	4.19E-02	4.57E-03
Metallothionein 2	*Mt2*	-4.0879	9.89E-06	2.56E-07
Chemokine (C-C motif) ligand 2	*Ccl2*	-3.6923	2.63E-03	1.53E-04
CD2 antigen	*Cd2*	-3.4363	6.10E-08	1.10E-09
Phospholipase A2, group VII (platelet-activating factor acetylhydrolase, plasma)	*Pla2g7*	-3.2754	8.39E-09	1.32E-10
Cytochrome b-245, beta polypeptide	*Cybb*	-3.2693	3.25E-06	7.67E-08
2'-5' oligoadenylate synthetase 3	*Oas3*	-3.2321	2.98E-43	3.35E-46
Histocompatibility 2, M region locus 3	*H2-M3*	-3.1173	1.28E-09	1.44E-11
Tumor necrosis factor	*Tnf*	-3.0967	2.07E-38	4.66E-41
Carcinoembryonic antigen-related cell adhesion molecule 13	*Ceacam13*	-3.0565	7.45E-13	5.02E-15
Bone marrow stromal cell antigen 1	*Bst1*	-3.0226	3.00E-04	1.08E-05
CD48 antigen	*Cd48*	-2.9478	2.17E-07	4.15E-09
2'-5' oligoadenylate synthetase-like 1	*Oasl1*	-2.9434	2.68E-37	9.03E-40

Chemokine (C-X-C motif) ligand 1	*Cxcl1*	-2.9432	8.20E-05	2.58E-06
SMAD family member 2	*Smad2*	-2.5089	4.98E-02	5.73E-03
Histone cluster 1, H1c	*Hist1h1c*	-2.4994	1.96E-12	1.54E-14
Chemokine (C-X-C motif) ligand 2	*Cxcl2*	-2.4367	1.95E-09	2.85E-11
Fucosyltransferase 4	*Fut4*	-2.4197	8.04E-11	7.23E-13
CD177 antigen	*Cd177*	-2.3846	4.40E-03	2.72E-04
Carbonic anhydrase 4	*Car4*	-2.3158	1.39E-03	6.86E-05
B lymphoid kinase	*Blk*	-2.1328	1.23E-05	3.32E-07
Lymphocyte antigen 75	*Ly75*	-2.0604	8.95E-04	4.12E-05
Histocompatibility 2, T region locus 24	*H2-T24*	-2.0561	1.29E-02	1.07E-03
CD74 antigen	*Cd74*	-1.9534	5.91E-04	2.46E-05
T cell receptor associated transmembrane adaptor 1	*Trat1*	-1.9484	3.03E-02	3.07E-03
Carboxypeptidase A3, mast cell	*Cpa3*	-1.8726	1.90E-02	1.73E-03
Kit oncogene	*Kit*	-1.8279	2.24E-13	1.26E-15
Lymphocyte transmembrane adaptor 1	*Lax1*	-1.8135	3.12E-02	3.19E-03
Kynureninase (L-kynurenine hydrolase)	*Kynu*	-1.7685	1.34E-09	1.81E-11
Interferon induced transmembrane protein 3	*Ifitm3*	-1.7126	6.18E-05	1.87E-06
Interferon regulatory factor 1	*Irf1*	-1.7119	2.69E-02	2.66E-03
CD22 antigen	*Cd22*	-1.6939	1.26E-02	1.00E-03
B and T lymphocyte associated	*Btla*	-1.6385	9.68E-10	9.78E-12
CD69 antigen	*Cd69*	-1.6102	1.48E-05	4.15E-07
Malic enzyme 1, NADP(+)-dependent, cytosolic	*Me1*	-1.5944	1.90E-02	1.71E-03
DEAD (Asp-Glu-Ala-Asp) box polypeptide 58	*Ddx58*	-1.5393	2.30E-03	1.27E-04
Beta-2 microglobulin	*B2m*	-1.5158	4.51E-03	2.84E-04
Spi-B transcription factor (Spi-1/PU.1 related)	*Spib*	-1.4302	1.34E-09	1.69E-11

Glypican 4	*Gpc4*	-1.4035	4.95E-02	5.56E-03
CD52 antigen	*Cd52*	-1.3942	5.39E-03	3.58E-04
2'-5' oligoadenylate synthetase 1G	*Oas1g*	-1.3506	4.18E-04	1.64E-05
Three prime repair exonuclease 1	*Trex1*	-1.3436	2.29E-03	1.23E-04
Optineurin	*Optn*	-1.3247	1.25E-08	2.11E-10
Apolipoprotein D	*Apod*	-1.2874	6.43E-03	4.55E-04
Myocyte enhancer factor 2C	*Mef2c*	-1.2523	1.53E-04	5.00E-06
Lectin, galactose binding, soluble 9	*Lgals9*	-1.2305	1.06E-02	8.10E-04
2'-5' oligoadenylate synthetase 1B	*Oas1b*	-1.2252	3.00E-03	1.79E-04
Signal transducer and activator of transcription 3	*Stat3*	-1.2118	3.33E-02	3.52E-03
DnaJ heat shock protein family (Hsp40) member B1	*Dnajb1*	-1.1764	3.00E-04	1.08E-05
LPS-responsive beige-like anchor	*Lrba*	-1.1744	8.80E-04	3.95E-05
Myelin and lymphocyte protein, T cell differentiation protein	*Mal*	-1.1117	4.98E-02	5.76E-03
Immunoglobulin kappa constant	*Igkc*	-1.1016	2.44E-03	1.37E-04
Interferon Induced Transmembrane Protein 3	*Ifitm3*	-1.1015	2.44E-03	1,37E-04
Serine (or cysteine) preptidase inhibitor, clade A, member 1B	*Serpina1b*	-0.9767	1.92E-02	1.77E-03
Acid phosphatase, prostate	*Acpp*	-0.9537	4.04E-04	1.54E-05
Membrane-spanning 4-domains, subfamily A, member 1	*Ms4a1*	-0.9392	3.14E-02	3.24E-03
B cell scaffold protein with ankyrin repeats 1	*Bank1*	-0.8961	5.07E-07	1.03E-08
Indoleamine 2,3-dioxygenase 1	*Ido1*	-0.8774	1.63E-02	1.43E-03
2'-5' oligoadenylate synthetase 2	*Oas2*	-0.8606	2.10E-02	1.99E-03
Protein tyrosine phosphatase, receptor type, C	*Ptprc*	-0.8081	1.63E-02	1.43E-03
Transient receptor potential cation channel, subfamily V, member 6	*Trpv6*	-0.7858	6.26E-03	4.22E-04
IKAROS family zinc finger 2	*Ikzf2*	-0.7351	6.40E-03	4.46E-04
Histocompatibility 2, O region alpha locus	*H2-Oa*	-0.6812	1.28E-02	1.05E-03

Carcinoembryonic antigen-related cell adhesion molecule 12	*Ceacam12*	-0.6733	4.92E-02	5.48E-03
Zinc and ring finger 1	*Znrf1*	-0.6444	3.93E-02	4.24E-03
Regulator of G-protein signaling 16	*Rgs16*	-0.6152	7.96E-03	5.82E-04
Paired box 5	*Pax5*	-0.5946	2.49E-02	2.38E-03
CD19 antigen	*Cd19*	-0.5853	3.25E-03	1.97E-04
Bone marrow stromal cell antigen 2	*Bst2*	-1.582	4.19E-02	4.61E-03
CD72 antigen	*Cd72*	-1.565	1.11E-02	8.72E-04
Lysophosphatidylcholine acyltransferase 4	*Lpcat4*	-1.355	2.42E-15	1.09E-17
Protein tyrosine phosphatase, receptor type, J	*Ptprj*	-1.196	1.37E-03	6.61E-05

Genes are shown in descending order (log2FC values).

Suppl. Tab. 7: *Pathways significantly altered by MC deficiency in sCRC preneoplastic lesions. Data were obtained by RNA-seq and analysed on DAVID (Bioinformatic Database).*

Pathway	Status	*p*-Value	Genes
Inflammatory bowel disease (IBD)	Upregulated	3.40E-08	*Smad3, H2-Aa, H2-Ab1, Il18, Il21r*
	Downregulated	3.40E-08	*Smad2, H2-Oa, Stat3, Tnf*
Cytokine-cytokine receptor interaction	Upregulated	1.20E-07	*Amhr2, Ccl19, Ccr6, Cxcl13, Cxcl5, Cxcr5, Il18, Il21r, Ltb, Tnfrsf10b*
	Downregulated	1.20E-07	*Ccl2, Cxcl1, Cxcl2, Tnf*
Antigen processing and presentation	Upregulated	6.30E-06	*H2-Aa, H2-Ab1*
	Downregulated	6.30E-06	*Cd74, B2m, H2-M3, H2-Oa, H2-T24, Tnf*
Cell adhesion molecules (CAMs)	Upregulated	9.80E-06	*H2-Aa, H2-Ab1, Madcam1, Selplg*
	Downregulated	9.80E-06	*Cd2, Cd22, H2-M3, H2-Oa, H2-T24, Ptprc*
Chemokine signaling pathway	Upregulated	4.50E-05	*Ccl19, Ccr6, Cxcl13, Cxcl5, Cxcr5, Nfbia*
	Downregulated	4.50E-05	*Ccl2, Cxcl1, Cxcl2, Stat3*
NOD-like receptor signaling pathway	Downregulated	1.30E-04	*Ccl2, Cxcl1, Cxcl2, Tnf*
Cytosolic DNA-sensing pathway	Upregulated	2.20E-04	*Zbp1, Irf7, Il18, Nfkbia*
	Downregulated	2.20E-04	*Ddx58, Trex1*
TNF signaling	Downregulated	2.50E-03	*Ccl2, Cxcl1, Cxcl2, Tnf*
B cell receptor signaling	Downregulated	3.10E-03	*Cd19, Cd22, Cd72, Cr2*
TGF-beta signaling	Upregulated	3.80E-02	*Smad3, Amhr2*
	Downregulated	3.80E-02	*Smad2, Tnf*

Acronyms meaning is given in Suppl. Tab. 6.

Suppl. Tab. 8. *Mast cells are drugable targets altering the development of early colon tumorigenic events (AOM vs AOM+CA). Data were obtained by RNA-seq.*

Name	Acronym	log2FC	*p*-Adj	*p*-Value
Upregulated genes				
ATP-binding cassette, sub-family G (WHITE), member 2	*Abcg2*	0.94418	1.38E-03	1.15E-05
CDC14 cell division cycle 14A	*Cdc14a*	0.6245	7.49E-03	1.34E-04
Frizzled class receptor 2	*Fzd2*	0.54644	4.26E-02	1.87E-03
Caspase 1	*Casp1*	0.46988	4.26E-02	1.77E-03
Abhydrolase domain containing 2	*Abhd2*	0.46076	4.64E-02	2.10E-03
Nedd4 family interacting protein 1	*Ndfip1*	0.45897	1.95E-02	5.34E-04
Chemokine (C-X-C motif) ligand 12	*Cxcl12*	0.44735	2.23E-02	7.68E-04
Downregulated genes				
Chemokine (C-C motif) ligand 19	*Ccl19*	-3.5472	6.04E-04	3.59E-06
Interleukin 13	*Il13*	-3.4608	4.91E-02	2.40E-03
T cell receptor associated transmembrane adaptor 1	*Trat1*	-2.8763	2.23E-02	7.54E-04
Membrane-spanning 4-domains, subfamily A, member 1	*Ms4a1*	-2.3658	4.91E-02	2.34E-03
Complement receptor 2	*Cr2*	-2.3086	4.90E-03	7.57E-05
CD19 antigen	*Cd19*	-1.9972	1.29E-03	9.18E-06
Carcinoembryonic antigen-related cell adhesion molecule 12	*Ceacam12*	-1.9074	1.53E-02	3.81E-04
Chemokine (C-X-C motif) ligand 5	*Cxcl5*	-1.794	8.22E-03	1.63E-04
Nitric oxide synthase 2, inducible	*Nos2*	-1.7376	4.26E-02	1.83E-03
Ubiquitin D	*Ubd*	-1.5843	3.95E-04	1.88E-06
CD22 antigen	*Cd22*	-1.5688	2.08E-02	5.93E-04
Dual specificity phosphatase 2	*Dusp2*	-1.5562	4.90E-03	7.42E-05
Granzyme A	*Gzma*	-1.5448	1.12E-02	2.40E-04
Suppressor of cytokine signaling 1	*Socs1*	-1.4443	1.38E-02	3.21E-04

Spi-B transcription factor	*Spib*	-1.4357	2.23E-02	7.69E-04
Chemokine (C-C motif) receptor 6	*Ccr6*	-1.3625	4.71E-02	2.19E-03
Zeta-chain associated protein kinase	*Zap70*	-1.1181	2.25E-02	8.01E-04
CD72 antigen	*Cd72*	-1.0918	3.63E-02	1.38E-03
Serine peptidase inhibitor, clade A, member 3N	*Serpina3n*	-1.0806	1.38E-02	3.27E-04
Proteasome subunit, beta type 9	*Psmb9*	-1.0404	1.91E-06	2.27E-09
Chemokine (C-C motif) ligand 5	*Ccl5*	-1.0292	1.58E-04	5.63E-07
Z-DNA binding protein 1	*Zbp1*	-0.964	3.60E-03	4.70E-05
Natural killer cell group 7 sequence	*Nkg7*	-0.8674	2.32E-03	2.21E-05
Transporter 1, ATP-binding cassette, sub-family B	*Tap1*	-0.8594	8.22E-03	1.66E-04
CD74 antigen	*Cd74*	-0.7109	4.47E-05	1.06E-07
Centromere protein F	*Cenpf*	-0.705	1.64E-02	4.28E-04
Histocompatibility 2, class II antigen A, β 1	*H2-Ab1*	-0.7036	6.03E-03	1.00E-04
Antigen identified by monoclonal antibody Ki 67	*Mki67*	-0.6661	2.39E-02	8.81E-04
Baculoviral IAP repeat-containing 5	*Birc5*	-0.6435	2.23E-02	7.02E-04
Histocompatibility 2, Q region locus 4	*H2-Q4*	-0.624	2.22E-02	6.60E-04
Histocompatibility 2, class II antigen A, α	*H2-Aa*	-0.5918	2.86E-03	3.40E-05
Histocompatibility 2, class II antigen E β	*H2-Eb1*	-0.5903	2.86E-03	3.20E-05
Histocompatibility 2, M region locus 3	*H2-M3*	-0.5693	3.97E-02	1.56E-03
Proteasome subunit, beta type 10	*Psmb10*	-0.4267	3.99E-02	1.61E-03

According to their log2FC values, genes are shown in descending order.

Suppl. Tab. 9. *Mast cells are drugable targets altering the development of early tumorigenic events in the colon (AOM vs AOM → CA). Data were obtained by RNA-seq.*

Name	Acronym	log2FC	*p*-Adj	*p*-Value
Upregulated genes				
γ-glutamyltransferase 1	*Ggt1*	2.69378	4.80E-02	2.10E-03
Chemokine (C-C motif) ligand 3	*Ccl3*	1.53774	4.76E-02	2.00E-03
Leucine rich repeat containing 32	Lrrc32	1.29369	2.59E-02	6.35E-04
CD36 antigen	*Cd36*	1.083	2.87E-02	7.37E-04
Interleukin 15	*Il15*	1.04341	4.90E-02	2.23E-03
Hairy/enhancer-of-split related with YRPW motif 1	*Hey1*	1.00961	4.76E-02	1.96E-03
Alanyl (membrane) aminopeptidase	*Anpep*	0.83758	3.15E-02	1.06E-03
Spondin 2. extracellular matrix protein	Spon2	0.80936	1.41E-02	1.97E-04
Cysteine-rich secretory protein LCCL domain containing 2	*Crispld2*	0.7985	2.38E-02	4.99E-04
CD34 antigen	*Cd34*	0.79222	1.23E-02	1.20E-04
Collagen. type III. alpha 1	*Col3a1*	0.61973	2.10E-02	3.91E-04
Frizzled class receptor 2	*Fzd2*	0.6149	2.16E-02	4.28E-04
Vascular endothelial growth factor C	Vegfc	0.59837	4.80E-02	2.13E-03
Acid phosphatase. prostate	*Acpp*	0.59654	4.44E-02	1.76E-03
Insulin-like growth factor binding protein 5	*Igfbp5*	0.56027	3.11E-02	9.31E-04
Chemokine (C-X-C motif) ligand 12	*Cxcl12*	0.54604	6.64E-03	3.87E-05
CDC14 cell division cycle 14A	*Cdc14a*	0.536	3.11E-02	9.68E-04
Downregulated genes				
Chemokine (C-C motif) ligand 19	*Ccl19*	-4.111	4.56E-05	5.32E-08
T cell receptor associated transmembrane adaptor 1	Trat1	-3.2211	1.23E-02	1.58E-04
Cochlin	*Coch*	-3.1581	4.44E-02	1.74E-03
Carcinoembryonic antigen-related cell adhesion molecule 12	*Ceacam12*	-2.6061	2.15E-04	7.51E-07

Membrane-spanning 4-domains. subfamily A. member 1	Ms4a1	-2.5536	3.11E-02	1.01E-03
Chemokine (C-C motif) receptor 7	*Ccr7*	-2.3446	1.23E-02	1.56E-04
Complement receptor 2	*Cr2*	-2.3063	1.06E-02	7.38E-05
CD19 antigen	*Cd19*	-2.2856	1.40E-04	3.26E-07
Cystatin F (leukocystatin)	*Cst7*	-2.2784	4.95E-02	2.31E-03
Histocompatibility 2. class II antigen E β2	*H2-Eb2*	-1.8299	2.55E-02	5.95E-04
CD22 antigen	*Cd22*	-1.7512	1.23E-02	1.18E-04
Histocompatibility 2. O region α locus	*H2-Oa*	-1.7194	3.56E-02	1.25E-03
B cell scaffold protein with ankyrin repeats 1	*Bank1*	-1.5358	2.55E-02	5.92E-04
Chemokine (C-X-C motif) ligand 5	*Cxcl5*	-1.5001	4.42E-02	1.65E-03
Chemokine (C-C motif) receptor 6	*Ccr6*	-1.4843	2.91E-02	7.79E-04
Dual specificity phosphatase 2	*Dusp2*	-1.4269	1.70E-02	2.77E-04
Spi-B transcription factor	Spib	-1.4116	3.11E-02	9.09E-04
Nuclear receptor subfamily 4. group A. member 2	Nr4a2	-1.3889	1.55E-02	2.35E-04
Tumor necrosis factor receptor superfamily. member 8	Tnfrsf8	-1.2221	4.99E-02	2.40E-03
Histocompatibility 2. T region locus 24	*H2-T24*	-1.1875	4.42E-02	1.64E-03
Histocompatibility 2. M region locus 2	*H2-M2*	-1.1742	4.99E-02	2.44E-03
Z-DNA binding protein 1	Zbp1	-0.9897	6.06E-03	2.82E-05
Epithelial membrane protein 1	*Emp1*	-0.9596	1.92E-02	3.36E-04
Melanophilin	Mlph	-0.936	1.23E-02	1.56E-04
Protein tyrosine phosphatase. receptor type. C	Ptprc	-0.8487	3.11E-02	9.96E-04
Centromere protein F	*Cenpf*	-0.705	1.64E-02	4.28E-04
Histocompatibility 2, class II antigen A, β 1	*H2-Ab1*	-0.7036	6.03E-03	1.00E-04
Antigen identified by monoclonal antibody Ki 67	*Mki67*	-0.6661	2.39E-02	8.81E-04
Baculoviral IAP repeat-containing 5	*Birc5*	-0.6435	2.23E-02	7.02E-04

Histocompatibility 2, Q region locus 4	*H2-Q4*	-0.624	2.22E-02	6.60E-04
Histocompatibility 2, class II antigen A, α	*H2-Aa*	-0.5918	2.86E-03	3.40E-05
Histocompatibility 2, class II antigen E β	*H2-Eb1*	-0.5903	2.86E-03	3.20E-05
Histocompatibility 2, M region locus 3	*H2-M3*	-0.5693	3.97E-02	1.56E-03
Proteasome subunit, beta type 10	*Psmb10*	-0.4267	3.99E-02	1.61E-03

Genes are shown in descending order (log2FC values).

Suppl. Tab. 10: *Pathways significantly altered by MC deficiency in early tumorigenic events in the colon (AOM vs AOM → CA). Data were obtained by RNA-seq and analysed on DAVID (Bioinformatic Database).*

Pathway	Status	*p*-Value	Genes
Cell adhesion molecules	Downregulated	1.2E-8	*Cd34, H2-M2, H2-M3, H2-Oa, H2-T24, H2-Ab1, H2-Aa, H2-Eb1, Ptprc*
Intestinal immune network for IgA production	Downregulated	6.9E-7	*H2-Oa, H2-Aa, H2-Ab1, H2-Eb1*
Intestinal immune network for IgA production	Upregulated	6.9E-7	*Cxcl12, Il15*
Antigen processing and presentation	Downregulated	8.9E-7	*H2-M2, H2-M3, H2-Oa, H2-T24, H2-Ab1, H2-Aa, H2-Eb1*
Cytokine-cytokine receptor interaction	Upregulated	4.8E-5	*Ccl3, Il15, Cxcl12*
	Downregulated	4.8E-5	*Ccl19, Ccr6, Ccr7, Cxcl5, Tnfrsf8*
Chemokine signaling pathway	Upregulated	1.2E-3	*Ccl9, Ccl3, Cxcl12*
	Downregulated	1.2E-3	*Ccr6, Ccr7, Cxcl5*
B cell receptor signaling pathway	Downregulated	3.4E-2	*Cd19, Cd22, Cr2*

Acronyms meaning is given in Suppl. Tab. 9.

Suppl. Tab 11: *Pathways significantly altered by MC deficiency in early tumorigenic events in the colon (AOM vs AOM+CA). Data were obtained by RNA-seq and analysed on DAVID (Bioinformatic Database).*

Pathway	Status	*p*-Value	Genes
Antigen processing and presentation	Downregulated	1.2E-5	*Cd74, H2-M3, H2-Aa, H2-Ab1, H2-Eb1, Tap1*
Intestinal immune network for IgA production	Downregulated	5.0E-4	*H2-Aa, H2-Ab1, H2-Eb1*
Inflammatory bowel disease (IBD)	Downregulated	1.4E-3	*H2-Aa, H2-Ab1, H2-Eb1, Il13*
Cytokine-cytokine receptor interaction	Downregulated	1.9E-3	*Ccl19, Ccl5, Ccr6, Cxcl5, Il13*
B cell receptor signaling pathway	Downregulated	2.2E-3	*Cd19, Cd22, Cd72, Cr2*
Cell adhesion molecules (CAMs)	Downregulated	3.0E-3	*Cd22, H2-M3, H2-Aa, H2-Ab1, H2-Eb1*
Chemokine signaling pathway	Downregulated	5.9E-3	*Ccl19, Ccl5, Ccr6, Cxcl5*
NF-kappa B signaling pathway	Downregulated	5.1E-2	*Ccl19, Zap70*

Acronyms meaning is given in Suppl. Tab. 9.

Suppl. Tab. 12. *Significantly altered genes by MC deficiency in allografic tumors (Kit^{B6} vs $Kit^{W/sh}$). Data were obtained by RNA-seq.*

Name	Acronym	log2FC	*p*-Adj	*p*-Value
Upregulated genes				
RNA binding motif protein 3	*Rbm3*	8.39E+14	1.37E+14	1.77E+09
Cell adhesion molecule 1	*Cadm1*	8.37E+14	1.18E+14	3.38E+14
Proteasome (prosome, macropain) subunit, alpha type 2	*Psma2*	8.01E+14	7.53E+14	1.79E+14
Proteasome (prosome, macropain) subunit, beta type 7	*Psmb7*	7.85E+14	1.44E+14	4.74E+14
Proteasome (prosome, macropain) inhibitor subunit 1	*Psmf1*	7.58E+14	4.88E+14	3.53E+14
Caspase 1	*Casp1*	7.57E+14	1.63E+14	2.56E+09
Tryptase alpha/beta 1	*Tpsab1*	7.50E+14	1.07E+02	3.07E-01
Proteasome (prosome, macropain) subunit, beta type 5	*Psmb5*	7.13E+14	4.49E+14	2.70E+14
Carboxypeptidase A3, mast cell	*Cpa3*	6.78E+14	6.11E-26	8.74E-29
Interferon induced transmembrane protein 3	*Ifitm3*	6.53E+14	1.18E+14	3.31E+14
Tryptase beta 2	*Tpsb2*	6.49E+14	1.57E+03	6.75E+00
Proteasome (prosome, macropain) activator subunit 1 (PA28 alpha)	*Psme1*	6.39E+13	2.00E+14	8.02E+14
Proteasome (prosome, macropain) 26S subunit, non-atpase, 6	*Psmd6*	6.13E+14	3.25E+14	1.48E+14
Proteasome (prosome, macropain) subunit, alpha type 4	*Psma4*	5.97E+14	3.47E+14	1.74E+14
Lectin, galactose binding, soluble 9	*Lgals9*	5.50E+14	4.88E+14	3.10E+14
Chemokine (C-C motif) receptor 5	*Ccr5*	5.50E+14	1.58E+14	5.87E+14
Vascular cell adhesion molecule 1	*Vcam1*	5.10E+14	3.47E+14	1.71E+14
Macrophage scavenger receptor 1	*Msr1*	4.89E+14	4.88E+14	3.30E+14
Proteasome (prosome, macropain) activator subunit 2 (PA28 beta)	*Psme2*	4.84E+14	1.84E+14	7.09E+14
Catalase	*Cat*	4.55E+14	4.46E+14	2.62E+14
Regulator of G-protein signaling 2	*Rgs2*	4.49E+14	4.36E+14	2.43E+14

Hepatitis A virus cellular receptor 2	*Havcr2*	4.38E+14	4.88E+14	3.37E+13
Beta-2 microglobulin	*B2m*	3.92E+14	4.18E+14	2.16E+14
Chemokine (C motif) ligand 1	*Xcl1*	1.00E+14	2.56E+13	1.09E+14
Downregulated genes				
Basic leucine zipper transcription factor, ATF-like	*Batf*	-5.87E+14	4.88E+14	3.56E+14
Chemokine (C-C motif) receptor 3	*Ccr3*	-2.03E+14	2.56E+13	1.10E+14
CD163 antigen	*Cd163*	-3.19E+12	5.71E+14	5.72E+08
CD5 antigen	*Cd5*	-1.27E+13	1.18E+14	3.34E+14
Class II transactivator	*Ciita*	-8.39E+14	1.91E+14	3.27E+09
C-type lectin domain family 10, member A	*Clec10a*	-1.99E+14	7.53E+14	1.83E+14
Colony stimulating factor 1 receptor	*Csf1r*	-6.71E+14	4.27E+14	2.32E+14
Dual specificity phosphatase 5	*Dusp5*	-8.73E+14	4.27E+14	2.32E+14
Coagulation factor XIII, A1 subunit	*F13a1*	-1.34E+14	1.46E+14	5.09E+14
Histocompatibility 2, class II antigen A, beta 1	*H2-Ab1*	-6.65E+14	9.83E+14	1.12E+09
Histocompatibility 2, class II antigen E beta	*H2-Eb1*	-8.66E+14	3.16E+14	2.71E+08
Histone cluster 1, h1c	*Hist1h1c*	-8.62E+14	3.25E+14	1.49E+14
Interleukin 13	*Il13*	-1.89E+14	4.88E+14	3.56E+14
K(lysine) acetyltransferase 6[a]	*Kat6a*	-5.78E+13	1.23E+14	3.78E+14
Leptin receptor overlapping transcript	*Leprot*	-8.37E+14	1.63E+14	2.50E+09
MAP-kinase activating death domain	*Madd*	-7.40E+14	4.44E+14	2.54E+14
Avian musculoaponeurotic fibrosarcoma oncogene homolog	*Maf*	-1.22E+14	1.46E+14	5.23E+13
Nuclear factor of kappa light polypeptide gene enhancer in B cells 1, p105	*Nfkb1*	-4.57E+14	6.19E+14	1.24E+13
Nudix (nucleoside diphosphate linked moiety X)-type motif 9	*Nudt9*	-6.03E+14	1.23E+14	3.87E+14
Programmed cell death 1 ligand 2	*Pdcd1lg2*	-1.56E+14	6.66E+14	1.43E+14
Proteoglycan 2, bone marrow	*Prg2*	-4.22E+14	2.19E+14	4.07E+09
Solute carrier family 15 (H+/peptide transporter), member 2	*Slc15a2*	-8.60E+13	1.67E+14	1.20E+08

Solute carrier family 7 (cationic amino acid transporter, y+ system), member 8	*Slc7a8*	-6.46E+14	4.83E+14	2.97E+14
Suppressor of cytokine signaling 1	*Socs1*	-5.57E+14	3.47E+14	1.65E+14
Spondin 2, extracellular matrix protein	*Spon2*	-1.61E+14	4.88E+14	3.28E+13
Tumor-associated calcium signal transducer 2	*Tacstd2*	-2.22E+13	4.88E+14	3.56E+14
Thrombospondin 4	*Thbs4*	-2.78E+14	3.85E+09	2.20E+07

According to their log2FC values, genes are shown in descending order.

Suppl. Tab. 13: *Pathways significantly altered by MC deficiency in in allografic tumors.. Data were obtained by RNA-seq and analysed on DAVID (Bioinformatic Database).*

Pathway	Status	*p*-Value	Genes
Proteasome	Downregulated	8.6E-10	*Psmd6, Psme1, Psme2, Psmf1, Psma2, Psma4, Psmb5, Psmb7*
Antigen processing and presentation	Upregulated	3.1E-5	*Ciita, H2-Ab1, H2-Eb1*
	Downregulated	3.1E-5	*B2m, Psme1, Psme2*
Inflammatory bowel disease (IBD)	Upregulated	1.4E-4	*Maf, H2-Ab1, H2-Eb1, Il13, Nfkb1*
Cell adhesion molecules (CAMs)	Upregulated	6.0E-3	*H2-Ab1, H2-Eb1, Pdcd1lg2*
	Downregulated	6.0E-3	*Cadm1, Vcam1*
Cytokine-cytokine receptor interaction	Downregulated	2.3E-2	*Ccr5, Xcl1*
	Upregulated	2.3E-2	*Ccr3, Csf1r, Il13*
Chemokine signaling pathway	Downregulated	5.9E-2	*Xcl1, Ccr5*
	Upregulated	5.9E-2	*Ccr3, Nfkb1*

Acronyms meaning is given in Suppl. Tab. 12.

Journal of Pathology
J Pathol 2019
Published online in Wiley Online Library
(wileyonlinelibrary.com) DOI: 10.1002/path.5285

ORIGINAL PAPER

Serotonin synthesis protects the mouse colonic crypt from DNA damage and colorectal tumorigenesis

Juliana Y Sakita[1], Michael Bader[2,3,4], Emerson S Santos[1], Sergio B Garcia[5], Stefania B Minto[5], Natalia Alenina[2,6], Mariângela O Brunaldi[5], Milene C Carvalho[7], Thiago Vidotto[8], Bianca Gasparotto[1], Ronaldo B Martins[9], Wilson A Silva Jr[8], Marcus L Brandão[7], Caio A Leite[10], Fernando Q Cunha[10], Gerard Karsenty[11], Jeremy A Squire[8,12], Sergio A Uyemura[1] and Vinicius Kannen[1]*

[1] *Department of Toxicology, Bromatology, and Clinical Analysis, University of Sao Paulo, Ribeirao Preto, Brazil*
[2] *Department of Biomedical and Molecular Sciences, Queen's University, Kingston, Canada*
[3] *Charité, University Medicine Berlin, Berlin, Germany*
[4] *Berlin Institute of Health (BIH), Berlin, Germany*
[5] *Department of Pathology, University of Sao Paulo, Ribeirao Preto, Brazil*
[6] *Institute of Translational Biomedicine, St. Petersburg State University, St. Petersburg, Russia*
[7] *Faculty of Philosophy, Sciences and Letters, University of São Paulo, Ribeirao Preto, Brazil*
[8] *Department of Genetics, University of Sao Paulo, Ribeirao Preto, Brazil*
[9] *Department of Cell and Molecular Biology, Virology Research Center, University of Sao Paulo, Ribeirao Preto, Brazil*
[10] *Department of Pharmacology, University of Sao Paulo, Ribeirao Preto, Brazil*
[11] *Department of Genetics and Development, Columbia University, New York, NY, USA*
[12] *Department of Pathology and Molecular Medicine, Queen's University, Kingston, Canada*

**Correspondence to: V Kannen, Department of Biomedical and Molecular Sciences, Queen's University, Kingston, ON K7L 2V5, Canada. E-mail: vkc@queensu.ca*

Abstract

Serotonin (5-HT) signaling pathways are thought to be involved in colorectal tumorigenesis (CRT), but the role of 5-HT synthesis in the early steps of this process is presently unknown. In this study, we used carcinogen treatment in the tryptophan hydroxylase 1 knockout (Tph1KO) and transgenic (Tph1$^{fl/fl}$Villin^{Cre}) mouse models defective in 5-HT synthesis to investigate the early mutagenic events associated with CRT. Our observations of the colonic crypt post-treatment followed a timeline designed to understand how disruption of 5-HT synthesis affects the initial steps leading to CRT. We found Tph1KO mice had decreased development of both allograft tumors and colitis-related CRT. Interestingly, carcinogenic exposure alone induced multiple colon tumors and increased cyclooxygenase-2 (*Ptgs2*) expression in Tph1KO mice. Deletion of interleukin 6 (*Il6*) in Tph1KO mice confirmed that inflammation was a part of the process. 5-HT deficiency increased colonic DNA damage but inhibited genetic repair of specific carcinogen-related damage, leading to CRT-related inflammatory reactions and dysplasia. To validate a secondary effect of 5-HT deficiency on another DNA repair pathway, we exposed Tph1KO mice to ionizing radiation and found an increase in DNA damage associated with reduced levels of ataxia telangiectasia and Rad3 related (*Atr*) gene expression in colonocytes. Restoring 5-HT levels with 5-hydroxytryptophan treatment decreased levels of DNA damage and increased *Atr* expression. Analysis of Tph1$^{fl/fl}$Villin^{Cre} mice with intestine-specific loss of 5-HT synthesis confirmed that DNA repair was tissue specific. In this study, we report a novel protective role for 5-HT synthesis that promotes DNA repair activity during the early stages of colorectal carcinogenesis.

Keywords: intestines; colon cancer; neuropeptide; γ-H2AX; DNA damage repair

Received 21 September 2018; Revised 19 March 2019; Accepted 26 April 2019

No conflicts of interest were declared.

Introduction

Colorectal cancer (CRC) is the third most common malignancy worldwide [1]. The majority of CRC is sporadic so that the disease is predominantly driven by changes in the human environment and lifestyle [2,3]. Although colitis is one of the recognized risk factors for CRC, less than 2% of CRC cases are attributed to this condition [4]. One of the best experimental mouse models to study the development of CRC uses colonotropic carcinogens to induce tumors in either a colitis-dependent or a colitis-independent manner [5]. Given that most carcinogen-induced tumors are nonmalignant, or otherwise classified as adenomas, the time frame from carcinogenic exposure until tumor detection may be better named colorectal tumorigenesis (CRT). Significantly, DNA damage repair (DDR) activity alters the development of colitis-independent CRT [1]. The cellular alterations and mutations leading to cancer are thought to take place in colonic stem cells

(CSCs) that reside at the base of crypts [6]. In keeping with this idea, CSCs have been known to give rise to enteroendocrine (EE) cells in a complex process of cellular differentiation. These EE cells release a large number of hormones, including serotonin (5-HT) [7]. Interestingly, β-catenin (*Ctnnb1*) mutations during the early stages of this process have been shown to induce tumors expressing 5-HT [8].

Signaling via 5-HT has been shown to play a role in a variety of different human cancers [9]. Tutton and Barkla first suggested in 1978 that 5-HT may also be involved in the development of CRC [10]. Our studies later confirmed that 5-HT signaling not only promoted the growth of CRC allograft tumors but also mediated tumor angiogenesis [11]. Recently, Li and colleagues showed that the 5-HT receptor 1D activated the Axin1/β-catenin/MMP-7 pathway promoting cell invasion and CRC metastasis [12]. However, this seems contradictory to the fact that 5-HT elicited radioprotective effects [13,14]. Moreover, some selective 5-HT reuptake inhibitors (SSRIs) increase 5-HT levels but appear to decrease the risk of CRC in humans [15]. We also found similar effects with SSRIs that reduced the CRC risk in rodent model systems [16]. In keeping with the idea that repression of 5-HT levels was protumorigenic, we found that experimental conditions promoting the development of CRC inhibited 5-HT synthesis in the colon [17,18].

As the largest neuroendocrine organ, the intestines make the greatest contribution to 5-HT levels in the body by hydroxylation of tryptophan, using the rate-limiting enzyme tryptophan hydroxylase I (Tph1) [19]. This neurohormone has controversial effects, as it can be either a pro-inflammatory or anti-inflammatory mediator according to the intensity or type of intestinal mucosa damaging stimulation [20]. It is noteworthy that in humans with ulcerative colitis the increased risk of CRC is based on both the extent and the duration of disease [21]. Although inflammation is a known risk factor for CRT in mice, the early steps of the disease process may be acquired independently of inflammatory responses [5]. In mice, CRT may also be a consequence of carcinogen-induced DNA damage leading to somatic mutations in CSCs [5].

In this study, we show that 5-HT synthesis alters the development of CRT in a DNA damage-dependent manner in the carcinogen-exposed colon of mice. Our analysis of the impact of 5-HT on the early steps leading to CRC reveals that 5-HT synthesis may lower the risk of this disease by promoting DDR mechanisms and protecting colonic crypts from subsequent inflammatory responses triggered by DNA damage.

Material and methods

Mouse strains and experiments

The Committee on Animal Research of the University of São Paulo (#14.1.296.53.3) approved all experiments according to the guidelines of the Committee on Care and Uses of Laboratory Animals of the National Research Council of the NIH (USA). Breeding and experimentation rooms remained at standard conditions (specific pathogen-free conditions; 24 ± 1 °C; light–dark cycles of 12:12 h). According to a previous detailed description, *Tph1* knockout (Tph1KO) mice were engineered to have the *Tph1* gene deleted [19]. *Tph1* WT (Tph1WT) mice were used as the control. Il6KO mice were acquired from the Jackson Laboratories (Bar Harbor, ME, USA) [22]. *Tph1* and *Il6* double knockout mice (Tph1-Il6DKO) were bred according to see supplementary material, Figure S1 and genotyped as described previously [19,22]. Also, mice carrying the *Tph1* floxed allele ($Tph1^{fl/fl}$) were bred to the $Villin^{Cre}$ and the $CDX2^{CreERT2}$ mouse strains to restrict 5-HT deficiency to the intestines ($Tph1^{fl/fl}Villin^{Cre}$; see supplementary material, Figure S2A) and to the colon ($Tph1^{fl/fl}CDX2^{CreERT2}$; see supplementary material, Figure S2B), respectively [23,24]. $CDX2^{CreERT2}$ mice (#022390) were also acquired from the Jackson Laboratories. Only male mice aged 8 weeks underwent experimentation.

A full-description of the 18 experiments on mice is provided in supplementary material, Supplementary materials and methods (DME 1–18; [5,11,19,24–28]). In brief, allograft tumors were induced by subcutaneously injecting 1×10^6 MC38 cells in each mouse [11]. Colitis-dependent CRT was induced by a single i.p. injection of azoxymethane (AOM; 10 mg/kg; Sigma-Aldrich, Heidenheim, BW, DE) and three cycles of dextran sodium sulfate (DSS; 3%; Sigma-Aldrich) in drinking water for 7 days and ordinary drinking water for 14 days [5]. At the 10th week, mice underwent euthanasia. Colitis-independent CRT was induced by six AOM injections throughout 6 weeks. A single AOM injection was given to mice to study DNA damage. Given that AOM-related metabolites are detected up to 48 h following carcinogenic exposure [28], mice underwent euthanasia 72 h after AOM injections to focus the analysis on DNA damage intensity and other related colonic effects occurring before carcinogenic bioactivity would have time to take place. To examine the impact of AOM on the development of aberrant crypts (AC) and determine the levels of colonic recovery, mice underwent euthanasia a week after AOM injections. To study the development of AC foci (ACF) and tumors, it was necessary to sacrifice mice at 6 or 18 weeks following the sixth AOM exposure, respectively [5]. Direct carcinogenic exposure was induced by either methylnitronitrosoguanidine (MNNG; 5 mg/ml; Sigma-Aldrich; [25]) or ionizing radiation (IR) provided by X-ray tube technology (RS-2000 Biological Research Irradiator, Rad Source, Kansas City, MO, USA) total dose 7 Gy at 1.75 Gy/min. A single tamoxifen injection (TAM; 100 mg/kg i.p.; Sigma-Aldrich) induced *Tph1* deletion by the $CDX2^{CreERT2}$ transgene [24].

Analytical methods

Details for the following methods are described in supplementary material, Supplementary materials and methods and in the references indicated: HPLC electrochemical detection (HPLC-ECD [16]), RT-qPCR [25], colonoscopy [5], histopathology [25], immunohistochemistry [IHC] [25], sequential IHC [29], qPCR array, immunofluorescence (IF) [25], TUNEL, immunoblotting [25] and quantitative methylation-specific PCR (qMSP) [30].

Statistical analysis

We analyzed our dataset with the GraphPad Prism 5.0 software (Graph Pad Software Inc., San Diego, CA, USA). We used two-tailed Mann–Whitney tests to analyze experiments with two different groups. One-way ANOVA tests (with Kruskal–Wallis *post hoc* test) were applied to analyze experiments with more than two groups. Two-way ANOVA tests (with Bonferroni's *post hoc* test) were applied to analyze different categorical independent endpoints with one dependent variable. A probability of $p < 0.05$ was considered to be statistically significant.

Results

5-HT synthesis elicits protection against DNA damage-related colorectal tumors

Since 5-HT signaling has been suggested to promote CRC [10–12], we evaluated how 5-HT synthesis altered the risk of CRC in different mouse models. In our initial experiments, allograft tumors were subcutaneously seeded in Tph1WT and Tph1KO mice. Our analysis confirmed that 5-HT promotes the development of CRC-like tumors (see supplementary material, Figure S3A, Supplementary materials and methods, DME 1) [10,11]. Since the synthesis of 5-HT has been found to promote colitis [31], a known risk factor of CRC [2], we studied Tph1KO mice to determine whether reducing 5-HT levels would also alter the incidence of colitis-related colorectal tumors. When we induced colitis-dependent CRT by AOM/DSS, fewer tumors developed in the Tph1KO mice, suggesting that 5-HT deficiency decreased the incidence of tumors in an inflammation-dependent manner (see supplementary material, Figure S3B,C; Supplementary materials and methods, DME 2).

Considering that colorectal tumors may develop in a colitis-independent manner [5], we investigated whether 5-HT synthesis activity was altered by longer exposure to a carcinogen in the colon. We found that protracted AOM exposures induced DNA damage and increased 5-HT levels (Figure 1A; see supplementary material, Supplementary materials and methods, DME 3). To clarify how further changes in the 5-HT system were affected by AOM-exposure, we analyzed some downstream serotonergic elements, such as DOPA decarboxylase (*Ddc*), monoamine oxidase A (*Maoa*), vesicular monoamine transporter 2 (Vmat2, encoded by *Slc18a2*) and 5-HT transporter (Sert, encoded by *Slc6a4*) following 72 h and 1 week from the last carcinogenic treatment (see supplementary material, Figure S4; Supplementary materials and methods, DME 4 [28]). At 1 week following AOM exposure, *Tph1* was highly expressed, suggesting that levels of the 5-HT precursor 5-hydroxytryptophan (5-HTP) were increased (see supplementary material, Figure S4A). AOM injections appear to increase the hydroxylation of 5-HTP into 5-HT by Ddc (see supplementary material, Figure S4B), which was followed by high expression of *Slc6a4* (Sert) (see supplementary material, Figure S4C).

These findings led us to explore what effects loss of 5-HT synthesis would have in a carcinogen-induced CRT model. Tph1KO mice had more AOM-induced colorectal tumors with increased multiplicity (Figure 1B; see supplementary material, Figure S5; Supplementary materials and methods, DME 5). Comparison between Tph1KO and Tph1WT mice showed that 5-HT deficiency increased (by 1.2-fold) low-grade dysplastic (LD) colorectal tumors but promoted proliferation in those high-grade dysplastic lesions (HD; Figure 1B–D; see supplementary material, Figure S6). Considering that ATR is activated due to errors in the replication fork [32–34], a second experiment showed the reproducibility of these findings and also revealed that the Tph1KO had a decreased number of cells immunopositive for phosphorylated ATR (pATR) (Figure 1E; see supplementary material, Figure S7). However, phosphorylated ATM (pATM) remained unchanged (Figure 1F). These findings collectively support that 5-HT synthesis promotes the expansion of CRC cells and colitis-dependent CRT, although it inhibited the development of DNA damage-related colorectal tumors by activating a DDR response.

5-HT synthesis activates DNA damage response in the preneoplastic colon

To clarify the role of 5-HT synthesis in DDR during CRT, we investigated whether 5-HT deficiency in Tph1KO mice reduced *Atr* levels before tumors were detectable in the colon. Colonic samples from AOM-exposed mice were analyzed 12 weeks before tumors are usually found (see timeline schematic, Figure 1A; see supplementary material, Supplementary materials and methods, DME 6). We observed that increased rates of ACFs occurred together with high CTNNB1 levels (Figure 2A,B; see supplementary material, Figure S8A,B). These increased rates were also associated with the upregulation of the CTNNB1 targets *Lef1*, *Tcf7* and *Myc* (see supplementary material, Figure S8C–E). Further analysis revealed proliferation was also increased (Figure 2C; see supplementary material, Figure S8F). Previous findings showed that increasing CTTNB1 activity facilitated CSCs to undergo DNA damage [35]. Therefore, we studied the abundance of cells at the crypt base containing γH2AX, and found

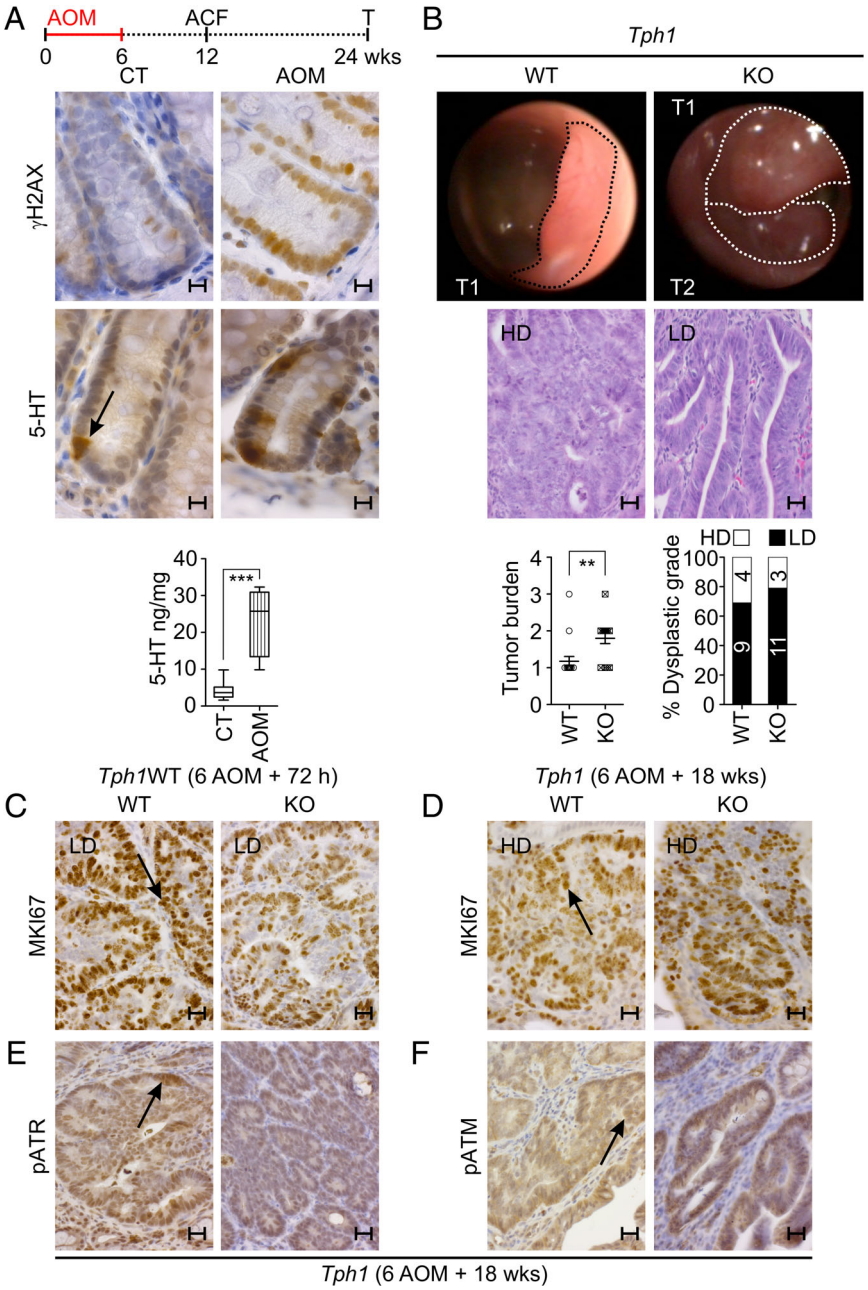

Figure 1. 5-HT synthesis deficiency promotes colorectal tumors to develop following DNA damaging events. (A) Timeline of AOM induction of DNA damage throughout 6 weeks, as well as detection of ACF and tumors (T) at weeks 12 and 24, respectively. Representative IHC images using anti-γH2AX and anti-5-HT antibodies; black arrows lead to positive cells; ×100. HPLC-ECD of 5-HT levels after AOM injections ($n = 14$; $^{***}p = 0.0006$) compared to control (CT); data are shown as the median, highest and lowest values, and upper and lower quartiles). (B) Representative images of colonoscopy in Tph1KO and Tph1WT mice (sectioned lines encircle tumors). Histopathological images of HD and LD tumors (×40). Graph depicts increased tumor numbers in Tph1KO mice ($n = 32$; $^{**}p = 0.0014$; data are shown as individual points with the mean ± SEM; two-tailed Mann–Whitney's tests). Tph1KO mice developed less HD tumors ($n = 27$; [HD; white box top] or not [LD; black box top]; the number of either HD or LD tumors are embedded within the column bars). (C,D) Representative IHC images of MKI67 antibody staining in LD (C) and HD (D) tumor samples from Tph1WT and Tph1KO mice (×100). (E,F) Representative IHC images of tumor samples stained for pATR (E) and pATM (F) (×100). Scale bars = 20 μm.

that genetic blockage of 5-HT synthesis increased DNA damage in the CSC niche (Figure 2D; see supplementary material, Figure S8G). Indeed, proliferation and DNA damaging events occurred at the same time in AOM-exposed Tph1KO mice (Figure 2E; see supplementary material, Figure S8H,I). This observation led us to assess whether proliferation-related DNA damage was associated with changes in DDR pathways. Out of 84 potential targets, *Atr* levels were significantly down-regulated ($p = 0.038$; Figure 2F; see supplementary material, Figure S7J). In agreement with this finding, we also observed a combined low level of *Atr*, *Chk1*, and *Trp53* mRNAs in AOM-exposed Tph1KO mice (Figure 2G).

To explore the role of 5-HT synthesis in the modulation of DNA damage and DDR activity further, we

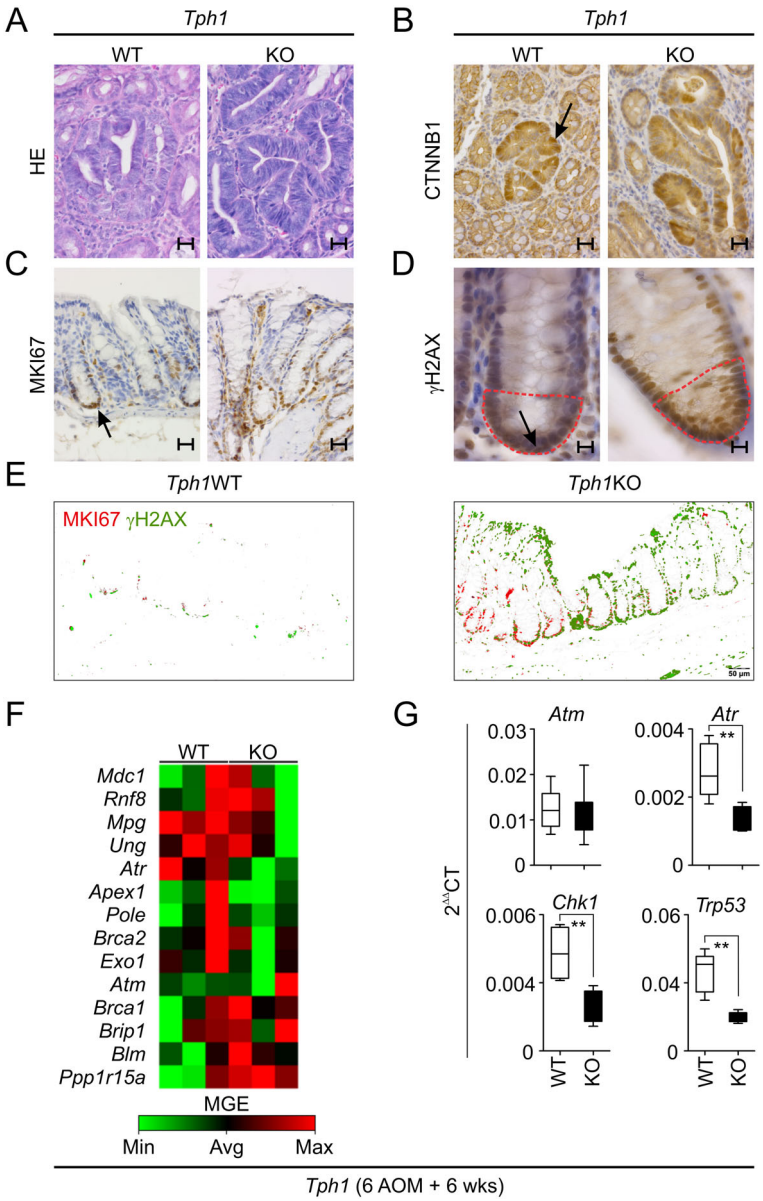

Figure 2. Increased development of preneoplastic lesions is related to DNA damage and genetic repair errors in 5-HT deficient mice. (A–D) Histopathological images depict ACFs stained by HE and anti-β-catenin antibody (CTNNB1) (A,B), as well as colonic samples stained for MKI67 and γH2AX (C,D); red sectioned lines encircle the CSC niche; nuclear-stained cells shown by black arrows. (E) Representative images of sequential IHC reactions against Ki67 and γH2AX, pseudo-colored in red and green, respectively. (F) Clustergram encloses 14 out of 84 DDR-related genes analyzed by a qPCR array. (G) Relative mRNA levels of the indicated DNA repair genes in colonic tissue samples from Tph1KO and Tph1WT by RT-qPCR ($n = 12$). Data are shown as the median, highest and lowest values, and upper and lower quartiles. *Atr* (**$p = 0.0087$), *Chk1* (**$p = 0.0079$), *Trp53* (**$p = 0.0079$), two-tailed Mann–Whitney's tests.

exposed Tph1KO mice to IR and analyzed samples 72 h later. These analyses confirmed that the irradiated mice had more DNA damage at the base of colonic crypts (Figure 3A; see supplementary material, Supplementary materials and methods, DME 7). We used gene expression array analysis to discover that *Atr* was downregulated (by 1.3-fold) in 5-HT deficient mice (Figure 3B). This observation was verified by RT-qPCR (Figure 3D). Rescuing 5-HT synthesis with 5HTP decreased DNA damage intensity at the crypt base (Figure 3E; see supplementary material, Supplementary materials and methods, DME 8). This anti-DNA damage effect of 5-HT was further related with increased proliferative activity in the colon (Figure 3F). Also, reactivating 5-HT synthesis by 5HTP treatment increased *Atm* (Figure 3G), *Atr* (Figure 3H), and *Trp53* mRNA levels in Tph1KO mice (Figure 3J). To verify whether this potential control of 5-HT on *Atr* expression could be an early event following induction of DNA damage, we analyzed colon samples 4 h after $Tph1^{fl/fl}$[1], and $Tph1^{fl/fl}Villin^{Cre}$ mice had been exposed to IR. This experiment confirmed that *Atr* levels were decreased in mice with constitutional deficiency of intestinal 5-HT synthesis (see supplementary material, Figure S9C; Supplementary materials and methods, DME 9).

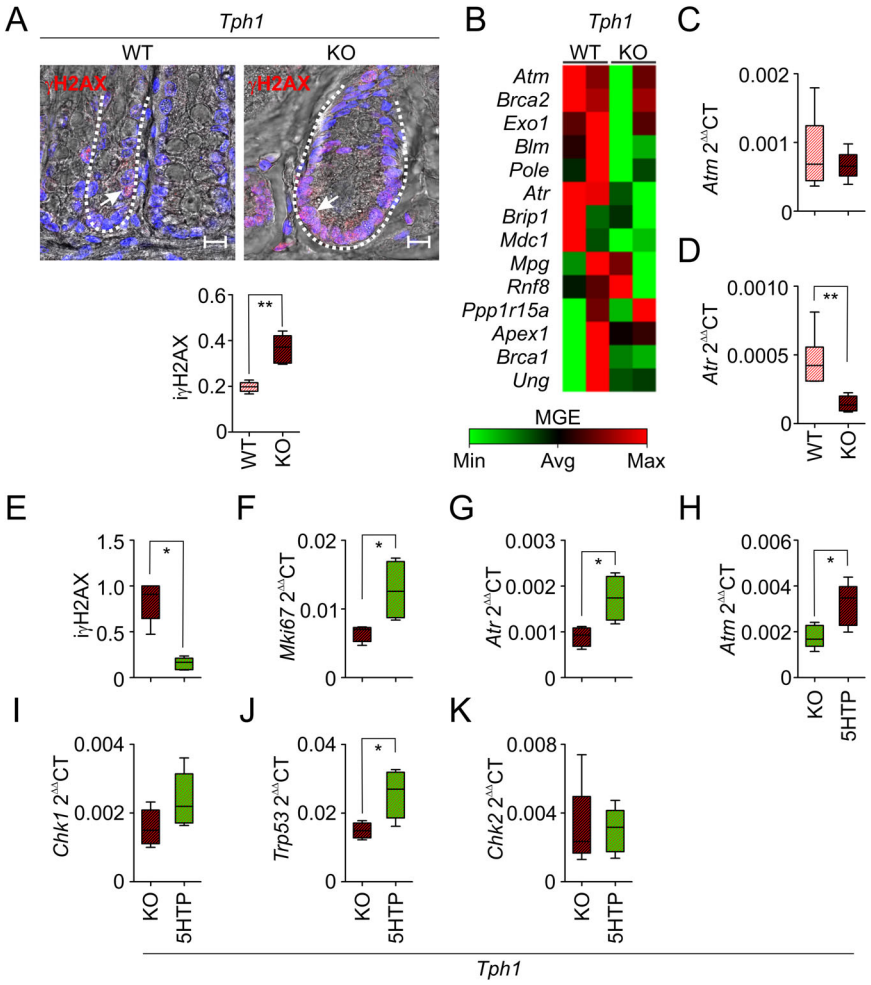

Figure 3. IR-related DNA damage and genetic repair errors are reduced by 5-HT synthesis. (A) Representative IF images show γH2AX in Tph1WT and Tph1KO mice. Dotted white lines encircle crypts. White arrows show γH2AX-positive cells (×63 optical magnification plus ×2 digital zoom). Graphs show index values [i]; iγH2AX; $n = 11$; $^{**}p = 0.0043$). (B) qPCR array analysis of DDR-related mRNA levels is summarized in a clustergram. (C,D) Relative *Atm* and *Atr* mRNA levels in IR-exposed WT and Tph1KO mice ($n = 11$; $^{**}p = 0.0043$). (E) Histopathological analysis of DNA damage and (F) qPCR for proliferation after rescuing 5-HT synthesis in Tph1KO mice ($n = 10$; $^{*}p = 0.0119$ and $^{*}p = 0.028$ for E and F, respectively). (G–K) Levels of the indicated mRNAs following IR-induced DNA damage and 5HTP treatment ($n = 10$; *Atr* $p = 0.0286$; *Atm* $p = 0.0317$; *Trp53* $p = 0.0317$). Data are shown as the median, highest and lowest values, and upper and lower quartiles. *P* values were calculated using two-tailed Mann–Whitney's test.

We further explored the potential protective effect of 5-HT synthesis against AOM-induced DNA damage with a time-course experiment. At 72 h after a single AOM exposure, we confirmed that DNA damage was increased in Tph1KO mice (Figure 4A; see supplementary material, Supplementary materials and methods, DME 10). However, we observed that the protective effect of 5-HT seemed to be related to 5-HT synthesis rather than this neurohormone replacement *per se*, since treating Tph1KO mice with exogenous 5-HT did not protect from DNA damage (see supplementary material, Figure S10; Supplementary materials and methods, DME 11). We further tested whether 5-HT synthesis could protect colonocytes from DNA damage by inhibiting Tph1 with 4-chloro-DL-phenylalanine (PCPA) (see supplementary material, Supplementary materials and methods, DME 12) before exposing mice to AOM (Figure 4B). Pharmacologically inhibiting 5-HT synthesis increased the development of colon preneoplastic lesions (Figure 4C; see supplementary material, Supplementary materials and methods, DME 13). Given that the 5-HT synthesis occurs in different cell types [19], we restricted loss of *Tph1* expression to the intestines to confirm that tissue specific 5-HT synthesis protected the colon from direct carcinogen-induced DNA damage (Figure 4D). Our findings supported the idea that intestinal deficiency of 5-HT synthesis promoted the development of preneoplastic lesions in the colon (Figure 4D; see supplementary material, Supplementary materials and methods, DME 14). We then engineered a mouse model with inducible deletion of Tph1 in the colon and exposed these mice to MNNG. This experiment provided further evidence that silencing 5-HT synthesis increased the number of preneoplastic lesions (Figure 4E; see supplementary material, Supplementary materials and methods, DME 15). Our findings support the idea that 5-HT synthesis modulates DNA damage and repair during the development of colorectal carcinogenesis.

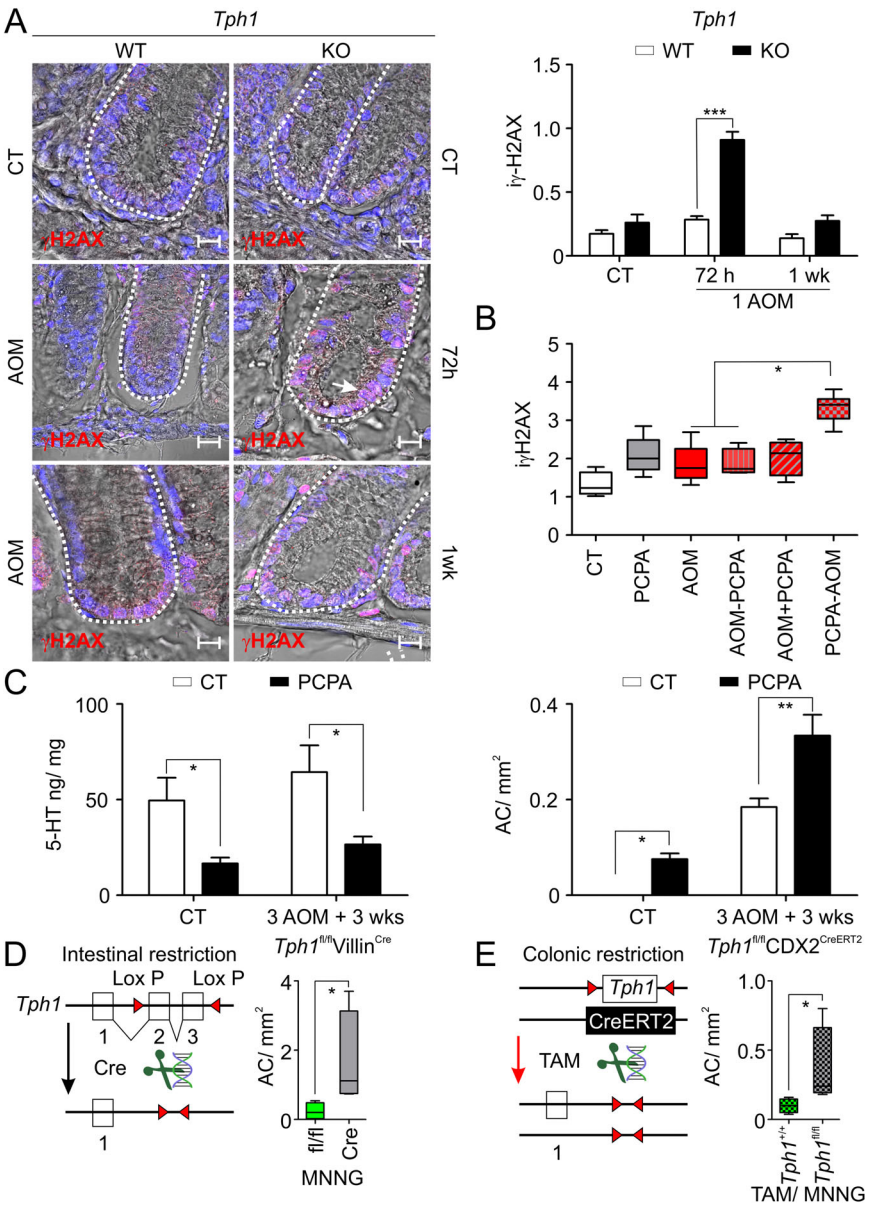

Figure 4. 5-HT synthesis protects colonocytes from DNA damage and early tumorigenic events. (A) Representative pictures of IF γ-H2AX in colon samples. Sectioned white lines encircle crypts. White arrows show γH2AX positive cells (×63 optical magnification plus ×2 digital zoom). The graph on the right shows index values [i]; data are mean ± SEM ($n = 35$; ***$p < 0.001$ two-way ANOVA with Bonferroni's *post hoc* test). (B) The effect of inhibiting 5-HT synthesis before carcinogenic induction on DNA damage in the colon. Data are the median, highest and lowest values, and upper and lower quartiles ($n = 30$; *$p < 0.05$ ANOVA with Kruskal–Wallis' *post hoc* test). (C) Left panel shows HPLC-ECD analysis of 5-HT levels with or without PCPA treatment. Right panel shows the development of preneoplastic lesions Data are shown as mean ± SEM ($n = 17$; *$p < 0.05$ and **$p < 0.001$; two-way ANOVA with Bonferroni's *post hoc* test). (D) Left panel; the targeting strategy for *Tph1* floxed allele and its specific intestinal deletion upon breeding these mice to the Villin^{Cre} mouse strain. Right panel; the numbers of preneoplastic lesions in the colon ($n = 8$; *$p = 0.028$). (E) Left panel; the strategy for CDX2 transgene activity induced by TAM to delete *Tph1* in the colon. Right panel; the development of preneoplastic lesions in the colon with MNNG exposure and *Tph1* deletion. Data are median, highest and lowest values, and upper and lower quartiles ($n = 8$; *$p = 0.028$; two-tailed Mann–Whitney's test).

Serotonergic activity induces specific AOM-related DNA damage response blocking the early steps of colorectal carcinogenesis

In keeping with the idea that 5-HT synthesis has a significant role on DDR mechanisms during the development of AOM-related colon tumors [5], we analyzed DNA damage intensity using a time-course experiment to study preneoplastic lesions 3 days after the sixth AOM exposure. We compared Tph1WT mice to Tph1KO and found that 5-HT synthesis protected the colon from AOM-induced DNA damage (Figure 5A; see supplementary material, Figure S11**;** Supplementary materials and methods, DME 16). However, analysis of *Atm* and *Atr* showed that the expression of both genes remained unchanged (Figure 5B,C). In contrast, Tph1KO mice (that lacked 5-HT synthesis) had intense methylation in the CpG islands of the *Mgmt* promoter, leading to decreased *Mgmt* mRNA levels (Figure 5D,E). At this same time-point, we also found *Alkb1* mRNA

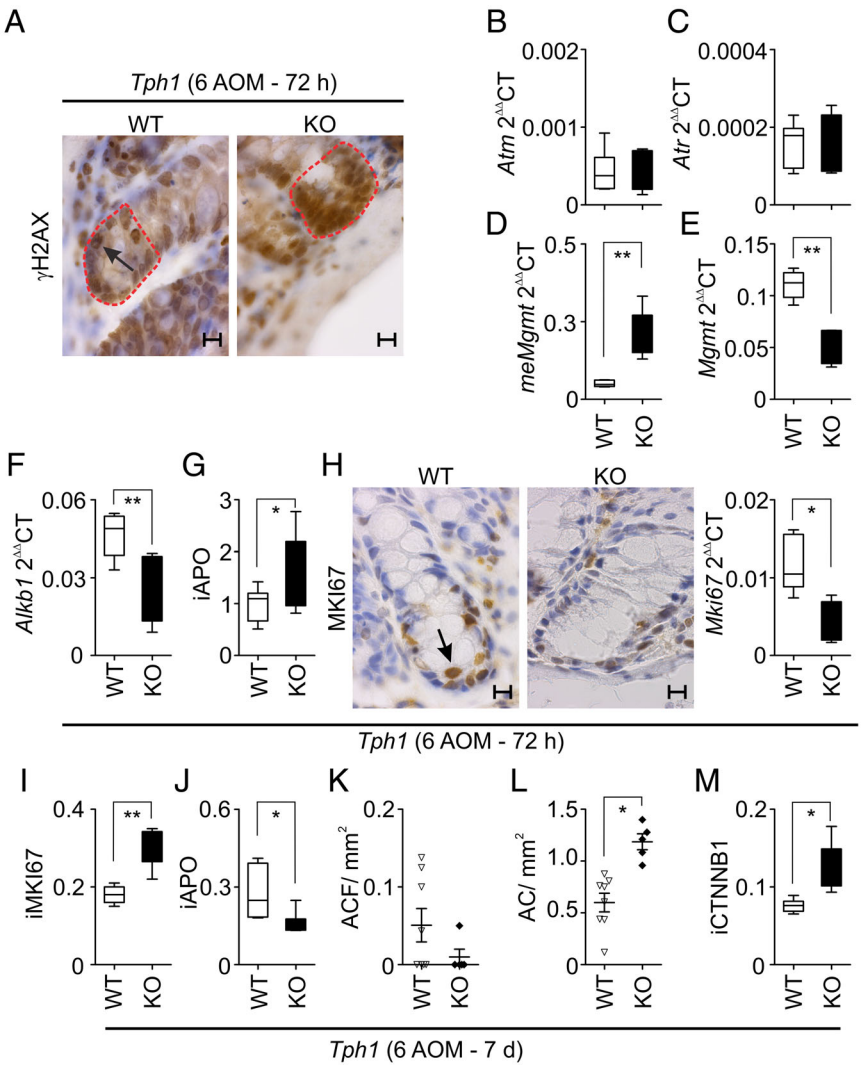

Figure 5. 5-HT synthesis deficiency promotes early carcinogenic events in the colon. (A) Representative IHC images of γH2AX in the colon of *Tph1*WT, and *Tph1*KO mice analyzed 72 h from the sixth AOM injection (red lines denote the stem cell niche, scale bar = 20 μm). (B,C) qPCR for *Atm* and *Atr*. (D) Methylation of *Mgmt* CpG region (*meMgmt*) and (E) *Mgmt* mRNA levels ($n = 12$; $p = 0.0022$ and $p = 0.0043$, respectively). (F) *Alkb1* mRNA levels ($n = 12$; $p = 0.0022$). (G) Apoptosis index (iAPO) in the colon; $n = 12$; $p = 0.0499$). (H) Representative images of colon sections stained for MKI67 and qPCR for *Mki67* mRNA 72 h from the sixth AOM exposure (scale bar = 20 μm; $n = 12$; $^*p = 0.0043$). (I,J) MKI67 index (iMKI67) and iAPO 1 week after the sixth AOM injection. Data are median, highest and lowest values, and upper and lower quartiles. ($n = 12$; $p = 0.0012$ and $p = 0.0140$, respectively). (K,L) Rates of ACF and AC in WT and Tph1KO mice ($n = 13$; data are shown as individual points with the mean ± SEM; $^*p = 0.0016$). (M) Numbers of CTNNB1 positive crypts (iCTNNB1; $n = 12$; $^*p = 0.0159$). Data are median, highest and lowest values, and upper and lower quartiles. *P* values were calculated using two-tailed Mann–Whitney's test.

was reduced (Figure 5F). We then checked to see if this downregulation in *Mgmt* occurred before or after the sixth AOM exposure. 5-HT deficiency decreased *Mgmt* mRNA levels 72 h after the first AOM injection, but there was no change at the sixth week after the last carcinogenic exposure (see supplementary material, Figure S12). Interestingly, the absence of 5-HT synthesis in Tph1KO mice led to apoptosis and reduced colonocyte proliferation shortly after the sixth AOM exposure (Figure 5G,H).

We then investigated CRT development 1 week from the sixth AOM injection. Throughout this period, 5-HT deficiency increased proliferation but inhibited apoptosis (Figure 5I,J). Also, this condition promoted the development of early preneoplastic lesions (Figure 5K,L) and increased CTNNB1 protein and *Lef1* mRNA (Figure 5M and see supplementary material, Figure S13, respectively). Collectively, our findings support that 5-HT synthesis could elicit protective effects against early steps of CRC by inducing specific genetic repair pathways.

Serotonergic activity controls DNA damage-related inflammatory reaction promoting the development of colon preneoplastic lesions

Finally, we considered the idea that cells with damaged DNA also require an inflammatory tissue microenvironment to develop into preneoplastic lesions and tumors [36]. Since macrophages are

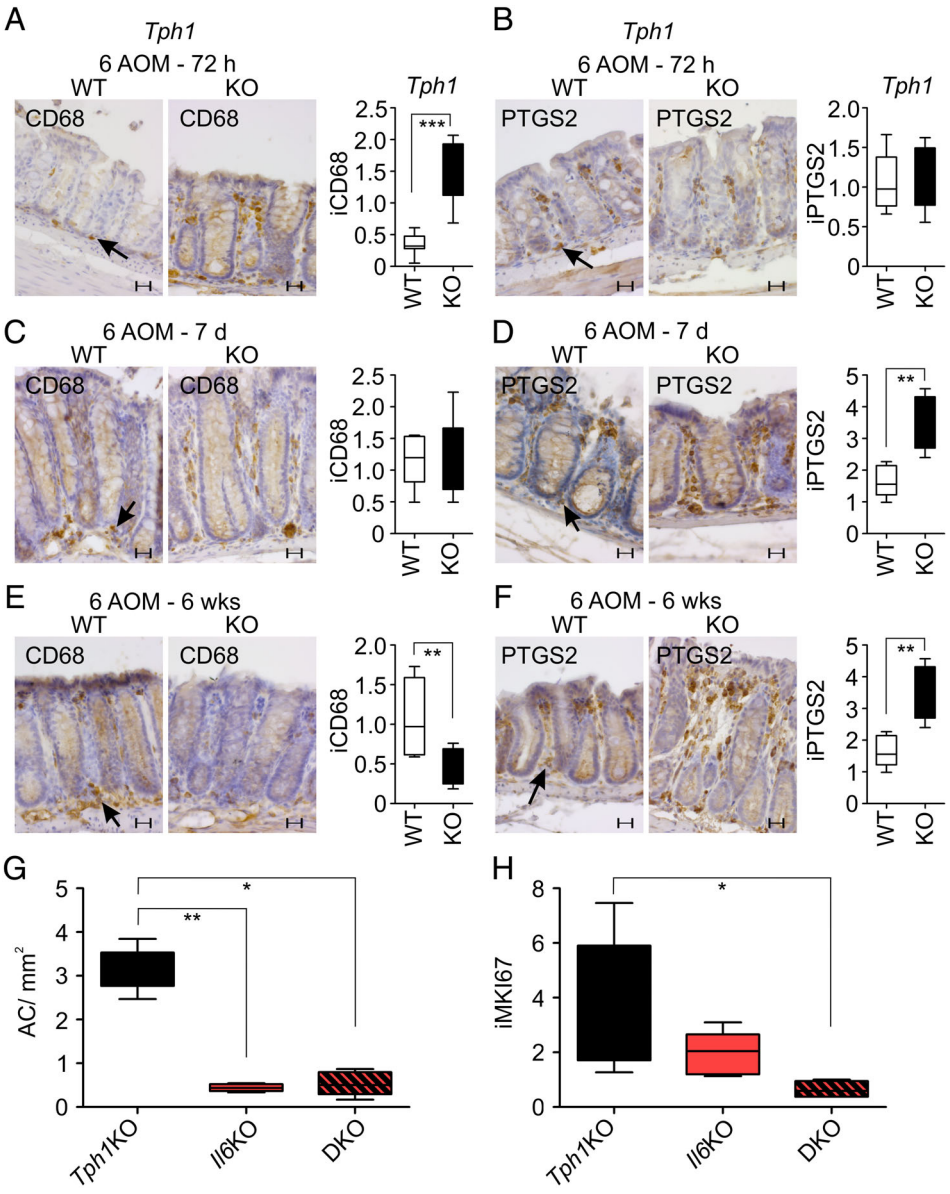

Figure 6. 5-HT deficiency activates inflammatory reaction following protracted carcinogenic exposure in the colon. (A,B) Representative IHC images and staining index (i) of CD8 (A; a black arrow indicates positive cells) and PTGS2 (B) 72 h after the sixth AOM exposure. $p = 0.0002$ for CD68 and $p = 0.752$ for PTGS2). (C,D) CD8 and PTGS2 immunostaining 1 week after the sixth carcinogenic injection ($p = 0.699$ and $p = 0.0012$, respectively). (E,F) CD68 and PTGS2 cell numbers at the sixth week following the last AOM exposure (**$p = 0.008$ and 0.0012, respectively). *P* values were calculated using two-tailed Mann–Whitney's test. Scale bars = 20 µm. (G,H) Preneoplastic lesions (G) ($p < 0.05$) and proliferation (H) ($p < 0.05$), one-way ANOVA with Kruskal–Wallis' *post hoc* test. Data are shown as the median, highest and lowest values, and upper and lower quartiles.

the most abundant immune cell population in the colon [37], we monitored their numbers by immunostaining for CD68 and we also immunostained for prostaglandin endoperoxide synthase 2 (PTGS2; also called cyclooxygenase 2), a biomarker that increases as CRC develops [38]. Our analysis showed an increase in the numbers of macrophages occurred 72 h after AOM injection, but PTGS2 did not increase until a week after AOM treatment (Figure 6A–D). We extended the time course and found that the number of macrophages decreased 6 weeks after the sixth AOM injection, but PTGS2 remained high in Tph1KO mice (Figure 6E,F).

To explore the idea that the absence of 5-HT could be permissive for inflammation-related events that promote sporadic CRC development, we genetically deleted the pro-inflammatory cytokine interleukin 6 gene (*Il6*) from Tph1KO mice (Tph1-Il6-DKO). In keeping with the idea that Il6 deficiency would block the tumor-promoting inflammatory reaction associated with CRC [39], we found that Tph1-Il6-DKO mice developed fewer preneoplastic lesions and showed reduced proliferative rates in the colorectal area (Figure 6G,H; see supplementary material, Supplementary materials and methods, DME 18). Our findings are consistent with a mechanism in which loss of 5-HT synthesis

increases DNA damaging events that also trigger an inflammatory microenvironment that is permissive for the development of CRC.

Discussion

It has been widely accepted that 5-HT signaling promotes the development of colon tumors through its receptors, as shown by Tutton and Barkla and others [10–12]. Our findings support this earlier idea, since those tumors classified as HD, or the more aggressive phenotype, showed increased proliferation when 5-HT signaling was absent. However, our study also draws attention to the important role of 5-HT synthesis in modulating DNA repair in the developing colon and providing protection against colorectal carcinogenesis. Our previous findings showed that 5-HT levels could alter the development of preneoplastic lesions and these are in keeping with other studies on the role of 5-HT in CRC [16–18]. For instance, although 5-HT was found to promote colon cancer in rats [10], it was unclear why increased 5-HT levels following serotonergic reuptake inhibition protected the colon from preneoplastic lesions [16]. Similar events reducing the CRC risk had also been reported in humans [40]. Tutton and Barkla reported that 5-HT promoted the proliferation of colon tumors but did not affect the normal colonocytes [10]. Since the serotonergic system provides initial protection against chemical or biological toxins in the colon [41], it seems possible that enhanced 5-HT levels could provide a primary damage response against a carcinogenic insult in the normal colon but is pro-tumorigenic after a cancer cell population has been established. In keeping with this idea, Leiter and colleagues reported that tumorigenic *Ctnnb1* mutations promoted 5-HT synthesis [8]. Similarly, our findings showed that chronic carcinogenic exposure also increased tumor burden when 5-HT is deficient, which decreased the number of lesions in colitis-driven colorectal carcinogenesis.

The rationale for 5-HT synthesis protecting the colon from DNA damage is at first counterintuitive. We believe that 5-HT synthesis might modulate pivotal genetic repair mechanisms against AOM-induced DNA adducts. The procarcinogen AOM requires complex metabolic transformations before hydroxylation releases its active form, methylazoxymethanol (MAM). Immediately, MAM yields a methyldiazonium ion that mainly methylates O^6 guanine, giving rise to O^6-methylguanine (O^6MeG) [42]. It seems that AlkB and Mgmt remove O^6MeG from colonocyte DNA. Whereas Mgmt shifts the O^6MeG methyl group onto its catalytic cleft, an event that promotes the Mgmt ubiquitin–proteasome-related decay, AlkB reaction with O^6MeG releases formaldehyde and the unmodified DNA base after a hydroxylated intermediate is generated [42]. Furthermore, Trp53 was reported to regulate Mgmt activity [43].

Our studies suggest 5-HT synthesis may lead to regulation of *Mgmt* expression in response to AOM exposure, with later downstream effects on the Atr repair activity. Kaina and colleagues suggested that changes in AOM-related genetic repair may also alter Atr-Chk1-p53 signaling and modify DNA damage levels in the CSC population [32]. It is possible that highly proliferative cells undergo replication stalling and DNA damage that leads to activation of Atr-Chk1-Trp53 arresting the cell cycle at the S/G2 phase [33,34]. Ropenga *et al.* reported that 5-HT release and neuroendocrine cell numbers were reduced following IR exposure [13]. Also, both 5-HT and 5-HTP have been shown to promote radioresistance in mammalian cells [13,14]. Myers and Cortez reported that IR-induced Chk1 activation relies on Atm/Atr signaling [33]. Löbrich and Jeggo suggested that Atm might activate Chk2 in cells with double-strand breaks that occurred during the G_1 cell-cycle phase, whereas Atr induces Chk1 and p53 activities when damage happens at the G_2 stage [33,34].

Our findings suggest that the absence of 5-HT synthesis promoted high levels of DNA damage in the stem cell-rich crypt base together with reduced CTNNB1 levels 72 h after the sixth carcinogen exposure. A week after this time point we found that CTNNB1 was reactivated. Clevers and colleagues have clearly shown that colonic cancer stem-like cells require activation of the Wnt signaling to survive and expand [44]. These findings suggest that promoting proliferation in crypt stem cells is more likely to lead to the development of CRC, since more somatic mutations will accumulate as increased levels of DNA damage take place in this progenitor population [32]. Hence, sporadic colon tumors develop following mutations in the crypt stem cell, as an initial unicryptal adenoma that expands into a tumor through crypt fission in a bottom-up pattern; although a top-down process could also promote the growth of these tumors afterwards [32].

We should also consider the dual-role of 5-HT synthesis on inflammatory reactions from different colorectal carcinogenic models. Our mouse model shows that 5-HT synthesis promotes the development of colitis-dependent colorectal tumors. However, in the colitis-independent tumor experimental model, we show that inhibiting 5-HT initially promotes high-macrophage numbers, and PTGS2 levels also increased later. Although these findings seem puzzling, they suggest that 5-HT synthesis could be a sensitive but complex reaction mechanism that determines tumor outcome according to the type of carcinogenic threat. A developing hypothesis suggests that 5-HT signaling may activate its receptor type 4 (5-HT4r) eliciting protective effects when intestines are challenged by experimental conditions close to normal, whereas pathological conditions could induce a serotonergic pro-inflammatory activity through 5-HT7r [20]. Given that the AOM/DSS protocol is a more aggressive colorectal tumor model than carcinogenic exposure to AOM alone [5], it is reasonable to suggest that 5-HT synthesis effects rely on the type and intensity of carcinogenic stimuli by which it has been challenged. Indeed, we have previously shown that carcinogenic exposure inhibiting

5-HT synthesis promoted PTGS2 expression and the development of preneoplastic lesions [16,17]. It further helps to clarify that 5-HT synthesis could determine the colonic microenvironment in which DNA-damaged crypt stem cells evolve into carcinogenic lesions [36].

Collectively, our results show that 5-HT synthesis protects the colorectal stem cell niche from DNA damage, thereby reducing early carcinogenic events, but later promotes the growth of established colorectal tumors. Moreover, our data suggest that the effects of 5-HT synthesis on DDR pathways may be dependent on the developmental stage of colorectal carcinogenesis. Our findings provide a new understanding of serotonergic activity in CRC onset and progression.

Acknowledgements

The authors disclose receipt of the following financial support for the development of this investigation: Sao Paulo Research Foundation (FAPESP; 2014/06428-5; 2015/01723-1; 2016/12619-3; 2017/01260-7). The funder had no role in the study design, data collection, analysis, decision to publish, or preparation of the manuscript.

Author contributions statement

VK contributed to the study concept and design. JYS, MB, ESS, SGB, SBM, NA, MOB, MCC, TV, BG, RBM, WASJ, MLB, CAL, FQC, GK, JAS, SAU contributed to the acquisition of data. VK contributed to the statistical analysis. All authors are contributed to the analysis and interpretation of data. VK contributed to the drafting the first version of the manuscript. All authors are contributed to the critical revision of the manuscript. VK contributed to the obtained funding. MB, ESS, RBM, WASJ, FQC, GK, JAS, SAU contributed to the technical and material support. VK contributed to the study supervision.

References

1. Sakita JY, Gasparotto B, Garcia SB, *et al.* A critical discussion on diet, genomic mutations and repair mechanisms in colon carcinogenesis. *Toxicol Lett* 2017; **265:** 106–116.
2. Siegel RL, Miller KD, Fedewa SA, *et al.* Colorectal cancer statistics, 2017. *CA Cancer J Clin* 2017; **67:** 177–193.
3. Arnold M, Sierra MS, Laversanne M, *et al.* Global patterns and trends in colorectal cancer incidence and mortality. *Gut* 2017; **66:** 683–691.
4. Triantafillidis JK, Nasioulas G, Kosmidis PA. Colorectal cancer and inflammatory bowel disease: epidemiology, risk factors, mechanisms of carcinogenesis and prevention strategies. *Anticancer Res* 2009; **29:** 2727–2737.
5. Neufert C, Becker C, Neurath MF. An inducible mouse model of colon carcinogenesis for the analysis of sporadic and inflammation-driven tumor progression. *Nat Protoc* 2007; **2:** 1998–2004.
6. Boman BM, Fields JZ, Cavanaugh KL, *et al.* How dysregulated colonic crypt dynamics cause stem cell overpopulation and initiate colon cancer. *Cancer Res* 2008; **68:** 3304–3313.
7. Basak O, Beumer J, Wiebrands K, *et al.* Induced quiescence of Lgr5+ stem cells in intestinal organoids enables differentiation of hormone-producing enteroendocrine cells. *Cell Stem Cell* 2017; **20:** 177–190.e174.
8. Wang Y, Giel-Moloney M, Rindi G, *et al.* Enteroendocrine precursors differentiate independently of Wnt and form serotonin expressing adenomas in response to active beta-catenin. *Proc Natl Acad Sci U S A* 2007; **104:** 11328–11333.
9. Sarrouilhe D, Clarhaut J, Defamie N, *et al.* Serotonin and cancer: what is the link? *Curr Mol Med* 2015; **15:** 62–77.
10. Tutton PJ, Barkla DH. The influence of serotonin on the mitotic rate in the colonic crypt epithelium and in colonic adenocarcinoma in rats. *Clin Exp Pharmacol Physiol* 1978; **5:** 91–94.
11. Nocito A, Dahm F, Jochum W, *et al.* Serotonin regulates macrophage-mediated angiogenesis in a mouse model of colon cancer allografts. *Cancer Res* 2008; **68:** 5152–5158.
12. Sui H, Xu H, Ji Q, *et al.* 5-Hydroxytryptamine receptor (5-HT1DR) promotes colorectal cancer metastasis by regulating Axin1/beta-catenin/MMP-7 signaling pathway. *Oncotarget* 2015; **6:** 25975–25987.
13. Ropenga A, Combes O, Chapel A, *et al.* Persistence of altered 5-hydroxytryptamine turnover following hemibody X-irradiation in the rat distal colon. *Int J Radiat Biol* 2004; **80:** 399–411.
14. Nakayama T, Nakamura W. Radioprotective effect of 5-hydroxytryptamine and 5-hydroxytryptophan on mammalian cells irradiated in vitro. *Int J Radiat Biol Relat Stud Phys Chem Med* 1978; **34:** 81–09.
15. Chubak J, Boudreau DM, Rulyak SJ, *et al.* Colorectal cancer risk in relation to antidepressant medication use. *Int J Cancer* 2011; **128:** 227–232.
16. Kannen V, Marini T, Turatti A, *et al.* Fluoxetine induces preventive and complex effects against colon cancer development in epithelial and stromal areas in rats. *Toxicol Lett* 2011; **204:** 134–140.
17. Kannen V, Zanette DL, Fernandes CR, *et al.* High-fat diet causes an imbalance in the colonic serotonergic system promoting adipose tissue enlargement and dysplasia in rats. *Toxicol Lett* 2012; **213:** 135–141.
18. Kannen V, Fernandes CR, Stopper H, *et al.* Colon preneoplasia after carcinogen exposure is enhanced and colonic serotonergic system is suppressed by food deprivation. *Toxicology* 2013; **312:** 123–131.
19. Walther DJ, Peter JU, Bashammakh S, *et al.* Synthesis of serotonin by a second tryptophan hydroxylase isoform. *Science* 2003; **299:** 76.
20. Spohn SN, Mawe GM. Non-conventional features of peripheral serotonin signalling - the gut and beyond. *Nat Rev Gastroenterol Hepatol* 2017; **14:** 412–420.
21. Jess T, Rungoe C, Peyrin-Biroulet L. Risk of colorectal cancer in patients with ulcerative colitis: a meta-analysis of population-based cohort studies. *Clin Gastroenterol Hepatol* 2012; **10:** 639–645.
22. Kopf M, Baumann H, Freer G, *et al.* Impaired immune and acute-phase responses in interleukin-6-deficient mice. *Nature* 1994; **368:** 339–342.
23. Yadav VK, Ryu JH, Suda N, *et al.* Lrp5 controls bone formation by inhibiting serotonin synthesis in the duodenum. *Cell* 2008; **135:** 825–837.
24. Feng Y, Sentani K, Wiese A, *et al.* Sox9 induction, ectopic Paneth cells, and mitotic spindle axis defects in mouse colon adenomatous epithelium arising from conditional biallelic Apc inactivation. *Am J Pathol* 2013; **183:** 493–503.
25. Kannen V, Hintzsche H, Zanette DL, *et al.* Antiproliferative effects of fluoxetine on colon cancer cells and in a colonic carcinogen mouse model. *PLoS One* 2012; **7:** e50043.
26. Zhu JX, Zhu XY, Owyang C, *et al.* Intestinal serotonin acts as a paracrine substance to mediate vagal signal transmission evoked by luminal factors in the rat. *J Physiol* 2001; **530:** 431–442.

27. Julio-Pieper M, O'Mahony CM, Clarke G, *et al.* Chronic stress-induced alterations in mouse colonic 5-HT and defecation responses are strain dependent. *Stress* 2012; **15:** 218–226.
28. Fiala ES. Investigations into the metabolism and mode of action of the colon carcinogens 1,2-dimethylhydrazine and azoxymethane. *Cancer* 1977; **40:** 2436–2445.
29. Glass G, Papin JA, Mandell JW. SIMPLE: a sequential immunoperoxidase labeling and erasing method. *J Histochem Cytochem* 2009; **57:** 899–905.
30. Yamada H, Vijayachandra K, Penner C, *et al.* Increased sensitivity of transforming growth factor (TGF) beta 1 null cells to alkylating agents reveals a novel link between TGFbeta signaling and O(6)-methylguanine methyltransferase promoter hypermethylation. *J Biol Chem* 2001; **276:** 19052–19058.
31. Margolis KG, Stevanovic K, Li Z, *et al.* Pharmacological reduction of mucosal but not neuronal serotonin opposes inflammation in mouse intestine. *Gut* 2014; **63:** 928–937.
32. Fahrer J, Frisch J, Nagel G, *et al.* DNA repair by MGMT, but not AAG, causes a threshold in alkylation-induced colorectal carcinogenesis. *Carcinogenesis* 2015; **36:** 1235–1244.
33. Myers JS, Cortez D. Rapid activation of ATR by ionizing radiation requires ATM and Mre11. *J Biol Chem* 2006; **281:** 9346–9350.
34. Lobrich M, Jeggo PA. The impact of a negligent G2/M checkpoint on genomic instability and cancer induction. *Nat Rev Cancer* 2007; **7:** 861–869.
35. Tao S, Tang D, Morita Y, *et al.* Wnt activity and basal niche position sensitize intestinal stem and progenitor cells to DNA damage. *EMBO J* 2015; **34:** 624–640.
36. Garcia SB, Stopper H, Kannen V. The contribution of neuronal-glial-endothelial–epithelial interactions to colon carcinogenesis. *Cell Mol Life Sci* 2014; **71:** 3191–3197.
37. Mowat AM, Agace WW. Regional specialization within the intestinal immune system. *Nat Rev Immunol* 2014; **14:** 667–685.
38. Wang D, Dubois RN. The role of COX-2 in intestinal inflammation and colorectal cancer. *Oncogene* 2010; **29:** 781–788.
39. Grivennikov S, Karin E, Terzic J, *et al.* IL-6 and Stat3 are required for survival of intestinal epithelial cells and development of colitis-associated cancer. *Cancer Cell* 2009; **15:** 103–113.
40. Lee HK, Eom CS, Kwon YM, *et al.* Meta-analysis: selective serotonin reuptake inhibitors and colon cancer. *Eur J Gastroenterol Hepatol* 2012; **24:** 1153–1157.
41. Gershon MD. Serotonin is a sword and a shield of the bowel: serotonin plays offense and defense. *Trans Am Clin Climatol Assoc* 2012; **123:** 268–280.
42. Fahrer J, Kaina B. O6-methylguanine-DNA methyltransferase in the defense against N-nitroso compounds and colorectal cancer. *Carcinogenesis* 2013; **34:** 2435–2442.
43. Grombacher T, Eichhorn U, Kaina B. p53 is involved in regulation of the DNA repair gene O6-methylguanine-DNA methyltransferase (MGMT) by DNA damaging agents. *Oncogene* 1998; **17:** 845–851.
44. Sato T, Stange DE, Ferrante M, *et al.* Long-term expansion of epithelial organoids from human colon, adenoma, adenocarcinoma, and Barrett's epithelium. *Gastroenterology* 2011; **141:** 1762–1772.

SUPPLEMENTARY MATERIAL ONLINE

Supplementary materials and methods

Supplementary figures legends

Figure S1. Development of a double-knockout mouse model

Figure S2. Development of transgenic mouse models

Figure S3. Allograft and colitis-related colorectal tumors develop in a 5-HT-dependent manner

Figure S4. AOM alters serotonergic elements

Figure S5. 5-HT deficiency blocks the development of sporadic colorectal tumors (Part I)

Figure S6. Effects of 5-HT deficiency on tumor proliferation

Figure S7. 5-HT deficiency blocks the development of sporadic colorectal tumors (Part II)

Figure S8. Increased development of colorectal preneoplastic lesions with 5-HT deficiency

Figure S9. Genetically deleting *Tph1* inhibits *Atr* expression in the colon of irradiated mice

Figure S10. 5-HT treatment does not protect from DNA damage

Figure S11. 5-HT deficiency facilitates DNA damage following protracted AOM exposure

Figure S12. *Mgmt* gene expression at different stages of colorectal tumorigenesis

Figure S13. 5-HT deficiency alters expression of CTNNB1-related genes during the early development of colorectal tumorigenesis

Table S1. qPCR array analysis in AOM-exposed mice

Table S2. qPCR array analysis of colons from radiation-exposed mice

Table S3. TaqMan probes used

Table S4. Antibodies used

Table S5. Primers used

Trends in Endocrinology & Metabolism

CellPress REVIEWS

Review

The Dual Role of Serotonin in Colorectal Cancer

Vinicius Kannen,[1,2,*] Michael Bader,[3,4,5] Juliana Y. Sakita,[2] Sergio A. Uyemura,[6] and Jeremy A. Squire[2,7]

Serotonin (5-HT) has complex effects on the central nervous system (CNS), neuroendocrine mechanisms, immunological reactions, intestinal microbiome, and cancer. It has been associated with more severe signs and symptoms of colitis, as well as promoting colorectal cancer (CRC) cells toward expansion. However, recent findings revealed that impairments in 5-HT synthesis lead to high levels of DNA damage in colonocytes, which is linked with inflammatory reactions promoting the development of CRC. Here, we review the diverse roles of 5-HT in intestinal homeostasis and in CRC and discuss how improved understanding of the modulation of the 5-HT pathway could be helpful for the design of novel anticancer therapies.

Highlights

Both brain and peripheral cells can synthesize 5-HT from the essential amino acid tryptophan, although intestinal enteroendocrine cells produce the most substantial amount of this hormone in the human body.

The serotonergic system encompasses a range of elements required for its synthesis, storage, release, transport, signaling, and degradation, from which it modulates essential functions in keeping with the body homeostasis.

Genetic, behavioral, or environmental factors may deregulate the serotonergic system functions, promoting a significant number of pathological conditions. This has been expanded to include different types of cancer.

A deregulated serotonergic system may be related to the development of colorectal cancer, because it can either promote or inhibit tumorigenesis in the colon through a combined modulation of DNA repair mechanisms and immune response.

Multiple Functions of Serotonin

5-HT is one of the most potent neuronal, peripheral, and gastrointestinal signaling molecules. It acts as a paracrine, endocrine, or exocrine messenger for a variety of cell -types, including the enteroendocrine cell (EC) population [1–12]. Erspamer and Asero showed that enteramine and 5-HT had the same chemical structure, ending the initial controversy over the discovery of this molecule [4,13]. Decades later, Tutton and Barkla reported that 5-HT promotes proliferation in CRC cells [14]. Recent findings confirmed that the 5-HT synthesis pathway not only promotes colitis and cell proliferation in colitis-related tumors, but also protects the colon from DNA damage and colitis-unrelated tumors [4,15]. CRC is a malignant disease in which colonocytes acquire aberrant functions related to their physiological features, such as abnormal growth and ability to invade and metastasize [16]. CRC is the third most frequent cancer and the second leading cause of cancer-related deaths in Western nations, showing increasing incidence rates each year [17].

The intestines are the primary source of 5-HT synthesis in the body (see Figure IA, in Box 1) [1–12]. This monoamine has complex and diverse effects on the central and peripheral nervous systems, neuroendocrine regulation, clotting-related mechanisms, immunological responses, the intestinal microbiome, epigenetics, and cancer [2,18–24]. An example of how 5-HT signaling can impact the immune system in completely different ways is illustrated by the varying effects of its receptors (HTr). Signaling from HTr4 decreases intestinal inflammation, whereas activating HTr7 promotes inflammation [25–27].

Recent findings have also shown that 5-HT synthesis levels could both alter or be altered by the intestinal microbiota [2,21]. This delicate balance between the microbiome and the host response is thought to have a pivotal role in modulating the risk of colitis and CRC [28]. We discuss these exciting discoveries in the context of the role of 5-HT in DNA damage- and immune response-related events throughout CRC development. We also consider how understanding the complex 5-HT activity promotes the development of novel therapeutic strategies in CRC.

Intestinal Serotonin Activity in Body Homeostasis

Serotonergic Signaling Defines Body Homeostasis

As a neurohormone with a range of receptors that differentially impacts many physiological events, 5-HT is important for the physiological functioning of the human body [29]. For example,

[1]Lunenfeld-Tanenbaum Research Institute, Mount Sinai Hospital, Toronto, Canada
[2]Department of Genetics, University of Sao Paulo, Ribeirao Preto, Brazil
[3]Max-Delbrück-Center for Molecular Medicine, Berlin, Germany
[4]Charité, University Medicine Berlin, Germany
[5]Institute for Biology, University of Lübeck, Lübeck, Germany
[6]Department of Toxicology, Bromatology, and Clinical Analysis, University of Sao Paulo, Ribeirao Preto, Brazil
[7]Department of Pathology and Molecular Medicine, Queen's University, Kingston, Canada

*Correspondence: vkannen@lunenfeld.ca (V. Kannen).

intestinal serotonergic activity modulates the homeostasis of the CNS through a microbiome–gut–brain axis [30]. Peripheral 5-HT has also been shown to inhibit the prothermogenic effects of noradrenaline (NA) and β-adrenergic receptors (βAR) [22]. Oh *et al.* used adipocyte-specific deletion of Tph1 via Cre-Lox recombination technology to reveal that serotonergic signaling from adipocytes can inhibit thermogenesis via blockage of βAR signaling in an HTr3-dependent manner [31], increasing the weight gain of mice [22,31]. Specifically, intestinal 5-HT synthesis might affect the risk of diabetes because it impacts glycemic control through the synthesis of glucagon-like peptide-1 (GLP-1), somatostatin, glucose-dependent insulinotropic polypeptide (GIP), and cholecystokinin (CCK) in pancreatic β cells [32]. In addition, this monoamine modulates insulin release from pancreatic β cells through HTr3 that, when impaired, has a pivotal role in diet-induced insulin resistance and type 2 diabetes mellitus [33]. Walther and colleagues revealed that a 5-HT-dependent mechanism referred to as serotonylation controls the activity of the small GTPases Rab3a and Rab27a and, thus, insulin secretion in pancreatic β cells (see Figure I in Box 2). 5-HT covalently binds to these GTPases, enhancing their constitutive activation, from which insulin release is promoted [34].

Intestinal 5-HT Synthesis in Brief

Two specific enzymes are responsible for maintaining the central and peripheral 5-HT synthesis, independently (see Figure IA in Box 1). In the intestines, uptake of tryptophan (TRP) is carried out by enteroendocrine units using an amino acid transport system, thereby activating TPH1 and initiating 5-HT synthesis (Figure 1A–C) [1–11]. Intestinal 5-HT biosynthesis further requires intense crosstalk between ECs and microbiota [2,21]. A healthy intestinal flora does not affect the number of ECs, but its presence provides these cells with high levels of short-chain fatty acids, which, in turn, promote enhanced TPH1 gene expression and 5-HT synthesis (Box 1) [2,21,35–39]. The

Box 1. Serotonin Synthesis and Signaling

5-HT synthesis is initiated by a biopterin-dependent monooxygenation of TRP that is catalyzed by tryptophan hydroxylase (TPH). This enzyme uses TRP, O_2, and tetrahydrobiopterin as substrates releasing 4a-hydroxytetrahydrobiopterin and 5-HTP. In the following reaction mediated by aromatic L-amino acid decarboxylase (AADC), 5-HT is synthesized from 5-HTP. Vesicular monoamine transporter 1 (VMAT1) transfers recently synthesized 5-HT from the cytosol to storage vesicles before its release. Following its release and proper signaling, 5-HT undergoes reuptake by SERT, from which monoamine oxidase A (MAOA) may degrade 5-HT into 5-hydroxyindoleacetic acid (5-HIAA) through oxidative deamination [1,4,11].

The activation of TPH requires calcium–calmodulin-dependent protein kinase (CAMK) and the 14-3-3 proteins. The N terminus of TPH acts as a regulatory domain for the catalytic C terminus. The phosphorylation of the N terminus by CAMK enables 14-3-3 protein to bind to the complex. Binding of the 14-3-3 acidic C terminus to basic residues of the TPH regulatory region leads to a conformational change activating this enzyme [6,7].

Two distinct TPH genes have been reported, located on chromosomes 11 and 12, and encoding TPH1 and TPH2, respectively (Figure IA). These enzymes have ~71% homology between them. Neurons express TPH2, while peripheral cells use TPH1 to synthesize 5-HT [1]. In the intestines, ECs have been suggested to synthesize most of the total 5-HT body content through TPH1 [12].

Specific spore-forming bacteria have also been shown to produce deoxycholate and α-tocopherol, which induce 5-HT synthesis through TPH1 activity in EC cells [2]. *Lactobacillus johnsonii* was found to promote intestinal-5-HT synthesis via H_2O_2, which, in turn, inhibits IDO, thereby reducing kynurenine synthesis [35]. Furthermore, susceptibility to intestinal infection by *Salmonella typhimurium* increased in butyrate-inducible zinc finger transcription factor-KO mice, which exhibit reduced butyrate-induced expression of *TPH1* and 5-HT synthesis [36]. Moreover, intestinal dysbiosis alters the 5-HT system by increasing the expression of SERT [37]. Although intestinal inflammation decreases SERT expression, inhibiting SERT activity promotes intestinal dysbiosis and impairs dendritic cell-induced antigen-related activation of T cells [38,39].

In addition, 5-HT has many receptors (HTr) to signal through (Figure IB). Thus, 5-HT binding to its receptors promotes a diverse range of effects in the human body, such as circadian rhythm, thermoregulation, food intake, nociception, locomotion, sexual behavior, gastrointestinal motility, blood coagulation, and cardiovascular homeostasis. Aside from HTr3 being a ligand-gated cation channel receptor, HTrs comprise six families of G-protein-coupled receptors [4,8,9].

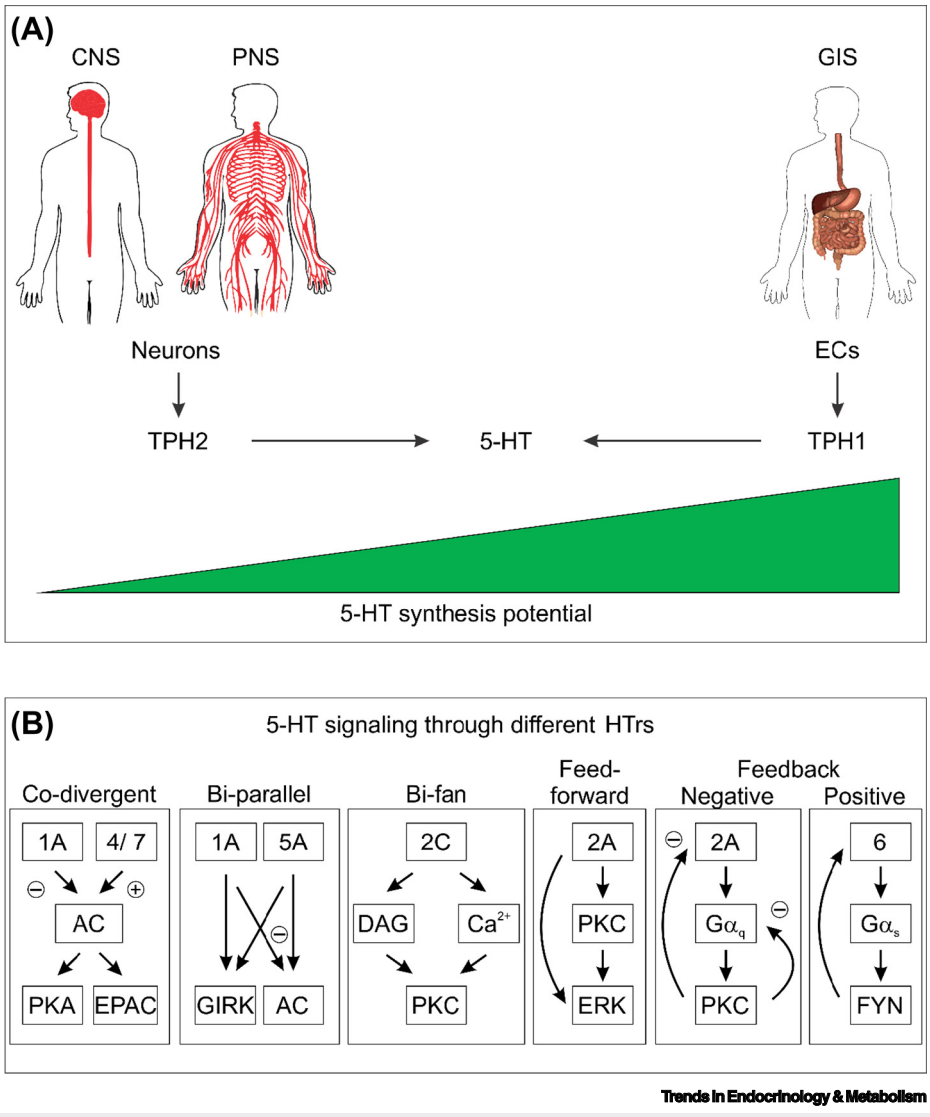

Figure I. Serotonin (5-HT) Synthesis and Signaling. (A) Neurons residing in the central (CNS) and peripheral nervous systems (PNS) synthesize 5-HT through tryptophan hydrolase 2 (TPH2), whereas enteroendocrine cells (ECs) in the gastrointestinal system (GIS) use TPH1. Almost 95% of the total 5-HT body content is released by intestinal ECs. (B) The complexity of serotonergic signaling is illustrated by the activity of several 5-HT receptor (HTr) units that convey multiple inputs into convergent or divergent stimulating effects, from which a multitude of outputs may arise and spread through several molecular pathways, promoting a range of effects. Input stimulation is positive unless shown by signals. For instance, Bi-fan 5-HT signaling converges inputs from HTr2C into protein kinase C (PKC) through different mediators such as diacylglycerol (DAG) and Ca^{2+}. Abbreviations: AC, adenylyl cyclase; DAG, diacylglycerol; EPAC, exchange factor directly activated by cAMP; ERK, extracellular-signal-regulated kinase; FYN, member of the protein-tyrosine kinase oncogene family; GIRK, G protein-coupled inwardly-rectifying potassium channel; PKA, protein kinase A; PKC, protein kinase C.

immune system then interacts with EC cells, intestinal bacteria, and enteric neurons, from which several intestinal functions are altered [21,40].

ECs arise from differentiating stem cells in the crypt bottom. This process requires precise modulation of the activation of the WNT and NOTCH signaling pathways that further regulate the

Box 2. Serotonylation

The 5-HT activation of intracellular processes by creating long-lasting covalent bonds to proteins has been named 'serotonylation'. 5-HT is incorporated into acceptor proteins in a transglutaminase (TGM)-dependent manner via glutamyl-amide bonds. During thrombus formation, the classical example of serotonylation in the body, the latter occurs in both extracellular and intracellular compartments. Extracellularly, fibrinogen and thrombospondin bind to serotonylated procoagulant proteins, stabilizing essential protein complexes [14]. In parallel, 5-HT binds to HTr2A, activating the phosphatidylinositol pathway in a $G_{\alpha q}$-protein-dependent manner that increases cytoplasmic Ca^{2+} levels and promotes TGM activity. Following 5-HT transportation into the cytoplasm, TGM crosslinks it to either RhoA or Rab4, which constitutively activate and induce α-granule exocytosis [13].

Recent findings revealed that serotonylation can also occur at the glutamine 5 residue in the N-terminal tail of H3 (H3Q5), which is the best-studied chromatin-regulatory region (Figure I) [7]. However, the addition of three methyl groups to the lysine 4 residue of histone H3 (H3K4) needs to occur before TGM2 serotonylates H3Q5. H3K4me3Q5ser appears to directly impact gene expression and chromatin remodeling since it supports the function of transcription factor II D (TFIID). Indeed, the RNA polymerase II preinitiation complex requires the binding of TFIID to the TATA box, which is one of the critical steps promoting the formation of the RNA polymerase II holoenzyme [7].

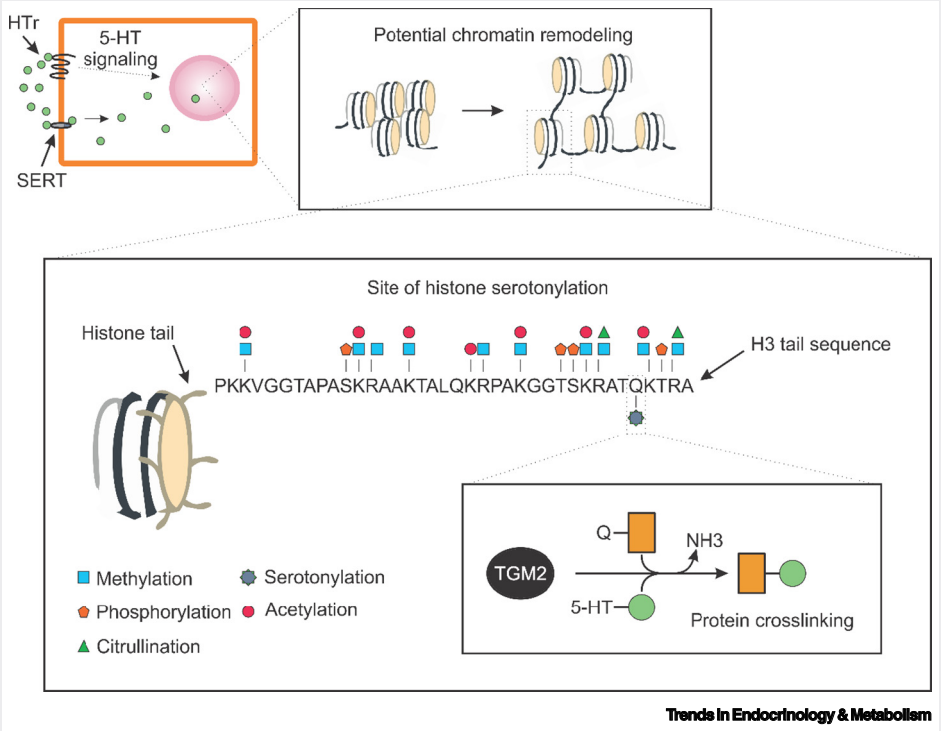

Figure I. The Epigenetic Effects of Serotonin (5-HT). 5-HT exerts epigenetic effects by 5-HT receptor 2A (HTr2A) signaling and by the transglutaminase 2 (TGM2)-mediated serotonylation of trimethylated lysine 4 residue of histone H3 (H3K4me3) at Q5, leading to the formation of H3K4me3Q5ser. While a transcriptionally active state of chromatin requires H3K4me3, H3K4me3Q5ser promotes gene expression even further.

rigorous homeostatic balance between secretory and absorptive cellular populations within the intestinal crypt (Figure 1B) [41]. Moreover, an orchestrated action of serotonergic elements controls intestinal motility (see Figure I in Box 3) [10–12,40,42–48].

5-HT Activity Modulates Intestinal Homeostasis

5-HT activity is a crucial signaling factor for essential intestinal functions, such as proliferation in intestinal crypts. Indeed, enteric neurons control epithelial cellular proliferation through 5-HT signaling [45]. Recent experiments based on *Tph1* and *Tph2*-knockout (KO) mouse models

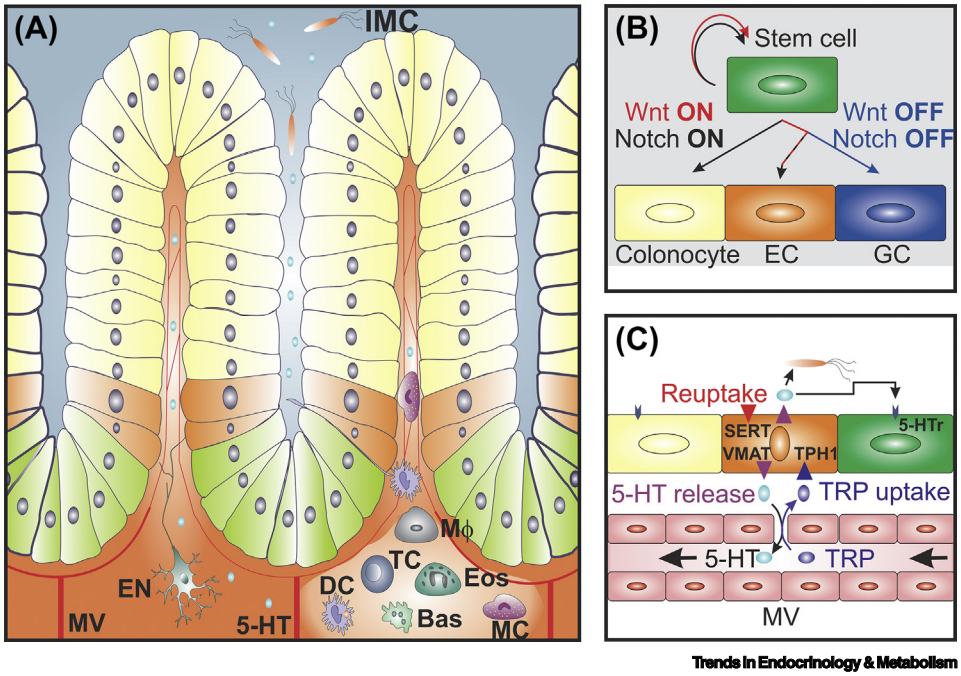

Figure 1. Serotonergic Activity in the Intestine. (A) Crypts have close contact with the intestinal microbiota (IMC), but are attached to the stromal cell layer to mediate interactions. Colonic stem cells (green) differentiate into enteroendocrine cells (EC; orange), goblet cells (GC), and colonocytes (yellow). These cells represent secretory (secret mucus and hormones) and absorptive cell populations (take up water and electrolytes), respectively. (B) Activation of WNT and NOTCH signaling pathways induces stem cells to differentiate into colonocytes. Blocking these signaling pathways increases GC numbers (blue), while their intermittent activation enhances the EC population. (C) A microvessel (MV) delivers tryptophan (TRP) to EC cells, which metabolize it into serotonin (5-HT) through tryptophan hydrolase 1 (TPH1). In addition, TRP can be directly delivered from the intestinal lumen to EC cells. The vesicular monoamine transporter (VMAT) stocks 5-HT into intracellular vesicles before its activation and release. 5-HT may bind to its receptors (HTr) promoting a significant number of events through complex molecular mechanisms. After release, 5-HT can also be taken up by the 5-HT transporter (SERT) for recycling or degradation. Abbreviations: Bas, basophil; DC, dendritic cells; EN, enteric neuron; Eos, eosinophil; MΦ, macrophage; MC, mast cell; TC, T cell.

revealed that serotonergic neurons synthesize 5-HT to activate HTr2A in cholinergic neurons. These neuronal units then activate muscarinic neurons, which stimulate intestinal epithelial cells to proliferate [40].

5-HT synthesis from both EC units and neurons appears to alter intestinal inflammation differentially. In *Tph1*-KO mice, epithelial 5-HT synthesis decreased chemically induced intestinal inflammation [49,50]. However, this inflammatory response increased in *Tph2*-KO mice [51,52]. It has been further suggested that 5-HT released by enteric neurons activates neurogenesis through HTr4, which may lead to control of inflammatory responses [51,53].

Since HTr4 signaling reduces the intestinal inflammatory response [25,40,52], pharmacological activation of HTr4 has been shown to reduce the development of colitis [25]. By contrast, the breakdown of intestinal homeostasis induces ECs to release 5-HT, which, in turn, stimulates HTr7 in dendritic cells, mobilizing immunological reactions toward intestinal inflammation [26,27]. Interestingly, intestinal inflammation is increased in *Sert*-KO mice, in which 5-HT is not able to undergo reuptake and degradation [54]. Thus, mucosal 5-HT initiates the inflammatory reaction, whereas enteric neuronal 5-HT provides the means for cellular survival by stimulating

epithelial cell proliferation, neuronal protection, and control over proinflammatory effectors [40,49,50,52,55].

5-HT has been shown to activate dendritic cells promoting their interleukin (IL)-2 production during intestinal inflammation. This 5-HT signaling further induces activation of nuclear factor κ-light-chain-enhancer of activated B cells (NF-κB) in dendritic cells, leading them to prime $CD4^+$ T cells, from which IL-17 and interferon (IFN)-γ are released [55]. Moreover, an immunoendocrine axis appears to impact intestinal adaptative immune reactions, where secretory products of $CD4^+$ T cells interact with ECs to enhance local 5-HT production via T helper (Th) 2-based mechanisms [56]. Using different mouse models with activated or deactivated Th2 responses, researchers observed that inhibiting this immunological reaction increased EC numbers and 5-HT levels [57].

EC cell-synthesized 5-HT also induces the release of proinflammatory cytokines by macrophages in an NF-κB-dependent manner [49]. Moreover, platelet-derived 5-HT synthesis contributes to the regulation of innate immunity since it determines neutrophil recruitment to acute inflammation sites [58]. These various regulatory mechanisms collectively illustrate some of the diverse homeostatic effects of 5-HT (Figure 2).

Serotonin Effects in CRC

The Multistep Development of CRC

The steady-state self-renewal of the intestinal stem cell niche in the epithelium requires precise molecular regulation of proliferation to avoid malignant transformation. In this process, colonic stem cells acquire DNA mutations, and the selective evolution of mutant clones can lead their progeny toward invasion and metastatic CRC. Mutations in only three driver genes have been proposed as sufficient to transform a normal cell into a metastatic cancer progenitor, because the acquired somatic mutations appear to be selected to bypass the molecular constraints of cell pluripotency and proliferation [59].

Box 3. 5-HT Activity in Intestinal Motility

To illustrate how an orchestrated action of serotonergic elements impacts intestinal motility, we define the motor patterns driving intestinal motility (Figure I). Peristalsis is an intestinal motor pattern propelling the bolus in either cranial (retrograde peristalsis) or caudal directions (antegrade peristalsis; Figure IA–C). However, the peristaltic reflex requires that the bolus stretches the intestinal wall, activating afferent enteric neurons that relax the intestinal musculature ahead (Figure ID). The intestinal content further activates efferent enteric neurons to induce muscular contractions at its rear end, propelling it in a caudal direction [10–12,42–44,46–48]. 5-HT has been known to have an active role in peristalsis for more than 50 years [30]. Regular bowel movements elicit mechanical forces that activate adenosine receptors, which in turn induce protein kinase A (PKA), phosphoinositide 3-kinase (PI3K), and mitogen-activated protein kinase (MAPK) signaling pathways promoting the activation of TPH1 and VMAT1 and the release of 5-HT [10]. This released 5-HT appears to activate HTr3 in mucosal enteric neurons, facilitating peristalsis [31]. Moreover, mechanical stimulation by the intestinal content leads to 5-HT release from ECs, from which 5-HT induces, together with the electrical enteric neuronal signaling, the peristaltic reflex (Figure ID–F) [11].

The reuptake of 5-HT by SERT has a significant role in intestinal motility. Although other transporters show some affinity for 5-HT, genetically deleting SERT negatively alters intestinal functions. Ablation of *Sert* expression promoted irregular intestinal motility, with either diarrhea or constipation occurring within a given timeframe [46]. Interestingly, hyperactivation of *Sert* through a Ala56 mutation decreased intestinal motility, because mice endured a significant neuronal hypoplasia [47]. A similar neuronal hypoplasia associated with changes in intestinal motility was also observed in mice bearing a genetic deletion of *Tph2* [48]. Similarly to what has been reported in *Sert*-KO mice, pharmacologically inhibiting this transporter with fluoxetine promoted intestinal hyperinnervation that led to complex but abnormal patterns of intestinal motility. However, a chemical sympathectomy with 6-hydroxydopamine normalized these abnormal motility patterns in both Sert-KO and fluoxetine-exposed animals, revealing a close relationship between central sympathetic control and 5-HT reuptake in intestinal motility [47]. Collectively, these observations provide an overview of the complex effects of serotonergic activity in intestinal motility.

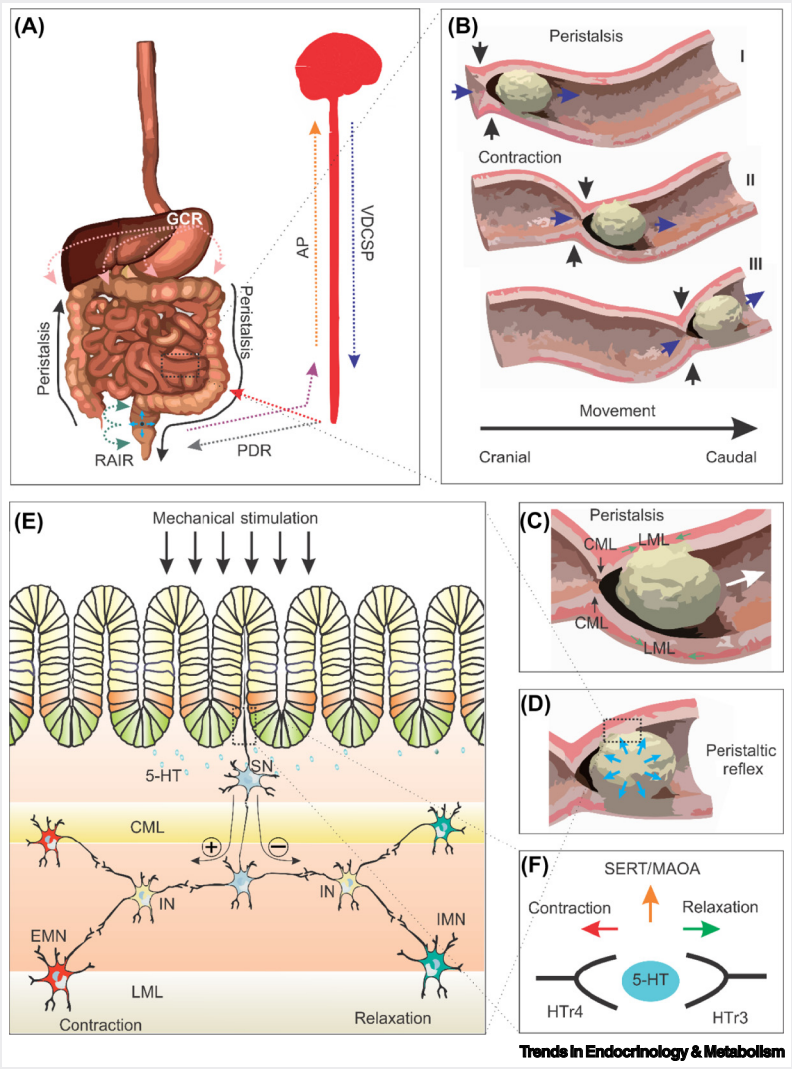

Figure I. Summarizing Gastrointestinal Motility. (A) Stomach distention, or even thoughts and food smells, may activate the gastrocolic reflex (GCR), which also promotes peristalsis. Rectal distention (light-blue arrows) promotes the rectoanal inhibitory reflex (RAIR) and a transient involuntary relaxation of the internal anal sphincter. This rectal distention also induces the parasympathetic defecation reflex (PDR; gray and red sectioned lines). In addition, an action potential (AP; purple and orange sectioned lines) migrates to the defecation reflex center in the spinal cord, which stimulates colorectal contraction while relaxing the internal anal sphincter. These APs reach the brain through ascending nerve tracts, from which voluntary defecation control signaling potential (VDCSP; dark-blue sectioned line) is released and controls the external anal sphincter. Further details are given about peristalsis in the next figure (magnification of a black-sectioned line square). (B) Although digestion requires a combined action of the enteric (ENS) and the central nervous systems (CNS), the ENS controls peristalsis aside from the CNS. The contraction effects (black arrows) promoting bolus displacement (blue arrows) throughout the intestines are shown in multiple figures. (C) These contractions occur in a coordinated manner between different intestinal muscle layers, such as circular (CML; black arrows) and longitudinal muscle layers (LML; blue arrows). (D–F) As contractions of the intestinal wall move the bolus forward, it also reacts from pressure against the epithelial cellular layer (D). EC units (orange cells) react to this mechanical stimulation, releasing serotonin (5-HT) into the extracellular space (E). Binding of 5-HT to 5-HT receptor 4 or 3 (HTr4 or HTr3), expressed by sensory neurons (SN; E), promotes contraction or relaxation of the intestinal wall, respectively (F). Following this stimulation phase, 5-HT undergoes reuptake and degradation by the 5-HT transporter (SERT) and monoamine oxidase A (MAO-A), respectively (F). These SN units interact with interneurons (IN), from which either stimulation or inhibition signaling is released to excitatory (EMN) or inhibitory myenteric neurons (IMN). Contraction or relaxation of CML or LML can be precisely coordinated by the ENS working through its neuronal network (E). Abbreviation: MAOA, monoamine oxidase A.

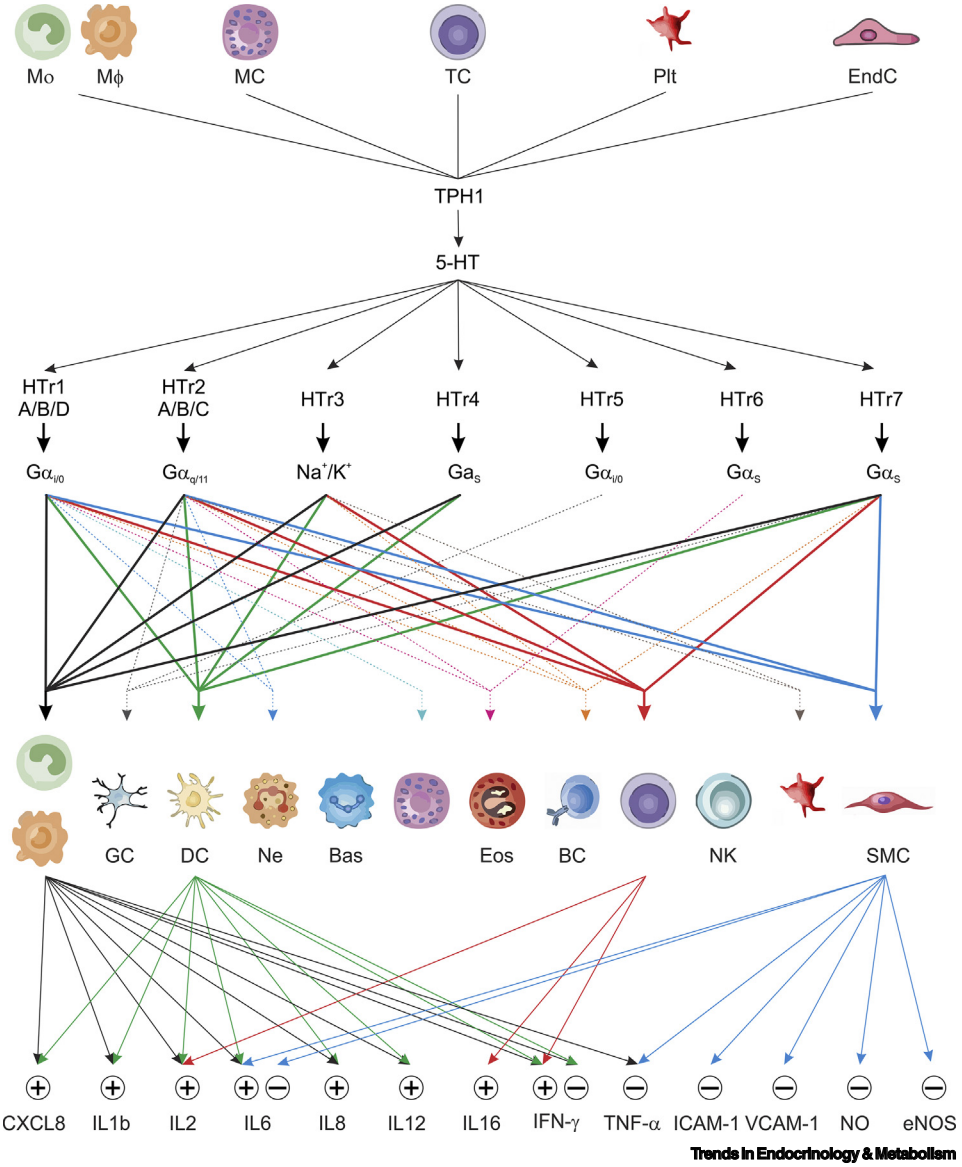

Figure 2. The Serotonergic System Impacts the Immune Response. Expression of the serotonin (5-HT) rate-limiting enzyme, tryptophan hydrolase 1 (TPH1), is shown by connecting lines in different immune cells (EndC, endothelial cell; MΦ, macrophage; MC, mast cell; MO, monocyte; Plt, platelet; TC, T cell). Following 5-HT binding, a given 5-HT receptor (HTr) may couple to specific G-protein isoforms, ion channels, or soluble second messengers according to its specific function and family. Aside from basophil (Bas) and natural killer (NK) cells, most immune cells express different HTrs. Black, green, red, and light-blue lines with arrows show immune cells that have well-defined expression of immunological factor after HTrs are stimulated in them. For instance, MΦs can express almost all serotonergic elements. Activation of TPH1, HTr2, and HTr3 appears to inhibit tumor necrosis factor α (TNF-α) synthesis and interferon γ (IFN-γ)-related effects. In dendritic cells (DC), activation of HTr3, HTr4, and HTr7 promotes the production of interleukin (IL) 1β, IL-6, and IL-8. MCs not only synthesize 5-HT through TPH1, but also alter their adhesion and migration functions through HTr1A-mediated serotonergic signaling. Sectioned lines with arrows illustrate immune cells that express HTrs but the effects of such signaling remain unknown. Abbreviations: BC, B cell; CXCL8, C-X-C motif chemokine ligand 8; eNOS, endothelial NO synthase; Eos, eosinophil; GC, glial cell; ICAM-1, intercellular adhesion molecule 1; Ne, neutrophil; NO, nitric oxide; SMC, smooth muscle cell; VCAM-1, vascular cell adhesion molecule 1.

Somatic mutations further enable growth factor receptors and signaling pathways to be activated through both direct and indirect mechanisms. This type of mutation is probably one of the first events to promote increased replicative potential, self-sufficiency for growth signals, and insensitivity to antigrowth signals in cancer cells [60]. Indeed, a carcinogenically initiated cell must follow the Darwinian evolutionary competition that enables further mutations to be accumulated and fixed, driving the most suitable clones towards malignant transformation [59,60]. Given that cancer-initiated cells initially express a multitude of antigens, immune cells are attracted to survey and kill them. However, this immunoediting process enables cancer cells to shut down immunological activities that would otherwise restrain tumor development [59–62].

5-HT Activity Inhibits CRC Initiation and Promotion Steps

The neuroendocrine system is one of many physiological mechanisms in the body that signal immunological reactions [63]. For instance, pancreatic neuroendocrine neoplasms have a low tumor mutation load compared with other types of gastrointestinal cancer [64], although these malignant lesions have a significant number of infiltrating immune cells, and a deregulated immune checkpoint system that alters the cytokine and chemokine milieu, and immunomodulatory factors [65]. Moreover, patients with midgut carcinoids showed high numbers of circulating regulatory T cells (Tregs) but a decreased Th1 immunological response and fewer proliferating T lymphocytes [66]. Olszewski and colleagues indicated that patients with colorectal neuroendocrine tumors do not benefit from prevention and treatment strategies that are efficient for most CRC cases [67].

Increased 5-HT levels are also associated with the severity of symptoms and clinical effects of colitis in patients [68], as well as promoting the development of colorectal tumors in mice [15]. However, 5-HT has been suggested to be a key element for intestinal protection, which might explain why selective 5-HT reuptake inhibitors administered to patients reduced their risk of CRC [69]. Thus, there has been some support for the idea that 5-HT is involved in intestinal diseases, such as CRC; however, further consideration of how 5-HT is involved in the complex intestinal protective mechanism suggests that this monoamine promotes malignancies only after its activity has been impaired [15,20,70–74].

There is increasing evidence that 5-HT activity may protect the colon against the development of early CRC-related events. Arisha and colleagues showed that, when fenitrothion treatment induced an increase in free radical levels, DNA damage, and apoptosis, this was associated with significantly decreased 5-HT levels [75]. Lubbe *et al.* reported that 5-HT reduced blood flow-constricting arterioles in CRC [76]. Inhibition of 5-HT reuptake by fluoxetine not only increased 5-HT levels in the colon, but also decreased the development of dysplastic lesions within a preneoplastic microenvironment in the colon [72,73]. Recently, it was shown that *Tph1*-deficient mice developed reduced numbers of colitis-promoted colorectal tumors, while at the same time this 5-HT deficiency increased numbers of colorectal tumors following a protracted carcinogenic exposure [15]. Indeed, these findings revealed that protracted carcinogenic exposure increased 5-HT levels in the colon and that either pharmacologically inhibiting or genetically silencing the 5-HT rate-limiting enzyme Tph1 increased DNA damage. When colonocytes lacking Tph1 activity were exposed to azoxymethane, promoter hypermethylation was associated with inhibiting expression of the DNA damage repair enzyme O^6-methylguanine-DNA methyltransferase (Mgmt). In Tph1-deficient cells subjected to ionizing radiation, 5-HT synthesis promoted DNA damage repair by ataxia telangiectasia and Rad3 related (Atr) [15].

In keeping with the idea that harmful compounds known to promote CRC might impair 5-HT activity, we should consider that high-fat diets have been known to promote early CRC steps

altering the intestinal microbiome [77]. Interestingly, it was found that 5-HT synthesis and reuptake were inhibited in carcinogen-exposed rats fed a fat-enriched diet, which did not significantly increase body weight but enlarged the visceral adipose tissue, promoted inflammation, and increased the CRC risk [78]. Singhal *et al.* observed that genetically silencing SERT activity promoted dysbiosis with similar features to those detected in obese mice [39]. Moreover, Loke *et al.* compared normal colon samples with CRC samples and found that cancer-associated dysbiosis occurred together with inhibition of the 5-HT synthesis pathway [79].

These recent discoveries underscore the close relationship between the neuroendocrine system and the development of malignant lesions. In the presence of a deregulated neuroendocrine system, early cancer-initiating cells may thrive due to an unbalanced immune system response selecting the most malignant clones toward expansion [80,81]. Changes in signaling from the neuroendocrine system could also promote cancer progression, because the imbalance in hormonal levels would induce the expansion of cancer-initiating cells but inhibit immunosurveillance activities against tumor growth [66,81].

5-HT Activity Promotes the CRC Progression Step

For a few decades, 5-HT has been thought to promote proliferation in CRC cells through the activation of its reuptake transporters and receptors [14]. Xia *et al.* showed not only that patients with CRC had increased plasma 5-HT levels compared with their counterparts who were either healthy or bearing benign colorectal polyps, but also that high-5-HT levels were closely associated with advanced tumor node metastasis, leading to poor recurrence-free survival and overall survival [82]. The cellular response to 5-HT stimulation differs between healthy colonocytes and CRC cells, as first observed by Tutton and Barkla. They observed that 5-HT did not increase the colonic crypt cell mitotic rate, although it did promote proliferation in CRC cells [14]. They later suggested that both endocrine and autonomic neural mechanisms control cell proliferation in healthy colonic crypts, whereas CRC cellular proliferation requires only endocrine signaling [83]. Nocito *et al.* supported these findings, because they showed that subcutaneous CRC allografts grew slower in mice with 5-HT deficiency [70].

It has recently been suggested that 5-HT-induced cancer cell expansion is closely related to HTr1 and HTr2 activities rather than to the effects of HTr3, HTr4, HTr6, and HTr7 [84]. Peters *et al.* studied the expression of HTr1B and HTr2B in 11 756 samples comprising 43 different cancer types. This report demonstrated that HTr2B overexpression mainly occurs in uveal melanomas, while HTr1B overexpression was usually detected in nasopharyngeal carcinoma. Another interesting observation was that HTr2B was largely expressed by stromal and endothelial cells in skin, colon, ovarian, breast, renal, and pancreatic malignancies [85]. In uveal melanomas, HTr2B promotes cell proliferation [86]. In pancreatic cancer cells, HTr1B and HTr1D units promote proliferation, clonogenicity, and invasion [87]. In CRC, subcutaneous tumor allografts treated with mirtazapine, an inhibitor of HTr2, underwent reduced growth by direct modulation of immunological mechanisms in the malignant microenvironment [71]. Moreover, HTr1D activates the Axin1/β-catenin/MMP-7 pathway underlying a significant tumor invasion mechanism in CRC [20].

Since tumor progression and metastasis heavily rely on angiogenesis to develop, significant insights have shown an impact of 5-HT signaling on angiogenesis. Notably, physiological 5-HT concentrations activate angiogenic signaling in human endothelial cells [88]. This serotonergic proangiogenic effect has been suggested to be related to the activation of HTr1, HTr2, and HTr3 [89]. Based on the observation that HTr1A, HTr1D, and HTr2B are expressed in prostate

and breast cancer samples [90–92], inhibition of 5-HT-induced angiogenesis through HTr1 was found to decrease tumor growth [93].

These findings illustrate that 5-HT has a pivotal but not yet fully understood role throughout CRC development. Although current evidence suggests that 5-HT is a regulatory factor by which colon tissue can react against different damaging conditions, it has become clear that 5-HT-related mechanisms can be easily tuned into procancer mechanisms facilitating CRC development.

5-HT Activity in Cancer Metabolism

5-HT activity also appears to alter cancer cell metabolism. First, glucose-stimulated CRC cells have shown increased 5-HT levels [94]. Then, 5-HT was found to activate its receptors HTr2A and HTr2C in breast cancer cells, from which the Jak1/STAT3 and ERK1/2 subcellular pathways promoted glucose metabolism through the upregulation of the pyruvate kinase M2 (PKM2) isoform. This HTr2A/ HTr2C signaling further activates adenylyl cyclase/PKA, leading to mitochondrial biogenesis and metabolism, from which lactate undergoes oxidation in cancer cells [95]. Similar metabolic effects of 5-HT have been reported in pancreatic ductal adenocarcinomas [96]. Then, it was observed that inhibiting SERT activity in CRC cells reduced tumor growth and microvessel density after it impaired cancer-related energy production. Specifically, this drug-induced SERT inhibition downregulated lactate transporters to break down essential cancer-related mitochondrial functions [74]. Recent findings have further revealed that pharmacologically inhibiting SERT inhibited energy consumption and energy production by mitochondrial Ca^{2+} overload in cancer cells [97].

Potential Serotonergic Targets for Anti-CRC Therapies

Serotonergic activity is one of the most versatile hormone-based mechanisms providing treatable targets for an almost uncountable number of human conditions, including cancer. For instance, more than four decades ago, treating carcinogen-exposed rats with d-bromolysergic acid diethylamide, which inhibits HTr2A, was shown to decrease proliferation in CRC cells [14]. However, recent discoveries illustrate the complexity of serotonergic activity in the onset of CRC. Drug-induced HTr3 inhibition was recently found to decrease the development of colitis-associated colorectal tumors in mice [98]. This same therapeutic strategy of inhibiting HTr3 was demonstrated to reduce 5-fluorouracil-induced intestinal mucositis, because it is a recurrent chemotherapy adverse effect in patients with CRC [99]. Another study of a different type of HTr revealed that pharmacologically inhibiting HTr1D reduced CRC-related pulmonary metastasis in mice [20]. Moreover, several studies support the idea that pharmacological inhibition of SERT not only decreases the risk of CRC, but also elicits oncostatic effects against this disease in different murine experimental models and patients [69,72–74]. These observations demonstrate that studying 5-HT activity has revealed promising therapeutic strategies against CRC.

Moreover, novel multitarget therapies have been recently designed that promote increased survival rates in experimental CRC models [100]. One of these promising therapeutic approaches has been epigenetic drugs that inhibit the histone methylation status and promote the survival of mice [101]. In this perspective scenario of personalized therapies against CRC, serotonergic activity provides a range of potential targets for future drug findings. While decreased trimethylation of histone H3 at lysine 4 (H3K4me3) has been associated with a poor prognosis in CRC [102], it was recently found that 5-HT activity directly controls this histone modification and thereby gene expression (see Figure I in Box 2) [18,103]. It means that serotonergic targets altering epigenetic mechanisms may enhance the limited potential of standard therapies in fighting cancer.

Concluding Remarks

The classical hypothesis that the endocrine system has a crucial role in body homeostasis through serotonergic signaling remains contemporary and provides a robust framework for future investigations on human cancer (Figure 3). Due to its complex effects in maintaining body homeostasis, 5-HT has vital activity in several gastrointestinal conditions, including the development of CRC. While the serotonergic activity could act protectively against early carcinogenic events in the colon, this same system might support CRC metastatic progression. Studying the role of 5-HT in different stages of CRC should reveal novel treatment strategies to enhance the potency of current anticancer therapies. Of particular importance are the newly discovered anti-DNA damage activity and the modulation of the immune response by 5-HT activity during CRC development. Both these functions of 5-HT provide novel opportunities for prophylactic therapies and anticancer alternative treatment strategies. Indeed, the diverse roles of 5-HT in intestinal homeostasis and CRC provide a resourceful pool of working targets for personalized therapies for patients with cancer. It appears likely that patients with either colitis-related or -unrelated CRC might benefit from specific inhibition or stimulation of certain serotonergic elements once their specific role in disease etiology is understood (see Outstanding Questions).

Outstanding Questions

How do the physiological interactions between the intestinal serotonergic system, immune response, and microbiota lead to the promotion of malignant processes in the colon?

What elements of the serotonergic system are significant targets for carcinogenic agents during the development of CRC?

Which of these compounds have the most harmful effects on humans?

What is the relationship between neuroendocrine deregulation and CRC?

How does this potential relationship limit cancer immunosurveillance and facilitate the establishment and expansion of cancer-initiating cells?

Could impairment of the serotonergic system be considered as one of the hallmarks of neuroendocrine disruption that increases the risk of CRC?

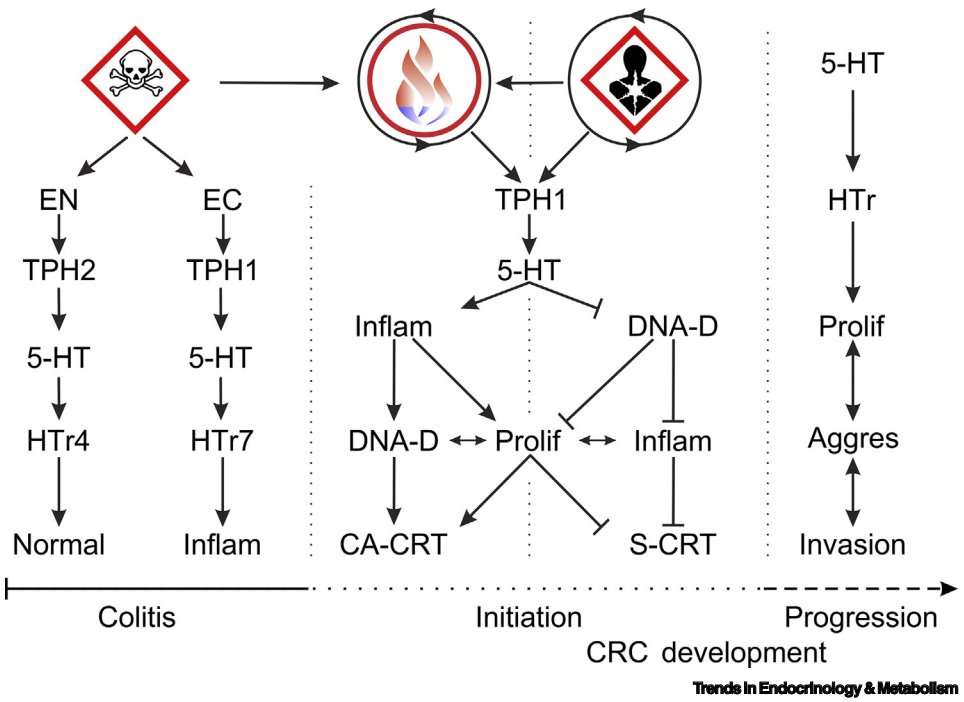

Figure 3. Serotonergic Activity Has a Pivotal Role in Maintaining Colorectal Homeostasis and Protection against Sporadic Colorectal Cancer (CRC). From the left to right side, exposure to hazardous chemicals (i.e., dextran sulfate; skull and crossbones) leads to serotonin (5-HT) release from either enteric neurons [EN; cells express tryptophan hydrolase (TPH)-2] or EC units (cells express TPH1). EN-induced 5-HT synthesis promotes the activation of 5-Ht receptor 4 (HT4r), leading to the resolution of inflammation. However, ECs appear to recruit an inflammatory response by activating HT7r following the synthesis and release of 5-HT by them. This mechanism may promote colitis. Colitis-associated colorectal tumorigenesis (CA-CRT) can be induced by the combined exposure of hazardous chemicals and carcinogens promoting the release of 5-HT and an intense inflammatory response, which promote DNA damage (DNA-D) and proliferation (Prolif) leading to the development of tumors. Since carcinogen-induced DNA-D is inhibited by 5-HT synthesis, sporadic colorectal tumorigenesis (S-CRT) is reduced by decreasing Prolif and inflammation (Inflam). However, 5-HT may promote latter steps of CRC development, because activation of HTrs promotes Prolif, tumor aggressiveness (Aggres), and tissue invasion.

References

1. Walther, D.J. *et al.* (2003) Synthesis of serotonin by a second tryptophan hydroxylase isoform. *Science* 299, 76
2. Yano, J.M. *et al.* (2015) Indigenous bacteria from the gut microbiota regulate host serotonin biosynthesis. *Cell* 161, 264–276
3. Stone, T.W. and Darlington, L.G. (2002) Endogenous kynurenines as targets for drug discovery and development. *Nat. Rev. Drug Discov.* 1, 609–620
4. Mawe, G.M. and Hoffman, J.M. (2013) Serotonin signalling in the gut–functions, dysfunctions and therapeutic targets. *Nat. Rev. Gastroenterol. Hepatol.* 10, 473–486
5. Nishizawa, S. *et al.* (1997) Differences between males and females in rates of serotonin synthesis in human brain. *Proc. Natl. Acad. Sci. U. S. A.* 94, 5308–5313
6. Kleppe, R. *et al.* (2011) The 14-3-3 proteins in regulation of cellular metabolism. *Semin. Cell Dev. Biol.* 22, 713–719
7. Kuhn, D.M. *et al.* (2007) Phosphorylation and activation of tryptophan hydroxylase 2: identification of serine-19 as the substrate site for calcium, calmodulin-dependent protein kinase II. *J. Neurochem.* 103, 1567–1573
8. Darmon, M. *et al.* (2015) Insights into serotonin receptor trafficking: cell membrane targeting and internalization. *Prog. Mol. Biol. Transl. Sci.* 132, 97–126
9. Day, M. and Vane, J.R. (1963) An analysis of the direct and indirect actions of drugs on the isolated guinea-pig ileum. *Br. J. Pharmacol. Chemother.* 20, 150–170
10. Chin, A. *et al.* (2012) The role of mechanical forces and adenosine in the regulation of intestinal enterochromaffin cell serotonin secretion. *Am. J. Physiol. Gastrointest. Liver Physiol.* 302, G397–G405
11. Heredia, D.J. *et al.* (2013) Important role of mucosal serotonin in colonic propulsion and peristaltic reflexes: in vitro analyses in mice lacking tryptophan hydroxylase 1. *J. Physiol.* 591, 5939–5957
12. Gershon, M.D. and Tack, J. (2007) The serotonin signaling system: from basic understanding to drug development for functional GI disorders. *Gastroenterology* 132, 397–414
13. Erspamer, V. and Asero, B. (1952) Identification of enteramine, the specific hormone of the enterochromaffin cell system, as 5-hydroxytryptamine. *Nature* 169, 800–801
14. Tutton, P.J. and Barkla, D.H. (1978) The influence of serotonin on the mitotic rate in the colonic crypt epithelium and in colonic adenocarcinoma in rats. *Clin. Exp. Pharmacol. Physiol.* 5, 91–94
15. Sakita, J.Y. *et al.* (2019) Serotonin synthesis protects the mouse colonic crypt from DNA damage and colorectal tumorigenesis. *J. Pathol.* 249, 102–113
16. Sakita, J.Y. *et al.* (2017) A critical discussion on diet, genomic mutations and repair mechanisms in colon carcinogenesis. *Toxicol. Lett.* 265, 106–116
17. Torre, L.A. *et al.* (2015) Global cancer statistics, 2012. *CA Cancer J. Clin.* 65, 87–108
18. Farrelly, L.A. *et al.* (2019) Histone serotonylation is a permissive modification that enhances TFIID binding to H3K4me3. *Nature* 567, 535–539
19. Kannen, V. *et al.* (2018) Mast cells and serotonin synthesis modulate Chagas disease in the colon: clinical and experimental evidence. *Dig. Dis. Sci.* 63, 1473–1484
20. Sui, H. *et al.* (2015) 5-hydroxytryptamine receptor (5-HT1DR) promotes colorectal cancer metastasis by regulating Axin1/beta-catenin/MMP-7 signaling pathway. *Oncotarget* 6, 25975–25987
21. Reigstad, C.S. *et al.* (2015) Gut microbes promote colonic serotonin production through an effect of short-chain fatty acids on enterochromaffin cells. *FASEB J.* 29, 1395–1403
22. Crane, J.D. *et al.* (2015) Inhibiting peripheral serotonin synthesis reduces obesity and metabolic dysfunction by promoting brown adipose tissue thermogenesis. *Nat. Med.* 21, 166–172
23. Walther, D.J. *et al.* (2003) Serotonylation of small GTPases is a signal transduction pathway that triggers platelet alpha-granule release. *Cell* 115, 851–862
24. Muma, N.A. and Mi, Z. (2015) Serotonylation and transamidation of other monoamines. *ACS Chem. Neurosci.* 6, 961–969
25. Spohn, S.N. *et al.* (2016) Protective actions of epithelial 5-hydroxytryptamine 4 receptors in normal and inflamed colon. *Gastroenterology* 151, 933–944
26. Kim, J.J. *et al.* (2013) Targeted inhibition of serotonin type 7 (5-HT7) receptor function modulates immune responses and reduces the severity of intestinal inflammation. *J. Immunol.* 190, 4795–4804
27. Holst, K. *et al.* (2015) The serotonin receptor 5-HT(7)R regulates the morphology and migratory properties of dendritic cells. *J. Cell Sci.* 128, 2866–2880
28. Elinav, E. *et al.* (2013) Inflammation-induced cancer: crosstalk between tumours, immune cells and microorganisms. *Nat. Rev. Cancer* 13, 759–771
29. Millan, M.J. *et al.* (2008) Signaling at G-protein-coupled serotonin receptors: recent advances and future research directions. *Trends Pharmacol. Sci.* 29, 454–464
30. Clarke, G. *et al.* (2013) The microbiome-gut-brain axis during early life regulates the hippocampal serotonergic system in a sex-dependent manner. *Mol. Psychiatry* 18, 666–673
31. Oh, C.M. *et al.* (2015) Regulation of systemic energy homeostasis by serotonin in adipose tissues. *Nat. Commun.* 6, 6794
32. Terry, N.A. *et al.* (2014) Impaired enteroendocrine development in intestinal-specific Islet1 mouse mutants causes impaired glucose homeostasis. *Am. J. Physiol. Gastrointest. Liver Physiol.* 307, G979–G991
33. Kim, K. *et al.* (2015) Functional role of serotonin in insulin secretion in a diet-induced insulin-resistant state. *Endocrinology* 156, 444–452
34. Paulmann, N. *et al.* (2009) Intracellular serotonin modulates insulin secretion from pancreatic beta-cells by protein serotonylation. *PLoS Biol.* 7, e1000229
35. Valladares, R. *et al.* (2013) *Lactobacillus johnsonii* inhibits indoleamine 2,3-dioxygenase and alters tryptophan metabolite levels in BioBreeding rats. *FASEB J.* 27, 1711–1720
36. Essien, B.E. *et al.* (2013) ZBP-89 regulates expression of tryptophan hydroxylase I and mucosal defense against *Salmonella typhimurium* in mice. *Gastroenterology* 144, 1466–1477
37. Sun, W. *et al.* (2018) Fecal microbiota transplantation can alleviate gastrointestinal transit in rats with high-fat diet-induced obesity via regulation of serotonin biosynthesis. *Biomed. Res. Int.* 2018, 8308671
38. Kwon, Y.H. *et al.* (2019) Modulation of gut microbiota composition by serotonin signaling influences intestinal immune response and susceptibility to colitis. *Cell. Mol. Gastroenterol. Hepatol.* 7, 709–728
39. Singhal, M. *et al.* (2019) Serotonin transporter deficiency is associated with dysbiosis and changes in metabolic function of the mouse intestinal microbiome. *Sci. Rep.* 9, 2138
40. Gross, E.R. *et al.* (2012) Neuronal serotonin regulates growth of the intestinal mucosa in mice. *Gastroenterology* 143, 408–417
41. Basak, O. *et al.* (2017) Induced quiescence of Lgr5+ stem cells in intestinal organoids enables differentiation of hormone-producing enteroendocrine cells. *Cell Stem Cell* 20, 177–190
42. Bayliss, W.M. and Starling, E.H. (1899) The movements and innervation of the small intestine. *J. Physiol.* 24, 99–143
43. Bulbring, E. and Crema, A. (1959) The action of 5-hydroxytryptamine, 5-hydroxytryptophan and reserpine on intestinal peristalsis in anaesthetized guinea-pigs. *J. Physiol.* 146, 29–53
44. Tuladhar, B.R. *et al.* (1997) Evidence for a 5-HT3 receptor involvement in the facilitation of peristalsis on mucosal application of 5-HT in the guinea pig isolated ileum. *Br. J. Pharmacol.* 122, 1174–1178
45. Tutton, P.J. (1974) The influence of serotonin on crypt cell proliferation in the jejunum of rat. *Virchows Arch. B Cell Pathol.* 16, 79–87
46. Chen, J.J. *et al.* (2001) Maintenance of serotonin in the intestinal mucosa and ganglia of mice that lack the high-affinity serotonin transporter: abnormal intestinal motility and the expression of cation transporters. *J. Neurosci.* 21, 6348–6361
47. Margolis, K.G. *et al.* (2016) Serotonin transporter variant drives preventable gastrointestinal abnormalities in development and function. *J. Clin. Invest.* 126, 2221–2235

48. Li, Z. *et al.* (2011) Essential roles of enteric neuronal serotonin in gastrointestinal motility and the development/survival of enteric dopaminergic neurons. *J. Neurosci.* 31, 8998–9009
49. Ghia, J.E. *et al.* (2009) Serotonin has a key role in pathogenesis of experimental colitis. *Gastroenterology* 137, 1649–1660
50. Kim, J.J. *et al.* (2015) Blocking peripheral serotonin synthesis by telotristat etiprate (LX1032/LX1606) reduces severity of both chemical- and infection-induced intestinal inflammation. *Am. J. Physiol. Gastrointest. Liver Physiol.* 309, G455–G465
51. Gershon, M.D. (2012) Serotonin is a sword and a shield of the bowel: serotonin plays offense and defense. *Trans. Am. Clin. Climatol. Assoc.* 123, 268–280 discussion 280
52. Margolis, K.G. *et al.* (2014) Pharmacological reduction of mucosal but not neuronal serotonin opposes inflammation in mouse intestine. *Gut* 63, 928–937
53. Belkind-Gerson, J. *et al.* (2015) Colitis induces enteric neurogenesis through a 5-HT4-dependent mechanism. *Inflamm. Bowel Dis.* 21, 87087–87088
54. Bischoff, S.C. *et al.* (2009) Role of serotonin in intestinal inflammation: knockout of serotonin reuptake transporter exacerbates 2,4,6-trinitrobenzene sulfonic acid colitis in mice. *Am. J. Physiol. Gastrointest. Liver Physiol.* 296, G685–G695
55. Li, N. *et al.* (2011) Serotonin activates dendritic cell function in the context of gut inflammation. *Am. J. Pathol.* 178, 662–671
56. Wang, H. *et al.* (2007) CD4+ T cell-mediated immunological control of enterochromaffin cell hyperplasia and 5-hydroxytryptamine production in enteric infection. *Gut* 56, 949–957
57. Motomura, Y. *et al.* (2008) Enterochromaffin cell and 5-hydroxytryptamine responses to the same infectious agent differ in Th1 and Th2 dominant environments. *Gut* 57, 475–481
58. Duerschmied, D. *et al.* (2013) Platelet serotonin promotes the recruitment of neutrophils to sites of acute inflammation in mice. *Blood* 121, 1008–1015
59. Vogelstein, B. and Kinzler, K.W. (2015) The path to cancer – three strikes and you're out. *N. Engl. J. Med.* 373, 1895–1898
60. Casey, S.C. *et al.* (2015) The effect of environmental chemicals on the tumor microenvironment. *Carcinogenesis* 36, S160–S183
61. Garcia, S.B. *et al.* (2014) The contribution of neuronal-glial-endothelial-epithelial interactions to colon carcinogenesis. *Cell. Mol. Life Sci.* 71, 3191–3197
62. Soto, A.M. and Sonnenschein, C. (2010) Environmental causes of cancer: endocrine disruptors as carcinogens. *Nat. Rev. Endocrinol.* 6, 363–370
63. Jacquelot, N. *et al.* (2019) Physiological regulation of innate lymphoid cells. *Front. Immunol.* 10, 405
64. Salem, M.E. *et al.* (2018) Landscape of tumor mutation load, mismatch repair deficiency, and PD-L1 expression in a large patient cohort of gastrointestinal cancers. *Mol. Cancer Res.* 16, 805–812
65. Zhang, W.H. *et al.* (2019) The tumor immune microenvironment in gastroenteropancreatic neuroendocrine neoplasms. *Biochim. Biophys. Acta Rev. Cancer* 1872, 188311
66. Vikman, S. *et al.* (2009) Midgut carcinoid patients display increased numbers of regulatory T cells in peripheral blood with infiltration into tumor tissue. *Acta Oncol.* 48, 391–400
67. Shafqat, H. *et al.* (2015) Survival of patients with neuroendocrine carcinoma of the colon and rectum: a population-based analysis. *Dis. Colon Rectum* 58, 294–303
68. Sikander, A. *et al.* (2015) Association of serotonin transporter promoter polymorphism (5-HTTLPR) with microscopic colitis and ulcerative colitis. *Dig. Dis. Sci.* 60, 887–894
69. Coogan, P.F. *et al.* (2009) Antidepressant use and colorectal cancer risk. *Pharmacoepidemiol. Drug Saf.* 18, 1111–1114
70. Nocito, A. *et al.* (2008) Serotonin regulates macrophage-mediated angiogenesis in a mouse model of colon cancer allografts. *Cancer Res.* 68, 5152–5158
71. Fang, C.K. *et al.* (2012) Mirtazapine inhibits tumor growth via immune response and serotonergic system. *PLoS ONE* 7, e38886
72. Kannen, V. *et al.* (2011) Fluoxetine induces preventive and complex effects against colon cancer development in epithelial and stromal areas in rats. *Toxicol. Lett.* 204, 134–140
73. Kannen, V. *et al.* (2012) Antiproliferative effects of fluoxetine on colon cancer cells and in a colonic carcinogen mouse model. *PLoS ONE* 7, e50043
74. Kannen, V. *et al.* (2015) Oncostatic effects of fluoxetine in experimental colon cancer models. *Cell. Signal.* 27, 1781–1788
75. Alam, R.T. *et al.* (2019) Amelioration of fenitrothion induced oxidative DNA damage and inactivation of caspase-3 in the brain and spleen tissues of male rats by N-acetylcysteine. *Life Sci.* 231, 116534
76. Lubbe, A.S. and Huhnt, W. (1994) Microvessel diameters of human colon adenocarcinoma during acute treatment with serotonin. *Int. J. Microcirc. Clin. Exp.* 14, 218–225
77. Schulz, M.D. *et al.* (2014) High-fat-diet-mediated dysbiosis promotes intestinal carcinogenesis independently of obesity. *Nature* 514, 508–512
78. Kannen, V. *et al.* (2012) High-fat diet causes an imbalance in the colonic serotonergic system promoting adipose tissue enlargement and dysplasia in rats. *Toxicol. Lett.* 213, 135–141
79. Loke, M.F. *et al.* (2018) Metabolomics and 16S rRNA sequencing of human colorectal cancers and adjacent mucosa. *PLoS ONE* 13, e0208584
80. Hristova, M.G. (2018) Neuroendocrine and immune disequilibrium as a probable link between metabolic syndrome and carcinogenesis. *Med. Hypotheses* 118, 1–5
81. Pierpaoli, W. (2013) Cancer and the endogenous "pineal clock": a means of early diagnosis and successful treatment as well as prevention of cancers. *Curr. Aging Sci.* 6, 108–114
82. Xia, Y. *et al.* (2018) Plasma serotonin level is a predictor for recurrence and poor prognosis in colorectal cancer patients. *J. Clin. Lab. Anal.* 32, e22263
83. Tutton, P.J. and Barkla, D.H. (1980) Neural control of colonic cell proliferation. *Cancer* 45, 1172–1177
84. Sarrouilhe, D. and Mesnil, M. (2019) Serotonin and human cancer: a critical view. *Biochimie* 161, 46–50
85. Peters, M.A.M. *et al.* (2019) Serotonin and dopamine receptor expression in solid tumours including rare cancers. *Pathol. Oncol. Res.* Published online September 2, 2019. https://doi.org/10.1007/s12253-019-00734-w
86. Weidmann, C. *et al.* (2018) Expression of the serotonin receptor 2B in uveal melanoma and effects of an antagonist on cell lines. *Clin. Exp. Metastasis* 35, 123–134
87. Gurbuz, N. *et al.* (2014) Down-regulation of 5-HT1B and 5-HT1D receptors inhibits proliferation, clonogenicity and invasion of human pancreatic cancer cells. *PLoS ONE* 9, e105245
88. Zamani, A. and Qu, Z. (2012) Serotonin activates angiogenic phosphorylation signaling in human endothelial cells. *FEBS Lett.* 586, 2360–2365
89. Peters, M.A. *et al.* (2014) Dopamine and serotonin regulate tumor behavior by affecting angiogenesis. *Drug Resist. Updat.* 17, 96–104
90. Dizeyi, N. *et al.* (2004) Expression of serotonin receptors and role of serotonin in human prostate cancer tissue and cell lines. *Prostate* 59, 328–336
91. Dizeyi, N. *et al.* (2005) Expression of serotonin receptors 2B and 4 in human prostate cancer tissue and effects of their antagonists on prostate cancer cell lines. *Eur. Urol.* 47, 895–900
92. Kopparapu, P.K. *et al.* (2013) Expression and localization of serotonin receptors in human breast cancer. *Anticancer Res.* 33, 363–370
93. Banskota, S. *et al.* (2016) BJ-1108, a 6-Amino-2,4,5-trimethylpyridin-3-ol analog, inhibits serotonin-induced angiogenesis and tumor growth through PI3K/NOX pathway. *PLoS ONE* 11, e0148133
94. Lieder, B. *et al.* (2017) The flavanone homoeriodictyol increases SGLT-1-mediated glucose uptake but decreases serotonin release in differentiated Caco-2 cells. *PLoS ONE* 12, e0171580
95. Sola-Penna, M. *et al.* (2020) Serotonin activates glycolysis and mitochondria biogenesis in human breast cancer cells through activation of the Jak1/STAT3/ERK1/2 and adenylate cyclase/PKA, respectively. *Br. J. Cancer* 122, 194–208
96. Jiang, S.H. *et al.* (2017) Increased serotonin signaling contributes to the Warburg effect in pancreatic tumor cells under

metabolic stress and promotes growth of pancreatic tumors in mice. *Gastroenterology* 153, 277–291
97. Charles, E. *et al.* (2017) The antidepressant fluoxetine induces necrosis by energy depletion and mitochondrial calcium overload. *Oncotarget* 8, 3181–3196
98. Amini-Khoei, H. *et al.* (2016) Tropisetron suppresses colitis-associated cancer in a mouse model in the remission stage. *Int. Immunopharmacol.* 36, 9–16
99. Yasuda, M. *et al.* (2013) 5-HT(3) receptor antagonists ameliorate 5-fluorouracil-induced intestinal mucositis by suppression of apoptosis in murine intestinal crypt cells. *Br. J. Pharmacol.* 168, 1388–1400
100. Zheng, D.W. *et al.* (2019) Phage-guided modulation of the gut microbiota of mouse models of colorectal cancer augments their responses to chemotherapy. *Nat. Biomed. Eng.* 3, 717–728
101. Segovia, C. *et al.* (2019) Inhibition of a G9a/DNMT network triggers immune-mediated bladder cancer regression. *Nat. Med.* 25, 1073–1081
102. Liu, H. *et al.* (2018) H3K4me3 and Wdr82 are associated with tumor progression and a favorable prognosis in human colorectal cancer. *Oncol. Lett.* 16, 2125–2134
103. Bader, M. (2019) Serotonylation: Serotonin signaling and epigenetics. *Front. Mol. Neurosci.* 12, 288

Journal of Gastrointestinal Cancer (2021) 52:280–288
https://doi.org/10.1007/s12029-020-00399-8

ORIGINAL RESEARCH

Age-Related and Gender-Related Increases in Colorectal Cancer Mortality Rates in Brazil Between 1979 and 2015: Projections for Continuing Rises in Disease

Francis L. Martin[1] · Camilo L. M. Morais[1] · Juliana Yumi Sakita[2] · Sergio Akira Uyemura[3] · Vinicius Kannen[2,4]

Published online: 4 April 2020

Abstract

Purpose Brazil is the largest country in South America. Although a developing nation, birth rates have been decreasing in the last few decades, while its overall population is undergoing lifestyle changes and ageing significantly. Moreover, Brazil has had increasingly high mortality rates related to colorectal cancer (CRC). Herein, we investigated whether the Brazilian population is exhibiting increasing mortality rates related to colon cancer (CC) or rectal cancer (RC) in recent years.

Methods We examined data from the Brazilian Federal Government from 1979 to 2015 to determine whether CRC mortality and the population ageing process may be associated.

Results Our mathematical modelling suggests that mortality rates related to CC and RC events in the Brazilian population may increase by 79% and 66% in the next 24 years, respectively. This finding led us to explore the mortality rates for both diseases in the country, and we observed that the highest levels were in the south and southeast regions from the year 2000 onwards. CC events appear to decrease life expectancy among people during their second decade of life in recent years, whereas RC events induced decreases in life expectancy in those aged >30 years. Additionally, both CC and RC events seem to promote significant mortality rates in the male population aged > 60 years and living in the southern states.

Conclusion Our dataset suggests that both CC and RC events may lead to a significantly increasing number of deaths in the Brazilian male population in coming years.

Keywords Ageing · Cancer mortality · Epidemiology · Lifestyle

Introduction

Colorectal cancer (CRC) is currently reported as one of the leading causes of cancer-related deaths worldwide, in males and females [1]. One should consider that CRC terminology comprises two types of cancer with similar risk factors: colon cancer (CC) and rectal cancer (RC). The colon has two anatomical components referred to as the proximal and distal, which respectively connects this organ to the small intestine and the rectum. The rectum connects the distal colon to the anal sphincter [2]. Both CC and RC have significant genetic similarities regarding the mutations promoting their development. Symptoms are quite similar for both diseases, although bleeding in CC patients may be observed in brown or black colours, while RC events are related to brighter red bleedings. Because of anatomical patterns, RC is prone to metastasize to the thorax, bones, and nervous system, while the peritoneum seems to be a recurrent target for CC metastases. Also, cancer recurrence seems to be more frequent in RC patients. Moreover, RC events seem to be somewhat more common in men than women [3]. We should stress that because aetiology and risk factors are almost the same for both CC and RC events, they are generally widely known together as CRC [1, 2, 4, 5].

✉ Francis L. Martin
FLMartin@uclan.ac.uk

✉ Vinicius Kannen
vkannen@lunenfeld.ca

[1] School of Pharmacy and Biomedical Sciences, University of Central Lancashire, Preston, UK

[2] Department of Genetics, University of Sao Paulo, Ribeirao Preto, Brazil

[3] Department of Toxicology, Bromatology, and Clinical Analysis, University of Sao Paulo, Ribeirao Preto, Brazil

[4] Lunenfeld-Tanenbaum Research Institute, Mount Sinai Hospital, Toronto, ON, Canada

Until the first half part of the last century, CRC was a rather rare disease even in countries currently with high rates [4]. Considering that most CRC cases are sporadic in aetiology, changes in lifestyle across the globe could thus be directly linked to the increasing incidence of this disease [1, 4, 6–8]. Although an uncountable number of factors may augment CRC rates in a given human cohort, ageing of the worldwide population may play the most pivotal role in this disease aetiology and can be considered one of the primary mechanisms driving the CRC development [5]. For instance, most CRC incidence and mortality occurs in elderly populations living in developed countries [6].

In keeping with this idea, Kuipers et al. observed that the average lifetime risk for CRC might be up to 5% in a general population set without a family history for the disease. In cases where a first-degree family member >50 years old has been diagnosed with CRC, this lifetime risk may double, while it could even triple if the first-degree relative were <50 years of age by the time of diagnosis [4]. However, on analysing CRC rates in Americans aged <50 years old, an increasing incidence of this disease in the younger US adult population is revealed [7, 9]. Interestingly, it has been reported that CRC incidence declined in the USA, generally [1]. On the contrary, another study suggests that about 60% of CRC cases will be found in developing countries by the year 2030 [8].

Brazil is the largest country in South America and has the fifth largest population worldwide. The elderly Brazilian population has been projected to achieve 64 million seniors by 2050 [10]. The country also faces significant social inequality among its elderly citizens, a factor that may impact on the incidence of chronic diseases and healthcare costs shortly [11]. The CRC incidence in Brazilians aged less than 50 years old has also been reported increased by 35% in recent years [12]. Although developed countries have shown a significant decrease in CRC death rates [1], the Brazilian population endured increased numbers of CRC-related deaths for the last 30 years [13]. In as much as CRC mortality rates vary in between different Brazilian states, a factor closely related to the economic development of each region, CRC mortality rates have significantly increased over recent years in the country [14]. These facts raise some concern that the Brazilian population could have a significant increase in CRC-related rates for both incidence and mortality soon, meaning that epidemiological studies on what regions have recently had the highest CRC mortality rates in the country are in significant need now. Herein, we studied the trend for CC and RC mortality during the next 24 years (from 2016 up to 2040), verified mortality rates for both diseases in different Brazilian regions throughout 36 years, as well as studied recent mortality rates according to age and gender.

Material and Methods

Data Collection

CRC mortality data were obtained from the Mortality Information System (SIM) of the Brazilian Ministry of Health, while population-based data were collected from the Brazilian Institute of Geography and Statistics (IBGE). According to the International Classification of Diseases (10^{th} revision, ICD-10) for CC (ICD-10, C18) and RC mortality rates (ICD-10, C19–21), mortality data were collected from 1979 to 2015 on an annual basis. According to the same timeframe, population-based data were also collected. This period has been chosen to further explore previous findings on CRC mortality rates in Brazil.

To statistically compare the Brazilian regions with the highest CRC mortality rates among themselves (Midwest [MW], Southeast [SE], and South regions [S]), we collected data that provides from regional health centres (RHCs). According to SIM, RHCs are government units responsible for coordinating the activities of the State Health Secretariat at the regional level of each Brazilian state. Thus, each Brazilian region is composed of different states with multiple RHCs in each one: Midwest region (Federal capital region [DF] had 1 RHC, Goias state [GO] had 16 RHCs, Mato Grosso do Sul [MS] had 12 RHCs, and Mato Grosso [MT] had 16 RHCs), Southeast region (Espirito Santo [ES] had 4 RHCs, Minas Gerais [MG] had 16 RHCs, Rio de Janeiro [RJ] had 9 RHCs, and Sao Paulo [SP] had RHCs), and South region (Parana [PR] had 16 RHCs, Santa Catarina [SC] had 16 RHCs, and Rio Grande do Sul [RS] had 16 RHCs).

Statistical Analyses

Prospective values for mortality from 2016 until 2040 were calculated according to a prediction function $m(y)$ described as follows:

$$m(y) = f(y)\frac{dp(y)}{dy}\left(\frac{dp_s(y)}{dy}\right)^{-1}\frac{o_{65}(y)}{o_{65}(2015)} \quad (1)$$

where $f(y)$ is a second-order polynomial function fitted to proportional mortality rates (PMR) recorded between the years y (1979 and 2015). This function represents the mortality growth regardless of factors such as population growth and ageing. Then, $p(y)$ is a second-order polynomial function fitted to the official estimate of the Brazilian population between 2014 and 2016. This function represents how a population will grow over time. To this end, $p_s(y)$ is a linear function fitted to the official records of the Brazilian population between 2010 and 2015, which represents the population growth in the years anticipating the future estimation. We should

also consider that $o_{65}(y)$ is the official percentage of people >65 years for the year y, while $o_{65}(2015)$ is the percentage of people >65 years in 2015 (the year that recorded data ends). The mortality function described in Eq. 1 was therefore adjusted to take into consideration variations in population growth and ageing over time. In summary, 1% of CC or RC mortality rates calculated by Eq. 1 means that 1% of the deaths in a determined year was caused by one of these diseases.

CC and RC mortality values were calculated as PMR, as described by Swaroop and Uemura [15]. One should note that any potential misclassification at diagnosis was not exposure-dependent, cause of death is precisely registered, all deaths are included, and population comparisons are consistent within the study [16]. According to Romeder and McWhinnie [17], years of potential life lost (YPLL) *per* 100,000 were determined by the number of deaths in the Brazilian population across different age ranges (between 15 and 79 years old) from 1979 to 2015. This calculation provides age-adjusted rates within a closed population. We further calculate the age-adjusted death rates (AADR) *per* 100,000 related to CC and RC events, according to the previous description of Yerushalmy (1951) [18]. These values were determined based on data from the regional health centres (RHCs) within each Brazilian state in the Midwest, Southeast, and South regions. Values have been adjusted to the Brazilian population of 2010.

Data analyses determined differences in mortality rates related to CC and RC events across different time points in various Brazilian regions by employing a two-way ANOVA model followed by the correction of multiple comparisons through the control of false discovery rates according to the two-stage step-up method of Benjamini, Krieger, and Yekutieli. These analyses were performed on MATLAB R2014b (MathWorks, Inc., Natick, MA, USA) and GraphPad Prism 8.1.0 (GraphPad, San Diego, CA, USA). P values of <0.05 were considered significant.

Results

CC and RC Mortality Across Different Brazilian Regions from 1979 to 2015

First, we analysed the mortality rates related to CC and RC events in Brazil. We observed that the number of deaths by CC and RC increased 2.8-fold and 3.1-fold throughout the last 36 years, respectively. Indeed, our mathematical modelling projected an upward trend in mortality for both diseases in the forthcoming 24 years (CC, from 6.2 to 7.8 per 100,000; RC, from 3.6 to 5.4 per 100,000; Fig. 1; Table 1).

This prospective analysis led us to investigate mortality rates by CC and RC in different regions of the country. Our dataset shows that the population living in the MW, SE, and S regions of Brazil exhibit a significant increase in CC and RC mortality rates in recent years when compared with the inhabitants of the North (N) and Northeast (NE) regions (Fig. 2). We also observe that RC-related mortality in the MW population increased to a level no different from that of the SE region (Fig. 2c, d). Whether CC-related mortality is higher

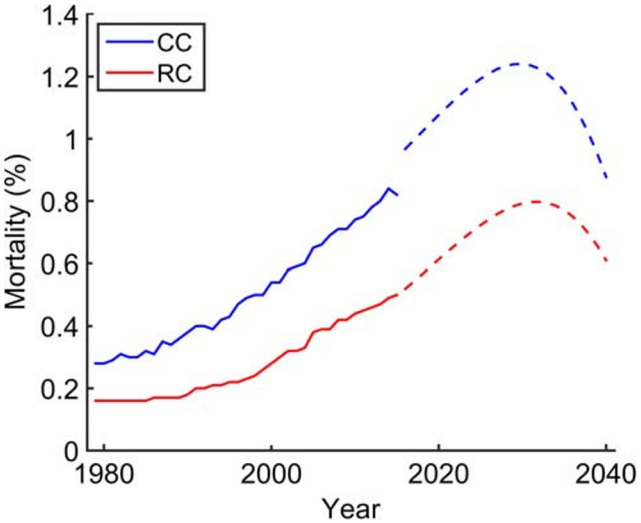

Fig. 1 Mortality rates related to colon (CC) and rectal cancer (RC) in Brazil. While the recorded period (1979–2015) is shown as continuous lines for both diseases, dashed lines represent the data collected from perspective calculations between 2016 and 2040

Table 1 Colon cancer (CC) and rectal cancer (RC) mortality rates *per* 100,000 in Brazil

Year	CC-related mortality	RC-related mortality
2010	4.71	2.80
2012	4.95	2.92
2014	5.35	3.12
2016	6.20	3.33
2018	6.61	3.66
2020	7.06	4.02
2022	7.52	4.39
2024	8.00	4.79
2026	8.46	5.18
2028	8.87	5.55
2030	9.19	5.87
2032	9.38	6.11
2034	9.39	6.22
2036	9.16	6.17
2038	8.64	5.92
2040	7.80	5.42

Values shown herein represent the recorded period between 2010 and 2014 for both CC and RC mortality rates, while a mathematical modelling projects these events from 2016 until 2040

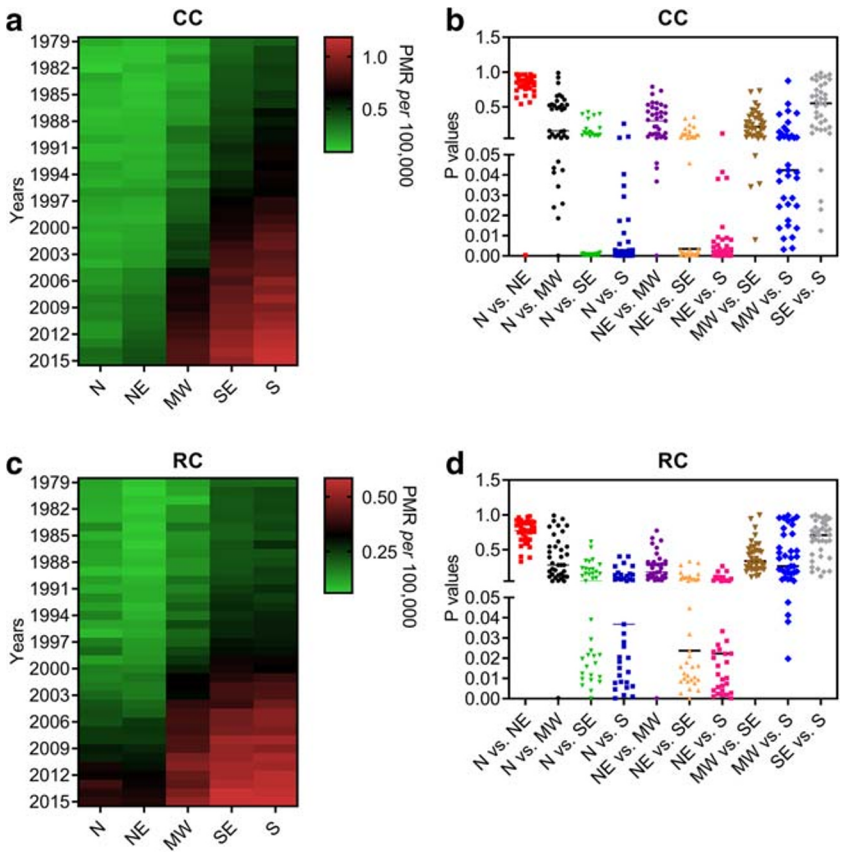

Fig. 2 Mortality rates for colon cancer (CC) and rectal cancer (RC) in Brazil. **a** and **b** Heatmaps illustrate proportional mortality rates (PMR) for CC (**a**) and RC (**b**) according to a population of 100,000 people in different regions of Brazil (North [N]; Northeast [NE]; Midwest [MW]; Southeast [SE]; South [S]) from 1979 until 2015. Whether bright green colours represent the lowest mean values of proportional mortality rates (PMR) in each Brazilian region, bright red colours represent the highest values. **c** and **d** Scatter dot plots show *P* values that have been calculated by the two-way ANOVA model followed by correction of multiple comparisons through the control of false discovery rates according to the two-stage step-up method of Benjamini, Krieger, and Yekutieli

in the S region than in the SE, no difference has been found for death rates related to RC events between both areas (Fig. 2).

Effects of Ageing on CC and RC Mortality in Recent Years

To better understand these events, we calculated the impact on life expectancy due to CC and RC events in the Brazilian population. Both CC and RC elevated the most shortening in life expectancy between the years 2009 and 2015 (Fig. 3). We further found that the decrease in life expectancy associated with CC started during the second decade of life, while RC induced similar effects in subjects not younger than 30 years old (Fig. 3).

We then calculated mortality rates adjusted by age to clarify these concerning findings in recent years. The AADR for male and female inhabitants from the MW, SE, and S regions of Brazil between 2014 and 2015 reveal that southern men and women aged 70 years old or more exhibited higher mortality rates related to CC than those living in the SE and MW regions (Fig. 4). While southern men in their seventieth decade of life onwards had the highest RC mortality rates, this same effect appeared to occur in the female population aged ≥80 years old (Fig. 5). Indeed, the southern male population died more frequently of CC and RC than women following their seventieth decade of life (Figs. 4 and 5). Similar differences between male and female populations for CC and RC mortality rates are observed in the SE region (Figs. 4 and 5). Irrespective of whether the MW male population exhibited the highest CC mortality rates following their eightieth decade of life (Fig. 4), RC promoted the highest mortality among female inhabitants of this area (Fig. 5).

Studying the MW states, we found that the oldest male and female populations living in the Federal District (DF) had the highest CC and CRC mortality rates in the region (Figs. 4 and 5). Interestingly, those men aged 70 years old or more and residing in the state of Mato Grosso (MT) showed the lowest values of CC and RC mortality (Figs. 4 and 5).

In the SE region, men aged ≥80 years old and living in the states of São Paulo (SP) and Rio de Janeiro (RJ) showed the highest CC and RC mortality rates (Figs. 4 and 5). It seems that the old male population in the state of Espirito Santo (ES) had the lowest values of RC mortality (Fig. 4). In comparison with the states of São Paulo (SP) and Rio de Janeiro (RJ), women residing in the state of Minas Gerais (MG) had lower rates of CC and RC mortality (Figs. 4 and 5). Indeed, the male population living in the state of SP died more of CC and RC than women from 70 years old age onwards (Fig. 5).

Following the seventieth decade of life, both men and women living in the southern state of Rio Grande do Sul

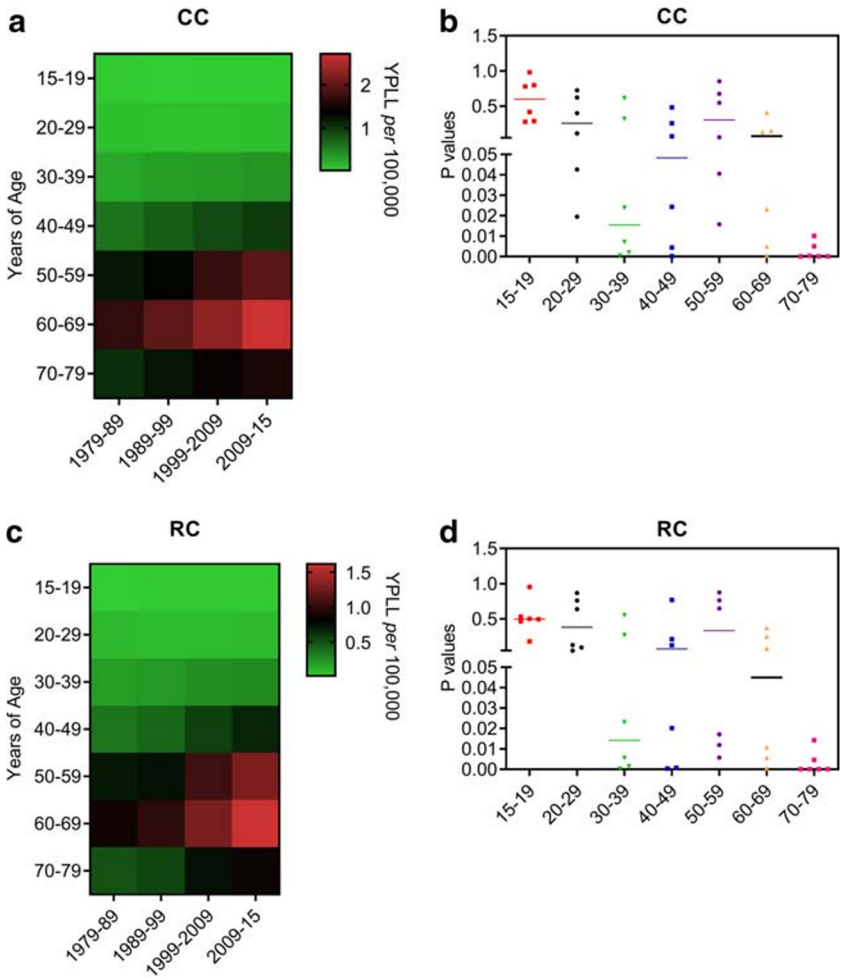

Fig. 3 Years of potential life lost (YPLL) due to colon cancer (CC) and rectal cancer (RC) events in Brazil. **a and b** Heatmaps illustrate YPLL values for CC (**a**) and RC (**b**) are shown in different populations with age ranging from 15 to 79 years old between 1979 and 2015 in Brazil. Whether bright green colours represent the lowest mean values of YPLL, bright red colours represent the highest values. **c** and **d** Scatter dot plots show *P* values that have been calculated by the two-way ANOVA model followed by correction of multiple comparisons through the control of false discovery rates according to the two-stage step-up method of Benjamini, Krieger, and Yekutieli

(RS) had the highest mortality rates of CC in the region (Fig. 4). Whether the Rio Grande do Sul (RS) male population had the highest mortality values due to RC events (Fig. 5), women living in the state of Parana (PR) showed the highest mortality for this disease when compared to the female population of other southern states (Fig. 5).

Discussion

Cancer mortality rates for both CC and RC cases have significantly increased over the years in Brazil. One should note that CC mortality was higher than RC-related deaths. Since RC events have been widely associated with poor patient survival [3], we believe that the Brazilian population has a higher incidence of CC than RC-related events. Arnold and colleagues have analysed CC and RC mortality rates in 42 countries and reported similar findings to ours in Brazil [19].

Our findings also suggest that CC and RC mortality rates may rise even higher in the coming years. This finding is in keeping with what has been reported by previous studies for a time range similar to ours [8, 19, 20]. Moreover, Jemal and colleagues predicted the number of CRC-related deaths worldwide (881,000 events) and ranked this disease second among the malignancies most related to fatal cases in 2018 [1]. Indeed, increased incidence and mortality rates of this disease have been suggested as a marker of socioeconomic development [1]. Bray et al. suggest that Brazil is one of those nations where CRC incidence and mortality have increased in recent years [1].

In contrast, countries observed to have a decreasing incidence and mortality rates have been the USA, Japan, and France [21]. In the USA and Japan, this effect could partially be related to the implementation of long-standing screening and early detection programmes against CRC [22]. However, food-related issues promoting obesity in the younger American adult population has also been suggested to be associated with increasing CRC incidence in patients aged < 50 years old [7, 9].

Analysing CC and RC mortality rates over time and across different Brazilian regions suggests that potential changes in lifestyle have occurred in recent years. This notion seems more evident when analysing YPLL rates found in the Brazilian population. One should consider that changes in

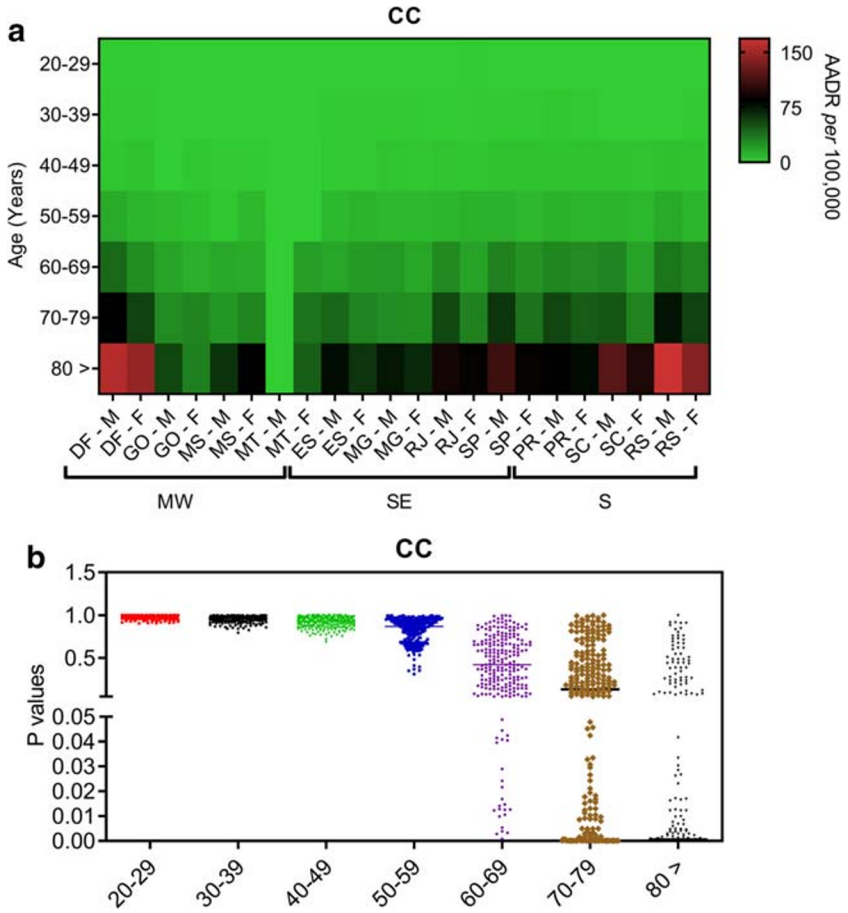

Fig. 4 Age-adjusted death rates (AADR) related to colon cancer events (CC) during the year of 2015 are shown for both male (M) and female populations (F) living in different Brazilian states according to their regional location in the country. **a** AADR values related to CC are shown in different populations with age ranging from 20 to 80 years old during the year of 2015 in Brazil. These values were determined based on data from regional health centres (RHCs) within each Brazilian state in the Midwest (MW; Federal capital region [DF; RHC = 1], Goias state [GO; RHC = 16], and Mato Grosso do Sul [MS; RHC = 12] and Mato Grosso [MT; RHC = 16] states), Southeast (SE; Espirito Santo [ES; RHC = 4], Minas Gerais [MG; RHC = 16], Rio de Janeiro [RJ; RHC = 9], and Sao Paulo [SP; RHC = 16] states), and South regions (S; Parana [PR; RHC = 16], Santa Catarina [SC; RHC = 16], and Rio Grande do Sul [RS; RHC = 16]). Values have been adjusted to the Brazilian population of 2010. Whether bright green colours represent the lowest mean values of AADR in each Brazilian region, bright red colours represent the highest values. **b** Scatter dot plots show *P* values that have been calculated by the two-way ANOVA model followed by correction of multiple comparisons through the control of false discovery rates according to the two-stage step-up method of Benjamini, Krieger, and Yekutieli

diet, body weight, and lifestyle could explain trends towards high CRC incidence, while best practices in cancer management and treatment may reduce mortality for this disease [21]. Besides the fact that a sound healthcare system decreases the number of cancer-related deaths, lifestyle profoundly impacts on both cancer risk and survival of patients. India seems to illustrate how changes in lifestyle impacts on CRC incidence and mortality. GLOBOCAN-based studies show that whether CRC incidence and mortality were lower in India than in Brazil by 2012 [21], analysing the same patterns 6 years later highlights a significant elevation of this disease in the Indian male population [1]. An Indian research group recently suggested that healthier lifestyle habits could reduce CRC incidence in the country [23]. In Brazil, research groups have been reporting frequent physical inactivity in the younger population, increasingly high intakes of red meat, and low consumption of fruits overall [24–27]. Folgueira and colleagues analysed 88 cases of gastric cancer and found that poor eating habits could be related to the development of this malignancy in younger adults living in Brazil [28].

The Brazilian population living in the southern regions of the country appear to exhibit the highest mortality rates for both CC and RC events. The male inhabitants of these Brazilian states may have a much higher mortality risk by either CC or RC than the female population. The Rio Grande do Sul (RS) state has previously been found to have the highest CRC mortality rates in Brazil [14]. Bray et al. have recently reported that the male population has a 50% higher chance of dying by any type of cancer than women worldwide [1]. A previous study carried out in the RS state revealed CRC to be the most prevalent type of cancer in both sexes combined, as prostate malignancies are the most common in men

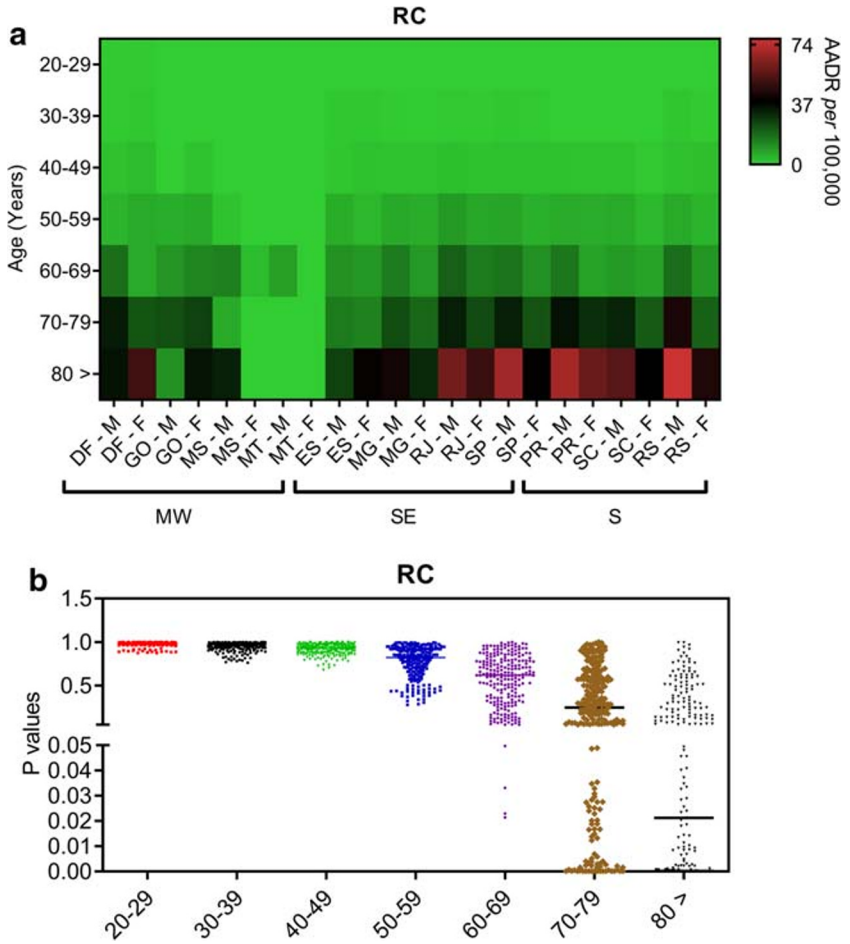

Fig. 5 Age-adjusted death rates (AADR) related to rectal cancer events (RC) during the year of 2015 are shown for both male (M) and female populations (F) living in different Brazilian states according to their regional location in the country. **a** AADR values related to RC are shown in different populations with age ranging from 20 to 80 years old during the year of 2015 in Brazil. These values were determined based on data from regional health centres (RHCs) within each Brazilian state in the Midwest (MW; Federal capital region [DF; RHC = 1], Goias state [GO; RHC = 16], and Mato Grosso do Sul [MS; RHC = 12] and Mato Grosso [MT; RHC = 16] states), Southeast (SE; Espirito Santo [ES; RHC = 4], Minas Gerais [MG; RHC = 16], Rio de Janeiro [RJ; RHC = 9], and Sao Paulo [SP; RHC = 16] states), and South regions (S; Parana [PR; RHC = 16], Santa Catarina [SC; RHC = 16], and Rio Grande do Sul [RS; RHC = 16]). Values have been adjusted to the Brazilian population of 2010. Whether bright green colours represent the lowest mean values of AADR in each Brazilian region, bright red colours represent the highest values. **b** Scatter dot plots show *P* values that have been calculated by the two-way ANOVA model followed by correction of multiple comparisons through the control of false discovery rates according to the two-stage step-up method of Benjamini, Krieger, and Yekutieli

and breast cancer in women [29]. Although heredity impact on CRC risk even in Brazil [30], two independent studies have shown that only specific rare mutations may impact a small percentage of the Brazilian population in general [31–33]. Assunção and colleagues reported that processed meats are now consumed very regularly by the Rio Grande do Sul (RS) inhabitants [34]. The Brazilian population seems to have acquired unhealthy eating habits in recent years [24, 25, 27, 28]. Consumption of red or processed meat seems to be an established risk factor promoting CRC [35]. Since the implementation of longer-standing screening and early detection programmes, CRC mortality seems to have decreased in other countries [22]. Frasca and colleagues report that testing for faecal occult blood could provide a significant strategy for early detection of CRC in the Brazilian population [36].

We must further consider that the Brazilian population is rapidly ageing and that this process has the potential to increase the risk of cancer besides the threat imposed by an unhealthy lifestyle [5, 10]. Recent studies have demonstrated that ageing decreases proliferation rates but increases the mutational load in humans or any other given organism [37, 38]. Although these findings seem controversial at first sight, DeGregori suggested that ageing provides the required length of time required for oncogenic mutations to accumulate and cancer to arise in a particular body site [39]. While the Brazilian population is undergoing significant changes in lifestyle factors to closely mirror those in developed Western societies, expansion of its elderly population is coupled with a lack of efficient anticancer health programmes reported to lower CRC incidence in developed Western regions [1, 10, 11,

13, 20, 40]. Thus, it is no surprise that we report herein increasing CC and CRC mortality in this Brazil region currently and in the coming decades. The current Brazilian scenario unfortunately seems to be set ideally for exponential increases in CRC incidence and mortality in the coming decades.

Although our findings are in keeping with previous national and international forecasting that CRC incidence and mortality rates would increase in Brazil [8, 20], this current study has some limitations that should be considered. First, we must consider that the period required for data consolidation in a public database results in a few years gap from the time that death events have been registered until the release of data to the public. This secondary data usage further limits the study design, as well as the interpretation of these results at an individual level. Moreover, registration errors at SIM can, in a hypothetical scenario, lead to under- or overestimation of incidence and mortality rates of any given disease. Nevertheless, mortality trends can also be slightly modified in case new diagnostic and therapeutic guidelines are implemented in the country during the predicted time-lapse [13, 20, 40, 41].

Our current findings suggest that mortality rates for CC and RC are rapidly rising throughout many Brazilian regions. This scenario may worsen in the coming years, as Brazilians are readily acquiring dietary and lifestyle habits from Western developed countries that have a consistent pattern for high incidence and mortality related to CRC. The most needed attention regarding healthcare strategy in treatment and prevention should be given to the inhabitants of the RS state, as high rates of CC and RC mortality have been observed here for consecutive decades now. New studies on cancer-related deaths in the RS state are required now, as future findings may help to decrease mortality rates for other types of cancer in different regions of Brazil.

Funding Information The authors disclose receipt of the following financial support for the development of this investigation: Sao Paulo Research Foundation (FAPESP; 2014/06428-5; 2015/01723-1). The funder had no role in the study design, data collection, analysis, decision to publish, or preparation of the manuscript.

Compliance with Ethical Standards

Conflict of Interest The authors declare that that they no competing interest.

References

1. Bray F, Ferlay J, Soerjomataram I, Siegel RL, Torre LA, Jemal A. Global cancer statistics 2018: GLOBOCAN estimates of incidence and mortality worldwide for 36 cancers in 185 countries. CA Cancer J Clin. 2018;68(6):394–424.
2. Sundling KE, Zhang R, Matkowskyj KA. Pathologic features of primary colon, rectal, and anal malignancies. Cancer Treat Res. 2016:168309–30.
3. Riihimaki M, Hemminki A, Sundquist J, et al. Patterns of metastasis in colon and rectal cancer. Sci Rep. 2016;629765.
4. Kuipers EJ, Grady WM, Lieberman D, et al. Colorectal cancer. Nat Rev Dis Prim. 2015;115065.
5. Wang T, Maden SK, Luebeck GE, Li CI, Newcomb PA, Ulrich CM, et al. Dysfunctional epigenetic aging of the normal colon and colorectal cancer risk. Clin Epigenetics. 2020;12(1):5.
6. Torre LA, Bray F, Siegel RL, et al. Global cancer statistics, 2012. CA Cancer J Clin. 2015;65(2):87–108.
7. Sung H, Siegel RL, Rosenberg PS, Jemal A. Emerging cancer trends among young adults in the USA: analysis of a population-based cancer registry. Lancet Public Health. 2019;4(3):e137–47.
8. Arnold M, Sierra MS, Laversanne M, et al. Global patterns and trends in colorectal cancer incidence and mortality. Gut. 2016.
9. Siegel RL, Fedewa SA, Anderson WF, et al. Colorectal cancer incidence patterns in the United States, 1974–2013. J Natl Cancer Inst. 2017;109(8).
10. Tramujas Vasconcellos Neumann L, Albert SM, Aging in Brazil. Gerontologist. 2018;58(4):611–617.
11. Sousa N, Medina LPB, Bastos TF, et al. Social inequalities in the prevalence of indicators of active aging in the Brazilian population: National Health Survey, 2013. Rev Bras Epidemiol. 2019;22Suppl 02(Suppl 02):E190013 SUPL 190012.
12. Silva ACB, Vicentini MFB, Mendoza EZ, Fujiki FK, da Fonseca LG, Braghiroli MIFM, et al. Young-age onset colorectal cancer in Brazil: analysis of incidence, clinical features, and outcomes in a tertiary cancer center. Curr Probl Cancer. 2019;43(5):477–86.
13. Oliveira RC, Rego MA. Mortality risk of colorectal cancer in Brazil from 1980 to 2013. Arq Gastroenterol. 2016;53(2):76–83.
14. Oliveira MM, Latorre M, Tanaka LF, et al. Disparities in colorectal cancer mortality across Brazilian States. Rev Bras Epidemiol. 2018;21e180012.
15. Swaroop S, Uemura K. Proportional mortality of 50 years and above; a suggested indicator of the component health, including demographic conditions in the measurement of levels of living. Bull World Health Organ. 1957;17(3):439–81.
16. Hansen ES. The proportionate mortality ratio and its relationship with measures of mortality. Stat Med. 1990;9(3):315–23.
17. Romeder JM, McWhinnie JR. Potential years of life lost between ages 1 and 70: an indicator of premature mortality for health planning. Int J Epidemiol. 1977;6(2):143–51.
18. Yerushalmy J. A mortality index for use in place of the age-adjusted death rate. Am J Public Health Nations Health. 1951;41(8 Pt 1):907–22.
19. Araghi M, Soerjomataram I, Jenkins M, et al. Global trends in colorectal cancer mortality: projections to the year 2035. Int J Cancer. 2019;144(12):2992–3000.
20. Souza DL, Jerez-Roig J, Cabral FJ, de Lima JR, Rutalira MK, Costa JA. Colorectal cancer mortality in Brazil: predictions until the year 2025 and cancer control implications. Dis Colon Rectum. 2014;57(9):1082–9.
21. Arnold M, Sierra MS, Laversanne M, et al. Global patterns and trends in colorectal cancer incidence and mortality. Gut. 2017;66(4):683–91.

22. Schreuders EH, Ruco A, Rabeneck L, et al. Colorectal cancer screening: a global overview of existing programmes. Gut. 2015;64(10):1637–49.
23. Sinha R, Doval DC, Hussain S, et al. Lifestyle and sporadic colorectal Cancer in India. Asian Pac J Cancer Prev. 2015;16(17):7683–8.
24. Nogueira Bezerra I, de Carvalho Gurgel AO, Bastos Barbosa RG, et al. Dietary behaviors among young and older adults in Brazil. J Nutr Health Aging. 2018;22(5):575–80.
25. de Carvalho AM, Cesar CL, Fisberg RM, et al. Excessive meat consumption in Brazil: diet quality and environmental impacts. Public Health Nutr. 2013;16(10):1893–9.
26. Duarte APP, Rodrigues PRM, Ferreira MG, et al. Socio-economic and demographic characteristics associated with risk behaviour patterns for chronic non-communicable diseases in Brazil: data from the National Health Survey. Public Health Nutr. 2013;2019:1–9.
27. de Carvalho AM, Cesar CL, Fisberg RM, et al. Meat consumption in Sao Paulo-Brazil: trend in the last decade. PLoS One. 2014;9(5): e96667.
28. Guindalini RSC, Cormedi MCV, Maistro S, et al. Frequency of CDH1 germline variants and contribution of dietary habits in early age onset gastric cancer patients in Brazil. Gastric Cancer. 2019.
29. da Silva FB, Binato M, da Silva JT, et al. Prevalence of solid neoplasms diagnosed between the years of 2011 to 2016 and oncologically treated at the University Hospital of Santa Maria. J Clin Med Res. 2019;11(4):275–82.
30. Abud J, Koehler-Santos P, Ashton-Prolla P, et al. CHEK2 1100DELC germline mutation: a frequency study in hereditary breast and colon cancer Brazilian families. Arq Gastroenterol. 2012;49(4):273–8.
31. Rossi BM, Palmero EI, Lopez-Kostner F, et al. A survey of the clinicopathological and molecular characteristics of patients with suspected lynch syndrome in Latin America. BMC Cancer. 2017;17(1):623.
32. Vaccaro CA, Lopez-Kostner F, Adriana DV, et al. From colorectal cancer pattern to the characterization of individuals at risk: picture for genetic research in Latin America. Int J Cancer. 2018.
33. Cossio SL, Koehler-Santos P, Pessini SA, et al. Clinical and histomolecular endometrial tumor characterization of patients at-risk for lynch syndrome in south of Brazil. Familial Cancer. 2010;9(2):131–9.
34. Schneider BC, Duro SM, Assuncao MC. Meat consumption by adults in southern Brazil: a population-based study. Cien Saude Colet. 2014;19(8):3583–92.
35. Bouvard V, Loomis D, Guyton KZ, Grosse Y, Ghissassi FE, Benbrahim-Tallaa L, et al. Carcinogenicity of consumption of red and processed meat. Lancet Oncol. 2015;16(16):1599–600.
36. Teixeira CR, Bonotto ML, Lima JP, et al. Clinical impact of the immunochemical fecal occult blood test for colorectal cancer screening in Brazil. Ann Gastroenterol. 2017;30(4):442–5.
37. Lee MB, Dowsett IT, Carr DT, Wasko BM, Stanton SG, Chung MS, et al. Defining the impact of mutation accumulation on replicative lifespan in yeast using cancer-associated mutator phenotypes. Proc Natl Acad Sci U S A. 2019;116(8):3062–71.
38. Rozhok AI, DeGregori J. Toward an evolutionary model of cancer: considering the mechanisms that govern the fate of somatic mutations. Proc Natl Acad Sci U S A. 2015;112(29):8914–21.
39. DeGregori J. Challenging the axiom: does the occurrence of oncogenic mutations truly limit cancer development with age? Oncogene. 2013;32(15):1869–75.
40. Dutra VGP, Parreira VAG, Guimaraes RM. Evolution of mortality for colorectal Cancer in Brazil and regions, by sex, 1996-2015. Arq Gastroenterol. 2018;55(1):61–5.
41. Martin FL, Martinez EZ, Stopper H, et al. Increased exposure to pesticides and colon cancer: early evidence in Brazil. Chemosphere. 2018:209623–31.

Journal for ImmunoTherapy of Cancer

Paradoxical interaction between cancer and long-term postsepsis disorder: impairment of de novo carcinogenesis versus favoring the growth of established tumors

Caio Abner Leite ,[1,2,3] Jose Mauricio Mota,[4] Kalil Alves de Lima,[5] Carlos Wagner Wanderley,[5] Leticia Almeida Nascimento,[5] Marcela Davoli Ferreira,[5] Camila Meirelles Souza Silva,[5] David Fernando Colon,[5] Juliana Yumi Sakita,[6] Vinicius Kannen,[6] Paula Ramos Viacava,[5] Maria Dirlei Begnami,[1] Roberto Cesar Pereira Lima-Junior,[7] Vladmir Claudio Cordeiro de Lima,[1] Jose Carlos Alves-Filho,[5] Fernando Queiroz Cunha,[2,5] Ronaldo Albuquerque Ribeiro[3,7]

To cite: Leite CA, Mota JM, de Lima KA, *et al*. Paradoxical interaction between cancer and long-term postsepsis disorder: impairment of de novo carcinogenesis versus favoring the growth of established tumors. *Journal for ImmunoTherapy of Cancer* 2020;**8**:e000129. doi:10.1136/jitc-2019-000129

► Additional material is published online only. To view please visit the journal online (http://dx.doi.org/10.1136/jitc-2019-000129).

Accepted 14 March 2020

For numbered affiliations see end of article.

Correspondence to
Dr Fernando Queiroz Cunha; fdqcunha@fmrp.usp.br

ABSTRACT

Background Previous data have reported that the growth of established tumors may be facilitated by postsepsis disorder through changes in the microenvironment and immune dysfunction. However, the influence of postsepsis disorder in initial carcinogenesis remains elusive.

Methods In the present work, the effect of postsepsis on inflammation-induced early carcinogenesis was evaluated in an experimental model of colitis-associated colorectal cancer (CAC). We also analyzed the frequency and role of intestinal T regulatory cells (Treg) in CAC carcinogenesis.

Results The colitis grade and the tumor development rate were evaluated postmortem or in vivo through serial colonoscopies. Sepsis-surviving mice (SSM) presented with a lower colonic DNA damage, polyp incidence, reduced tumor load, and milder colitis than their sham-operated counterparts. Ablating Treg led to restoration of the ability to develop colitis and tumor polyps in the SSM, in a similar fashion to that in the sham-operated mice. On the other hand, the growth of subcutaneously inoculated MC38luc colorectal cancer cells or previously established chemical CAC tumors was increased in SSM.

Conclusion Our results provide evidence that postsepsis disorder has a dual effect in cancer development, inhibiting inflammation-induced early carcinogenesis in a Treg-dependent manner, while increasing the growth of previously established tumors.

INTRODUCTION

Colorectal cancer (CRC) is a major health issue worldwide and inflammation has been directly linked to CRC development and tumor progression.[1 2] Among many other factors, proinflammatory mediators and increased oxidative stress were postulated as initiator mechanisms of carcinogenesis in CRC.[3] This is supported by the increased risk of CRC in patients with inflammatory bowel disease and by the reduced incidence of polyps and CRC after the long-term use of cyclooxygenase inhibitors.[4]

Beyond local inflammation, additional systemic immune modifications, such as immunosuppression, are expected to modify cancer development.[5] Sepsis is a life-threatening organ dysfunction caused by a deregulated host response to an infectious agent.[6] Patients who survive to severe sepsis commonly develop a profound anti-inflammatory response, which predisposes to secondary infections,[7] higher mortality, and possibly cancer.[8 9 10] In the experimental setting, accumulating evidence have demonstrated that regulatory T cells (Treg) mediate the immune paralysis in the late-phase sepsis.[11]

Tregs are crucial for intestinal homeostasis through the regulation of local immune response.[12] The adoptive transfer of Tregs inhibits the development of experimental colitis-associated colorectal cancer (CAC), and CRC associated with *APC* mutation.[13 14] Accordingly, the systemic ablation of Tregs in experimentally established CAC attenuates tumor growth through the expansion of $CD8^+$ T cells.[15] Altogether, these findings shed light on a potential dual role of Tregs in CRC carcinogenesis.

The question that comes up is whether postsepsis disorder may interfere with initial inflammation-induced CRC carcinogenesis

and whether Treg expansion during postsepsis may interfere in this scenario. The present study shows that postsepsis disorder decreases inflammation-induced colorectal tumors in a Treg-dependent manner while promoting the growth of previously established colorectal tumors.

MATERIAL AND METHODS

Mice

Six-week to 8-week-old male C57BL/6 mice and *Foxp3*^{DTR} knock-in mice (depletion of regulatory T cell (DEREG); Jackson Laboratory, USA) mice were bred and housed in the laboratory animal facility of the Ribeirao Preto Medical School (Sao Paulo, Brazil) and were kept in appropriate cages in temperature-controlled rooms with 12 hours dark–light cycles. They received sterilized food and acidified water ad libitum.

Sepsis and postsepsis model

Polymicrobial sepsis was induced by cecal and ligation puncture (CLP), as described previously.[16] To save approximately 50% of mice after severe sepsis, the animals were treated with ertapenem (20 mg/kg, i.p., Merck Research Laboratory, Whitehouse Station, NJ) 6 hours after surgery, and every 12 hours for 3 days. The controls were sham operated, and they also received treatment with ertapenem (figure 1A).

AOM/DSS protocol

CAC was induced as described before with minor alterations.[17] Azoxymethane (AOM)/dextran sodium sulfate (DSS) is a protocol composed of two hits. At first, AOM transforms some cells into a malignant phenotype, and DSS promotes colitis and CAC. Fifteen days after CLP, the mice were injected with the carcinogen AOM (10 mg/kg, i.p.; Sigma Chemical Co. St. Louis, Missouri, USA). After 5 days, the mice received drinking water supplemented with 2% DSS (Sigma Chemical Co.; MW, 36–50 kDa) for 5 days. Each cycle of DSS was repeated three times every 15 days. The mice were euthanized at day 65 (figure 1A). The colon length was registered as an indirect measure of colitis. Samples of colon tissue were harvested for histological analysis, cytokine measurement via ELISA, and Treg quantification via flow cytometry.

Colonoscopy

The animals were anesthetized with isoflurane (1 mL/mL, Cristalia, Brazil) and were submitted to a warm saline enema prior to colonoscopy. A high-resolution mouse video endoscope (TELE PACK VET X, Karl Storz) was used for monitoring colitis and local tumorigenesis, following a described protocol.[18] The material consists of a camera, a light source, a monitor, a HOPKINS Forward-Oblique Telescope 30° (diameter 1.9 mm, length 10 cm) and a protection sheath. Colonoscopies were performed by a blinded examiner.

Colitis grading and tumor development quantification

Colitis was scored by four parameters (perianal findings, wall transparency, intestinal bleeding, and focal lesions), and the sum of scores ranged from 0 to 12 (0 being the absence of colitis and 12 being the most severe colitis).[18]

Tumor development was assessed by measuring the number and size of neoplastic lesions. Tumor load was determined by size, as described: score 1, just detectable; score 2, tumor covering up to one-eighth of the colonic circumference; score 3, tumor covering up to one-fourth of the colonic circumference; score 4, tumor covering up to half of the colonic circumference; score 5, tumor covering more than half of the colonic circumference (figure 2A).[19]

Histological analysis

All colonic lesions (inflammation, polyps and tumors) were fixed in phosphate-buffered formalin and unblocked in paraffin. Tissue sections (4.0 µm) were prepared from the paraffin-embedded tissue blocks, stained with H&E, and evaluated in a blinded fashion by an experienced pathologist, MDB.

Colitis was scored from 0 to 6 according to cell infiltration and tissue damage.[20] Focally increased numbers of inflammatory cells in the lamina propria were scored as 1, inflammatory cells extending into the submucosa as 2 and transmural infiltration as 3. For tissue damage, mild lymphoepithelial lesions were scored as 1, erosions as 2, and extensive mucosal damage as 3.

All polyps and suspected lesions were microscopically evaluated and were classified as follows: normal colon, polyp without dysplasia, adenoma with low-grade dysplasia, adenoma with high-grade dysplasia, and invasive adenocarcinoma.

Western blotting assay

Following euthanasia 3 days after AOM injection, colon samples were harvested in radioimmunoprecipitation assay buffer (Thermo Scientific, USA) supplemented with a protease (Roche) and phosphatase (Calbiochem) inhibitors. The protein concentration was determined using the Pierce BCA Protein Assay Kit (Thermo Scientific, USA). Equivalent amounts of protein (30 µg) in each extract were separated by electrophoresis on polyacrylamide gel followed by transfer to blotting membrane (GE Healthcare Life Sciences, GE). Next, membranes were incubated at 4°C overnight antibodies against γH2A.X (ab81299; 1:5000; ABCAM, USA) and anti-glyceraldehyde-3-phosphate dehydrogenase (GAPDH) antibody (ab181602; 1:10,000; ABCAM, USA). Next, the membrane was incubated with a secondary antibody conjugated with peroxidase. Chemiluminescence reactions on membranes were imaged using the ChemiDocTM XRS+System (BioRad, Life Technologies, Carlsbad, California, USA).

Real-time PCR qRT-PCR was conducted for specific genes related with DNA repair e cell proliferation (*ATM*, *ATR*, *MGMT* (O-6-methylguanine-DNA

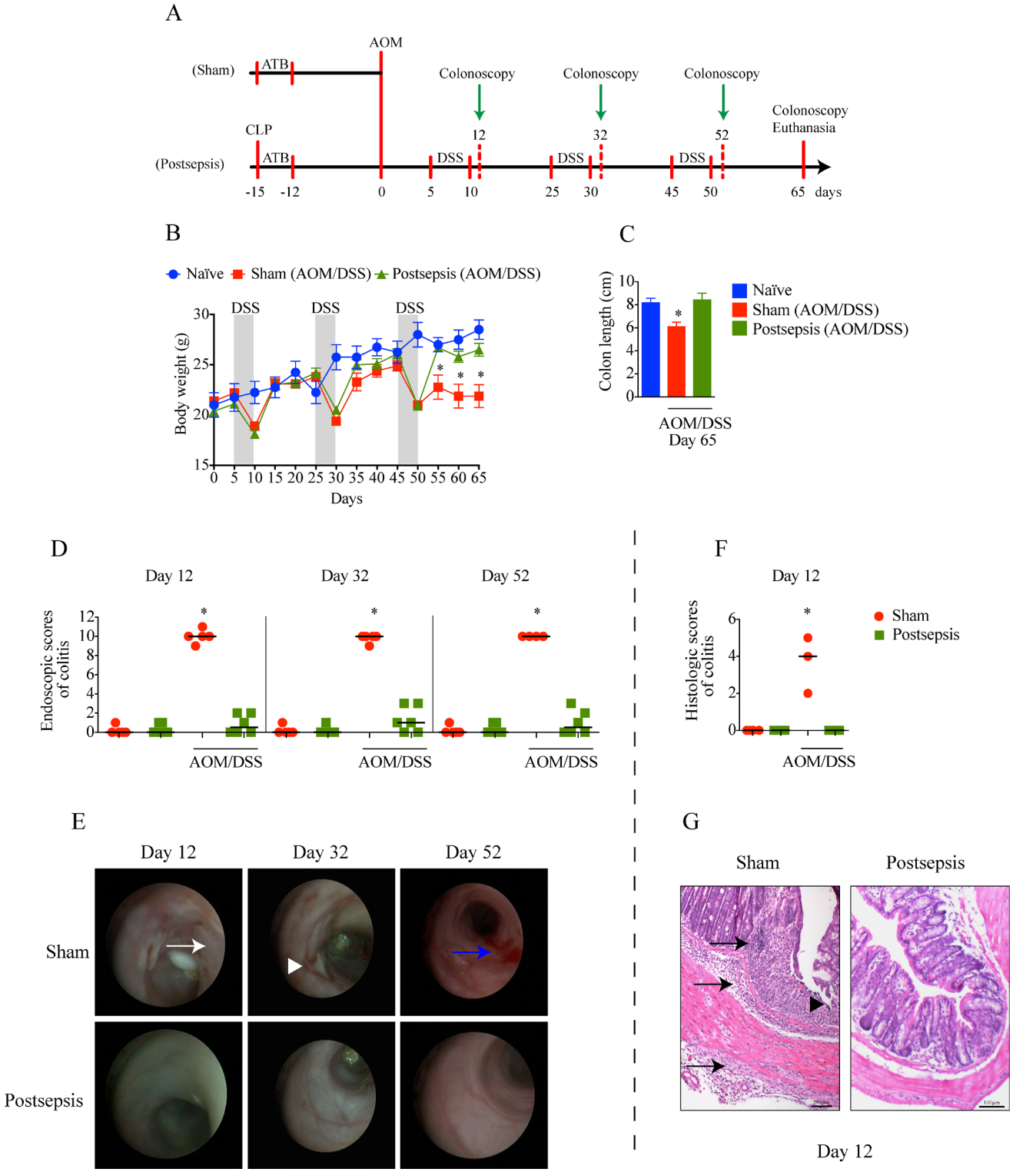

Figure 1 Postsepsis state prevents the development of azoxymethane (AOM)/dextran sodium sulfate (DSS)-induced colitis. (A) Schematic schedule of the administration of AOM and DSS in sham and postsepsis mice. (B) Temporal weight change of naive mice (blue, n=4), AOM/DSS-treated sham mice (red, n=10) and AOM/DSS-treated postsepsis mice (green, n=10). (C) Comparison of colon length at day 65 in naïve mice (n=4), AOM/DSS-treated sham (n=10) and postsepsis mice (n=10). (D) Endoscopic scores of colitis at days 12, 32, and 52 post-AOM administration. (E) Representative endoscopic images from the distal colon of sham (red circles) and postsepsis mice (green squares) at days 12, 32 and 52. (F) Histological scores of colitis at day 12 post-AOM administration. (G) Photomicrographs of representative (H&E staining) colons of sham-operated and postsepsis mice at day 12. White arrow: thick wall; white arrowhead: ulcer; blue arrow: bleeding; black arrow: transmural leukocyte infiltration; black arrowhead: erosion. The experiments were repeated three times. Data demonstrate a representative experiment. Data, mean±SEM. * (B) p=0.0006, (C) p=0.0076, (D) p<0.0001, (F) p<0.0001. CLP, cecal and ligation puncture; ATB, antibiotic.

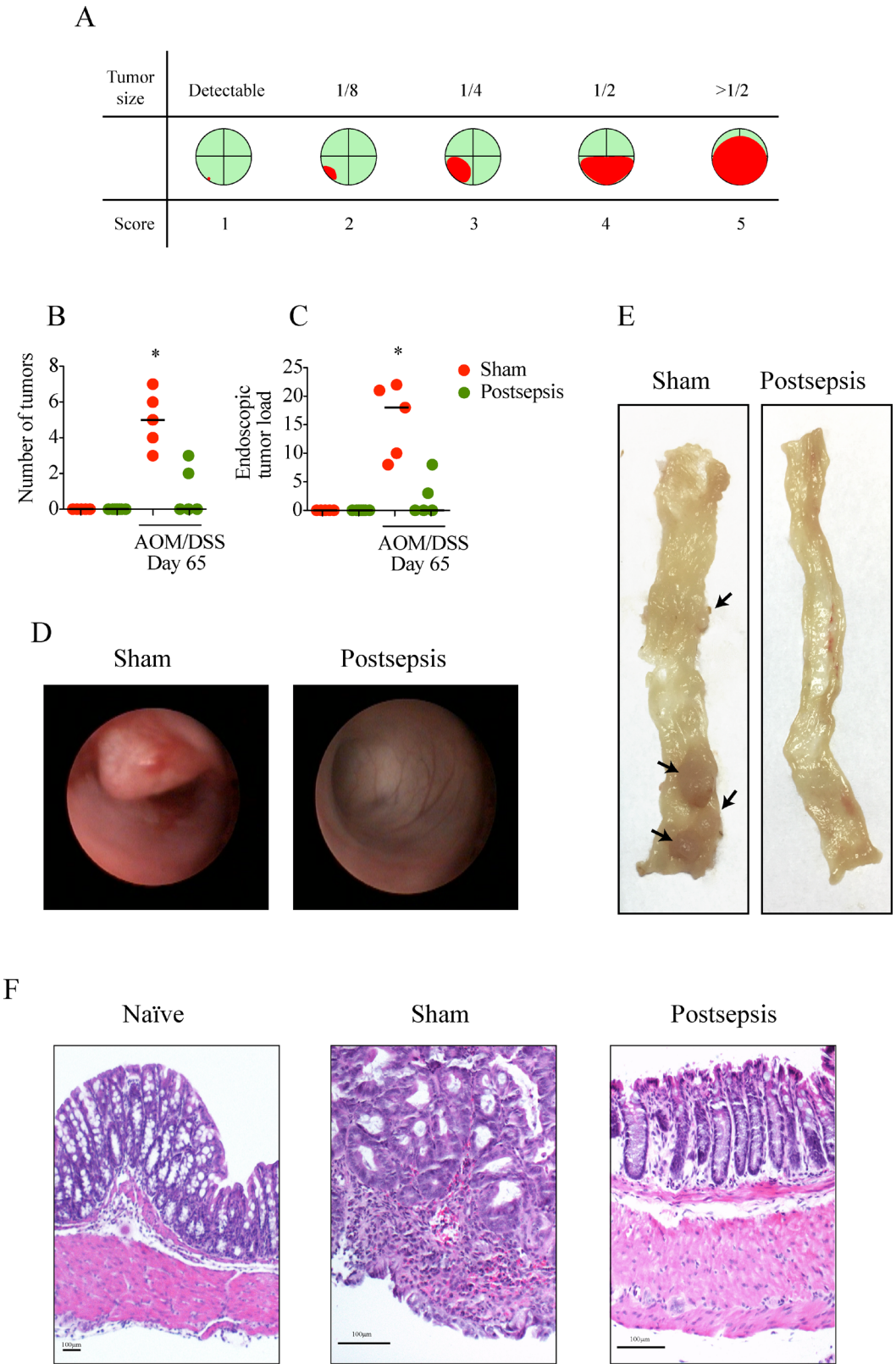

Figure 2 Colitis-associated cancer is impaired in sepsis-surviving mice. (A) Schematic schedule of the tumor-load scoring system. The red color indicates how polyps/tumors occupy the intestinal lumen as seen in colonoscopy. (B) Endoscopic number of colonic tumors and (C) tumor load per mice in sham (red circles) and postsepsis mice (green circles) following azoxymethane (AOM)/dextran sodium sulfate (DSS)-induced colitis (n=5 per group). (D) Representative endoscopic images from the distal colon of sham (left) and postsepsis mice (right) at day 65. (E) Representative images of colons of sham (left) and postsepsis mice (right) evidencing tumor development only in the sham group. (F) Photomicrographs of representative (H&E staining) tumor samples from sham and postsepsis mice. The experiments were repeated three times. Data demonstrate a representative experiment. Data, mean±SEM. *, p<0.0001.

methyltransferase), *ALKB1, P53, KI67* and *βCAT* (β-catenin)). Total RNA was obtained using RNeasy Mini Kit (Qiagen, DE) and total RNA was reverse transcribed using high-capacity cDNA RT Kit (Applied Biosystem) according to manufacturer's instructions. cDNA was used as template for qPCR of genes of interest using Taqman Universal Master Mix II with UNG (Applied Biosystems). TaqMan probes were acquired from Thermo Fisher Scientific (USA): *Atm* (Mm01177457), *Atr* (Mm01223626), *MGMT* (Mm00485014), *ALKB1* (Mm012968822), *Trp53* (Mm01731290), *Ki67* (Mm01278617), *β-Catenin* (Ctnnb1; Mm00483039_m1) and *Gapdh* (Mm99999915_g1). Data were collected and analyzed using an Eppendorf Mastercycler RealPlex2 system (Eppendorf, DE). The fold change was calculated using the $2^{-\Delta\Delta Ct}$ method (Gapdh as a housekeeping gene).

Cytokine quantification

On days 0, 12, 52 and 65, the mice were euthanized, and the colons were collected and homogenized in a lysis buffer containing protease inhibitors. Interferon (IFN)-γ, interleukin (IL)-1β, IL-6, keratinocyte chemoattractant (KC), tumor necrosis factor (TNF), IL-33 and tumor growth factor (TGF)-β in intestinal mucosa were quantified using the Milliplex Map Kit (Cat. MCYTOMAG-70K, Merck, USA), according to the manufacturer's recommendations. The assay was run on a Luminex MagPix instrument (Luminex Corporation, USA).

Isolation of colonic intraepithelial lymphocytes (IELs)

Colonic IELs were isolated as described previously,[21] with minor alterations. Briefly, the colons were flushed with phosphate-buffered saline (PBS) to remove feces, opened longitudinally, and cut transversally into 1.0 cm fragments. The tissue fragments were washed with PBS, were placed in RPMI-1640 containing EDTA 0.5 M and DTT 1 M for 30 min at 37°C with rotation and were vortexed thoroughly. To obtain IELs, the cell suspension was passed through a 40 µm cell strainer and was washed twice with cold culture medium.

Flow cytometry analysis

The IELs were stained with fluorochrome-labeled anti-mouse CD4 (RM4-5, BD Biosciences, USA). Intracellular detection of Foxp3 was performed using the Foxp3 Staining Kit from BD Bioscience with anti-Foxp3 (MF-23, BD Biosciences, USA), according to the manufacturer's recommendations. The cells were quantified via flow cytometry on a FACSCanto (BD Biosciences, USA) and were blindly analyzed using the FlowJo software V.9 (FlowJo, LLC, USA).

In vivo depletion of Tregs

Aiming to deplete Tregs, we designed two different protocols using sham or postsepsis animals. In the first set of experiments, the mice received cyclophosphamide (CYP; 100 mg/kg, i.p., Baxter, USA) 1 day before the AOM injection. The second experiment consisted of two injections of diphtheria toxin (DTX; 0.5 mg/animal/day, i.p., Sigma, USA) starting 2 days before AOM in DEREG animals. Treg depletion was confirmed via flow cytometric analysis of the splenic tissue. Colitis and tumor formation were monitored via colonoscopy, as aforementioned.

Growth of previously established tumors in postsepsis mice

To address the potential dual role of the postsepsis state in carcinogenesis, CLP was performed in animals with tumors that were already established. In the first set of experiments, the mice were submitted to the AOM/DSS protocol and were later randomized to the sham operation or CLP group on day 65. All animals received ertapenem, as described above. Tumor development and growth were measured using serial colonoscopy. In another set of experiments, the mice were submitted to CLP or sham operation and were subcutaneously inoculated with 10^5 MC38luc cells derived from C57BL6 murine colon adenocarcinoma 15 days after surgery.[22] Tumor growth was quantified via digital caliper or bioluminescence quantification (IVIS Lumina; Caliper Lifesciences, USA) following D-luciferin administration (150 mg/kg, i.p., Caliper Lifesciences, USA).

Statistical analysis

All results were expressed as the mean±SEM. The differences were assessed using Student's t-test or analysis of variance, followed by Bonferroni's correction when appropriate. Kaplan-Meier plots were used to estimate survival, using the log-rank test to calculate differences between groups. Statistical analysis was performed using the Prism V.5.0 software (GraphPad). Statistical significance was set at a level of $p<0.05$.

RESULTS

Postsepsis disorder prevents AOM/DSS-induced colitis

In a previous report, our group showed that postsepsis disorder increases the tumor growth of subcutaneously inoculated B16 melanoma cells.[10] To investigate the role of the postsepsis condition on the early phases of the inflammation-induced carcinogenic process, we compared the effects of AOM/DSS in sepsis-surviving or sham-operated mice (figure 1A). As depicted in figure 1B, all animals developed weight loss after each cycle of DSS. However, the development of colitis was observed only in the sham-operated group, as quantified by the reductions in colon length (figure 1C) and bowel inflammation and determined both by colonoscopy (figure 1D,E) and microscopic analysis (figure 1F,G). Sham-operated animals submitted to AOM/DSS cycles presented significant thickening, bleeding, erosions, and ulcers by colonoscopy analysis (figure 1E) and edema, transmural leukocyte infiltration and erosion according to microscopic analysis (figure 1G). Notably, none of the above-mentioned parameters were detected in the sepsis-surviving group. Collectively, these results indicate that

the postsepsis state impairs the development of AOM/DSS-induced colitis.

CAC development is impaired in sepsis-surviving mice

Next, tumor development in sham-operated mice was compared with tumor development following sepsis induction. Consistent with our previous data, a significant impairment in the development of CRC was found in sepsis-surviving animals at day 65 after AOM administration (figure 2). The tumor burden (mean number of tumors per colon, figure 2B) and tumor load (figure 2C) were significantly higher in the sham-operated mice than in the sepsis-surviving mice. Notably, 5/5 mice (100%) that were administered AOM/DSS developed tumorous lesions, as identified via colonoscopy (figure 2D) and via gross examination following necropsy (figure 2E). On the other hand, only 40% of postsepsis mice exhibited tumorous lesions (Fisher's exact test—$p<0.05$).

In terms of histopathological features, 25% of sham-operated animals developed invasive adenocarcinoma, one quarter exhibited adenomas with low-grade dysplasia, and 50% presented adenomas with high-grade dysplasia (figure 2F, online supplementary table S1). Conversely, only 25% of sepsis-surviving mice exhibited adenomas with low-grade dysplasia. Importantly, these animals did not develop adenomas with high-grade dysplasia or invasive adenocarcinomas (figure 2F, online supplementary table S1). In summary, these observations demonstrate that the postsepsis condition might modify the colonic environment, and it has a profound impact on the colitis-associated initiation of CRC.

Impairment of CRC development in postsepsis mice is associated with reduced DNA damage and colonic inflammation

Given our previous results and because DNA damage and proinflammatory mediators have been described as crucial for cancer initiation,[23 24] we hypothesized that the immunosuppression observed postsepsis may interfere with colon carcinogenesis by local inhibition of AOM-induced DNA damage and the inflammatory response.

To address this hypothesis, at first, we quantified the amount of histone phosphorylated (γ-H2AX) after the single injection of AOM (figure 3A). As depicted in figure 3B, postsepsis state reduced AOM-induced DNA damage in colon. Since this result did not appear to be related to non-inflammatory gene alterations (figure 3C, D, E, F, G, H, I), we performed a screening of cytokines and chemokines throughout different phases of colitis development (figure 4). By the end of the first DSS cycle (day 12), we found higher levels of proinflammatory cytokines in colonic samples isolated from the sham-operated group compared with those obtained from the sepsis-surviving animals (IFN-γ, IL-1β, IL-6, KC, TNF, and IL-33). These mediators were still elevated at day 65 following AOM treatment (figure 4B, C, D, E, F, G). Of note, the anti-inflammatory cytokine TGF-β was increased in the colon tissues of sham mice only at day 65 of the AOM/DSS protocol (figure 4H). Together, these findings support the idea that the anti-inflammatory postsepsis environment negatively regulates CAC development.

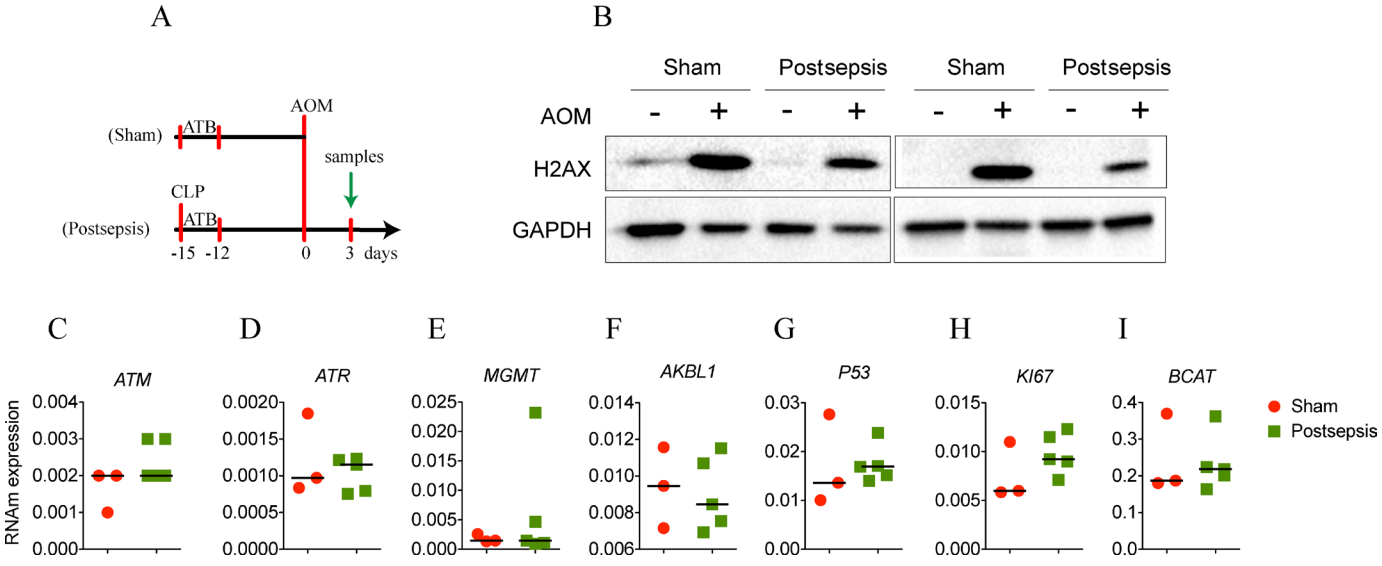

Figure 3 Postsepsis disorder reduces the azoxymethane (AOM)-induced DNA damage. (A) Schematic schedule of DNA-damage evaluation in the model of colitis-associated colorectal cancer. (B) Representative images of western blotting assay of histone phosphorylated (γ-H2AX). The gene expression of (C) *ATM*, (D) *ATR*, (E) *MGMT*, (F) *AKBL1*, (G) *P53*, (H) *KI67*, and (I) *BCAT* was investigated with no differences between sham and postsepsis mice. The experiments were repeated twice. Data demonstrate a representative experiment. Data, mean±SEM. CLP, cecal and ligation puncture; GAPDH, glyceraldehyde-3-phosphate dehydrogenase.

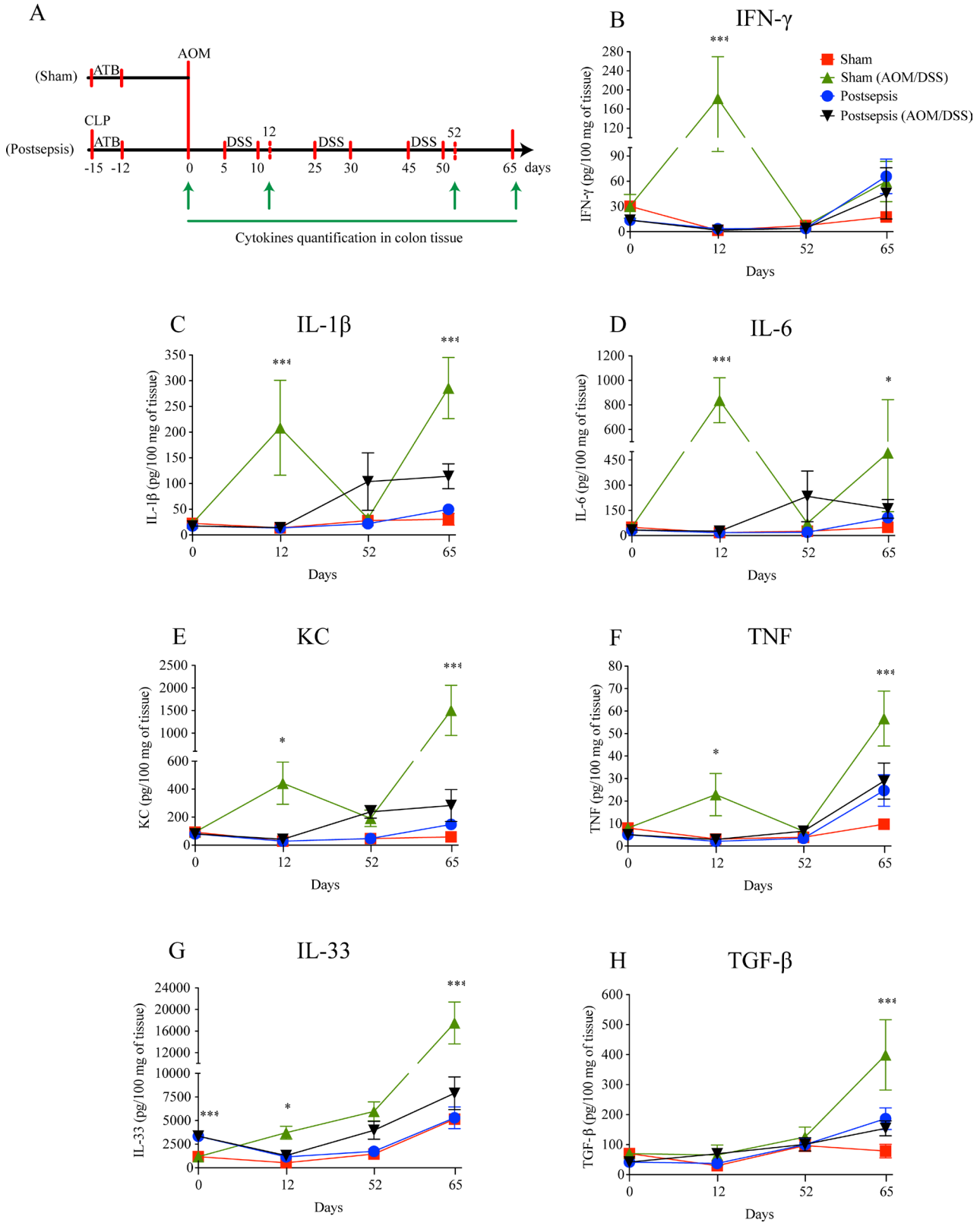

Figure 4 Postsepsis disorder impairs the increase of inflammatory cytokines after colitis induction. (A) Schematic schedule of cytokine quantification in the bowel wall following the model of colitis-associated colorectal cancer. (B) Interferon (IFN)-γ, (C) interleukin (IL)-1β, (D) IL-6, (E) keratinocyte chemoattractant (KC), and (F) tumor necrosis factor (TNF) concentrations peak at day 12 in the sham mice but not in the postsepsis mice. The concentrations of regulatory cytokines (G) IL-33 and (H) tumor growth factor (TGF)-β are increased at day 65 only in the sham mice but not in the postsepsis mice (n=5 per group). The experiments were repeated twice. Data demonstrate a representative experiment. Data, mean±SEM. ***, p<0.0001. *, (D) p=0.0410, (E) p=0.0385, (F) p=0.0097, (G) p=0.0230. AOM, azoxymethane; CLP, cecal and ligation puncture; DSS, dextran sodium sulfate.

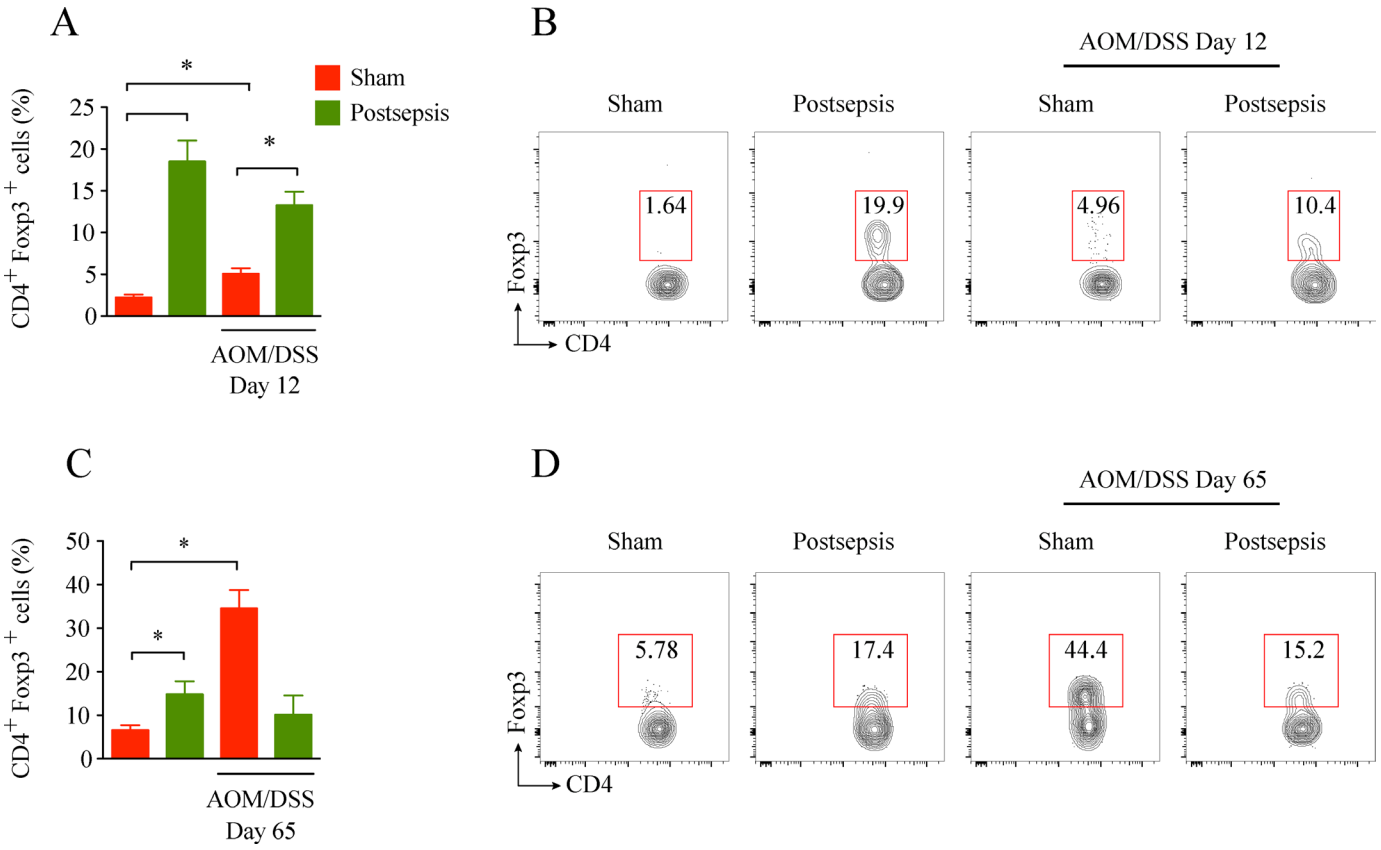

Figure 5 Intraepithelial Tregs are increased at baseline in the bowel of postsepsis mice. (A) Intraepithelial lymphocyte (IEL) infiltration of Tregs in postsepsis mice at the baseline, and after dextran sodium sulfate (DSS) cycle in sham mice (n=5 per group). The graph is representative of two independent experiments. (B) Representative dot plots of flow cytometric analysis performed at day 12. (C) IEL infiltration of Tregs in postsepsis mice at day 65 and in sham mice that were administered azoxymethane (AOM)/DSS (n=5). (D) Representative dot plots of flow cytometric analysis performed at day 65. The experiments were repeated twice. Data demonstrate a representative experiment. Data, mean±SEM. (A) *, p=0.0002, **, p=0.0571, ***, p=0.0253. (B) *, p=0.2904 (not significant), **, p=0.0002, ***, p=0.0013.

Intraepithelial Tregs are increased in the colon of postsepsis mice

T regulatory cells are crucial players during the immunosuppression condition observed after sepsis resolution.[11] To investigate their participation in the impairment of early colorectal carcinogenesis during postsepsis disorder, the frequency of colonic intraepithelial Tregs was measured in our experimental model. As depicted in figure 5 and in accordance with previous reports,[9 11] we found a higher frequency of colonic intraepithelial T CD4$^+$ regulatory cells in the sepsis-surviving mice than in the sham-operated mice. A higher percentage of Tregs cells was observed in the colon of postsepsis mice after the first cycle of DSS (day 12 after AOM administration, figure 5A, B). On the other hand, Tregs were found in higher frequencies among the sham-operated mice when the colon tumors were already established (day 65; figure 5C, D). Collectively, these results suggest that Treg expansion following sepsis resolution is related to the anti-inflammatory colonic environment and the impairment of the initiation of CRC.

Treg depletion restores colonic inflammation and fosters cancer development in postsepsis mice

We next sought to investigate the participation of Tregs in colitis impairment and directly tested its impact on CAC initiation in postsepsis disorder. By taking advantage of DEREG harboring Treg subsets tagged with a human DTX receptor, we were able to efficiently ablate these cells on in vivo DTX administration.[15]

As depicted in figure 6A, in contrast to the sepsis-surviving group, the sham-operated animals depleted of Tregs did not survive after the first cycle of DSS (figure 6A), likely due to severe colitis, as seen on necropsy. The depletion of Tregs in the sepsis-surviving mice restored their competence to develop colitis and colonic tumors, in a similar fashion to sham-operated mice (figure 6B, C, D). Accordingly, the pharmacological depletion of Tregs through low-dose CYP just before the AOM/DSS protocol restored the development of colitis and colorectal tumors in the sepsis-surviving mice (see online supplementary figure S1). In summary, these results support the idea that colonic Treg expansion after sepsis resolution promotes a local anti-inflammatory response and negatively impacts colitis-associated colorectal carcinogenesis.

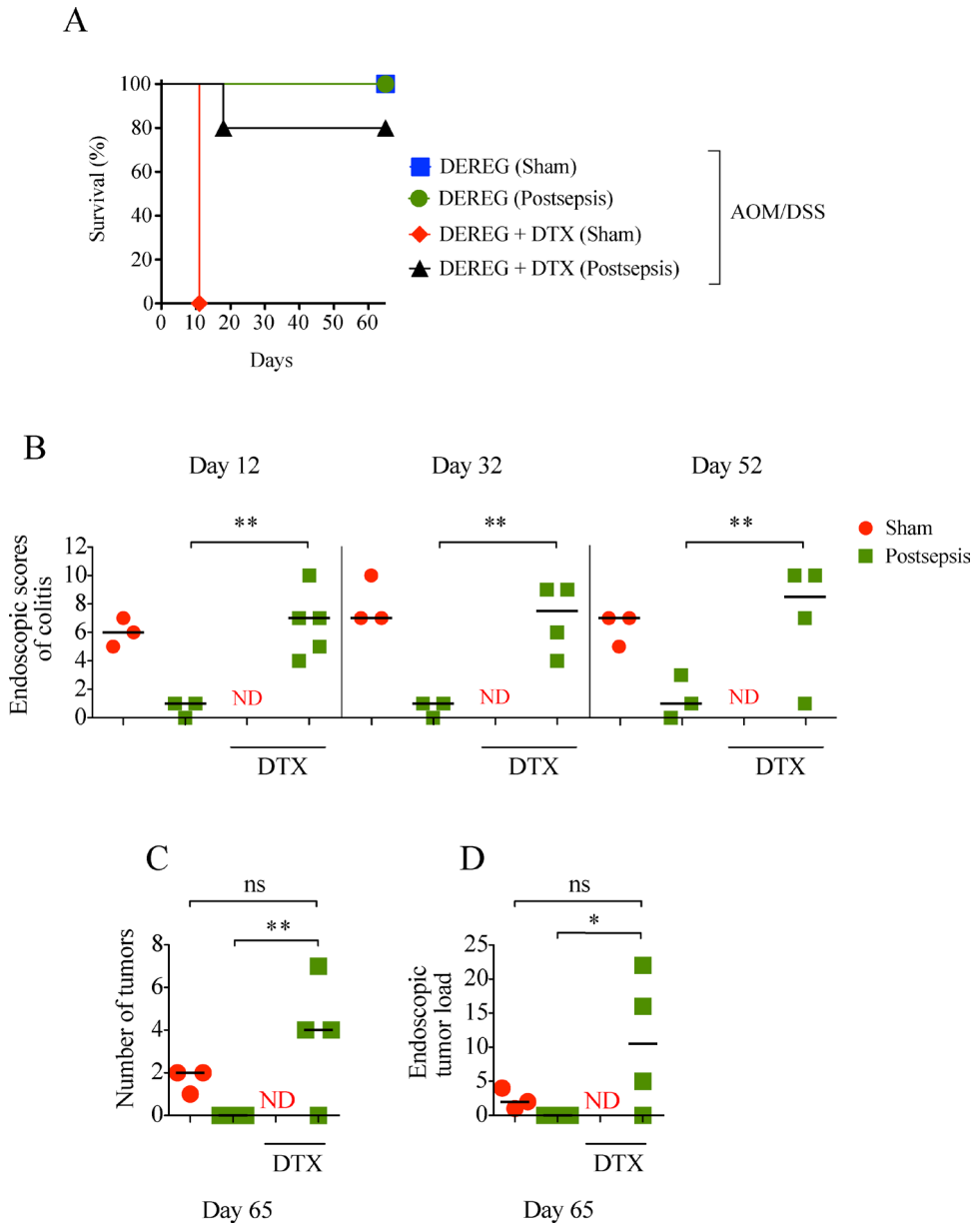

Figure 6 Treg depletion restores colon inflammation and facilitates cancer development in postsepsis mice. (A) Higher mortality in Treg-depleted sham mice after first dextran sodium sulfate (DSS) cycle (depletion of regulatory T cell (DEREG) sham, n=3; DEREG postsepsis, n=3; DEREG +diphtheria toxin (DTX) sham n=6; DEREG +DTX postsepsis, n=5). (B) Endoscopic scores of colitis at days 12, 32, and 52, evidencing colitis in Treg-depleted postsepsis mice. Endoscopic number of colonic tumors (C) and tumor load (D) showing that Treg-depletion postsepsis mice also developed tumors. The experiments were repeated twice. Data demonstrate a representative experiment. Data±SEM. (B) **, p=0.0015, p=0.0031, p=0.0406. (C) *, p=0.0075. (D) *, p=0.0450. ns, not significant; ND, not determined.

Postsepsis disorder is associated with increased growth of established tumors

Since the immunosuppression following sepsis resolution has been described as a relevant promoter of the growth of lung carcinoma and melanoma,[9 10] the effect of postsepsis status was investigated in the context of previously established CAC. For this purpose, we first induced CAC development through the AOM/DSS protocol, which was followed by sepsis induction using the CLP model, as detailed in figure 7A. Notably, the mice were randomly distributed at day 65 of the protocol into 2 groups, the sham operated or postsepsis group, which had an equivalent tumor burden. After 15 days of CLP, both groups maintained a similar number of tumors and tumor load (figure 7B,C).

In contrast to our previous findings in the cancer-initiation protocol, sepsis induction enhanced the number of polyps and the tumor load when colorectal tumors were previously formed (figure 7D, E, F). Assessment of tumor counting is limited by the fact that, during disease progression, two or more polyps/tumors may coalesce which can result in a reduction of the total

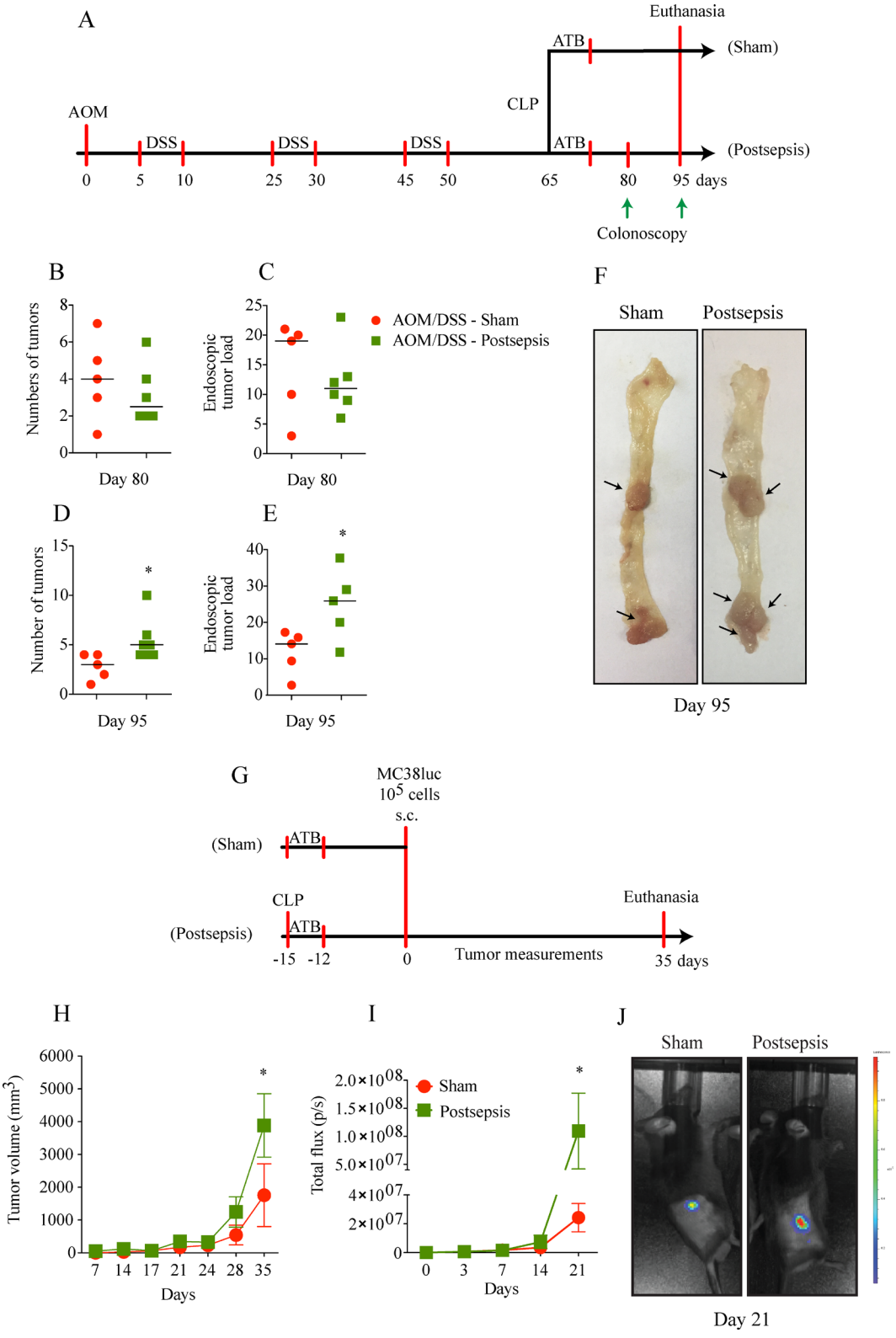

Figure 7 Tumor growth of established tumors is increased in the postsepsis state. (A) Schematic schedule of the azoxymethane (AOM)/dextran sodium sulfate (DSS) protocol, followed by cecal and ligation puncture (CLP). (B)–(E) Number of tumors and tumor load at days (B)–(C) 80 and (D)–(E) 95, respectively, showing increased tumor load in postsepsis group at day 95. (F) Representative images of colons of sham (left) and postsepsis mice (right) evidencing a higher tumor development in postsepsis group. Arrows point to the grossly observed tumors. (G) Schematic schedule of s.c. injection of MC38luc cells in sham and postsepsis mice. (H) and (I) Increased tumor growth in postsepsis group measured via (H) digital caliper and (I) bioluminescence (n=10 per group). (J) Representative animal from each group was analyzed at day 21 for the tumor bioluminescence quantification. The experiments were repeated twice. Data demonstrate a representative experiment. Data, means±SEM. *, (D) p=0.0363, (E) p=0.0336, (H) p=0.0089, (I) p=0.0307.

number of polyps/tumors (figure 7D, E). Furthermore, in the model of subcutaneously implanted MC38luc cells, the postsepsis mice showed increased tumor growth compared with the sham-operated mice (figure 7H, I), which was confirmed by detecting the increased tumor burden following luciferin administration (figure 7J). Together, these findings indicate a potential dual role for postsepsis disorder in the cancer context, which on one hand promotes cancer development in previously established tumors and on the other hand impairs early inflammation-induced carcinogenesis.

DISCUSSION

In the present work, we demonstrated that inflammation-induced carcinogenesis is hampered in postsepsis disorder in a Treg-dependent fashion, while the tumor growth of previously established CRC is increased. To our knowledge, this is the first evidence showing that inflammation-induced early carcinogenesis is impaired following sepsis resolution.

The postsepsis period is characterized by an anti-inflammatory condition,[25] associated with high susceptibility to subsequent infections and/or other diseases, leading to consequent higher mortality rates.[26] The long-term downregulation of the acquired immune response that occurs after sepsis episodes has been described in humans and experimental models.[10 26] In the present study, a lack of an intestinal inflammatory response to DSS was observed after more than 60 days following sepsis induction, as shown by the reduced severity of colitis and reduced proinflammatory cytokine concentration in mice previously submitted to sepsis. Moreover, we have shown that sepsis-surviving subjects also presented a significant reduction in the inflammation-induced development of colorectal adenomas and adenocarcinomas.

Inflammatory bowel disease (ie, ulcerative rectocolitis and Crohn's disease) has been implicated as a causative factor for CRC.[27] The clinical relevance of inflammation in colon carcinogenesis is reinforced by the cancer-preventive effect of long-term intake of cyclooxygenase inhibitors, which suppress local eicosanoid production and other inflammatory parameters.[28–30] Thus, the reduced DNA damage and production of proinflammatory cytokines during DSS-induced colitis and of other inflammatory events following sepsis may explain, at least in part, the reduction in AOM/DSS-induced CRC.

Many of the connecting mechanisms between CRC and inflammation are still under discussion. Resident cells surrounding the inflammatory site secrete inflammatory cytokines and other mediators, including eicosanoids and oxygen-derived and nitrogen-derived free radicals,[31] which mediates several inflammatory events. Consequently, other leukocytes are recruited to the inflammatory site, where they release new waves of inflammatory mediators and free radicals, which could trigger carcinogenesis through inducing DNA damage in the epithelial cells and other cell types.[31] Cytokines such as IFN-γ, IL-1β, IL-6, IL-8 and TNF were previously described to play a crucial role in the CRC carcinogenesis as well.[32–37] In line with this view, we observed that the inhibition of AOM/DSS-induced CRC in sepsis-surviving mice was associated with a reduction of DNA-damage and inflammatory cytokines production.

It is noteworthy that we observed a significant expansion of intestinal Tregs when animals were previously submitted to sepsis. Accordingly, the previous literature has shown a systemic expansion of Tregs following acute sepsis resolution.[11] IL-33, an alarmin found in epithelial cells and related to Treg polarization, is directly implicated in postsepsis-induced Treg expansion.[38] In the present work, IL-33 was also found in increased concentrations in the postsepsis intestine before colitis induction

To evaluate if Tregs could be causative players in the reduction of early carcinogenesis observed in postsepsis mice, Tregs were depleted using DTX in DEREG mice or CYP in wild-type mice. The depletion of Tregs in control mice led to fulminant colitis and death, as previously described,[15] while restoring the development of colitis, adenomatous intestinal polyps, and colorectal adenocarcinomas induced by the AOM/DSS protocol in the sepsis-surviving group.

These findings ultimately indicate that Tregs mediate the reductions in colitis and AOM/DSS-induced carcinogenesis in the postsepsis state. The mechanism through which Tregs reduce colitis is not the aim of the present study; however, the literature indicates that Tregs suppress the Th1 response by producing the anti-inflammatory cytokines TGF-β, IL-10 and adenosine, which induce T $CD8^+$ exhaustion and stimulate suppressive cells, namely, myeloid-derived suppressor cells, and macrophage polarization towards an immunotolerant profile.[39–42] In addition, Tregs promote tumor immune evasion and facilitate tumor growth and metastatic spread.[43–45]

The postsepsis state is related to a boost in Treg population and function,[11] which mediates the increased growth of previously established tumors.[9] Accordingly, depleting Tregs in mice with established tumors reduced the tumor growth and precluded the progression from adenomas to adenocarcinomas.[15] This shed light on the fact that these cells may have a dual role during colorectal-cancer initiation and progression, that is, impairing early inflammation-inducing carcinogenesis at the same time as promoting the growth of well-established tumors.

Collectively, our results introduce the concept that the postsepsis state impairs the inflammation-induced early carcinogenesis of CRC through the expansion of intestinal Tregs (see online supplementary figure S2). We postulate that in the early phase of colorectal carcinogenesis, postsepsis disorder reduces local inflammatory-related cancer initiators and early promoters, leading to a global impairment of cancer

initiation; however, during the late stages of cancer progression (ie, established tumors), postsepsis spurs tumor growth through reduced antitumor immunity and changes in the tumor microenvironment, as previously described.[9 10] These results may translate into the clinical setting. Prospective clinical studies are highly expected to evaluate how inflammation-induced carcinogenesis occurs in patients who have recovered from severe sepsis and septic shock and how the modulation of Treg activity can be explored as a therapeutic or preventative strategy. In addition to contributing to a better understanding of the pathogenesis involved in colorectal carcinogenesis, clinical confirmation and the further evaluation of our findings might hereafter impact screening and the further development of chemoprevention strategies to help reduce the cancer burden in the general population.

Author affiliations
[1]A.C. Camargo Cancer Center, Sao Paulo, Brazil
[2]Center for Research in Inflammatory Diseases (CRID), University of Sao Paulo, Ribeirao Preto, Brazil
[3]Cancer Institute of Ceara, Fortaleza, Brazil
[4]Instituto do Cancer do Estado de Sao Paulo, University of Sao Paulo, Sao Paulo, Brazil
[5]Ribeirao Preto Medical School, University of Sao Paulo, Ribeirao Preto, Brazil
[6]Department of Toxicology, Bromatology, and Clinical Analysis, University of Sao Paulo, Ribeirao Preto, Brazil
[7]Federal University of Ceara, Faculty of Medicine, Fortaleza, Brazil

Acknowledgements The authors are grateful to Ieda Regina dos Santos, Ana Kátia dos Santos, Marco Antônio de Carvalho, Giuliana Bertozzi Francisco, Diva Amábile Montanha de Sousa, Tadeu Franco Vieira and Sérgio Roberto Rosa for their technical support.

Contributors Conceived and designed the experiments: CAL, JMM, FQC and RAR. Performed the experiments: CAL, JMM, KAdL, CWW, LAN, MDF, CMSS, DFC, JYS, PRV and MDB. Analysed the data: CAL, JMM, KAdL, MDB, JCAF, VCCdL, FQC, VK and RAR. Contributed reagents/materials/analysis tools: VK, JCAF and FQC. Drafted the first version of the manuscript: CAL, JMM and FQC. All authors approved the final version of the paper.

Funding This work was supported by the São Paulo Research Foundation (FAPESP) under grant agreement no. 2013/08216-2 (Center for Research in Inflammatory Diseases).

Competing interests None declared.

Patient consent for publication Not required.

Ethics approval The experimental protocols and procedures were previously approved by the local Ethics Committee (protocol number: 195/2013) and were in accordance with the Declaration of Helsinki and the Guide for Care and Use of Laboratory Animals (National Institutes of Health, Bethesda, MD).

Provenance and peer review Not commissioned; externally peer reviewed.

Data availability statement Data are available upon reasonable request. All data relevant to the study are included in the article or uploaded as supplementary information. The datasets used and/or analyzed during the current study are available from the corresponding author on reasonable request.

ORCID iD
Caio Abner Leite http://orcid.org/0000-0002-9661-4378

REFERENCES

1 Torre LA, Bray F, Siegel RL, *et al*. Global cancer statistics, 2012. *CA Cancer J Clin* 2015;65:87–108.
2 Lasry A, Zinger A, Ben-Neriah Y. Inflammatory networks underlying colorectal cancer. *Nat Immunol* 2016;17:230–40.
3 Frick A, Khare V, Paul G, *et al*. Overt increase of oxidative stress and DNA damage in murine and human colitis and colitis-associated neoplasia. *Mol Cancer Res* 2018;16:634–42.
4 Johnson CM, Wei C, Ensor JE, *et al*. Meta-analyses of colorectal cancer risk factors. *Cancer Causes Control* 2013;24:1207–22.
5 Ghirelli C, Hagemann T. Targeting immunosuppression for cancer therapy. *J Clin Invest* 2013;123:2355–7.
6 Singer M, Deutschman CS, Seymour CW, *et al*. The third International consensus definitions for sepsis and septic shock (Sepsis-3). *JAMA* 2016;315:801–10.
7 Angus DC, Opal S. Immunosuppression and secondary infection in sepsis: part, not all, of the story. *JAMA* 2016;315:1457–9.
8 Davis JS, He V, Anstey NM, *et al*. Long term outcomes following hospital admission for sepsis using relative survival analysis: a prospective cohort study of 1,092 patients with 5 year follow up. *PLoS One* 2014;9:e112224.
9 Cavassani KA, Carson WF, Moreira AP, *et al*. The post sepsis-induced expansion and enhanced function of regulatory T cells create an environment to potentiate tumor growth. *Blood* 2010;115:4403–11.
10 Mota JM, Leite CA, Souza LE, *et al*. Post-Sepsis state induces tumor-associated macrophage accumulation through CXCR4/CXCL12 and favors tumor progression in mice. *Cancer Immunol Res* 2016;4:312–22.
11 Nascimento DC, Alves-Filho JC, Sônego F, *et al*. Role of regulatory T cells in long-term immune dysfunction associated with severe sepsis. *Crit Care Med* 2010;38:1718–25.
12 Barnes MJ, Powrie F. Regulatory T cells reinforce intestinal homeostasis. *Immunity* 2009;31:401–11.
13 Erdman SE, Poutahidis T, Tomczak M, *et al*. CD4+ CD25+ regulatory T lymphocytes inhibit microbially induced colon cancer in Rag2-deficient mice. *Am J Pathol* 2003;162:691–702.
14 Erdman SE, Sohn JJ, Rao VP, *et al*. CD4+CD25+ regulatory lymphocytes induce regression of intestinal tumors in Apcmin/+ mice. *Cancer Res* 2005;65:3998–4004.
15 Pastille E, Bardini K, Fleissner D, *et al*. Transient ablation of regulatory T cells improves antitumor immunity in colitis-associated colon cancer. *Cancer Res* 2014;74:4258–69.
16 Nascimento DC, Melo PH, Piñeros AR, *et al*. IL-33 contributes to sepsis-induced long-term immunosuppression by expanding the regulatory T cell population. *Nat Commun* 2017;8:14919.
17 Thaker AI, Shaker A, Rao MS, *et al*. Modeling colitis-associated cancer with azoxymethane (AOM) and dextran sulfate sodium (DSS). *J Vis Exp* 2012;67:4100.
18 Kodani T, Rodriguez-Palacios A, Corridoni D, *et al*. Flexible colonoscopy in mice to evaluate the severity of colitis and colorectal tumors using a validated endoscopic scoring system. *J Vis Exp* 2013:e50843.
19 Becker C, Fantini MC, Neurath MF. High resolution colonoscopy in live mice. *Nat Protoc* 2006;1:2900–4.
20 Bauer C, Duewell P, Mayer C, *et al*. Colitis induced in mice with dextran sulfate sodium (DSS) is mediated by the NLRP3 inflammasome. *Gut* 2010;59:1192–9.
21 Weigmann B, Tubbe I, Seidel D, *et al*. Isolation and subsequent analysis of murine lamina propria mononuclear cells from colonic tissue. *Nat Protoc* 2007;2:2307–11.
22 de Camargo MR, Gorgulho CM, Rodrigues CP, *et al*. Low concentration of 5-fluorouracil increases the effectiveness of tumor RNA to activate murine dendritic cells. *Cancer Biother Radiopharm* 2017;32:302–8.
23 Sakita JY, Bader M, Santos ES, *et al*. Serotonin synthesis protects the mouse colonic crypt from DNA damage and colorectal tumorigenesis. *J Pathol* 2019;249:102–13.
24 Luo C, Zhang H. The role of proinflammatory pathways in the pathogenesis of colitis-associated colorectal cancer. *Mediators Inflamm* 2017;2017:5126048.
25 Hotchkiss RS, Monneret G, Payen D. Sepsis-induced immunosuppression: from cellular dysfunctions to immunotherapy. *Nat Rev Immunol* 2013;13:862–74.
26 Prescott HC, Angus DC. Enhancing recovery from sepsis: a review. *JAMA* 2018;319:62–75.
27 Beaugerie L, Itzkowitz SH. Cancers complicating inflammatory bowel disease. *N Engl J Med* 2015;372:1441–52.
28 Burn J, Gerdes A-M, Macrae F, *et al*. Long-term effect of aspirin on cancer risk in carriers of hereditary colorectal cancer: an analysis from the CAPP2 randomised controlled trial. *Lancet* 2011;378:2081–7.

29 Rothwell PM, Fowkes FGR, Belch JFF, *et al*. Effect of daily aspirin on long-term risk of death due to cancer: analysis of individual patient data from randomised trials. *Lancet* 2011;377:31–41.
30 Cao Y, Nishihara R, Wu K, *et al*. Population-wide impact of long-term use of aspirin and the risk for cancer. *JAMA Oncol* 2016;2:762–9.
31 Taniguchi K, Karin M. NF-κB, inflammation, immunity and cancer: coming of age. *Nat Rev Immunol* 2018;18:309–24.
32 Zhan Y, Seregin SS, Chen J, *et al*. Nod1 limits colitis-associated tumorigenesis by regulating IFN-γ production. *J Immunol* 2016;196:5121–9.
33 Voronov E, Apte RN. IL-1 in colon inflammation, colon carcinogenesis and invasiveness of colon cancer. *Cancer Microenviron* 2015;8:187–200.
34 Grivennikov S, Karin E, Terzic J, *et al*. IL-6 and Stat3 are required for survival of intestinal epithelial cells and development of colitis-associated cancer. *Cancer Cell* 2009;15:103–13.
35 Asfaha S, Dubeykovskiy AN, Tomita H, *et al*. Mice that express human interleukin-8 have increased mobilization of immature myeloid cells, which exacerbates inflammation and accelerates colon carcinogenesis. *Gastroenterology* 2013;144:155–66.
36 Popivanova BK, Kitamura K, Wu Y, *et al*. Blocking TNF-alpha in mice reduces colorectal carcinogenesis associated with chronic colitis. *J Clin Invest* 2008;118:560–70.
37 Kim ER, Chang DK. Colorectal cancer in inflammatory bowel disease: the risk, pathogenesis, prevention and diagnosis. *World J Gastroenterol* 2014;20:9872–81.
38 Schiering C, Krausgruber T, Chomka A, *et al*. The alarmin IL-33 promotes regulatory T-cell function in the intestine. *Nature* 2014;513:564–8.
39 Fantini MC, Becker C, Tubbe I, *et al*. Transforming growth factor beta induced FoxP3+ regulatory T cells suppress Th1 mediated experimental colitis. *Gut* 2006;55:671–80.
40 Schmitt EG, Haribhai D, Williams JB, *et al*. IL-10 produced by induced regulatory T cells (iTregs) controls colitis and pathogenic ex-iTregs during immunotherapy. *J Immunol* 2012;189:5638–48.
41 Lee C-R, Kwak Y, Yang T, *et al*. Myeloid-Derived suppressor cells are controlled by regulatory T cells via TGF-β during murine colitis. *Cell Rep* 2016;17:3219–32.
42 Tiemessen MM, Jagger AL, Evans HG, *et al*. CD4+CD25+Foxp3+ regulatory T cells induce alternative activation of human monocytes/macrophages. *Proc Natl Acad Sci U S A* 2007;104:19446–51.
43 Facciabene A, Motz GT, Coukos G. T-Regulatory cells: key players in tumor immune escape and angiogenesis. *Cancer Res* 2012;72:2162–71.
44 Halvorsen EC, Mahmoud SM, Bennewith KL. Emerging roles of regulatory T cells in tumour progression and metastasis. *Cancer Metastasis Rev* 2014;33:1025–41.
45 Chaudhary B, Elkord E. Regulatory T cells in the tumor microenvironment and cancer progression: role and therapeutic targeting. *Vaccines* 2016;4:28.